

**UNIVERSIDADE DE SÃO PAULO
INSTITUTO DE QUÍMICA**

Programa de Pós-Graduação em Ciências Biológicas (Bioquímica)

ISAAC DE ARAUJO MATOS

Design of Myeloperoxidase Inhibitors as New Anti-inflammatory Agents: An *in silico*, *in vitro* and *in vivo* Study

Versão corrigida

São Paulo

Data do Depósito na SPG:
04/02/2022

ISAAC DE ARAUJO MATOS

**Planejamento de Inibidores da Enzima Mieloperoxidase
como novos Agentes Anti-inflamatórios: Um Estudo *in silico*,
in vitro e *in vivo***

*Tese apresentada ao Instituto de Química da
Universidade de São Paulo para obtenção do Título de
Doutor em Ciências (Bioquímica)*

Orientadora: Prof^ª. Dr^ª. Flávia Carla Meotti

São Paulo
2022

Autorizo a reprodução e divulgação total ou parcial deste trabalho, por qualquer meio convencional ou eletrônico, para fins de estudo e pesquisa, desde que citada a fonte.

Ficha Catalográfica elaborada eletronicamente pelo autor, utilizando o programa desenvolvido pela Seção Técnica de Informática do ICMC/USP e adaptado para a Divisão de Biblioteca e Documentação do Conjunto das Químicas da USP

Bibliotecária responsável pela orientação de catalogação da publicação:
Marlene Aparecida Vieira - CRB - 8/5562

M425p Matos, Isaac de Araujo
 Planejamento de Inibidores da Enzima
 Mieloperoxidase como novos Agentes Anti-
 inflamatórios: Um Estudo in silico, in vitro e in
 vivo / Isaac de Araujo Matos. - São Paulo, 2022.
 90 p.

 Tese (doutorado) - Instituto de Química da
 Universidade de São Paulo. Departamento de
 Bioquímica.
 Orientador: Meotti, Flávia Carla

 1. Mieloperoxidase. 2. Triagem virtual. 3.
 Inibidores. 4. Inflamação. 5. Artrite gotosa. I. T.
 II. Meotti, Flávia Carla, orientador.



Universidade de São Paulo
Instituto de Química

"Planejamento de inibidores da enzima mieloperoxidase como novos agentes anti-inflamatórios: um estudo *in silico*, *in vitro* e *in vivo*"

ISAAC DE ARAUJO MATOS

Tese de Doutorado submetida ao Instituto de Química da Universidade de São Paulo como parte dos requisitos necessários à obtenção do grau de Doutor em Ciências obtido no Programa Ciências Biológicas (Bioquímica) - Área de Concentração: Bioquímica.

Profa. Dra. Flavia Carla Meotti
(Orientadora e Presidente)

APROVADO(A) POR:

Profa. Dra. Ohara Augusto
IQ - USP

Prof. Dr. Laurent Emmanuel Dardenne
LNCC

Prof. Dr. Raphael Ferreira Queiroz
UESB

SÃO PAULO
09 de março de 2022

*Dedico esta tese a todos os Professores da minha Família,
Em especial à minha mãe, a Prof^a Maria Gorete de Araujo Matos e a minha tia avó,
A Prof^a Izaura Jaqueira Poderoso (in memoriam)*

AGRADECIMENTO(S)

Primeiramente agradeço à minha Família por todo o suporte, em especial à minha mãe, a Prof^a. Maria Gorete de Araujo Matos que durante seu magistério sempre me incentivou à ciência de forma indireta, quando propiciava um ambiente familiar da vida de um professor, como durante suas correções de dezenas de avaliações, onde eu sempre pedia um papel e uma caneca para rabiscar e de forma direta por todo suporte e educação, como quando me presenteava com exemplares de revistas de ciência ainda durante minha infância. Gestos esses que foram cruciais à escolha da carreira acadêmica/científica.

Agradeço também à minha tia avó Prof^a. Izaura Jaqueira Poderoso (*in memoriam*), a primeira professora da minha família, por todo o suporte durante minha formação e pelo incentivo mesmo que involuntário durante as horas que eu passava em sua cozinha ainda criança e ela me introduzia a ciência quando descrevia os estados físicos da matéria, a molécula da água, de quando falava sobre as galáxias e das válvulas cardíacas e como se deveria pronunciar a palavra *Washington*. Tudo isso me recorda o quanto fui privilegiado ao nascer num ambiente onde a educação estava sempre presente.

Agradeço também à minha tia a Prof^a. MSc. Miriam Ferreira Matos pelas contribuições à minha formação e pelos importantes momentos de discussão sobre os mais diversos assuntos incluindo literatura.

Agradeço também a todos meus Professores do ensino básico do Colégio Estadual Almirante Tamandaré – N. Sra. De Lourdes - SE, em especial à minha primeira

Professora de ciências, Tia Valdenice (*in memoriam*), pela introdução do método científico.

Agradeço também ao Professor Dr. Humberto Reis Matos por propiciar um ambiente de aprendizado nas disciplinas de bioquímica e farmacologia, bem como diversas outras áreas das ciências biológicas/farmacêuticas ainda durante minha iniciação científica em seu laboratório.

Agradeço ainda à minha orientadora, a Professora Dr^a Flávia Carla Meotti, por ter aceito a ideia do projeto de pesquisa que veio a se tornar esta tese, como também a todo suporte necessário para o desenvolvimento da mesma.

Agradeço também a todos os colegas e técnicos do Instituto de Química da USP, em especial à Cheila Cesar Gomes, pelos momentos de desabafo e à técnica bioterista Flávia Prates Moura e toda sua equipe do biotério, pelo excelente suporte com a experimentação animal.

Agradeço também ao Professor Dr. Nicolas Hoch pela confiança em um projeto paralelo relacionado à pandemia do Sars-Cov-2, expandindo minha formação para além do meu objeto de estudo.

Agradeço ainda a todos os colaboradores que tornaram este projeto viável, em especial à Professora do ICB Dr^a, Soraia Katia Pereira Costa e ao seu aluno, o doutorando Jorge Luiz Dallazen pelo valioso suporte com a experimentação animal.

Finalmente, agradeço à agência de fomento CAPES, pelo suporte financeiro para o desenvolvimento desta tese.

*Ninguém ignora tudo. Ninguém sabe tudo. Todos nós sabemos alguma coisa.
Todos nós ignoramos alguma coisa. Por isso aprendemos sempre.”*

Paulo Freire

*Nobody ignores everything. Nobody knows everything. We all know something.
We all ignore something. That's why we always learn.”*

Paulo Freire

RESUMO

(Matos, I.A.) Planejamento de inibidores da mieloperoxidase como novos agentes anti-inflamatórios: Um estudo *in silico*, *in vitro* e *in vivo*. 2021. 200p. Tese de Doutorado – Programa de Pós-graduação em Bioquímica. Instituto de Química, Universidade de São Paulo, São Paulo.

Esta tese disserta acerca do uso de métodos computacionais e experimentais para o desenvolvimento de novos inibidores da mieloperoxidase (MPO). A MPO é uma enzima chave na inflamação, ela está presente em neutrófilos e usa o peróxido de hidrogênio para oxidar cloreto ao ácido hipocloroso, um forte agente microbicida. Embora a MPO possua um importante papel no controle de infecções, sua atividade está associada ao descontrole da inflamação e ao dano tecidual. Além de catalisar a oxidação de haletos e pseudo-haletos através de um ciclo clorinante, a MPO pode oxidar outros substratos endógenos como urato, ascorbato, serotonina e tirosina através do ciclo peroxidásico. A oxidação de substratos via ciclo peroxidásico produz radicais livres, sendo um gatilho à reação em cadeia de radicais livres. Nesse contexto, inibidores da MPO surgem como novos candidatos anti-inflamatórios. Assim, para superar as limitações de metodologias prévias na busca de novos inibidores da MPO, um fluxo de trabalho utilizando diversas abordagens computacionais e experimentais foi desenvolvido. Inibidores já reportados para a MPO permitiram a elaboração de uma regra MPO inibidor-símile. Compostos que satisfazem essa regra possuem maior probabilidade de inibição e de atividade *in vivo*. A aplicação desta regra ao banco de dados ZINC12 recuperou uma sub-biblioteca de 6546 moléculas. Após etapas de docagem molecular, esse conjunto foi reduzido para 242 moléculas. Em uma validação experimental inicial, 10 compostos foram testados e 6 inibiram a atividade clorinante. O composto mais potente, ZINC9089086, exibiu um modo de inibição reversível, com um IC₅₀ de 2,2 µM, além de inibir a produção de ácido hipocloroso produzido por células. Para confirmar a previsibilidade da metodologia, 18 novos compostos foram selecionados. Confirmando a robustez da metodologia, 12 desses compostos foram ativos no ensaio de atividade clorinante da enzima, enquanto 13 inibiram a atividade peroxidásica. Os compostos mais potentes, RL6 e RL7, exibiram IC₅₀ na faixa nanomolar (270 nM e 560 nM, respectivamente) e os ensaios celulares também indicaram modulação na produção/disponibilidade do ácido hipocloroso e na NETose. Estudos mecanísticos indicaram que RL6 é um inibidor reversível e que não é oxidado pela enzima ou pelo produto da reação. Enquanto RL7 é um sequestrante de ácido hipocloroso. Para confirmar que a regra inibidor-símile não apenas seleciona inibidores *in vitro*, mas também compostos ativos *in vivo*, foi usado

um modelo murinho de artrite gotosa. Corroborando nossa hipótese, todos os compostos testados (RL6, RL7, RL21 e ZINC9089086), inibiram o edema de pata quando administrados por via intraperitoneal e 3 também foram oralmente ativos (RL6, RL7 e RL21). Finalmente, a integração de métodos computacionais e experimentais provou ser uma abordagem de ouro para a descoberta de inibidores de MPO ativos *in vivo*.

Palavras-chave: Mieloperoxidase, Triagem virtual, Inibidores, Inflamação, Artrite de gotosa.

ABSTRACT

(Matos, I.A.) Design of Myeloperoxidase Inhibitors as new anti-inflammatory drugs: A *in silico*, *in vitro* and *in vivo* study. 2021. 200p. PhD Thesis – Graduate Program in Biochemistry. Chemistry Institute, University of São Paulo, São Paulo.

This thesis discusses the use of computational and experimental methods for the development of new myeloperoxidase (MPO) inhibitors. MPO is a key enzyme present majority in neutrophil cells. Using hydrogen peroxide, MPO oxidizes chloride generating hypochlorous acid, a strong microbicidal agent. Although MPO has a microbicidal role, its activity is associated to inflammation progression and tissue damage. Beside the oxidation of halides and pseudo-halides in a chlorinating cycle, MPO can oxidize other endogenous substrates, such as urate, ascorbate, serotonin and tyrosine through a peroxidatic cycle. The oxidation of substrates in the peroxidatic cycle produces free radicals and can trigger a free radical chain reaction. In this context, MPO inhibitors emerge as new candidates to anti-inflammatory drugs. To overcome the limitations of the current methodologies available in the search of new MPO inhibitors, a pipeline of several computational and experimental approaches was developed in this thesis. Initially, known potent MPO inhibitors were used to elaborate an inhibitor-like rule. This rule suggests that compounds that match this criterion are more likely to both inhibit MPO and be orally active. By applying this rule to the ZINC12 database, a sub-library of 6546 molecules was recovered. After molecular docking steps, this set was reduced to 242 molecules with good stereospecificity for the active site of MPO. In a first experimental validation, 10 compounds were tested and 6 inhibited MPO chlorinating activity. The most potent compound, ZINC9089086, reversibly inhibited the enzyme with a $IC_{50} = 2.2 \mu M$. It also inhibited hypochlorous acid production by cells. To confirm the predictability of the virtual screening methodology, 18 additional compounds were selected. Confirming the methodology robustness, 12 of these compounds inhibited the chlorinating activity of the enzyme, while 13 inhibited the peroxidatic one. The most potent compounds, RL6 and RL7, exhibited IC_{50} in the nanomolar range (270 nM and 560 nM, respectively). Both compounds decreased hypochlorous acid production and NETosis in dHL-60 cells and peripheral blood neutrophils. Mechanistic studies indicate that RL6 is a reversible non-oxidizable MPO inhibitor, while RL7 is an hypochlorous acid scavenger. To confirm that the MPO inhibitor-like rule do not only select MPO inhibitors but also *in vivo* active compounds, a murine model of gouty arthritis was used. Corroborating our hypothesis, all tested compounds (RL6, RL7, RL21 and

ZINC9089086) inhibited paw edema when administered intraperitoneally and 3 compounds were also orally active (RL6, RL7 and RL21). Finally, the integration of computational and experimental methods has proven to be a golden approach for the discovery of *in vivo* active MPO inhibitors.

Keywords: Myeloperoxidase, Virtual screening, Inhibitors, Inflammation, Gout arthritis,

LIST OF ABBREVIATIONS

ABAH	4-Aminobenzoic acid hydrazide
AINES	Non-steroidal anti-inflammatory
AMP	Adenosine monophosphate
CTAC	Cetyltrimethylammonium chloride
DAG	Diacyl glycerol
DAMPs	Damage-associated molecular patterns
G-CSF	Granulocyte colony-stimulating factor
GMPs	Granulocyte–monocyte progenitors
HSC	Hematopoietic stem cells
HTS	High-Throughput Scree
IL-1 β	Interleukin-1 β
LBDD	Ligand-based drug design
LMPPs	Lymphoid primed multipotent progenitors
MPO	Myeloperoxidase
MPP	Multipotent progenitor
NMR	Nuclear magnetic resonance
NOS	Nitric oxide synthase
PAD4	Peptidylarginine deiminase 4
PAMPS	Pathogen-associated molecular patterns
PKC	Protein kinase C
PMA	Phorbol 12-myristate 13-acetate
PTU	Propylthiouracil
QSAR	Quantitative structure-activity relationship
SARS-CoV-2	Severe acute respiratory syndrome coronavirus 2
SBDD	Structure-based drug design
TNF- α	Tumor necrosis factor- α
TPSA	Topological polar surface area
VLA1	Integrin alpha 1 beta 1

SUMMARY

1. INTRODUCTION.....	15
1.1. Neutrophils and inflammation.....	15
1.2. Uric acid metabolism and gouty arthritis.....	19
1.3. MPO: Structure and catalysis.....	23
1.4. MPO inhibitors.....	27
1.5. MPO as a pharmacological target.....	29
1.6. Computer-aided drug discovery process.....	30
CHAPTER I.....	34
INTRODUCTION.....	35
MATERIALS AND METHODS.	36
▪ MPO inhibitor-like rule design.....	36
▪ Receptor structure preparation.....	36
▪ Calculation of heme group charges.....	36
▪ Molecular docking simulation.....	36
▪ Virtual screening validation.....	36
▪ MPO inhibition assay.....	37
▪ Theoretical ADME/Tox study.....	37
▪ Cell culture.....	37
▪ Human neutrophil isolation.....	37
▪ Hypochlorous acid production in cells.....	37
▪ Reversibility test.....	38
RESULTS AND DISCUSSION.....	38
▪ MPO inhibitor-like rule.....	38
▪ Structure-based step one.....	38
▪ Structure-based step two.....	39
▪ Hit validation and characterization.....	40
▪ ADME/Tox profile.....	41
▪ Inhibition of hypochlorous acid production <i>in vitro</i>	42
▪ Mechanism of inhibition.....	42
CONCLUSIONS.....	42

REFERENCES.....	43
SUPPORTING INFORMATIONS.....	46
CHAPTER II.....	51
INTRODUCTION.....	53
RESULTS.....	54
▪ Revalidation of the molecular docking protocol.....	54
▪ Identification of new MPO inhibitors.....	54
▪ Active compounds exhibit diversified interaction mode.....	57
▪ RL6 is a nanomolar reversible inhibitor.....	60
▪ RL6 and RL7 are not consumed by MPO.....	61
▪ MPO inhibitors decrease NETosis and HOCl production by dHL-60 cells and neutrophils.....	63
▪ RL6 does not inhibit PARP1.....	63
▪ <i>In vivo</i> candidates have good theoretical ADME/Tox profile.....	65
▪ MPO inhibitors and the HOCl scavenger decreased MSU-induced paw edema in mice.....	65
DISCUSSION.....	68
MATERIALS AND METHODS.....	69
▪ Virtual screening.....	69
▪ Chlorinating activity assay.....	70
▪ Peroxidatic activity assay.....	70
▪ Taurine chloramine scavenger assay	70
▪ Reversibility test.....	70
▪ Kinetics for the oxidation of the compounds.....	70
▪ HOMA calculation.....	71
▪ Cell culture.....	71
▪ Peripheral blood neutrophils.....	71
▪ Preparation of urate crystals.....	71
▪ HOCl cell production.....	71
▪ NETosis experiment.....	71
▪ PARP1 off-target assay.....	72

▪ Animals.....	72
▪ MSU-induced paw edema.....	72
▪ Statistical analysis.....	73
▪ References.....	74
▪ Supplementary materials.....	78
REFERENCES.....	84
APPENDIX.....	94
CURRICULLUM VITAE.....	145

1. INTRODUCTION

1.1. Neutrophils and Inflammation

Neutrophils are the most abundant leucocytes in blood, representing about 70% of their total. They are produced by the bone marrow at an approximated rate of 10^{11} cells per day(1). During differentiation the precursor cells undergo alteration in nucleus shape to a lobulated form, acquire granules and change receptors expression(1). As part of hematopoiesis, neutrophil production is named granulopoiesis. The hematopoietic stem cells (HSC) differentiate to multipotent progenitor (MPP) cells(2) (**Figure 1**). MPPs are categorized into three subsets MMP2, MMP3 and MMP4. The MMP3 is the most efficient in neutrophil polarization(3). MPPs cells differentiate to lymphoid primed multipotent progenitors cells (LMPPs) and, subsequently, to granulocyte–monocyte progenitors (GMPs)(1). Under granulocyte colony-stimulating factor (G-CSF) stimulus, GMPs obligatory follow to neutrophil production and are differentiated into myeloblasts (**Figure 1**). After five maturation steps, including promyelocyte, myelocyte, metamyelocyte and band cells, the mature neutrophil is able to leave the bone marrow(4).

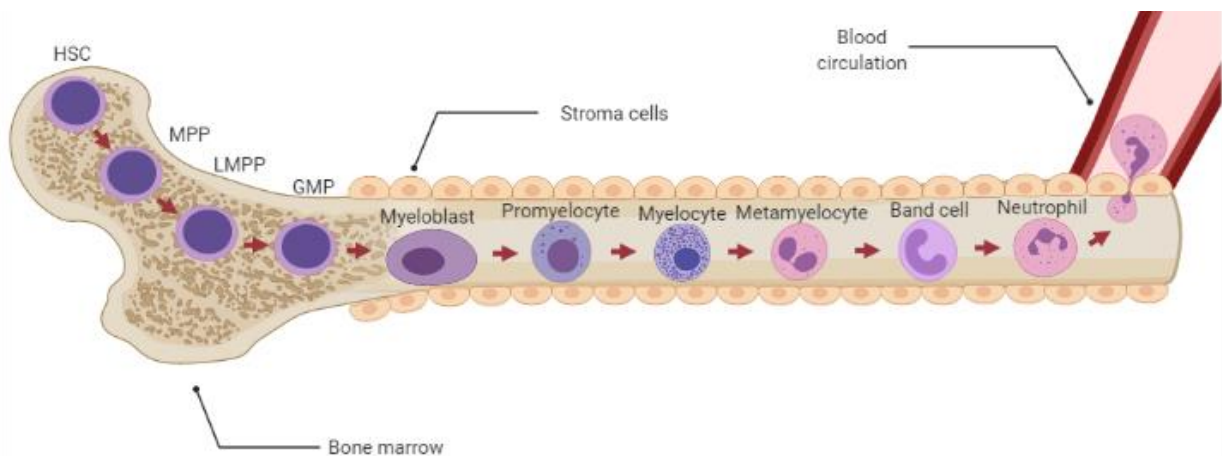


Figure 1. Neutrophil granulopoiesis in blood marrow. HSC – hematopoietic stem cell; MPP – multipotent progenitor cell; LMPP - lymphoid-primed multipotent progenitors and GMP - granulocyte-monocyte progenitor cells.

During granulopoiesis, expression of several receptors are modified, for instance there is a downregulation of integrin alpha 1 beta 1 (VLA1), CXC chemokine receptor 4, CXCR2 and Toll-like receptor 4(1). These receptors are important to maintain immature neutrophil progenitors into the bone marrow. For example, the stroma cells express ligands for VLA4 and CXCR4 receptors, VCAM1 and CXCL12, respectively(1).

From promyelocyte stage, the cells exhibit a different number of cytoplasmatic compartments. In mature neutrophils the secretory vesicles also known as secretory or granules are named: gelatinase or tertiary, specific or secondary and azurophilic or primary(5). Secretory vesicles are smaller compared to the others vesicles and the most to undergo exocytosis. This compartment contains several membrane-associated receptors that are important to the earliest phase of inflammatory responses as the contact between neutrophil and activated vascular endothelium, diapedesis and chemokine-mediated migration during chemotaxis(6).

Tertiary or gelatinase granules are secreted for the initial contact with the activated endothelium(7). Besides gelatinase, which digest extracellular matrix, these granules contain arginase I, an enzyme that degrades arginine, impairs oxide nitric synthesis by nitric oxide synthase (NOS) and promotes penetration into inflamed regions(8).

Specific (secondary) granules contain several microbicide agents that are secreted into the phagosome or released to the extracellular medium(5). This type of granule contains lactoferrin, a antimicrobial protein with bacteriostatic and bactericidal action active against Gram-positive and negative bacteria, fungi and viruses(9). Lactoferrin has several action mechanisms, including iron chelation, impairment of nutrients uptake by microorganisms, abstraction of pro-inflammatory lipopolysaccharides, resulting in a positive impact in sepsis and tissue damage. It also acts as a mediator between innate and adaptive immune response(10).

Azurophilic, also named primary granules, have variable size and form(5). This type of granule is composed by acidic hydrolases and microbicide proteins, with abundant content of the heme protein myeloperoxidase (MPO). MPO represents about 5% of the neutrophil's total protein(11,12). It plays important microbicide role into phagolysosome and in extracellular environment(13). This enzyme oxidizes chloride to hypochlorous acid, a strong oxidant with microbicidal activity(14). Other enzymes present in azurophilic granules are neutrophil elastase, proteinase 3 and cathepsin G, they digest extracellular matrix proteins(15).

Neutrophils are the first line of defense against infection. They migrate to inflamed tissues through endothelial capture, followed by rolling, slow rolling, arrest, adhesion, intravascular crawling and diapedesis between endothelial cells that coat the blood vessels(16,17). The release of pro-inflammatory cytokines as interleukin-1 β (IL-1 β), IL-8 and tumor necrosis factor- α (TNF- α) induce expression and translocation of the selectins P, E and L on the endothelium surface(18). Thus, neutrophils adhere to endothelium through selectin receptors(16). After that, they migrate

into the interstitial space using chemotactic gradient. An additional recruitment can be performed by macrophages, which release IL-1 β that stimulates IL-8 production by endothelial cells(16).

At the infection site, neutrophils can act through three antimicrobial mechanisms: degranulation, phagocytosis and NETosis(1). In degranulation, neutrophil granules release their content to the extracellular medium(1). Initially, gelatinase granules are released, followed by specific and then, the azurophilic granules(5). The azurophilic degranulation depends on a great stimulus, as a high content of pathogens, being great part of granules translocated to phagosomes and not exocytosed(19,20).

When neutrophils phagocyte pathogens, the signaling is triggered by pathogen-associated molecular patterns (PAMPs) that bind to Toll-like receptors and/or by opsonins as proteins from microbe surface, antibodies and complement molecules, that activate phagocytosis through opsonin receptors(16). After activation, phagocytes engulf the pathogen by endocytosis forming the phagosome. This vesicle fuses with the lysosome to form the phagolysosome(21), this new organelle contains microbicidal proteins (e.g. lactoferrin), proteases (e.g. neutrophil elastase) and oxidants enzymes as NADPH oxidase and MPO that work together to eliminate the pathogen(22).

Activation of neutrophils is not restrict to infection control(1). These cells are also involved in the pathophysiology of inflammatory diseases, as autoimmune, cancer, cardiovascular and neurodegenerative diseases(23). In this context, many pharmacological strategies have been employed to modulate neutrophil response(23).

A more recently described process in neutrophil-inflammatory and antimicrobial response is NETosis(23,24)(25). In NETosis, cells eject a conjunct of chromatin and antimicrobial enzymes, as elastase and MPO(26), to capture microbes like a “net”. NETosis is classified in lytic and non-lytic forms. In the lytic NETosis, neutrophil undergoes a slow death that initiates with the formation of a granule-chromatin complex, nuclear delobulation and dissolution, followed by cell depolarization, chromatin decondensation and, finally, rupture of plasm membrane, ejecting the NETs to all directions(26). In non-litic NETosis, NETs are rapidly ejected unidirectionally with granule-chromatin complex formation in extracellular medium and a remaining cytoplasm with phagocytic capacity is generated(26).

If in one hand NETs are important for pathogens eradication(27,28), on the other hand it contributes to the pathogenesis of chronic inflammation, autoimmune, cancer and neurodegenerative disease(26–30). In an atherosclerosis animal model, NETosis process was

implicated in atherothrombotic events(31). NETs also was implicated in cystic fibrosis, a disorder caused by mutation of the cystic fibrosis trans-membrane conductance regulator(32). In this condition, NETs favored bacterial colonization in parallel to lung tissue injury(32).

Recently, a clinical study reported NETosis contributions in Covid-19 pathophysiology(33). In these patients, NETs in blood, tracheal aspirate and lung autopsies were elevated when compared to healthy individuals. Additionally, neutrophils of Covid-19 positive individuals had a higher “NETotic” capacity and experiments using viral particle showed that SARS-CoV-2 virus was able to induce NETosis *in vitro*, promoting epithelial cell death(33).

Different stimuli are able to induce NETs, for instance bacteria, fungi and virus(34–36), sterile agents as platelets, antibodies and crystals as well the chemical agents PMA (phorbol 12-myristate 13-acetate) and ionomycin(37)(38). In some cases, NETosis is dependent on NADPH oxidase, MPO and neutrophil elastase(39). Following neutrophil activation, the protease elastase migrates from azurophilic granules to nucleus promoting chromatin decompaction by histones degradation. MPO helps elastase in chromatin decompaction by a mechanism independent of its catalytic activity. However, inhibition of MPO activity retards NETosis(39,40). A recent study showed that a MPO inhibition by ABAH (4-Aminobenzoic Acid hydrazide) inhibited NETosis induced by PMA(38).

The elastase/MPO pathway was observed in NETosis induced by different agents, including pathogens, cholesterol and urate crystals(26,38,41). Alternatively, NETosis can be regulated by citrullination of histones with peptidylarginine deiminase 4 (PAD4), which is involved in chromatin decompaction(31,42,43). In the NETosis induced by PMA and urate crystals citrullination was unnecessary(26). PMA is a phorbol ester that mimetics diacyl glycerol (DAG), it targets protein kinase C (PKC) by bind to C1A domain promoting conformational changes that culminates in C1A/PMA complex translocation to membrane(44). In sequence, a second PMA molecule bind to C1B domain that also translocates to membrane generating conformational changes to an active PKC(44).

PKC phosphorylates the NADPH oxidase p47phox subunit to produce the anion radical superoxide and hydrogen peroxide(45). These species, along with MPO and neutrophil elastase promote chromatin decompaction and NETs ejection(39). Differently from PMA and fungi stimuli, NETosis induced by urate crystals occurs by a mechanism independent of oxidants, with neutrophil elastase mediating chromatin decompaction after cell death(38). Additionally, NETs

induced by urate crystals are less susceptible to enzymatic degradation than the PMA-stimulated one. In addition, there are an abundance in actin and actin binding proteins, suggesting an alternative pathway.

1.2. Uric acid Metabolism and Gouty Arthritis

Gouty Arthritis is a very common inflammatory condition characterized by elevation of serum urate levels (hyperuricemia) caused by an unbalance in the production or elimination of urate(46,47). Urate may precipitate as crystals in the joints causing inflammation and acute pain(48,49). The global incidence of gout is estimated up to 6.8%, reaching between 0.58 and 2.89 per 1,000 person-year with prevalence in man and correlated with age and ethnical groups(48). Hyperuricemia is an essential condition to gout, being characterized by a serum urate level > 7 mg/L(49).

Urate is a subproduct of purine metabolism (Figure 2)(50). In this pathway, phosphate groups in AMP (adenosine monophosphate) and GMP (guanosine monophosphate) nucleotides are removed by nucleosidases. The products, adenosine and guanosine follow different routes(50). In a new reaction with nucleosidase, guanosine is converted to guanine that, after deamination by guanine deaminase yields uric acid. In the case of adenosine, the enzyme adenosine deaminase deaminates it into inosine and, in the next step, the nucleosidase converts inosine to hypoxanthine. Hypoxanthine is converted into uric acid by two oxidation steps catalyzed by xanthine oxidase(50).

Uricase, an enzyme that catabolizes urate to 5-hydroxyisourate, is expressed and active in all mammals but not in humans and great apes(51). Thus, uric acid accumulates in their blood reaching concentrations between 2.5 and 7.0 mg/dL in men and 1.5 to 6.0 mg/dL in women(50). The loss of uricase has been attributed to an adaptation to increase serum antioxidant capacity(52). However, the levels of serum uric acid are associated with cardiovascular damage(53,54).

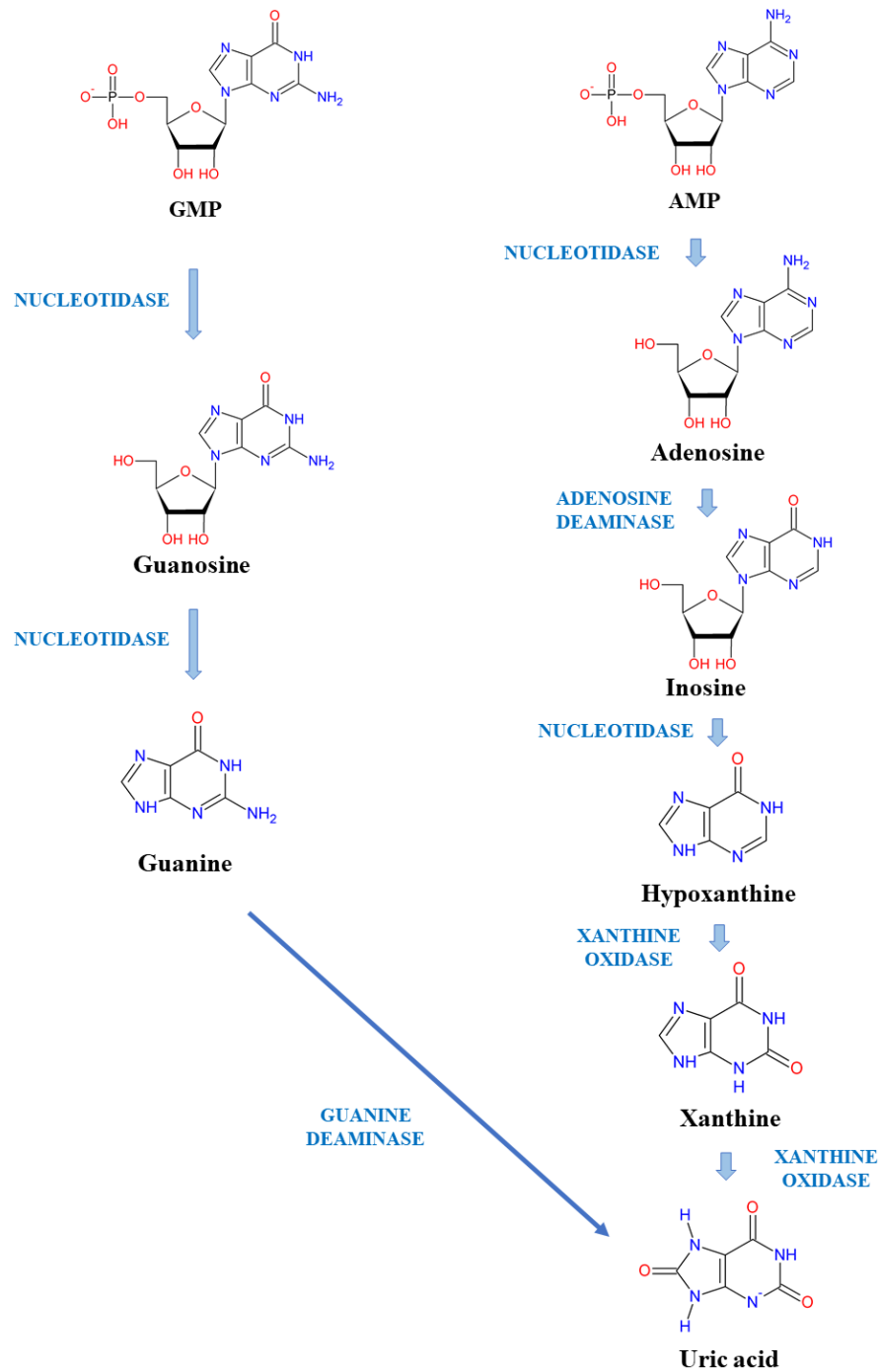


Figure 2. Uric acid production in humans.

Beside an endogenous production, uric acid can also be obtained from diet, mostly from animal protein. The endogenous production occurs mainly in liver, kidneys, intestines, vascular endothelium and muscles (**Figure 3**)(55). Factors that increase the cell turnover such as fructose

intolerance, alcohol ingestion, use of drugs like aspirin, cyclosporine and thiazide diuretics as well as dehydration and impaired renal function affect uric acid homeostasis(56).

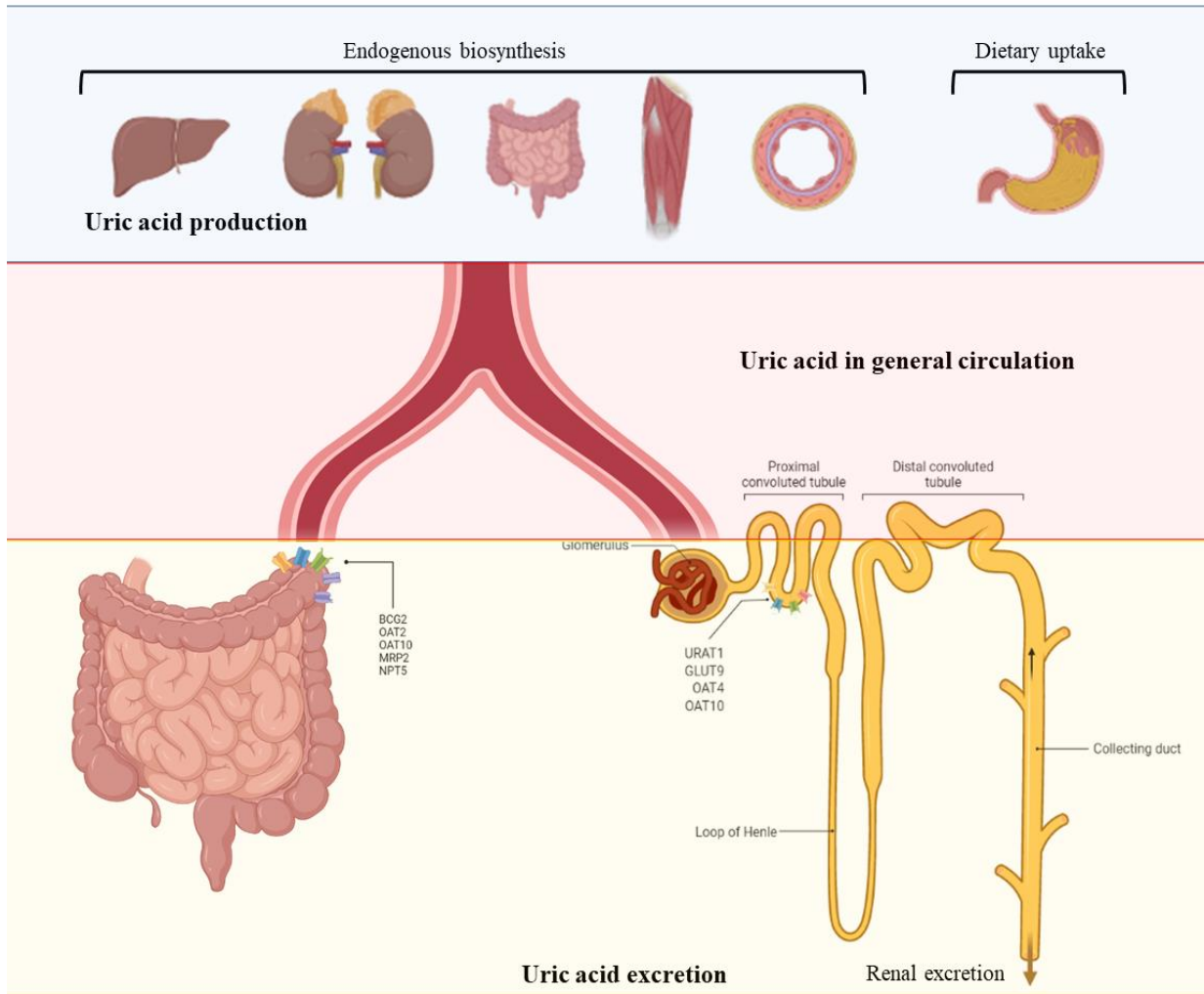


Figure 3. Uric acid production and excretion. Uric acid can be generated endogenously by the liver, kidneys, intestine, muscles and endothelium or obtained in the diet. It is excreted by the intestinal tract through ABCG2, OAT2, OAT10, MRP2 or NPT5 (57). In renal excretion, it is filtrated in the glomerulus and reabsorbed by URAT1, GLUT9, OAT4 and OAT10 transporters at proximal tubule. ABCG2 - ATP-binding cassette transporter G2, OAT2 - organic anion transporter 2, OAT10 - organic anion transporter 10, NPT5 - sodium-dependent phosphate co-transporter, URAT1 - urate transporter 1, GLUT9 - glucose transporter 9, OAT4 - organic anion transporter 4 and OAT10 - organic anion transporter 10.

Elimination of uric acid by the renal tract represents two-thirds of total clearance, whilst the other third is via gastrointestinal(50). Intestinal excretion occurs via BCG2, OAT2, OAT10, MRP2 or NPT5 transporters (**Figure 3**)(57). Kidney excretion occurs via MRP4, ABCG2, SLC17A1 and SLC17A3 transporters, whereas 90% is reabsorbed in the proximal tubule by URAT1, GLUT9,

OAT4 and OAT10 transports. Mutations in these transporters are related with gout in different populations(57–59).

Hyperuricemia is virtually present in every gout patient. However, individuals with hyperuricemia do not necessarily develop gout(60). Among hyperuricemia individuals a percentage of 25% exhibit monosodium urate deposition crystal in joint(61,62). This deposition is a check point to gout progression.

Monosodium urate crystals are damage-associated particles that activate NLRP3 inflammasome in monocytes and macrophages producing gout crisis(63). Inflammasome is a protein complex composed by receptors and sensors that, when assembled, activates caspase-1, inducing the inflammatory response against endogenous and exogenous stimulus(64).

Activation of NLRP3 inflammasome depends on Toll-like receptors 2 and 4 (TLR2 and TLR4)(65). The binding of DAMPs (damage-associated molecular patterns) or PAMPs (pathogen-associated molecular patterns) to TLR2 or TLR4 results in stimulation of NF- κ B transcription factor that promotes the expression of inflammasome components-related genes and synthesis of pro-IL-1 β cytokine(66). Then, inflammasome assembly is triggered, pro-caspase 1 is cleaved to caspase 1, which converts pro-IL-1 β to mature IL-1 β (67). This pathway is activated by monosodium urate crystals. However, the mechanisms are not very clear(49). Mature IL-1 β leaves the cell and binds to IL-1 β receptor, promoting the activation and release of other pro-inflammatory cytokines and neutrophil recruitment(49).

In a mice experimental model of acute gouty arthritis induced by intra-articular administration of monosodium urate crystals, neutrophils were not essential to gout resolution(68). In this study, neutrophil depletion strongly decreased MSU-crystal-induced paw edema and MPO activity, a marker of neutrophil infiltration/inflammation. This data supports the modulation of neutrophil activation to counteract gout(23,24).

Gout is managed by pharmacological and nonpharmacological therapies. The latter include lifestyle and nutritional changes, such as avoidance of alcohol and uricogenic-based diets to lower serum uric acid. However, they may be insufficient to control gout(69). Pharmacological therapies can be used both to reduce hyperuricemia and to manage inflammation in acute attacks(65). Hypouricemic drugs include xanthine oxidase inhibitors as allopurinol and febuxostat, both decrease uric acid biosynthesis(70). Drugs that block urate transporters and its renal reabsorption include benzbromarone and probenecid(71). Acute gout episodes, known as gout flare, are

managed with analgesic, non-steroidal anti-inflammatory drugs (AINEs) and corticosteroids. However, their adverse effects limit the use(65), making the search for new pharmacological agents still necessary.

1.3. MPO: Structure and catalysis

MPO (E.C. 1.11.2.2) is an oxidoreductase that reduces hydrogen peroxide to water incorporating an oxygen atom into its hemic iron(72). This enzyme is present in leukocytes and very abundant in neutrophils. It represents approximately 5% of the total protein in this cell(11,12). MPO is a homodimer with a total molecular mass of 146 kDa. Each monomer is composed by a light (15.5 kDa) and a heavy (58.5 kDa chain (**Figure 4A, B and C**)(73).

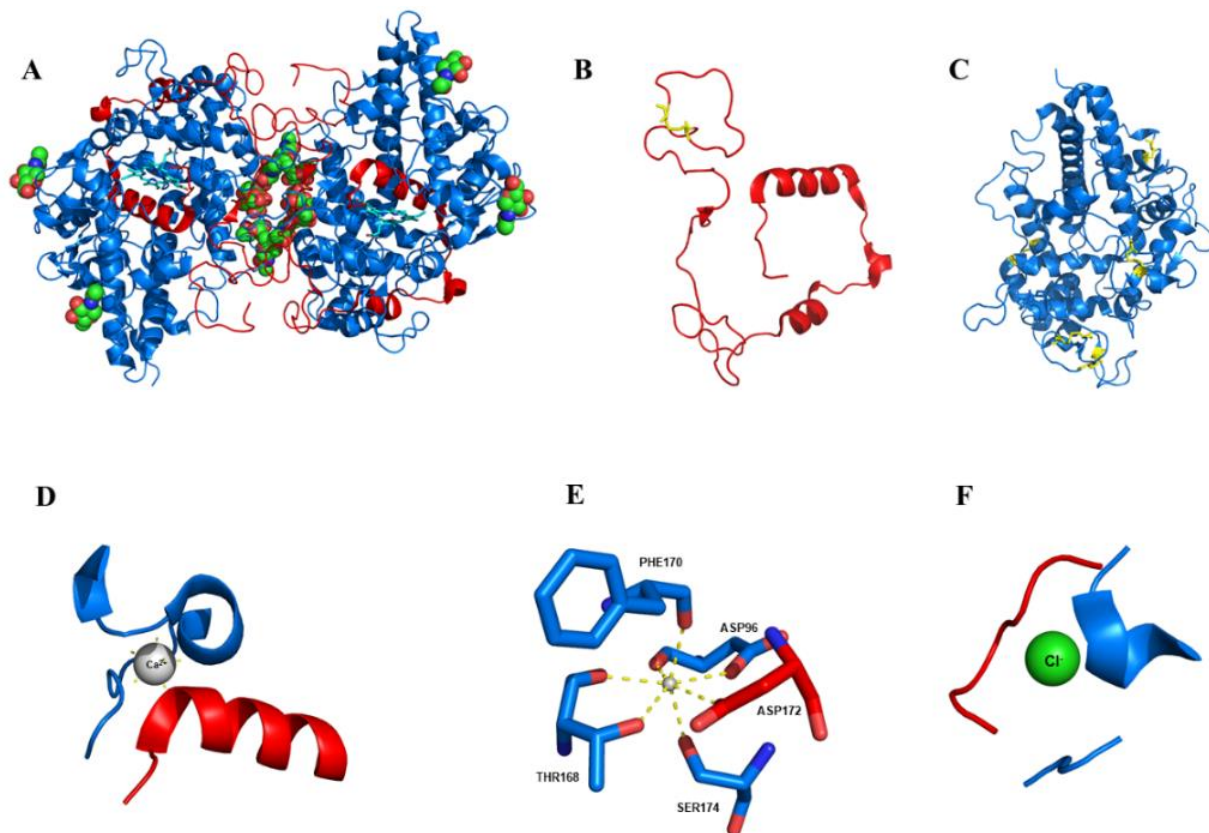


Figure 4. Structure of MPO. A – Structure of MPO dimer with glycosylations (green spheres). B - light chain with a disulfide bond between two cysteine in yellow. C - heavy chain exhibiting five disulfide bonds. D, E – Calcium atom coordinated in pentagonal bipyramidal geometry with residues of light and heavy chain. F – Chloride binding site. Protein Data Bank 1CXP code.

To reach its mature form, MPO undergoes several post-translational modifications(74). Initially, in endoplasmic reticulum, MPO is expressed as a primary product preMPO (80 kDa). It

is glycosylated into five asparagine residues to form the inactive apoproMPO (90 kDa). This glycosylation is essential to the optimal enzyme activity(75). Supported by ERp57, calreticulin and calnexin chaperones, the heme group is attached to the protein through an autocatalytic mechanism dependent on hydrogen peroxide. This active proMPO monomer (90 kDa) is then exported from endoplasmic reticulum. In the cytoplasm, proMPO is cleaved by a protease that removes the *pro* peptide, generating a monomeric intermediate (75 kDa). To finally reach the mature form, a proteolysis between the light and the heavy chains is necessary, as well as the disulfide bond formation between the heavy chains of the two monomers.

In addition to the disulfide bond between the heavy chains, MPO is stabilized by one cysteine within the light chain and five others in the heavy chain (**Figure 4B and C**). MPO also has a calcium in a pentagonal bipyramid geometry that coordinates with residues from the light and the heavy chains (**Figure 4D e E**). Interestingly, in presence of chelating agents MPO precipitates in an inactive form(76). Supporting these findings, mutations in the calcium bind site abolish MPO catalytic activity(77), indicating that calcium acts as an “atomic glue” by stabilizing MPO structure.

MPO active site contains a heme group attached by three covalent bonds with the lateral chain of Asp94, Glu242 and Met243. Met243 has the sulfur atom methylated and charged (**Figure 5A**). This vinyl-sulphonium bond is indispensable for chloride and bromide oxidation and the mutation of Met243 to Val reduced 98.1% and 87.4% the chlorinating and brominating activities, respectively(78). MPO active site contains a distal (His95) and a proximal (His336) histidine (**Figure 5B**). Raman spectroscopy data and molecular dynamics simulations indicate that the imidazole in proximal histidine is negatively charged as an imidazolate(79,80). Differently from proximal histidine, distal histidine directly participates in catalysis, its imidazole ring is neutral and in the epsilon tautomerization state (**Figure 5B**)(73). The Gln91 and Arg239 residues in the internal MPO pocket are also important to catalysis, whereas the external residues Phe336, Phe407 and Glu102 contribute to the ligand’s stabilization in the MPO active site (**Figure 5C**). Additionally, MPO has a defined catalytic pocket with a surface predominantly negative with some neutral regions (**Figure 5D**).

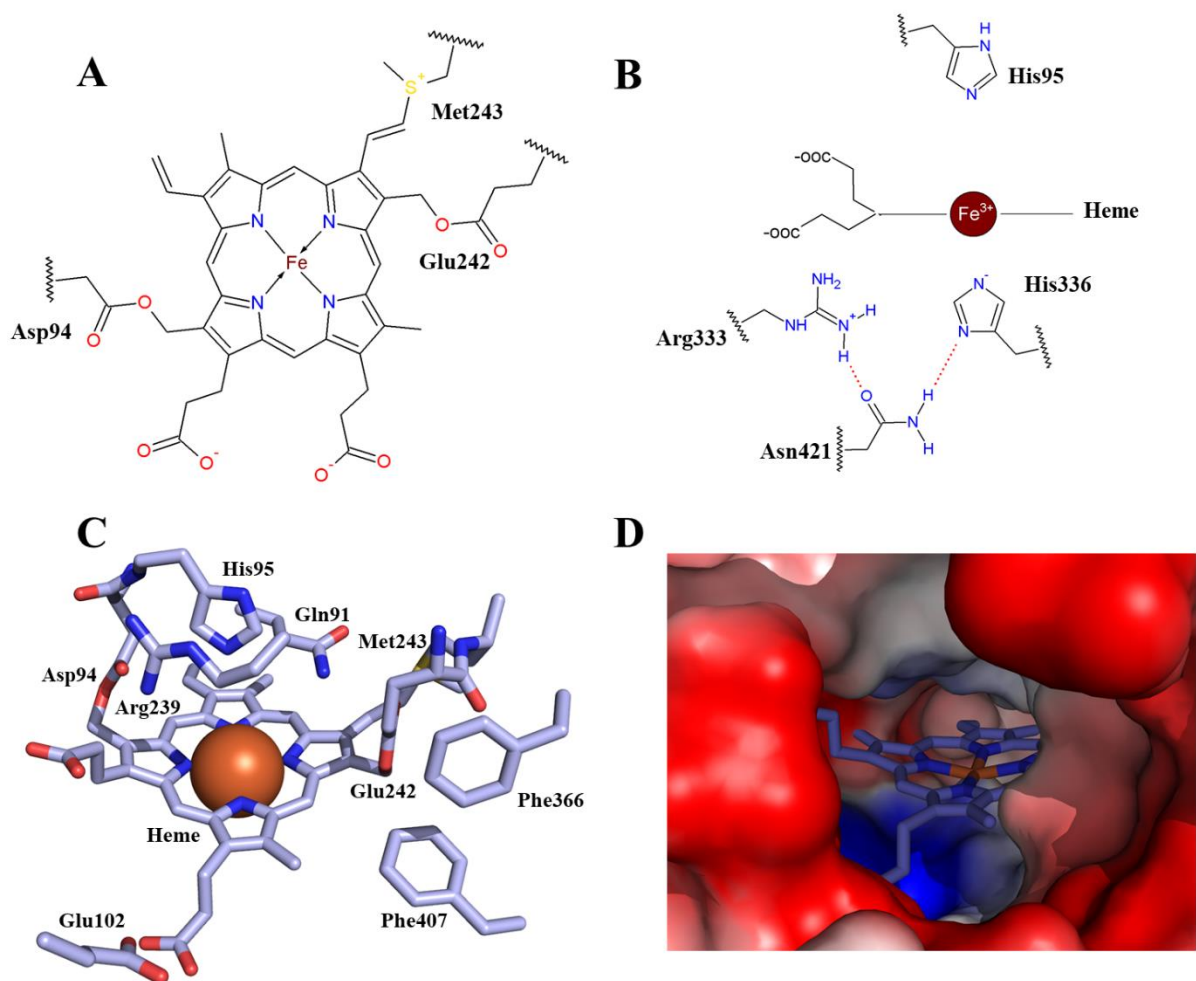


Figure 5. Amino acids residues and heme group in the MPO active site. A – MPO heme group top view showing the covalent bonds with Asp94, Glu242 and Met243. B - Side view of the heme and His95, Arg333, His336 and Ans421 residues. C – The most relevant residues in MPO active site. D – Potential electrostatic map of the active site surface showing negative (red) and apolar (grey) regions. Protein Data Bank 1CXP code.

MPO is a non-typical enzyme with diverse catalytic activities and multi substrate(73). For this, MPO uses the chemical potential from its main substrate, hydrogen peroxide, as driving force to promote the generation of redox species. In this process, hydrogen peroxide binds to iron in the ferric state (Fe III, high spin) and uses a water molecule as a bridge, performing a hydrogen bond with the distal histidine (His95) (**Figure 6**)(73). During catalysis, two electrons are removed from heme, an oxygen atom is transferred to the iron yielding a peroxy (Fe IV) named compound I(72). This specie is a π -cation radical that is rapidly formed in hydrogen peroxide presence ($k = 2 \times 10^7 \text{ M}^{-1} \text{ s}^{-1}$) and has a high reduction potential for abstraction of one or two electrons(73,81).

Compound I can be reduced by either a peroxidatic or halogenation cycles, oxidizing a myriad of substrates (**Figure 6**). In the halogenation cycle, compound I removes two electrons from chloride ($k = 2.5 \times 10^4 \text{ M}^{-1} \text{ s}^{-1}$), bromide ($k = 1.1 \times 10^6 \text{ M}^{-1} \text{ s}^{-1}$), iodide ($k = 7.2 \times 10^6 \text{ M}^{-1} \text{ s}^{-1}$) or from the pseudohalide thiocyanate ($k = 9.6 \times 10^6 \text{ M}^{-1} \text{ s}^{-1}$)(82), generating the respective hypohalous acid. By halogenation, the enzyme is regenerated to its ferric native form (**Figure 6**). Moreover, hypochlorous acid is also a substrate for ferric MPO, converting the native enzyme to compound I ($k = 2 \times 10^8 \text{ M}^{-1} \text{ s}^{-1}$)(83). Additionally, hydrogen peroxide is a compound I substrate in a catalase-like reaction ($k = 2 \times 10^6 \text{ M}^{-1} \text{ s}^{-1}$)(84). Alternatively, the ferric species can be oxidized by superoxide ($k = 1.1 \times 10^6 \text{ M}^{-1} \text{ s}^{-1}$) forming the so called compound III and the reverse reaction is a superoxide dismutase catalysis generating hydrogen peroxide(85).

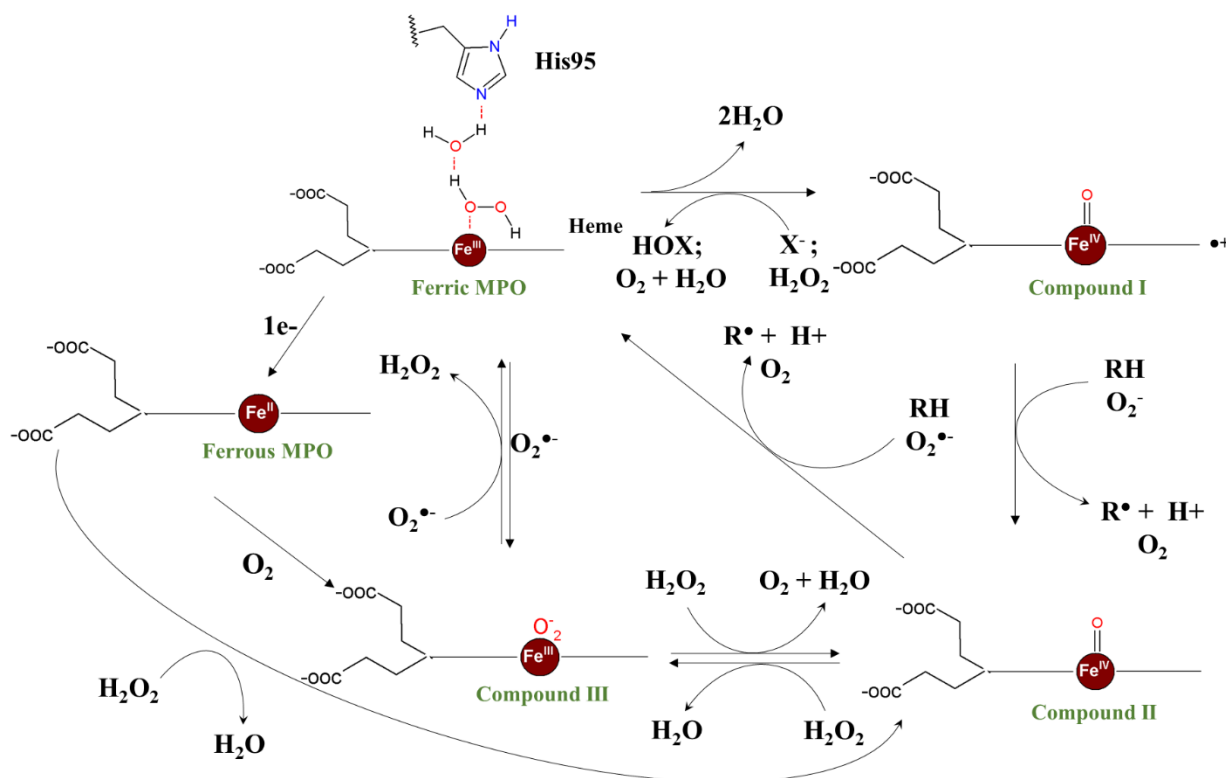


Figure 6. MPO catalytic mechanism. HOX – hypohalous acid, X⁻ - halide ion, RH – oxidable substrate.

In the peroxidatic cycle, compound I oxidizes several substrates via one electron generating compound II and a free radical product. Endogenous substrates for compound I include tyrosine(86), urate(87), melatonin(88), serotonin(89), hydrogen sulfide(90) and ascorbate(91). Superoxide is also a compound I substrate ($k = 1 \times 10^8 \text{ M}^{-1} \text{ s}^{-1}$) and the one electron oxidation

generates molecular oxygen and the intermediate compound II (92). Compound II can be reduced by one electron abstraction from superoxide ($k = 4 \times 10^6 \text{ M}^{-1} \text{ s}^{-1}$) or organic substrates regenerating the enzyme to ferric form(92).

Alternatively, compound II can react with hydrogen peroxide being converted to compound III. The reverse of this reaction is a catalase-like catalysis and produces molecular oxygen and water from hydrogen peroxide (**Figure 6**). Furthermore, compound III can be generated from the oxidation of ferrous MPO by molecular oxygen(93). The ferrous intermediate is formed from one electron reduction of the ferric one by free radical products of the peroxidatic cycle. In addition, at anaerobic conditions ferrous MPO degrades hydrogen peroxide directly forming compound II(94).

The different redox forms of MPO have distinct absorption spectra(95). Ferric MPO absorbs at 430, 570 and 625 nm. The conversion of the ferric form to compound I decreases the *Soret* band in 430 nm and the ferrous MPO presents a shift to 473nm in *Soret* band(96). *Soret* bands of compound II and III are similar at 456 nm. However, at 625 nm compound II has a low broad band while compound III is higher and sharper. The ratio 625/456 is used to distinguish these two species(97). The decrease in the isosbestic band at 441 nm is used to evaluate the conversion of compound III or ferric form to compound I, whereas its increase reveals the conversion of compound I to compound II.

1.4. MPO inhibitors

Since MPO can be at different intermediate forms, mechanisms of inhibition are varied. Thus, inhibitors can be classified into compound II accumulators, mechanism-based irreversible inhibitors or those that exhibit a reversible binding to ferric MPO(98). Compound II accumulator inhibitors are good substrates to compound I but not to compound II. Therefore, they trap MPO as compound II decreasing enzyme turnover. This class includes nitroxides(99), indoles(100) and flavonoids (Figure 7) (101,102). Compound II accumulators have a limitation at physiological conditions, since compound II contains relevant endogenous substrates: tyrosine(103,104), urate(87) and ascorbate(105), it can efficiently return to ferric form, reverting the inhibition(106).

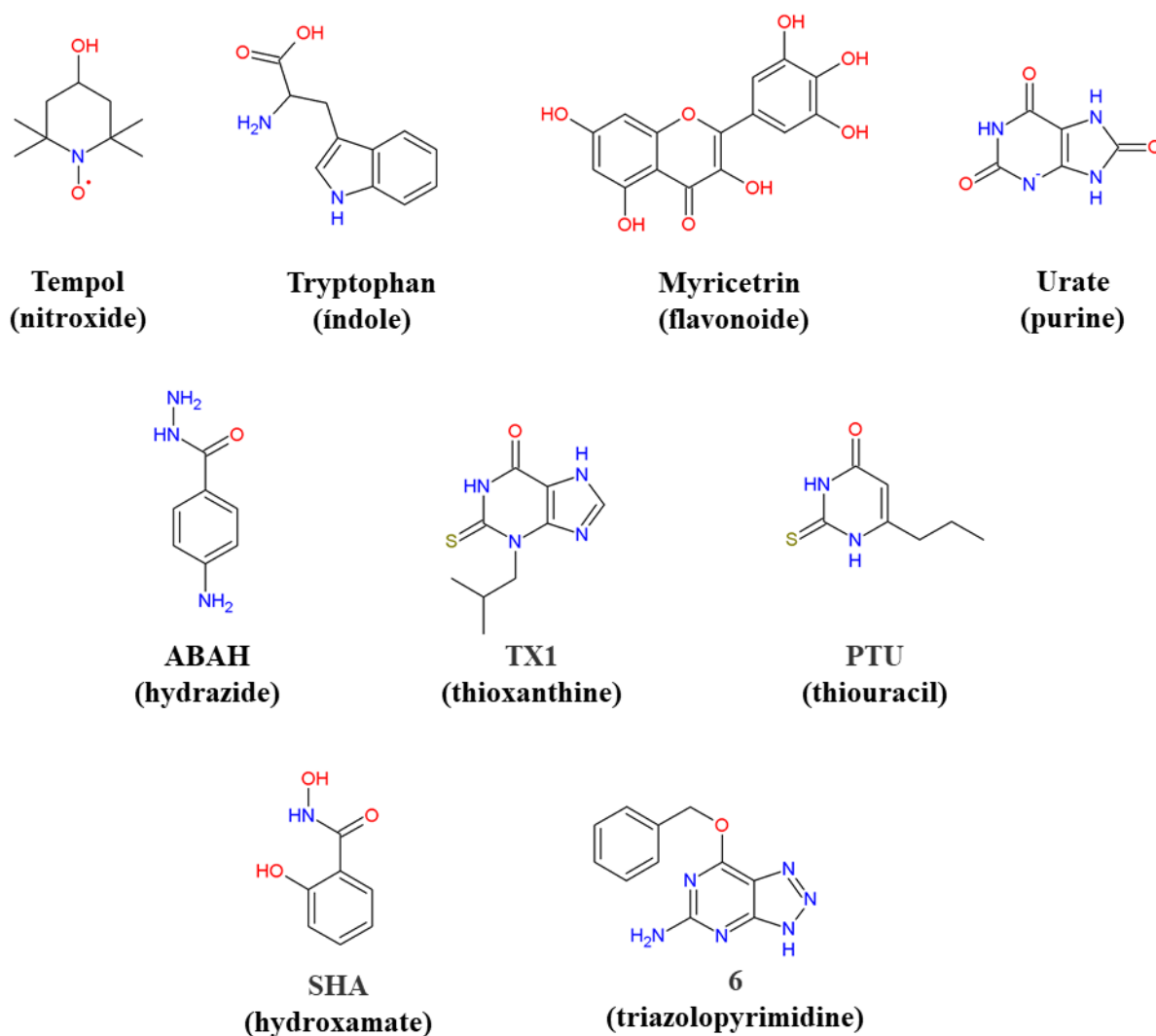


Figure 7. Structure of MPO inhibitors. ABAH - 4-Aminobenzoic Acid hydrazide, TX1-thioxanthine 1, PTU – propylthiouracil, salicylhydroxamic acid.

The second class of inhibitors, also known as suicide substrates, is formed by compound I substrates but different of compound II accumulators, after the one electron abstraction from substrate, the free radical product rapidly reacts with the enzyme, forming a covalent bond with the heme group, inactivating it(107). This class comprises hydrazides(107), thioxanthines(108) and thiouracil analogs(109). Although they are effective inhibitors at physiological conditions, their high reactivity and poor selectivity results in several off-target effects and toxicity.

The third class is formed by tight binding inhibitors. These compounds are reversible inhibitors that bind to the MPO ferric form obstructing the entry of hydrogen peroxide and/or chloride(98). This class is the least studied and few compounds have been reported by having this inhibition mechanism. Hydroxamates were proposed as the first MPO tight binding inhibitors. However, they are also substrates for compound I accumulating compound II and trapping MPO to ferrous and nitrosyl ferrous forms(98). Recently, a triazolopyrimidine was reported as the first tight binding inhibitor which is not a MPO substrate(110). This compound has high potency *in vitro* and was active in an animal model of inflammation(110). Although do not enzyme degrades, this mode of inhibition has shown promise, equilibrating efficacy and safety(98).

1.5. MPO as a pharmacological target

The inhibition of MPO is a promising approach to the development of a new class of anti-inflammatory agents(111,112). MPO activity is key in the pathogenesis of different inflammatory conditions(113), including multiple sclerosis(114), chronic obstructive pulmonary disease(115), multiple system atrophy(116), Parkinson disease(117), cardiovascular disease(118) and, recently, in the severe acute respiratory syndrome coronavirus 2 (SARS-CoV-2)(33).

MPO is also involved in gout disease. In this case, two complementary mechanisms occur, first urate crystals activate neutrophils and release MPO. Second, MPO oxidizes urate to urate free radical, contributing to tissue damage and inflammation(87,119). Supporting this data, the depletion of neutrophils in a murine model of gout induced by urate crystals decreased paw edema and MPO activity, indicating the strong pro-inflammatory component of these cells(68). In this context, the modulation of neutrophil enzymes as MPO emerges as promisor target to control the inflammatory process associated to gout, considering the MPO importance to neutrophil function(113).

Several preclinical studies have revealed the benefit of inhibiting MPO. In an atherosclerosis model, the inhibitor INV-315 decreased the volume of atherosclerotic plaque and improved endothelial function(120). Inhibition of MPO also protected against damage in a myocardial infarction model. The inhibitor PF-1355 attenuated ventricular dilatation and the inflammatory cell infiltrate(121). In an atrophy of multiple system model, a neuro-inflammatory disease, inhibition of MPO decreased motor impairment and alpha-synuclein aggregates(116). In another study, MPO

inhibition reduced the evolution of neuroinflammation and neurodegeneration, increasing animal survival by 70% in a multiple sclerosis-like model(122).

Although MPO inhibition presents a promising approach, this modulation is not free of side effects. In an animal model of *Klebsiella pneumonia* infection, MPO deficient mice were more susceptible to infection and death when compared to wild-type mice(123). In another study using *Salmonella*, MPO was important to induce an oxidative protection and for animal survival(124).

Corroborating these findings, the first MPO mutations detected in humans were associated with severe sepsis (125–127). In the contrary, a recent study indicated a prevalence of MPO deficiency one in 2000-4000 individuals and most of them were healthy(109). Although these recent studies encourage MPO inhibition as a safe strategy to treatment of inflammation conditions, protocols for detection of immunosuppressive effects must be performed in chronic pre-clinical and clinical studies.

Although a large number of MPO inhibitors have been studied, they usually fail in clinical tests. Currently, potent inhibitors from thioxanthines class are in clinical trials(128). However, serious toxic effects have already been reported for this pharmacological class, including inhibition of the synthesis of thyroid hormone, hepatotoxicity, pancytopenia, agranulocytosis and aplastic anemia(129–131). Inhibitors belonging to the tryptamine, hydroxamate, nitroxide, carboxylic acid, amine and quinone chemical classes exhibit metabolic instability and reactivity generating poor bioavailability and toxicity(101,132–135).

In this context, the search for new inhibitors with good pharmacokinetic and pharmacodynamic properties and low toxicity is necessary. and computational methods are an intelligent, time and resource saving strategy for the discovery of new bioactive compounds(136).

1.6. Computer-aided Drug Discovery Process

The drug discovery process is a risky investment from an economic point of view requiring budgets of up to 2.5 million dollars(137). Currently, around 90 % compounds are reprovved during drug discovery process despite the fact that the research and development (R&D) has grown due to technology in both academia and industry (138).

The drug discovery process can be summarized in four phases, development, preclinic, clinic and approval(139). The development phase includes target identification, target validation, target assay construction and hit/lead optimization. The cost is estimated in \$1 to 4 million. In preclinical

phase, the drug candidate is tested for pharmacokinetic, efficacy and safety, using several animal species, with an estimated cost of \$ 12-15 million.

After preclinical phase, the candidates are subjected to four phases of clinical trials(140), called Phase I, II, III and IV(139). Phase I is composed by a low number of healthy individuals (< 20) and the main objective is to obtain data on safety, tolerability and dose adjustment(141). Phase II, uses a greater number of individuals that carry the disease to what the candidate has been planned for. The candidates are tested for effectiveness dose-response and toxicity. Phase III has the same purpose as phase II but it is a larger trial to confirm the effectiveness and safety of the drug candidate(141). The last study, Phase IV, aims to assess the drug's effectiveness in the real world. This phase can also assess potential rare risks in a post-marketing surveillance (PMS) study(142). Clinical trials are the most expensive among all the studies. Phases I, II, and III cost around \$ 3.4, 8.6, and 21.4 million, respectively(143).

In this expensive, slow and complex process, computational chemistry emerges to support the drug development process mainly in the early stages of discovery and development(136). Virtual screening has been shown to be a useful tool, accelerating the identification of hits and promoting collaborations in modern drug discovery process(144).

Virtual screening methods can be classified in ligand-based drug design (LBDD) and structure-based drug design (SBDD)(145). In absence of a target structure, LBDD methods focus on structural information from known active compounds to design new scaffolds with optimized properties or even compounds with greater chemical diversity but retaining privileged structural or electronic characteristics. Within LBDD are methods based on 2D, 3D similarity, pharmacophoric research and QSAR (quantitative structure-activity relationship)(146).

In the SBDD approach, knowledge of the target structure allows the design of ligands with optimized stereochemical characteristics to interact with the receptor(145). The target structure can be obtained by crystallography, 3D electron microscopy, nuclear magnetic resonance (NMR) or homology modelling(147,148). Molecular docking and molecular dynamics are part of these methods(149). SBDD methods are expected to expand greatly with the development of AlphaFold2, a sophisticated 3D prediction algorithm that can achieve atomic resolution in some cases(150). Furthermore, machine learning methods are being successfully applied in the drug development process(151,152).

Another strategy widely used in virtual screening protocols includes the use of ADME filters for the pre-selection of molecules with promising characteristics for **Administration, Distribution, Metabolization and Excretion**(153). The most used filters are those preconized by Lipinski and Veber. Lipinski filter, also known as rule-of-five, was developed to analyze the potential bioavailability in humans, predicting poor bioavailability for compounds with more than 10 hydrogen bond acceptors, 5 hydrogen bond donors, a Log P greater than 5 and a molecular weight greater than 500 Da(154).

Interestingly in Veber rule, that uses bioavailability data obtained in rats, the number of hydrogen bond donors and acceptors has been confirmed as a good predictor for oral bioavailability. However, the other Lipinski parameters were proved to be poor predictors (155). The best capability to predict was found by Veber when the compounds presented a polar surface area (TPSA) up to 140 \AA^2 and rotatable bonds count less than 7.

Although Lipinski's and Veber's rules are still widely used, recent studies have suggested an update in some parameters. For instance, the increase in molecular weight maximum to 600 Da, the number of hydrogen bond acceptors to 12 and the rotatable bonds count to 14(156). Interestingly, the values of the clogP and TPSA parameters are still the same predicted by Lipinski and Veber(154–156).

ADME filters have been used with success in the search of MPO inhibitors. The first virtual screening workflow to discover MPO inhibitors integrated physicochemical filters, pharmacophoric search and molecular docking. This studied obtained a high hit rate but a low chemical diversity(157). In a subsequent study, the application of successive molecular docking steps proved limit success rate. However, it has reached high chemical diversity(158).

Recently, a virtual screening methodology using numerous pharmacophores and molecular docking showed high success rates. However, close inspection revealed a high number of analogs and known inhibitors(159). In addition, **High-Throughput Screen (HTS)** was also used for the search of new MPO inhibitors. The experimental evaluation of 124,000 compounds led to the discovery of a potent MPO inhibitor, although the hit rate was well below 1%, beside to the high cost associated with HTS methods(160,161).

Although several efforts have culminated in the discovery of hundreds of MPO inhibitors, none of these compounds or their derivatives have been approved by regulatory agencies worldwide. In this context, computational methods to discover new putative therapeutic agents

against inflammation are still needed. Taking this into account, this thesis reports a new virtual screening methodology that has recovered several compounds that inhibited HOCl production by purified MPO and on cells. The compounds are also active in a mice model of gout arthritis. As a direct result from this thesis, a paper containing details on the screening method has been published (doi.org/10.1021/acs.jcim.0c00813 – first chapter in this thesis) and a patent has been deposited INPI (BR102021021677-8, appendix in this thesis).

CHAPTER I

Integration of an Inhibitor-like Rule and Structure-based Virtual Screening for the Discovery of Novel Myeloperoxidase Inhibitors

Isaac de Araújo Matos,* Nivan Bezerra da Costa Júnior, and Flavia Carla Meotti*


 Cite This: *J. Chem. Inf. Model.* 2020, 60, 6408–6418


Read Online

ACCESS |



Metrics & More

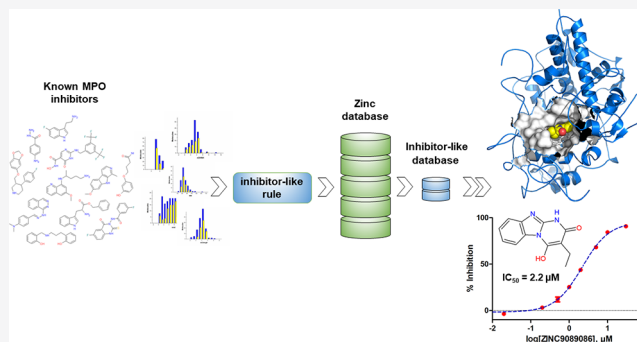


Article Recommendations



Supporting Information

ABSTRACT: Myeloperoxidase (MPO) is an attractive therapeutic target against inflammation. Herein, we developed an inhibitor-like rule, based on known MPO inhibitors, and generated a target database containing 6546 molecules with privileged inhibitory properties. Using a structure-based approach validated by decoys, robust statistical metrics, redocking, and cross-docking, we selected 10 putative MPO inhibitors with high chemical diversity. At 20 μM , six of these 10 compounds (*i.e.*, 60% success rate) inhibited more than 20% of the chlorinating activity of the enzyme. Additionally, we found that compound ZINC9089086 forms hydrogen bonds with Arg233 and with the hemic carboxylate. It makes a π -stacking interaction with the heme group and displays a high affinity for the enzyme active site. When incubated with purified MPO, ZINC9089086 inhibited the chlorinating activity of the enzyme with an IC_{50} of $2.2 \pm 0.1 \mu\text{M}$ in a reversible manner. Subsequent experiments revealed that ZINC9089086 inhibited hypochlorous acid production in dHL-60 cells and human neutrophils. Furthermore, the theoretical ADME/Tox profile indicated that this compound exhibits low toxicity risks and adequate pharmacokinetic parameters, thus making ZINC9089086 a very promising candidate for preclinical anti-inflammatory studies. Overall, our study shows that integrating an inhibitor-like rule with a validated structure-based methodology is an excellent approach for improving the success rate and molecular diversity of novel MPO inhibitors with good pharmacokinetics and toxicological profiles. By combining these tools, it was possible to increase the assurance rate, which ultimately diminishes the costs and time needed for the acquisition, synthesis, and evaluation of new compounds.



INTRODUCTION

Neutrophils are the most abundant leukocyte cells in the blood and represent the first line of defense against microbes.¹ The cytoplasm of neutrophils contains many azurophilic granules, which harbor large amounts of the heme-containing enzyme myeloperoxidase (MPO) (E.C. 1.11.1.7). In human neutrophils, MPO represents more than 5% of the total protein.²

It is well known that after microbe ingestion and complete phagosome formation, MPO reacts with hydrogen peroxide and is converted to the highly reactive intermediate compound I. This species can oxidize halide ions such as chloride, iodide, and bromide, as well as the pseudohalide thiocyanate to generate hypochlorous, hypiodous, hypobromous, and hypothiocyanous acids, respectively.³ While the production of these oxidants is essential for the killing activity of the neutrophils, this aggressive response can cause tissue damage and exacerbate inflammation, thus hindering the resolution of the insult.

In this sense, MPO contributes to many chronic inflammatory conditions, including cardiovascular disease.^{4–8} For example, it has been shown that this enzyme promotes fibrosis and increases the vulnerability to atrial fibrillation during myocardial infarction.^{5,8} Additionally, the chlorinating

activity of MPO can oxidize apoA-I, which impairs cholesterol efflux from the cell and is intimately associated with high-density lipoprotein dysfunction.⁷ The pathogenesis of neurodegenerative diseases, including Parkinson's,⁹ multiple sclerosis,¹⁰ and multiple system atrophy,¹¹ as well as rheumatoid arthritis,¹² chronic obstructive pulmonary disease,¹³ and systemic organ failure¹⁴ have also been associated with MPO. Furthermore, the emerging disease COVID-19 produces an inflammatory response, during the severe acute respiratory syndrome phase, which is associated with significant pulmonary neutrophilic infiltrate and elevated levels of circulating MPO.^{15,16}

Because of the prominent role of MPO in a variety of diseases and conditions, previous studies have investigated the effects of knocking out or inhibiting MPO and showed that

Received: July 17, 2020

Published: December 3, 2020



attenuating the activity of this enzyme provides protective effects in inflammatory models.^{5,8,9,11–13,17} In this sense, MPO appears to be a promising target for novel therapeutic agents that could be used to treat inflammatory and chronic diseases.^{18–20}

Currently, a diverse chemical class of MPO inhibitors exists. Initially, hydroxamates and hydrazides were the first MPO inhibitors reported.^{21–23} Later, other chemical classes were identified, including polyphenols, indoles, antimalarials, benzodioxols, tryptamines, nitroxides, naphthalenes, thiouracils, and thioxanthines.¹⁹ However, all of these prospective MPO inhibitors have failed clinical trials, and the regulatory agencies have approved none. Therefore, the search for new inhibitors with higher potency, bioavailability, and specificity is particularly relevant.²⁴

Several computational strategies have been employed to identify new MPO inhibitors. The first virtual screening methodology was developed by Malvezzi *et al.*²⁵ and used a ligand and structure-based approach with the GOLD docking program and one pharmacophore model. This methodology exhibited a high success rate but low chemical diversity because all fitted inhibitors were hydrazides. A short time later, using only the molecular docking software Glide, Aldib *et al.*²⁶ recovered a set of MPO inhibitors with a diverse number of new scaffolds but with a low success rate. More recently, Soubhye *et al.*²⁷ achieved the best success rate, using several pharmacophore models and the FlexX docking program. However, a more detailed analysis of active compounds revealed many analogues and previously reported inhibitors.¹⁹

In this context, we analyzed the molecular properties of 143 previously published MPO inhibitors and generated an inhibitor-like profile for creating an enriched target database. We then applied a validated virtual screening methodology to this library, followed by molecular docking with the GOLD and AutoDock programs. Computational hits were selected based on their stereospecificity to the active site, which included analyzing the number of hydrogen bonds, binding energy, and clustering histogram profile. We then validated the hits by assessing the inhibition of MPO chlorinating activity *in vitro*. Based on these results, the IC₅₀ of each compound was calculated. The reversibility of inhibition was evaluated using a dilution method, and the inhibition of chlorinating activity was also tested in dHL-60 cells and peripheral blood neutrophils. The present study demonstrated that integrating an inhibitor-like rule and a validated structure-based methodology is an excellent approach for discovering enzyme inhibitors. In this case, by improving the success rate and molecular diversity of the drug candidates, we identified several novel and potent MPO inhibitors.

MATERIALS AND METHODS

MPO Inhibitor-like Rule Design. A set of 143 previously reported MPO inhibitors^{19,21–23,25–45} was used to characterize the chemical space of these inhibitors and generate the inhibitor-like rule. Molecular properties including molecular mass (MM), rotatable bond count (RBC), topological polar surface area (TPSA), hydrogen bond donor (OH, NH), and acceptor (O, N) numbers were calculated by Molinspiration (www.molinspiration.com). The octanol–water partition coefficient (log *P*) was estimated by ChemSketch (<https://www.acdlabs.com/>).

Receptor Structure Preparation. Three MPO crystal structures (PDB IDs 1CXP,⁴⁶ 4C1M,⁴⁵ and SWDJ⁴⁷) were

used for all molecular docking studies. The protein structures were edited using the CAChe WorkSpace software⁴⁸ where all ligands and water molecules were removed and hydrogen atoms added. Flexible amino acids were identified by superpositioning the following MPO PDB IDs: 1DNU, 1DNW, 1MHL, 3F9P, 3ZS0, 3ZS1, 4C1M, 4DL1, 5FIW, 1CXP, 1D2V, 1D5L and 1D7W. Because the conformations and tautomeric forms of some residues in the MPO crystals are incompatible with the catalytic mechanism of the enzyme, we performed some adjustments to make them compatible with MPO catalytic properties. For example, the distal histidine (His95) in the native enzyme exhibits an uncharged N^π tautomeric form that is essential for coordination with hydrogen peroxide.⁴⁹ Additionally, resonance Raman spectroscopy and molecular dynamic simulations demonstrated that the ionization of imidazole to imidazolate in the proximal histidine (His336) maximizes hydrogen bonds and changes the orientation of Asn421.^{50,51}

Calculation of Heme Group Charges. In the docking studies with AutoDock 4.2.3, the iron and nearby atom charges were calculated with MOPAC2016⁵² software, using the keywords PRECISE, UHF, MS=2.5, CHARGE=1, METAL=(FE(+3)), PDBOUT, PL, GRADIENTS, NOOPT OPT-H, and XYZ. The Hamiltonians PM6, PM6-D3, PM6-D3H4, PM6-D3H4X, PM6-DH+, PM6-DH2, PM6-DH2X, and PM7 were also evaluated. For this calculation, the active site was represented by the heme group and the following amino acids: Asn421, Arg424, Arg333, His336, Glu242, Met243, Asp94, Asp98, Phe99, and Thr100.

Molecular Docking Simulation. The molecular docking simulations were performed with the programs AutoDock 4.2.3, AutoDock Vina 1.1.2, and GOLD 5.4. During the simulations, the protein was kept rigid, and the ligands were flexible. In the simulations with AutoDock Vina, nonpolar hydrogens were merged, and Gasteiger charges were added. The grid box was 36 × 40 × 40 Å in size, with a lattice point distance of 0.375 Å, and was centralized in the coordinates 24.123 × 3.191 × 43.257. Each docking simulation consisted of 100 runs, and the Lamarckian Genetic algorithm was selected as the optimization method.

For the docking studies using GOLD 5.4, the radius of the simulation was set to 10 Å, the ASP, ChemPLP, GoldScore, and ChemScore scoring functions were tested, and the efficiency parameter was set at 30%. All of the other parameters were set to the default values.

Following the molecular docking simulations, the results were validated by cross-docking. For this, the crystal conformation of the hydroxamate ligand (HX1) in PDB ID 4C1M and the triazole analogue in PDB ID SWDJ were aligned to the redocked pose of PDB ID 1CXP, and VMD⁵³ was used to calculate the RMSD distances between the ligand atoms.

Virtual Screening Validation. To validate the different structure-based virtual screening methodologies, we used the DUD-E server⁵⁴ to generate a set of 456 decoys from 24 known MPO inhibitors (Table S1). The statistical metrics, area under the receiver operating characteristic curve (AUC), enrichment factor (EF), robust initial enhancement (RIE), and Boltzmann-enhanced discrimination of receiver operating characteristic (BEDROC),⁵⁵ were calculated using Rv3.3.2 (www.r-project.org) and RStudio1.0.1.3.6 (www.rstudio.com) software.

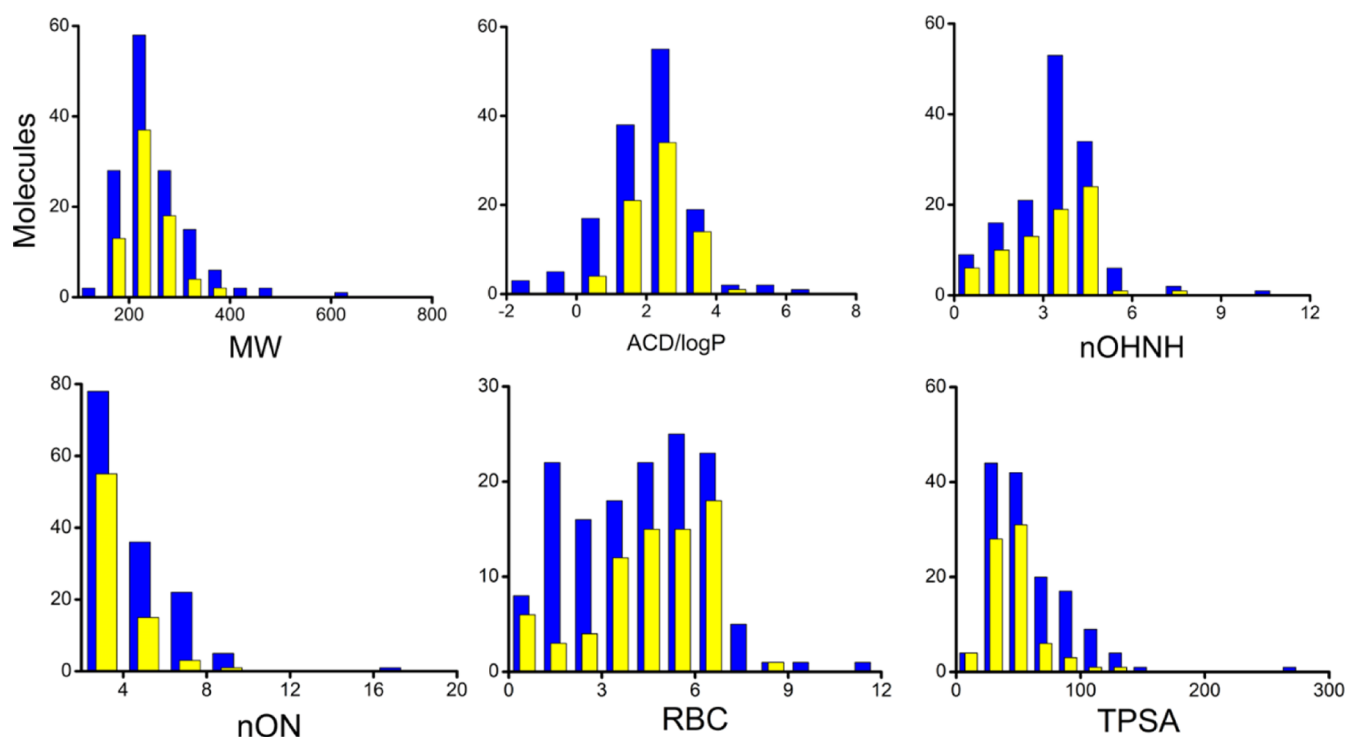


Figure 1. Molecular property frequency distribution for 143 known MPO inhibitors. The blue bars represent the frequency distribution considering all of the inhibitors, and the yellow bars represent the inhibitors with IC_{50} values lower than 500 nM. Abbreviations: MW—molecular weight, ACD/log P —octanol/water partition coefficient, $nOHNH$ —hydrogen donor number, nON —hydrogen acceptor number, RBC—rotatable bond count, and TPSA—topological polar surface area.

MPO Inhibition Assay. The compounds selected by virtual screening were experimentally validated by measuring MPO-mediated chlorination activity. The reaction mixture included, MPO (10 nM), 140 mM NaCl, 5 mM taurine, 0.03% cetyltrimethylammonium chloride (CTAC), 0.1 mM diethylenetriaminepentaacetic acid (DTPA), 20 mM phosphate buffer pH 7.4, and the compound to be tested (20 μ M). All of these components were incubated for 15 min at 37 $^{\circ}$ C, and then, the reaction was initiated by adding 40 μ M H_2O_2 . After 8 min, the reaction was stopped with 20 μ g/mL catalase. Taurine chloramine was quantified by monitoring the oxidation of TMB (3,3',5,5'-tetramethylbenzidine) by iodide. For this assay, 240 μ L of the above reaction mixture was mixed with 60 μ L of 2 mM TMB containing 10% dimethylformamide and 100 μ M KI in 400 mM acetate buffer (pH 5.4).⁵⁶ After 8 min, the absorbance at 650 nm was measured in a microplate reader. The degree of inhibition was based on the activity of the control sample, which contained 0.3% DMSO (vehicle). The concentration that inhibited 50% of the enzyme activity (IC_{50}) was determined using eight different concentrations of each compound, and the curves were fit using nonlinear regression with the GraphPad Prism 5 software.

Theoretical ADME/Tox Study. The following theoretical pharmacokinetic parameters, namely, gastrointestinal absorption, oral bioavailability, blood–brain barrier (BBB) permeation, and the P-glycoprotein substrate of the active compounds were calculated by SwissADME (<http://www.swissadme.ch/>). Cardiotoxicity was measured by the risk of the h-ERG channel block using the Pred-hERG 4.3 server (<http://predherg.labmol.com.br/>). The toxicological potential, including the risk of carcinogenicity, cytotoxicity, hepatotoxicity, immunotoxicity, and acute toxicity, was calculated using ProTox-II (http://tox.charite.de/prottox_II/).

Cell Culture. Human promyelocytic leukemic cells (HL-60) (BCRJ, RJ, Brazil) were grown in RPMI 1640 medium with bovine fetal serum (20%) and penicillin (100 U/mL) in a humidified atmosphere of 5% CO_2 at 37 $^{\circ}$ C. To differentiate the HL-60 cells into dHL-60 cells, dimethyl sulfoxide (1.25%) was added to the above growth media, and the cells were incubated for 4 days.⁵⁷

Human Neutrophil Isolation. Peripheral blood neutrophils were isolated from the blood of healthy volunteers (ethical committee approval CEPISH-ICB 1435/18) by centrifugation over a histopaque and dextran gradient, sedimentation, and hypotonic lysis of the red blood cells.⁵⁸

Hypochlorous Acid Production in Cells. Before measuring hypochlorous acid production, the dHL-60 cells and human neutrophils were centrifuged at 1400 rpm for 10 min, washed with sterile saline and suspended in PBS glucose (10 mM Na_2HPO_4 , 2 mM KH_2PO_4 , 140 mM NaCl, 1 mM $CaCl_2$, 0.5 mM $MgCl_2$, and 1 g/L glucose). Then, the cells (1×10^6) were activated with 100 nM phorbol myristate acetate (PMA) and the rate of superoxide production, based on the reduction of cytochrome c ($\lambda_{550nm} = 21,000 M^{-1} cm^{-1}$), was calculated to verify the oxidative burst. Hypochlorous acid was quantified using the same TMB method described above.⁵⁶ In brief, the dHL-60 or human neutrophils (1×10^6) were incubated in PBS glucose containing 0.1 mM DTPA, 5 mM taurine, 20 μ M test compounds, and 100 nM PMA for 1 h at 37 $^{\circ}$ C. Control cells were incubated with 0.3% DMSO. Samples were centrifuged at 1400 rpm by 10 min, an aliquot of the supernatant was diluted (threefold) in the same buffer, and 240 μ L of this mixture was incubated with 60 μ L 0.4 M acetate buffer pH 5.4 containing 0.1 mM NaI and 2 mM TMB dissolved into 10% dimethylformamide (DMF). The absorbance at 655 nm was used to monitor the oxidation of TMB.

Reversibility Test. The compounds (20 μM) were incubated with 100 nM MPO in 20 mM phosphate buffer pH 7.4 containing 0.03% CTAC at 37 °C for 30 min. The reaction was initiated by adding 40 μM hydrogen peroxide. Then, an aliquot was diluted 200-fold in acetate buffer 0.2 M pH 5.4 containing 2 mM TMB (10% DMF), and residual peroxidase activity was measured by monitoring TMB oxidation at 655 nm after a new addition of 40 μM hydrogen peroxide.⁵⁹

RESULTS AND DISCUSSION

MPO Inhibitor-like Rule. Initially, we analyzed a set of 143 known MPO inhibitors to verify the frequency distribution of critical molecular properties related to oral bioavailability and toxicity. As shown in Figure 1, the most potent compounds (*i.e.*, $\text{IC}_{50} \leq 500$ nM, yellow bars) have a similar distribution profile when compared to all of the inhibitors (blue bars). It is important to note that most of the selected MPO inhibitors to construct the MPO inhibitor-like rule were not discovered by methodologies that included bioavailability filters.^{19,21–23,25–45}

Moreover, when analyzing all of the compounds together, the frequency distribution indicated limited oral bioavailability, according to the Lipinski and Veber rules^{60,61} (Table 1). On

Table 1. Molecular Properties of MPO Inhibitors^a

rules	properties	range	
		all	most potent
Lipinski	molecular weight (≤ 500)	136–610 (no)	174–396 (yes)
Lipinski	ACD/log P (≤ 5)	–1,59–6,26 (no)	0,1–4,37 (yes)
Lipinski	$n\text{OHNH}$ (≤ 5)	0–10 (no)	0–7 (no)
Lipinski	$n\text{ON}$ (≤ 10)	2–16 (no)	2–9 (yes)
Veber	RBC (≤ 10)	0–11 (no)	0–8 (yes)
Veber	TPSA ($\leq 140 \text{ \AA}^2$)	18–269 (no)	18–122 (yes)

^aAbbreviations: ACD/log P —octanol/water partition coefficient, $n\text{OHNH}$ (hydrogen bond donor), $n\text{ON}$ (hydrogen bond acceptor), RBC (rotatable bond count), and TPSA (topological polar surface area).

the other hand, when the most potent inhibitors ($\text{IC}_{50} \leq 500$ nM) were grouped separately, they obeyed the Lipinski and Veber rules, except when the $n\text{OHNH}$ property was analyzed (Table 1).

These results demonstrate a good overlap between the high potency and oral bioavailability chemical spaces, a requirement when searching for new orally active inhibitors. Additionally, the most potent compounds exhibit lower log P and higher TPSA values, indicating lower toxicity⁶² and a higher therapeutic window for this subset.

Analysis of the descriptor values indicated that Lipinski and Veber rules have only the upper limit.^{60,61} Comparing these values with the upper and lower limits of the MPO inhibitor-like rule (Table 1), it is possible to note that the MPO inhibitor-like rule is a subspace into Lipinski and Veber chemical spaces but with a small outside zone (OH/NH) (Figure 2).

The virtual screening workflow employed herein is outlined in Figure 3. Using the Zinc 12 database (<http://zinc.docking.org>), which contains more than 35 million compounds, we applied the MPO inhibitor-like rule to search for compounds

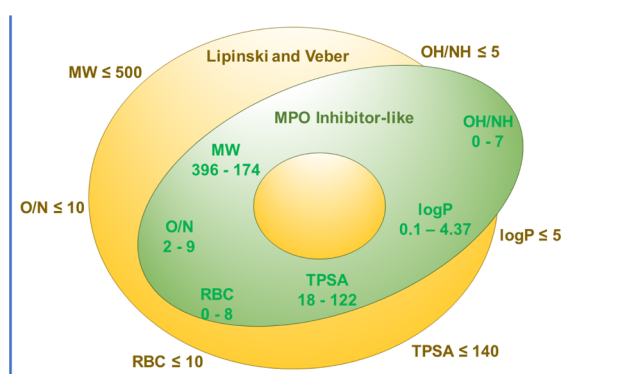


Figure 2. 2D representation of the Lipinski/Veber (orange) and MPO inhibitor-like (green) chemical spaces. MW—molecular weight, ACD/log P —octanol/water partition coefficient, $n\text{OHNH}$ —hydrogen donor number, $n\text{ON}$ —hydrogen acceptor number, RBC—rotatable bond count, and TPSA—topological polar surface area.

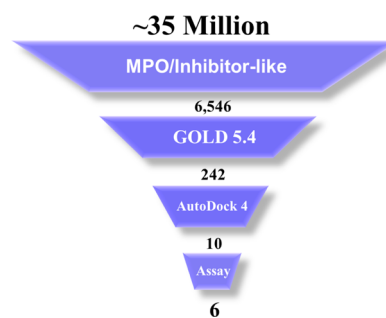


Figure 3. Virtual screening workflow for the identification of new MPO inhibitors using the inhibitor-like rule and molecular docking approach.

exhibiting inhibitory properties and oral bioavailability. This filtering approach yielded 6546 potential ligands.

Structure-based Step One. Prior to the molecular docking simulations, we overlaid the MPO crystal structures to detect flexible amino acids. The resultant superposition of the structures showed that the Glu116, Asp218, and Met411 side chains are flexible but distant from the active site (Figure S1). Based on these observations, we opted to configure MPO as a rigid body during the simulations.

Next, we tested and validated the molecular docking protocols for the structure-based virtual screening, using decoys, redocking, and cross-docking approaches with three crystallographic structures of MPO (PDB IDs 1CXP,⁴⁶ 4C1M,⁴⁵ and SWDJ⁴⁷). To validate the GOLD 5.4 and AutoDockVina programs, 456 decoys from 24 MPO inhibitors were generated (Table S1). According to Mysinger (2012),⁵⁴ because of the high number of available search algorithms and score functions, it is important to evaluate the performance of these programs statistically.⁵⁴ For this purpose, we assessed the following four statistical metrics: the area under the curve ROC (AUC-ROC), BEDROC, RIE, and EF.

AUC-ROC values, an indicator of capacity to distinguish between inhibitors and noninhibitors,⁵⁵ were highly similar among five methodologies, but ASP and CHEMPLP had significantly higher values (Figure 4A). Similarly, the RIE (Figure 4B) and BEDROC (Figure 4C) values for ASP and CHEMPLP also significantly increased when compared to ChemScore, GoldScore, and AutoDockVina, which were determined to have a low performance. Furthermore, these

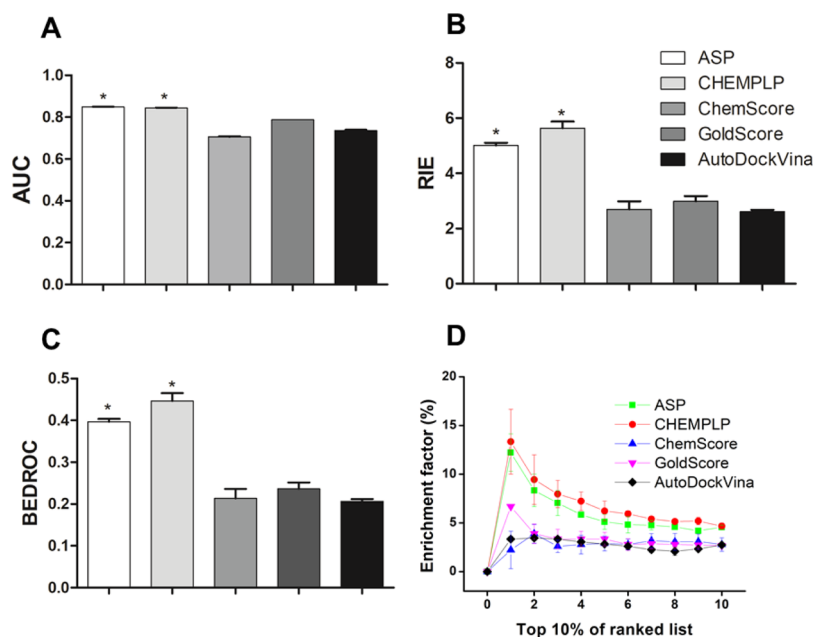


Figure 4. Statistical metrics used to validate virtual screening protocols. (A) AUC, (B) RIE, (C) BEDROC, and (D) EF. Data are presented as the mean \pm S.E.M of three independent simulations. The results were statistically analyzed using one-way ANOVA, followed by the Bonferroni posthoc test. The asterisk (*) represents a statistical difference ($p < 0.05$) when compared to the ChemScore, GoldScore, or AutoDockVina groups.

two methods exhibited elevated EF values (Figure 4D). These results demonstrate that ASP and CHEMPLP performed the best in terms of early MPO inhibitor recognition. Thus, the ASP and CHEMPLP score functions were selected for the structure-based virtual screening.

Interestingly, a previous study searching for β -glucuronidase inhibitors reported that ASP performed the worst in recovering inhibitors, whereas ChemScore was the best.⁶³ These data suggest that the performance of the molecular docking program and its score function is dependent on the target enzyme, thus, reinforcing the underlying importance of validating each program before starting a virtual methodology. Implementing this validation step will undoubtedly improve the probability of discovering novel inhibitors.

Herein, the GOLD 5.4 molecular docking simulations, in a fast screening mode, effectively reduced the previously identified 6546 MPO inhibitor candidates to 242 (Figure 3). In this selection, the molecular binding mode of the 50% top compounds (3273) was analyzed by visual inspection, taking their stereochemical complementarity into account. The latter was analyzed through binding energy, the number of hydrogen bonds, number of π -stacking interactions, and docking histogram profile.

Structure-based Step Two. To improve the accuracy of our approach and confirm the conformations of the docked ligands, we added a new molecular docking step, using the AutoDock 4 program, to the structure-based virtual screening method. In this case, hemic atom charges were calculated using different semiempirical Hamiltonians (see Methods) in the MOPAC package. As summarized in Table 2, some of the added charges improved the redocking simulation of the HX1 ligand into the PDB ID 4C1M structure. For example, the semiempirical Hamiltonian PM7 iron charge produced the structure with the best RMSD (1.04 Å) for both the most populous and the lowest energy cluster. Additionally, the PM7 iron charge presented a high population in both clusters. It is plausible that the PM7 method enhances the description of

Table 2. Cluster Data of Hydroxamate HX1 in Redocking Simulation using Different Semiempirical Charges in MPO Structure PDB ID 4C1M

method	RMSD (Å) of the most populous cluster/ population	RMSD (Å) of the lowest energy cluster/ population	total cluster number
Gasteiger	1.19 (57)	1.19 (57)	12
PM6	1.07 (60)	1.07 (60)	13
PM6-D3	1.07 (65)	1.07 (65)	9
PM6-D3H4	1.13 (69)	1.13 (69)	9
PM6-D3H4X	1.20 (64)	1.20 (64)	9
PM6-DH+	1.19 (61)	1.19 (61)	13
PM6-DH2	1.32 (62)	3.23 (20)	8
PM6-DH2X	1.22 (57)	3.41 (17)	15
PM7	1.04 (69)	1.04 (69)	11

noncovalent interactions present in this Hamiltonian, which are important for intermolecular interactions.⁶⁴

For the cross-docking validation, HX1 and a triazole analogue, the MPO ligands present in crystal structures of PDB IDs 4C1M and SWDJ, respectively, were docked to the MPO crystal structure PDB ID 1CXP using the AutoDock 4 program (Figure 5). The RMSD values of MPO cross-docked with HX1 and the triazole analogue were 1.09 and 0.75 Å, respectively. Because these values were less than 2 Å, the molecular docking protocol was validated.⁶⁵

With the AutoDock validated protocol, the 242 previously identified compounds were docked to MPO (PDB ID 1CXP). Using the same criteria described for the previous selection (6546 to 242 candidates) and also selecting a chemical diverse group (by removing replicates), all 242 molecular docking complexes were analyzed and the top 10 potential MPO inhibitors were purchased to test upon the enzyme activity (Figure 3).

Noteworthy, some chemical classes previously reported as MPO inhibitors were also recovered in the virtual screening methodology presented here (data not shown). These

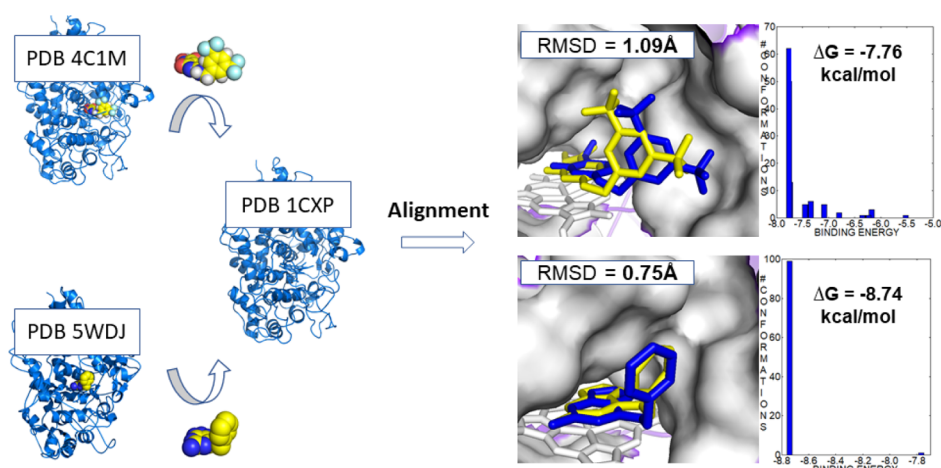


Figure 5. Molecular docking validation. Crystallographic ligands HX1 (PDB ID 4C1M, upper panel) and triazole analogue (PDB ID SWDJ, lower panel) were cross-docked into the PDB 1CXP structure. The RMSD values were calculated between docked (blue) and crystallographic pose (yellow). The respective clustering histograms and binding energies are displayed in the panels to the right of the active site images.

included flavonoids,³⁰ hydrazines,²¹ and hydroxamates.⁴⁵ Additionally, the methodology selected an identical guanidine quinazoline and derivatives previously reported as irreversible MPO inhibitors.²⁷ Because the inhibitory effect of these compounds upon MPO has already been established, they were not included for testing against the enzyme as it would overestimate the success rate of the virtual screening methodology. The recent described MPO inhibitors aminopyridines and a new indole scaffold matched with the MPO inhibitor-like profile in all parameters (Table S2),^{66,67} despite the fact that they were not included in the MPO inhibitor-like rule elaboration. Together, these data corroborate the accuracy of the MPO inhibitor-like rule to discover new MPO inhibitors.

Hit Validation and Characterization. The 10 identified compounds were subsequently acquired from Specs (Zoetermeer, Netherlands), and the structure and purity of each were confirmed by mass spectrometry. Then, an MPO chlorination assay⁵⁶ was employed to evaluate the inhibitory action of these compounds. When applied at 20 μM , six of the 10 compounds inhibited MPO-related chlorination by greater than 20% (range 20–74%) when compared to control (vehicle) samples (Table 3). The inhibition exhibited by the other four compounds ranged between 0–8% (Table 3). These results were interpreted as a success rate of 60%. The compounds presented high chemical diversity, and none have been previously reported as MPO inhibitors. Four of the inhibitors have a benzimidazole ring similar to the indole present in many known MPO inhibitors.^{33,39,68} Notably, compound ZINC9089086 inhibited MPO chlorination activity by more than 70% at 20 μM , and the dose–response curve indicated an IC_{50} of $2.2 \pm 0.1 \mu\text{M}$ (Figure S2).

The compounds that failed to inhibit MPO-mediated chlorination were ZINC208265, ZINC4134843, ZINC19796886, and ZINC4450397 (Table 3). It should be pointed out that the absence of inhibition by ZINC208265 and ZINC4134843 was unexpected because these compounds contain a benzodioxole and a purine fragment, respectively, which are present in well-known, previously described MPO inhibitors.^{41,69} The absence of inhibition by these two compounds revealed that other properties, that were not included in the molecular docking simulations (e.g., the redox potential) and potentially modified depending on the global

Table 3. List of the 10 Compounds Selected for the MPO Chlorinating Assay and the Respective Zinc Codes, Specs Codes, Structures, Binding Energies, and Inhibitory Activities

Zinc code	Specs Code	Structure	Binding energy (kcal/mol)	Inhibition at 20 μM (%)
9089086	AI-204/31685032		-8.31	74 \pm 15
99474	AK-968/41705263		-9.35	60 \pm 10
660255	AM-807/13614268		-8.57	51 \pm 5.0
478529	AH-262/34342005		-7.31	48 \pm 1.0
13466360	AH-262/32490010		-6.29	40 \pm 1.0
4471880	AH-034/04864059		-7.18	20 \pm 1.0
208265	AH-034/11650405		-9.07	8.0 \pm 8.0
4134843	AG-690/40721604		-8.47	0.0 \pm 8.0
19796886	AO-476/43407309		-8.77	1.0 \pm 2.0
4450397	AM-807/41928974		-8.78	3.0 \pm 1.0

compound structure, are also important to confer MPO inhibition.³⁹

Table 4. Theoretical ADME/Tox Profiles of Active Compounds

zinc code	pharmacokinetics				toxicity					LD ₅₀ mg/kg
	GI absorption	bioavailability score	BBB permeant	P-gp substrate	hERG inhibitor	carcinogenicity	cytotoxicity	hepatotoxicity	immunotoxicity	
9089086	high	0.56 ^a	yes	no	no	no	no	no	no	300
99474	high	0.55 ^a	yes	yes	yes	no	no	no	yes	595
660255	high	0.55 ^a	no	no	yes	no	no	yes	no	900
478529	high	0.55 ^a	yes	yes	yes	yes	no	no	no	374
13466360	high	0.55 ^a	no	no	no	yes	no	no	no	348
4471880	high	0.55 ^a	yes	no	no	no	no	yes	no	4617

^aProbability of $F > 10\%$ in rat; GI—gastrointestinal; BBB—brain–blood barrier; P-gp—glycoprotein-P; hERG—human ether-a-go-go-related gene.

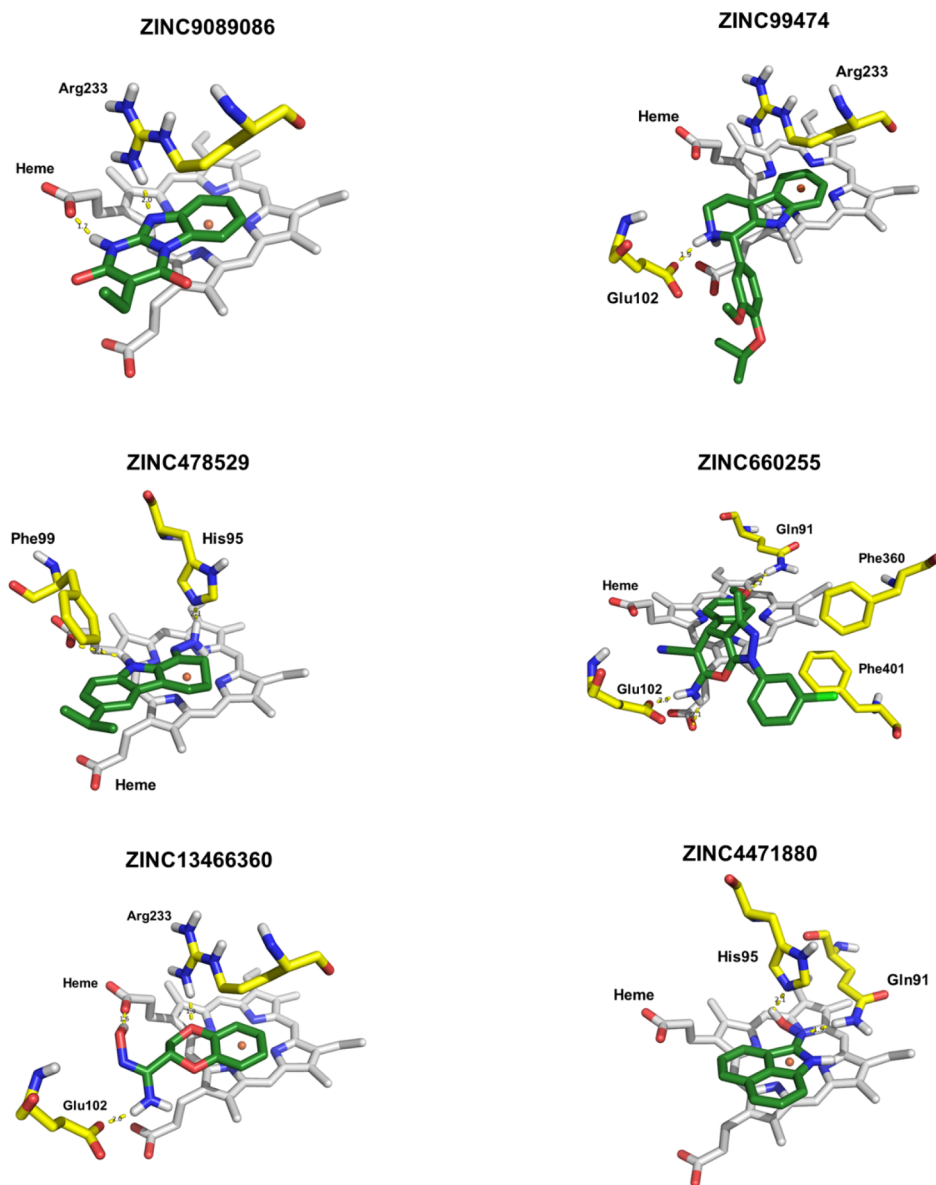


Figure 6. Molecular docking of active compounds into MPO active site. Inhibitors are shown in green, heme group in grey, and amino acids and hydrogen bonds in yellow.

ADME/Tox Profile. The analysis of the pharmacokinetic parameters gastrointestinal absorption, bioavailability score, and P-gp (Glycoprotein-P) substrate revealed that all of the active compounds have a high probability of gastrointestinal absorption and oral bioavailability (Table 4). Moreover, these

results provide further evidence that applying an inhibitor-like filter in the virtual screening workflow facilitates the recovery of compounds with privileged molecular characteristics for oral administration. Surprisingly, we identified three inhibitors (ZINC 9089086, ZINC99474, and ZINC478529) that were

BBB-permeable, even though no filter for BBB penetration was applied (Figure 3). This observation is particularly relevant because it was previously reported that BBB-permeable MPO inhibitors could treat neuroinflammatory diseases.⁷⁰

Additionally, the ADME/Tox profile showed that around 20% of the compounds exhibit toxicological risks, except to cardiotoxicity, where 50% of the compounds likely inhibit hERG. However, the selected compounds present low acute toxicity, as evidenced by LD₅₀ values above 300 mg/kg. Notably, the integrative analysis of these pharmacokinetic parameters showed that ZINC9089086, the most potent MPO inhibitor, show reduced calculated toxicity risks. Therefore, this compound was considered the best candidate for optimizing and testing the inflammatory model.

Importantly, the molecular docking histograms show a clear predominance of a single cluster for five of the six active compounds (Figure S3). The compound ZINC660255 exhibited two distinct binding modes. The lower energy conformation (less populous) was selected for presenting more hydrogen bonds (data not shown). The compounds ZINC9089086, ZINC99474, and ZINC660255 exhibited lower binding energies (Table 3) than the cocrystallized HX1 ligand (Figure 5), and compound ZINC99474 had a lower binding energy than the cocrystallized triazole (Figure 5).

The molecular docking simulations showed that the most potent inhibitor, ZINC9089086, forms hydrogen bonds with Arg233 and the hemic carboxylate. Moreover, this compound makes a π -stacking interaction between its benzimidazole ring and the hemic pyrrole (Figure 6). Compound ZINC99474 presents a similar stacking indole orientation and forms one salt bridge with the hemic carboxylate. Compound ZINC660255 makes one hydrogen bond with Glu102 and another with Gln91 and π -stacking interactions with the heme, Phe360, and Phe401. Compound ZINC478529 contains a three-ring system orientation, similar to ZINC9089086 and ZINC99474, that forms a hydrogen bond with the hemic carboxylate, a hydrazine group that participates in a hydrogen bond with His95 and a phenyl ring that makes a T-shaped interaction with Phe99. Compound ZINC13466360 forms hydrogen bonds with Arg233, Glu102, and the hemic carboxylate and a shifted π -stacking interaction with the hemic pyrrole. Lastly, compound ZINC4471880 makes a π -stacking interaction between the tricyclic ring and the heme and forms hydrogen bonds with Gln91 and His95.

These results are consistent with previous studies, demonstrating that these interactions are essential for molecular recognition between the MPO active site and inhibitors.^{25,26,42,45} Indeed, the orientation of hydrazine and oxime groups between the iron atom and His95, as in ZINC478529 and ZINC4471880, is analogous to the proposed catalytic conformation of hydrogen peroxide in the active site of native MPO.⁷¹ Based on the fact that the most frequently observed interaction was between the hemic pyrrole and the aromatic system of the ligands, it appears that aromaticity is an essential property to the inhibitory action. Furthermore, interactions with the hemic carboxylate and Glu102 were also commonly identified, indicating the importance of these structural elements. Interestingly, the latter interaction with Glu102 is also present in several potent MPO inhibitors.^{26,27,35}

Inhibition of Hypochlorous Acid Production *In Vitro*. Inhibition of MPO chlorinating activity was evaluated using dHL-60 cells. It was previously shown that differentiating HL-

60 cells by adding 1.25% DMSO to the culture media for 4–5 days increases the expression of NADPH oxidase subunits, which substantially increases the production of superoxide, hydrogen peroxide, and, consequently, hypochlorous acid (HOCl) by these cells.^{57,72} As shown in Table 5,

Table 5. Hypochlorous Acid Production in Cells^a

	HOCl production (% of control)	
	dHL-60	human neutrophils
PTU	6.2 ± 0.4*	22 ± 4.2*
ZINC9089086	31 ± 2.7*	53 ± 4.2*

^adHL-60 or human neutrophils (1×10^6) were incubated in PBS glucose containing 0.1 mM DTPA, 5 mM taurine, 20 μ M test compound, and 100 nM PMA for 1 h at 37 °C. Samples were then centrifuged at 1400 rpm for 10 min. An aliquot of the supernatant was diluted (threefold) in the same buffer. The reaction mixture contained 240 μ L of the dilute supernatant, 60 μ L 0.4 M acetate buffer pH 5.4 containing 0.1 mM NaI, and 2 mM TMB dissolved into 10% DMF. The oxidation of TMB was measured at 655 nm. The values are expressed as the means \pm DP, $n = 4$. Statistical analyses involved one-way ANOVA, followed by the Bonferroni posthoc test. The asterisk (*) represents statistically different ($p < 0.05$) results when compared to control (DMSO). Abbreviation: PTU, propylthiouracil.

ZINC9089086, the most potent inhibitor of purified MPO chlorinating activity, decreased hypochlorous acid production in dHL-60 cells. To confirm the inhibition of MPO-mediated chlorination, we then performed a similar set of experiments using human neutrophils and observed a similar inhibition profile (Table 5). While compound ZINC9089086 was less efficient at inhibiting MPO than the irreversible inhibitor propylthiouracil (PTU), it displayed higher inhibition in neutrophils than other recently discovered MPO inhibitors.²⁷

Mechanism of Inhibition. Previous studies have determined that there are three groups of MPO inhibitors: (i) tight-binding inhibitors (e.g., hydroxamates),⁴⁵ (ii) mechanism-based inhibitors (e.g., 2-thiouracil),⁷³ and (iii) compound II accumulators (e.g., indoles).³³ To elucidate the mechanism of ZINC9089086-mediated MPO inhibition, we incubated the drug with MPO for 30 min, diluted the reaction mixture 200-fold, and measured the residual peroxidase activity (see Materials and Methods). As shown in Figure 7, the residual MPO activity was completely restored following sample dilution. This result demonstrates that ZINC9089086 is a reversible inhibitor and means that it is either a tight-binding inhibitor or a compound II accumulator. Concerning compound II accumulators, this group of MPO inhibitors is not considered to be the best because physiological substrates of MPO compound II (e.g., tyrosine, uric acid, and ascorbate) can restore the enzyme to its native ferric form.⁴⁵ Thus, further studies focused on discriminating between these two inhibitory mechanisms are necessary.

CONCLUSIONS

Because of the role MPO plays in various inflammatory conditions, this enzyme represents a promising molecular target for the development of novel anti-inflammatory agents. However, no MPO inhibitor tested so far has been approved for clinical use. In the present study, we created an integrative virtual screening methodology that consisted of an MPO inhibitor-like filter and a validated structure-based protocol. Following the virtual screening of more than 35 million

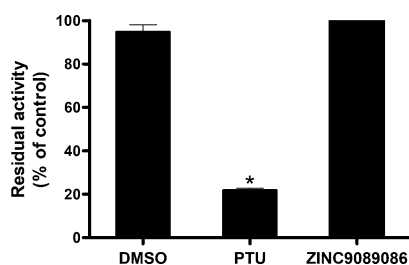


Figure 7. Reversibility of compound ZINC9089086. MPO (100 nM) was incubated with PTU or ZINC9089086 (20 μ M) for 30 min at 37 $^{\circ}$ C, and diluted 200-fold diluted in acetate buffer (0.2 M pH 5.4) with TMB (2 mM in DMF 10%). Next, hydrogen peroxide (40 μ M) was added to initiate the reaction. Residual peroxidase activity is expressed as the percent of control (0.33% DMSO). Abbreviations: DMSO—dimethyl sulfoxide, PTU—propylthiouracil. Data are presented as the mean \pm S.E.M of three independent experiments. Statistical analysis was performed by one-way ANOVA, followed by Bonferroni posthoc test. The asterisk (*) indicates statistically different results ($p < 0.01$) when compared to the DMSO group.

compounds in the ZINC12 database, we identified 10 candidate compounds and subsequently evaluated each using enzymatic and cellular assays. We found that six of these compounds effectively blocked MPO chlorinating activity *in vitro* and that this group of compounds displayed diverse chemical properties. Notably, compound ZINC9089086 proved to be the best inhibitor. This compound exhibited an IC_{50} of 2.2 μ M when incubated with purified MPO and inhibited hypochlorous acid production in dHL-60 cells and human neutrophils. While we demonstrated reversible ZINC9089086-mediated MPO inhibition, it remains unclear whether this compound is a tight-binding inhibitor or a compound II accumulator. Furthermore, the theoretical ADME/Tox study indicated that ZINC9089086 has an attractive pharmacokinetic and toxicological profile; however, studies in an animal model need to be undertaken to prove the *in vivo* anti-inflammatory effect of ZINC9089086. In conclusion, during our search for novel MPO inhibitors with a favorable ADME/Tox profile, we found that integrating an inhibitor-like rule with a validated structure-based methodology could effectively generate an enriched target database and identify compounds with a high success rate and chemical diversity.

■ ASSOCIATED CONTENT

Supporting Information

The Supporting Information is available free of charge at <https://pubs.acs.org/doi/10.1021/acs.jcim.0c00813>.

Smiles input of MPO inhibitors used to generate decoys; superposition of MPO crystal structures from PDB; dose–response curve for ZINC9089086; and molecular docking histograms of the active compounds (PDF)

■ AUTHOR INFORMATION

Corresponding Authors

Isaac de Araújo Matos – Department of Biochemistry, Institute of Chemistry, University of São Paulo, São Paulo 05508-000, Brazil; Phone: +55 11 3091-1763; Email: isaacbioquim@usp.br

Flavia Carla Meotti – Department of Biochemistry, Institute of Chemistry, University of São Paulo, São Paulo 05508-000,

Brazil; orcid.org/0000-0002-7217-3352;

Email: flaviam@iq.usp.br

Author

Nivan Bezerra da Costa Júnior – Department of Chemistry, Federal University of Sergipe, Sergipe 49100-000, Brazil

Complete contact information is available at:

<https://pubs.acs.org/10.1021/acs.jcim.0c00813>

Author Contributions

I.A.M conceived the study, performed all the experiments, analyzed the data, and wrote the manuscript. N.B.C.J discussed and reviewed all computational data; F.C.M reviewed the project and the manuscript; I.A.M. and F.C.M discussed all results and led the investigation.

Funding

This study was supported by Fundação de Amparo à Pesquisa do Estado de São Paulo (FAPESP): CEPID Redoxoma 2013/07937-8; Young Investigator 2018/14898-2 and Conselho Nacional de Pesquisa Tecnológica (CNPq) 472105/2012-4. I.A.M. received scholarship from CNPq.

Notes

The authors declare no competing financial interest.

■ REFERENCES

- (1) Soehnlein, O.; Steffens, S.; Hidalgo, A.; Weber, C. Neutrophils as Protagonists and Targets in Chronic Inflammation. *Nat. Rev. Immunol.* **2017**, *17*, 248–261.
- (2) Schultz, J.; Kaminker, K. Myeloperoxidase of the Leucocyte of Normal Human Blood. I. Content and Localization. *Arch. Biochem. Biophys.* **1962**, *96*, 465–467.
- (3) Kettle, A. J.; Winterbourn, C. C. Myeloperoxidase: Structure and Function of the Green Heme Peroxidase of Neutrophils. *Heme Peroxidases*; The Royal Society of Chemistry, 2016; pp 272–308.
- (4) Nicholls, S. J.; Hazen, S. L. Myeloperoxidase and Cardiovascular Disease. *Arterioscler., Thromb., Vasc. Biol.* **2005**, *25*, 1102–1111.
- (5) Rudolph, V.; Andrié, R. P.; Rudolph, T. K.; Friedrichs, K.; Klinke, A.; Hirsch-Hoffmann, B.; Schwoerer, A. P.; Lau, D.; Fu, X.; Klingel, K.; Sydow, K.; Didié, M.; Seniuk, A.; Von Leitner, E.-C.; Szoecs, K.; Schrickel, J. W.; Treede, H.; Wenzel, U.; Lewalter, T.; Nickenig, G.; Zimmermann, W.-H.; Meinertz, T.; Böger, R. H.; Reichenspurner, H.; Freeman, B. A.; Eschenhagen, T.; Ehmke, H.; Hazen, S. L.; Willems, S.; Baldus, S. Myeloperoxidase Acts as a Profibrotic Mediator of Atrial Fibrillation. *Nat. Med.* **2010**, *16*, 470–474.
- (6) Anatoliotakis, N.; Deftereos, S.; Bouras, G.; Giannopoulos, G.; Tsounis, D.; Angelidis, C.; Kaoukis, A.; Stefanadis, C. Myeloperoxidase: Expressing Inflammation and Oxidative Stress in Cardiovascular Disease. *Curr. Top. Med. Chem.* **2013**, *13*, 115–138.
- (7) Shao, B.; Oda, M. N.; Oram, J. F.; Heinecke, J. W. Myeloperoxidase: An Oxidative Pathway for Generating Dysfunctional High-Density Lipoprotein. *Chem. Res. Toxicol.* **2010**, *23*, 447–454.
- (8) Ali, M.; Pulli, B.; Courties, G.; Tricot, B.; Sebas, M.; Iwamoto, Y.; Hilgendorf, I.; Schob, S.; Dong, A.; Zheng, W.; Skoura, A.; Kalgukar, A.; Cortes, C.; Ruggeri, R.; Swirski, F. K.; Nahrendorf, M.; Buckbinder, L.; Chen, J. W. Myeloperoxidase Inhibition Improves Ventricular Function and Remodeling After Experimental Myocardial Infarction. *J. Am. Coll. Cardiol. Basic Trans. Science* **2016**, *1*, 633–643.
- (9) Choi, D.-K.; Pennathur, S.; Perier, C.; Tieu, K.; Teismann, P.; Wu, D. C.; Jackson-Lewis, V.; Vila, M.; Vonsattel, J. P.; Heinecke, J. W.; Przedborski, S. Ablation of the Inflammatory Enzyme Myeloperoxidase Mitigates Features of Parkinson's Disease in Mice. *J. Neurosci.* **2005**, *25*, 6594–6600.
- (10) Nagra, R. M.; Becher, B.; Tourtellotte, W. W.; Antel, J. P.; Gold, D.; Paladino, T.; Smith, R. A.; Nelson, J. R.; Reynolds, W. F.

Immunohistochemical and Genetic Evidence of Myeloperoxidase Involvement in Multiple Sclerosis. *J. Neuroimmunol.* **1997**, *78*, 97–107.

(11) Stefanova, N.; Georgievska, B.; Eriksson, H.; Poewe, W.; Wenning, G. K. Myeloperoxidase Inhibition Ameliorates Multiple System Atrophy-Like Degeneration in a Transgenic Mouse Model. *Neurotoxic. Res.* **2012**, *21*, 393–404.

(12) Odobasic, D.; Yang, Y.; Muljadi, R. C. M.; O'Sullivan, K. M.; Kao, W.; Smith, M.; Morand, E. F.; Holdsworth, S. R. Endogenous Myeloperoxidase Is a Mediator of Joint Inflammation and Damage in Experimental Arthritis. *Arthritis Rheumatol.* **2014**, *66*, 907–917.

(13) Churg, A.; Marshall, C. V.; Sin, D. D.; Bolton, S.; Zhou, S.; Thain, K.; Cadogan, E. B.; Maltby, J.; Soars, M. G.; Mallinder, P. R.; Wright, J. L. Late Intervention with a Myeloperoxidase Inhibitor Stops Progression of Experimental Chronic Obstructive Pulmonary Disease. *Am. J. Respir. Crit. Care Med.* **2012**, *185*, 34–43.

(14) Carr, A. C.; Spencer, E.; Hoskin, T. S.; Rosengrave, P.; Kettle, A. J.; Shaw, G. Circulating Myeloperoxidase Is Elevated in Septic Shock and Is Associated with Systemic Organ Failure and Mortality in Critically Ill Patients. *Free Radical Biol. Med.* **2020**, *152*, 462–468.

(15) Li, H.; Liu, L.; Zhang, D.; Xu, J.; Dai, H.; Tang, N.; Su, X.; Cao, B. SARS-CoV-2 and Viral Sepsis: Observations and Hypotheses. *Lancet* **2020**, *395*, 1517–1520.

(16) Arazna, M.; Pruchniak, M. P.; Zycinska, K.; Demkow, U. Neutrophil Extracellular Trap in Human Diseases. In *Respiratory Regulation - The Molecular Approach*; Pokorski, M., Ed.; Springer Netherlands: Dordrecht, 2013; pp 1–8.

(17) Zheng, W.; Warner, R.; Ruggeri, R.; Su, C.; Cortes, C.; Skoura, A.; Ward, J.; Ahn, K.; Kalgutkar, A.; Sun, D.; Maurer, T. S.; Bonin, P. D.; Okerberg, C.; Bobrowski, W.; Kawabe, T.; Zhang, Y.; Coskran, T.; Bell, S.; Kapoor, B.; Johnson, K.; Buckbinder, L. PF-1355, a Mechanism-Based Myeloperoxidase Inhibitor, Prevents Immune Complex Vasculitis and Anti-Glomerular Basement Membrane Glomerulonephritis. *J. Pharmacol. Exp. Ther.* **2015**, *353*, 288–298.

(18) Ray, R. S.; Katyal, A. Myeloperoxidase: Bridging the Gap in Neurodegeneration. *Neurosci. Biobehav. Rev.* **2016**, *68*, 611–620.

(19) Soubhye, J.; Aldib, I.; Delporte, C.; Prévost, M.; Dufasne, F.; Antwerpen, P. Myeloperoxidase as a Target for the Treatment of Inflammatory Syndromes: Mechanisms and Structure Activity Relationships of Inhibitors. *Curr. Med. Chem.* **2016**, *23*, 3975–4008.

(20) Taylor, A. M. The Resurrection of Myeloperoxidase as a Therapeutic Target: Is It Lazarus or Just an Apparition? *J. Am. Coll. Cardiol. Basic Trans. Science* **2016**, *1*, 644–646.

(21) Kettle, A. J.; Gedye, C. A.; Hampton, M. B.; Winterbourn, C. C. Inhibition of Myeloperoxidase by Benzoic Acid Hydrazides. *Biochem. J.* **1995**, *308*, 559–563.

(22) Kettle, A. J.; Gedye, C. A.; Winterbourn, C. C. Mechanism of Inactivation of Myeloperoxidase by 4-Aminobenzoic Acid Hydrazide. *Biochem. J.* **1997**, *321*, 503–508.

(23) Davies, B.; Edwards, S. W. Inhibition of Myeloperoxidase by Salicylhydroxamic Acid. *Biochem. J.* **1989**, *258*, 801–806.

(24) Malle, E.; Furtmüller, P. G.; Sattler, W.; Obinger, C. Myeloperoxidase: a target for new drug development? *Br. J. Pharmacol.* **2007**, *152*, 838–854.

(25) Malvezzi, A.; Queiroz, R. F.; de Rezende, L.; Augusto, O.; Amaral, A. T.-d. MPO Inhibitors Selected by Virtual Screening. *Mol. Inf.* **2011**, *30*, 605–613.

(26) Aldib, I.; Soubhye, J.; Zouaoui Boudjeltia, K.; Vanhaeverbeek, M.; Rousseau, A.; Furtmüller, P. G.; Obinger, C.; Dufasne, F.; Nève, J.; Van Antwerpen, P.; Prévost, M. Evaluation of New Scaffolds of Myeloperoxidase Inhibitors by Rational Design Combined with High-Throughput Virtual Screening. *J. Med. Chem.* **2012**, *55*, 7208–7218.

(27) Soubhye, J.; Chikh Alard, J.; Aldib, I.; Prévost, M.; Gelbcke, M.; De Carvalho, A.; Furtmüller, P. G.; Obinger, C.; Flemmig, J.; Tadrent, S.; Meyer, F.; Rousseau, A.; Nève, J.; Mathieu, V.; Zouaoui Boudjeltia, K.; Dufasne, F.; Van Antwerpen, P. Discovery of Novel Potent Reversible and Irreversible Myeloperoxidase Inhibitors Using Virtual Screening Procedure. *J. Med. Chem.* **2017**, *60*, 6563–6586.

(28) Forbes, L. V.; Furtmüller, P. G.; Khalilova, I.; Turner, R.; Obinger, C.; Kettle, A. J. Isoniazid as a Substrate and Inhibitor of Myeloperoxidase: Identification of Amine Adducts and the Influence of Superoxide Dismutase on Their Formation. *Biochem. Pharmacol.* **2012**, *84*, 949–960.

(29) Regasini, L. O.; Velloso, J. C. R.; Silva, D. H. S.; Furlan, M.; de Oliveira, O. M. M.; Khalil, N. M.; Brunetti, I. L.; Young, M. C. M.; Barreiro, E. J.; Bolzani, V. S. Flavonols from Pterogyne Nitens and Their Evaluation as Myeloperoxidase Inhibitors. *Phytochemistry* **2008**, *69*, 1739–1744.

(30) Shiba, Y.; Kinoshita, T.; Chuman, H.; Taketani, Y.; Takeda, E.; Kato, Y.; Naito, M.; Kawabata, K.; Ishisaka, A.; Terao, J.; Kawai, Y. Flavonoids as Substrates and Inhibitors of Myeloperoxidase: Molecular Actions of Aglycone and Metabolites. *Chem. Res. Toxicol.* **2008**, *21*, 1600–1609.

(31) Van Antwerpen, P.; Dufasne, F.; Lequeux, M.; Boudjeltia, K. Z.; Lessgyer, I.; Babar, S.; Moreau, P.; Moguilevsky, N.; Vanhaeverbeek, M.; Ducobu, J.; Nève, J. Inhibition of the Myeloperoxidase Chlorinating Activity by Non-Steroidal Anti-Inflammatory Drugs: Flufenamic Acid and Its 5-Chloro-Derivative Directly Interact with a Recombinant Human Myeloperoxidase to Inhibit the Synthesis of Hypochlorous Acid. *Eur. J. Pharmacol.* **2007**, *570*, 235–243.

(32) Van Antwerpen, P.; Prévost, M.; Zouaoui-Boudjeltia, K.; Babar, S.; Lessgyer, I.; Moreau, P.; Moguilevsky, N.; Vanhaeverbeek, M.; Ducobu, J.; Nève, J.; Dufasne, F. Conception of Myeloperoxidase Inhibitors Derived from Flufenamic Acid by Computational Docking and Structure Modification. *Bioorg. Med. Chem.* **2008**, *16*, 1702–1720.

(33) Sliskovic, I.; Abdulhamid, I.; Sharma, M.; Abu-Soud, H. M. Analysis of the Mechanism by Which Tryptophan Analogs Inhibit Human Myeloperoxidase. *Free Radical Biol. Med.* **2009**, *47*, 1005–1013.

(34) Ruggeri, R. B.; Buckbinder, L.; Bagley, S. W.; Carpino, P. A.; Conn, E. L.; Dowling, M. S.; Fernando, D. P.; Jiao, W.; Kung, D. W.; Orr, S. T. M.; Qi, Y.; Rocke, B. N.; Smith, A.; Warmus, J. S.; Zhang, Y.; Bowles, D.; Widlicka, D. W.; Eng, H.; Ryder, T.; Sharma, R.; Wolford, A.; Okerberg, C.; Walters, K.; Maurer, T. S.; Zhang, Y.; Bonin, P. D.; Spath, S. N.; Xing, G.; Hepworth, D.; Ahn, K.; Kalgutkar, A. S. Discovery of 2-(6-(5-Chloro-2-Methoxyphenyl)-4-Oxo-2-Thioxo-3,4-Dihydropyrimidin-1(2H)-yl)acetamide (PF-06282999): A Highly Selective Mechanism-Based Myeloperoxidase Inhibitor for the Treatment of Cardiovascular Diseases. *J. Med. Chem.* **2015**, *58*, 8513–8528.

(35) Soubhye, J.; Meyer, F.; Furtmüller, P.; Obinger, C.; Dufasne, F.; Van Antwerpen, P. Characterization of Chemical Features of Potent Myeloperoxidase Inhibitors. *Future Med. Chem.* **2016**, *8*, 1163–1177.

(36) Li, Y.; Ganesh, T.; Diebold, B. A.; Zhu, Y.; McCoy, J. W.; Smith, S. M. E.; Sun, A.; Lambeth, J. D. Thioxo-Dihydroquinazolinone Compounds as Novel Inhibitors of Myeloperoxidase. *ACS Med. Chem. Lett.* **2015**, *6*, 1047–1052.

(37) Zeraik, M. L.; Ximenes, V. F.; Regasini, L. O.; Dutra, L. A.; Silva, D. H. S.; Fonseca, L. M.; Coelho, D.; Machado, S. A. S.; Bolzani, V. S. 4'-Aminochalcones As Novel Inhibitors of the Chlorinating Activity of Myeloperoxidase. *Curr. Med. Chem.* **2012**, *19*, 5405–5413.

(38) Rosso, R.; Vieira, T.; Leal, P.; Nunes, R.; Yunes, R.; Creczynskipasa, T. Relationship between the Lipophilicity of Gallic Acid N-Alquil Esters' Derivatives and Both Myeloperoxidase Activity and HOCl Scavenging. *Bioorg. Med. Chem.* **2006**, *14*, 6409–6413.

(39) Soubhye, J.; Aldib, I.; Elfving, B.; Gelbcke, M.; Furtmüller, P. G.; Podrecca, M.; Conotte, R.; Colet, J.-M.; Rousseau, A.; Reye, F.; Sarakbi, A.; Vanhaeverbeek, M.; Kauffmann, J.-M.; Obinger, C.; Nève, J.; Prévost, M.; Zouaoui Boudjeltia, K.; Dufasne, F.; Van Antwerpen, P. Design, Synthesis, and Structure-Activity Relationship Studies of Novel 3-Alkylindole Derivatives as Selective and Highly Potent Myeloperoxidase Inhibitors. *J. Med. Chem.* **2013**, *56*, 3943–3958.

(40) Soubhye, J.; Prévost, M.; Van Antwerpen, P.; Zouaoui Boudjeltia, K.; Rousseau, A.; Furtmüller, P. G.; Obinger, C.; Vanhaeverbeek, M.; Ducobu, J.; Nève, J.; Gelbcke, M.; Dufasne, F.

o. Structure-Based Design, Synthesis, and Pharmacological Evaluation of 3-(Aminoalkyl)-5-Fluoroindoles as Myeloperoxidase Inhibitors. *J. Med. Chem.* **2010**, *53*, 8747–8759.

(41) Soubhye, J.; Aldib, I.; Prévost, M.; Elfving, B.; Gelbcke, M.; Podrecca, M.; Conotte, R.; Colet, J.-M.; Furtmüller, P. G.; Delporte, C.; Rousseau, A.; Vanhaeverbeek, M.; Nève, J.; Obinger, C.; Zouaoui-Boudjeltia, K.; Van Antwerpen, P.; Dufrasne, F. Hybrid Molecules Inhibiting Myeloperoxidase Activity and Serotonin Reuptake: A Possible New Approach of Major Depressive Disorders with Inflammatory Syndrome. *J. Pharm. Pharmacol.* **2014**, *66*, 1122–1132.

(42) Aldib, I.; Gelbcke, M.; Soubhye, J.; Prévost, M.; Furtmüller, P. G.; Obinger, C.; Elfving, B.; Alard, I. C.; Roos, G.; Delporte, C.; Berger, G.; Dufour, D.; Zouaoui Boudjeltia, K.; Nève, J.; Dufrasne, F.; Van Antwerpen, P. Novel Bis-Arylalkylamines as Myeloperoxidase Inhibitors: Design, Synthesis, and Structure-Activity Relationship Study. *Eur. J. Med. Chem.* **2016**, *123*, 746–762.

(43) Kettle, A. J.; Winterbourn, C. C. Mechanism of Inhibition of Myeloperoxidase by Anti-Inflammatory Drugs. **1991**, *41* (), 1485–1492. DOI: 10.1016/0006-2952(91)90565-m

(44) Roth, A.; Ott, S.; Farber, K. M.; Palazzo, T. A.; Conrad, W. E.; Haddadin, M. J.; Tantillo, D. J.; Cross, C. E.; Eiserich, J. P.; Kurth, M. J. Inhibition of Myeloperoxidase: Evaluation of 2H-Indazoles and 1H-Indazolones. *Bioorg. Med. Chem.* **2014**, *22*, 6422–6429.

(45) Forbes, L. V.; Sjögren, T.; Auchère, F.; Jenkins, D. W.; Thong, B.; Laughton, D.; Hemsley, P.; Paireadeau, G.; Turner, R.; Eriksson, H.; Unitt, J. F.; Kettle, A. J. Potent Reversible Inhibition of Myeloperoxidase by Aromatic Hydroxamates. *J. Biol. Chem.* **2013**, *288*, 36636–36647.

(46) Fiedler, T. J.; Davey, C. A.; Fenna, R. E. X-ray Crystal Structure and Characterization of Halide-binding Sites of Human Myeloperoxidase at 1.8 Å Resolution. *J. Biol. Chem.* **2000**, *275*, 11964–11971.

(47) Duclos, F.; Abell, L. M.; Harden, D. G.; Pike, K.; Nowak, K.; Locke, G. A.; Duke, G. J.; Liu, X.; Fernando, G.; Shaw, S. A.; Vokits, B. P.; Wurtz, N. R.; Viet, A.; Valente, M. N.; Stachura, S.; Sleph, P.; Khan, J. A.; Gao, J.; Dongre, A. R.; Zhao, L.; Wexler, R. R.; Gordon, D. A.; Kick, E. K. Triazolopyrimidines Identified as Reversible Myeloperoxidase Inhibitors. *Medchemcomm* **2017**, *8*, 2093–2099.

(48) Fujitsu CaChe Workspace; Fujitsu: Toronto, 2004.

(49) Raven, E.; Dunford, B. Heme Peroxidases. *Metallobiology*, 1st ed.; The Royal Society of Chemistry, 2016.

(50) Zederbauer, M.; Furtmüller, P. G.; Brogioni, S.; Jakopitsch, C.; Smulevich, G.; Obinger, C. Heme to Protein Linkages in Mammalian Peroxidases: Impact on Spectroscopic, Redox and Catalytic Properties. *Nat. Prod. Rep.* **2007**, *24*, 571–584.

(51) Capena, X.; Vidossich, P.; Schrottner, K.; Calisto, B. M.; Banerjee, S.; Stampler, J.; Soudi, M.; Furtmüller, P. G.; Rovira, C.; Fita, I.; Obinger, C. Essential Role of Proximal Histidine-Asparagine Interaction in Mammalian Peroxidases. *J. Biol. Chem.* **2009**, *284*, 25929–25937.

(52) Stewart, J. J. P. MOPAC. Colorado, 2016.

(53) Humphrey, W.; Dalke, A.; Schulten, K. VMD: Visual Molecular Dynamics. *J. Mol. Graphics* **1996**, *14*, 33–38.

(54) Mysinger, M. M.; Carchia, M.; Irwin, J. J.; Shoichet, B. K. Directory of Useful Decoys, Enhanced (DUD-E): Better Ligands and Decoys for Better Benchmarking. *J. Med. Chem.* **2012**, *55*, 6582–6594.

(55) Truchon, J.-F.; Bayly, C. I. Evaluating Virtual Screening Methods: Good and Bad Metrics for the “Early Recognition” Problem. *J. Chem. Inf. Model.* **2007**, *47*, 488–508.

(56) Dypbukt, J.; Bishop, C.; Brooks, W.; Thong, B.; Eriksson, H.; Kettle, A. A Sensitive and Selective Assay for Chloramine Production by Myeloperoxidase. *Free Radical Biol. Med.* **2005**, *39*, 1468–1477.

(57) Carvalho, L. A. C.; Lopes, J. P. P. B.; Kaihama, G. H.; Silva, R. P.; Bruni-Cardoso, A.; Baldini, R. L.; Meotti, F. C. Uric Acid Disrupts Hypochlorous Acid Production and the Bactericidal Activity of HL-60 Cells. *Redox Biol.* **2018**, *16*, 179–188.

(58) Böyum, A. Isolation of Mononuclear Cells and Granulocytes from Human Blood. Isolation of Mononuclear Cells by One Centrifugation, and of Granulocytes by Combining Centrifugation

and Sedimentation at 1 G. *Scand. J. Clin. Lab. Invest., Suppl.* **1968**, *97*, 77–89.

(59) Josephy, P. D.; Eling, T.; Mason, R. P. The horseradish peroxidase-catalyzed oxidation of 3,5,3',5'-tetramethylbenzidine. Free radical and charge-transfer complex intermediates. *J. Biol. Chem.* **1982**, *257*, 3669–3675.

(60) Veber, D. F.; Johnson, S. R.; Cheng, H.-Y.; Smith, B. R.; Ward, K. W.; Kopple, K. D. Molecular Properties That Influence the Oral Bioavailability of Drug Candidates. *J. Med. Chem.* **2002**, *45*, 2615–2623.

(61) Lipinski, C. A.; Lombardo, F.; Dominy, B. W.; Feeney, P. J. Experimental and Computational Approaches to Estimate Solubility and Permeability in Drug Discovery and Development Settings. *Adv. Drug Delivery Rev.* **2012**, *64*, 4–17.

(62) Hughes, J. D.; Blagg, J.; Price, D. A.; Bailey, S.; DeCrescenzo, G. A.; Devraj, R. V.; Ellsworth, E.; Fobian, Y. M.; Gibbs, M. E.; Gilles, R. W.; Greene, N.; Huang, E.; Krieger-Burke, T.; Loesel, J.; Wager, T.; Whiteley, L.; Zhang, Y. Physicochemical Drug Properties Associated with in Vivo Toxicological Outcomes. *Bioorg. Med. Chem. Lett.* **2008**, *18*, 4872–4875.

(63) Yousuf, M.; Shaikh, N. N.; Ul-Haq, Z.; Choudhary, M. I. Bioinformatics: A rational combine approach used for the identification and in-vitro activity evaluation of potent β -Glucuronidase inhibitors. *PLoS One* **2018**, *13*, No. e0200502.

(64) Stewart, J. J. P. Optimization of Parameters for Semiempirical Methods VI: More Modifications to the NDDO Approximations and Re-Optimization of Parameters. *J. Mol. Model.* **2013**, *19*, 1–32.

(65) Hevener, K. E.; Zhao, W.; Ball, D. M.; Babaoglu, K.; Qi, J.; White, S. W.; Lee, R. E. Validation of Molecular Docking Programs for Virtual Screening against Dihydropteroate Synthase. *J. Chem. Inf. Model.* **2009**, *49*, 444–460.

(66) Marro, M. L.; Patterson, A. W.; Lee, L.; Deng, L.; Reynolds, A.; Ren, X.; Axford, L.; Patnaik, A.; Hollis-Symynkywicz, M.; Casson, N.; Custeau, D.; Ames, L.; Loi, S.; Zhang, L.; Honda, T.; Blank, J.; Harrison, T. J.; Papillon, J. P. N.; Hamann, L. G.; Marcinkeviciene, J.; Regard, J. B. Discovery of 1-((6-Aminopyridin-3-yl)methyl)-3-(4-Bromophenyl)urea as a Potent, Irreversible Myeloperoxidase Inhibitor. *J. Pharmacol. Exp. Ther.* **2018**, *367*, 147–154.

(67) Patnaik, A.; Axford, L.; Deng, L.; Cohick, E.; Ren, X.; Loi, S.; Kecman, S.; Hollis-Symynkywicz, M.; Harrison, T. J.; Papillon, J. P. N.; Dales, N.; Hamann, L. G.; Lee, L.; Regard, J. B.; Marcinkeviciene, J.; Marro, M. L.; Patterson, A. W. Discovery of a Novel Indole Pharmacophore for the Irreversible Inhibition of Myeloperoxidase (MPO). *Bioorg. Med. Chem.* **2020**, *28* (). DOI: DOI: 10.1016/j.bmc.2020.115548.

(68) Jantschko, W.; Furtmüller, P. G.; Zederbauer, M.; Neugschwandtner, K.; Lehner, I.; Jakopitsch, C.; Arnhold, J.; Obinger, C. Exploitation of the Unusual Thermodynamic Properties of Human Myeloperoxidase in Inhibitor Design. *Biochem. Pharmacol.* **2005**, *69*, 1149–1157.

(69) Meotti, F. C.; Jameson, G. N. L.; Turner, R.; Harwood, D. T.; Stockwell, S.; Rees, M. D.; Thomas, S. R.; Kettle, A. J. Urate as a Physiological Substrate for Myeloperoxidase. *J. Biol. Chem.* **2011**, *286*, 12901–12911.

(70) Lazarevic-Pasti, T.; Leskovic, A.; Vasic, V. Myeloperoxidase Inhibitors as Potential Drugs. *Curr. Drug Metab.* **2015**, *16*, 168–190.

(71) Forbes, L. V.; Kettle, A. J. Myeloperoxidase Power, Unleashing the Peroxide, of Hydrogen. In *Hydrogen Peroxide Metabolism in Health and Disease*; Vissers, M.; C. M.; Hampton, M.; Kettle, A. J., Eds.; Taylor and Francis Group, 2018; pp 281–203.

(72) Hua, J.; Hasebe, T.; Someya, A.; Nakamura, S.; Sugimoto, K.; Nagaoka, I. Evaluation of the Expression of NADPH Oxidase Components during Maturation of HL-60 Cells to Neutrophil Lineage. *J. Leukocyte Biol.* **2000**, *68*, 216–224.

(73) Dong, J. Q.; Varma, M. V.; Wolford, A.; Ryder, T.; Di, L.; Feng, B.; Terra, S. G.; Sagawa, K.; Kalgutkar, A. S. Pharmacokinetics and Disposition of the Thiouracil Derivative PF-06282999, an Orally Bioavailable, Irreversible Inactivator of Myeloperoxidase Enzyme, across Animals and Humans. *Drug Metab. Dispos.* **2016**, *44*, 209–219.

Supporting information

Integration of an Inhibitor-like Rule and Structure-based Virtual Screening for the Discovery of Novel Myeloperoxidase Inhibitors

Isaac de Araújo Matos^{1}, Nivan Bezerra da Costa Júnior², and Flavia Carla Meotti^{1*}*

¹Department of Biochemistry, Institute of Chemistry, University of São Paulo, São Paulo, Brazil

²Department of Chemistry, Federal University of Sergipe, Sergipe, Brazil

*To whom correspondence should be addressed:

Flavia Carla Meotti or Isaac de Araújo Matos

Department of Biochemistry, Institute of Chemistry, University of São Paulo, São Paulo, Brazil

Av. Prof Lineu Prestes, 748. Office 1004

CEP 05508-000, Tel.: +55 11 3091-1763

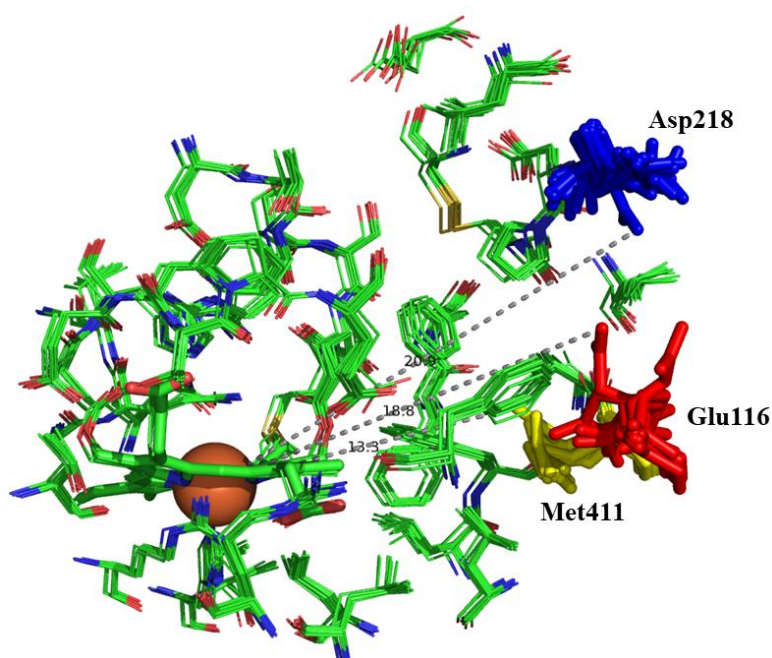
Email: flaviam@iq.usp.br, isaacbioquim@usp.br

Table S1. Smiles input of MPO inhibitors used to generate decoys.

```

O(c1cc(NC(C)CCC[NH3+])c2ncccc2c1)C
Oc1ccccc1C[NH+]3CCN(Cc2c(O)cccc2)CC3
Oc1ccccc1C[NH2+]CCc2cccc2
O=C(c1ccc(N)cc1)\C=C\c2ccc(F)cc2
Oc1ccccc1C[NH+]3CCCN(Cc2c(O)cccc2)C3
O=C3c1c(nc(n1CCCOc2cccc2)NCC[NH3+])N(C(=O)N3)C
FC(F)(F)c1cc(ccc1)Nc2cccc2C([O-])=O
O=C(OCc1ccccc1)C([NH3+])Cc3c2cccc2nc3
[O-]c3cc(O)c1c(OC(=C(O)C1=O)c2ccc(O)c(O)c2)c3
Oc2cc(\C=C\c1ccc(O)cc1)cc(O)c2
[O-]C(=O)c1cc(O)c(O)c(O)c1
Fc1cc2c(cc1)ncc2CCCC[NH3+]
O=C(c1ccc(N)cc1)NN
O=C(C1=CN=C(NC1=O)NCc2cc(cc(c2)C(F)(F)F)C(F)(F)F)NO
O=C(c1ccc(cc1O)Cc2cccc2)NO
n1c2cccc2c(OC)n1C(C)C
n1c3cccc3c2SCCn12
Fc1cccc2c1ncc2CCSCC[NH3+]
Fc1cc2c(cc1)ncc2CCCSC#N
O(c1ccc2c(c1)nc3c2CC[NH+]=C3C)C
[O-]C=2c1sc(C1)cc1S(=O)(=O)N(C=2C(=O)Nc3ncccc3)C
Fc1ccc(cc1)C2CC[NH2+]CC2COc3ccc4OCOc4c3
n2nc(c1ccccc1c2)N/N=C/c3ccc(N(C)C)cc3
Clc2ccc1[N-]C(=S)N(C(=O)c1c2)CCC[NH+](C)C

```

**Figure S1.** Alignment of MPO crystal structures PDB codes 1DNU, 1DNW, 1MHL, 3F9P, 3ZS0, 3ZS1, 4C1M, 4DL1, 5FIW, 1CXP, 1D2V, 1D5L and 1D7W.

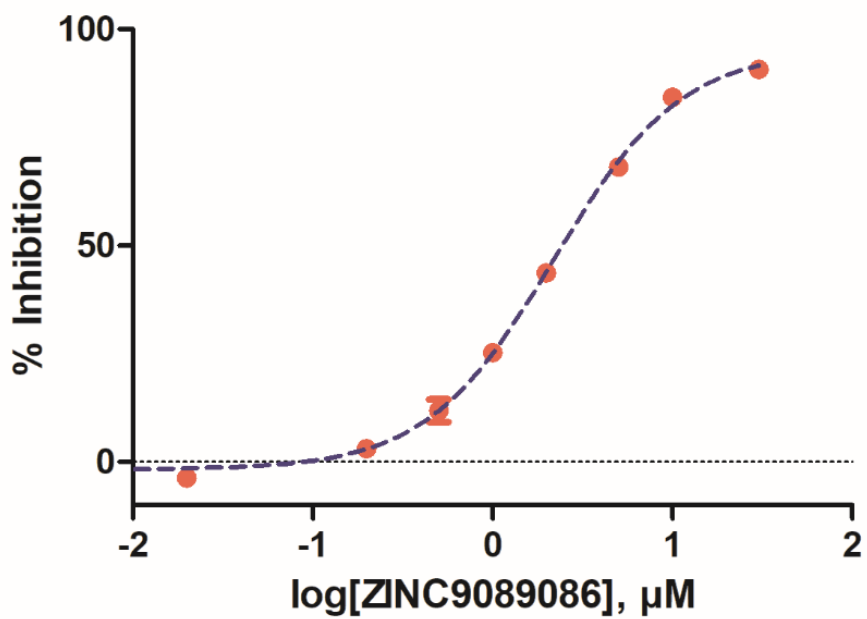


Figure S2. Dose-response curve for ZINC9089086.

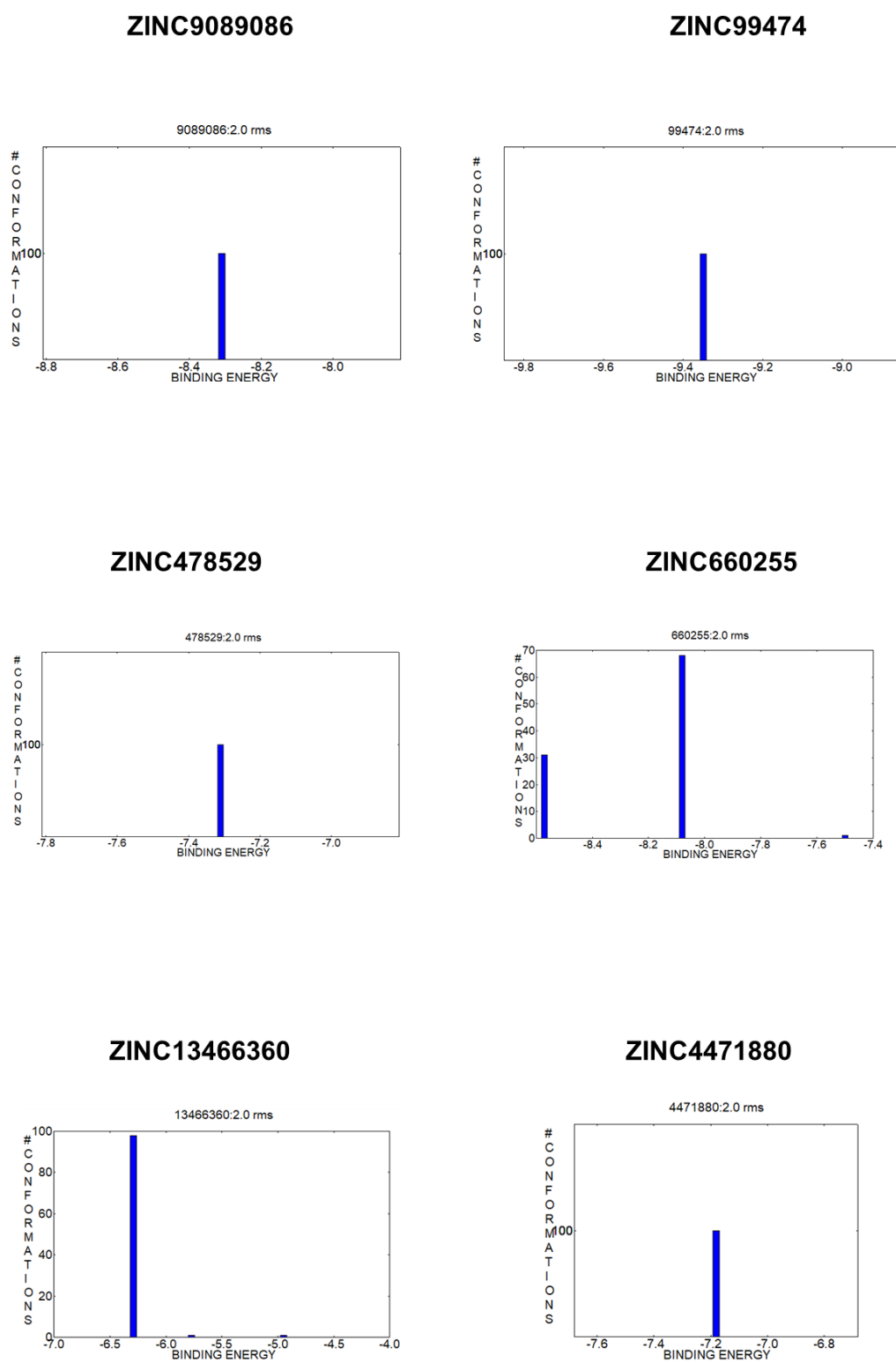


Figure S3. Molecular docking histograms of active compounds.

Table S2. MPO inhibitors not included in the construction of the MPO inhibitor-like rule

Inhibitor	MW	logP	TPSA	RBC	nON	nOHNH
HTS indole Hit						
<chem>Nc1ncnc4c1c(c3ccc2cc[nH]c2c3)cn4c5ccc(OCCNCCO)cc5</chem>	428	2.75	114	8	8	5
Aminopyridine 1						
<chem>Nc2ccc(CNC(=O)Nc1cccc(Br)c1)cn2</chem>	321	2.45	80	3	5	4

CHAPTER II

Targeting Myeloperoxidase Ameliorates Gouty Arthritis in Mice: A Virtual Screening Success Story

Isaac de Araujo Matos, Jorge Luiz Dallazen, Nivan Bezerra da Costa Júnior, Lorena Rocha Reis, Graziella Eliza Ronsein, Luiz Felipe de Souza, Nicolas Hoch, Soraia Kátia Pereira Costa, Flávia Carla Meotti.

ABSTRACT

Here we report a new pipeline to search for myeloperoxidase inhibitors (MPO) with successful inhibition *in vivo*. The virtual screening approach used recovered a varied chemical class of reversible inhibitors and HOCl scavengers with nanomolar potency. This methodology revealed success hits rates between 66% and 72%. Mechanistic studies indicated that the nanomolar reversible inhibitor RL6 is a MPO inhibitor and RL7 is potent HOCl scavenger. Moreover, these molecules were able to inhibit HOCl production and NETosis in HL-60 cells and neutrophils. Finally, using a mice model of gouty arthritis, the compounds reduced paw edema when administered either by intraperitoneal or oral route. Together, this study demonstrates that an inhibitor-like rule and receptor-based virtual screening is a golden approach to discover MPO inhibitors with *in vivo* anti-inflammatory effect.

TEASER

Structure-based virtual screening and inhibitor-like rule are good approaches to discover potent anti-inflammatory compounds by targeting myeloperoxidase.

INTRODUCTION

Myeloperoxidase (MPO), EC 1.11.2.2, is a homodimeric glycosylated enzyme and along with thyroid peroxidase (TPO), eosinophil peroxidase (EPO) and lactoperoxidase (LPO) belongs to the mammalian peroxidases superfamily (1). MPO is mostly expressed in neutrophils, although it is present in monocytes, macrophages and glial cells (2–4). The main physiological function of MPO is to catalyze chloride oxidation by hydrogen peroxide, generating hypochlorous acid, a powerful oxidant with microbicidal activity (5). Although MPO has an important microbicide role, under sterile conditions, MPO activity has been associated with tissue damage and chronic inflammation, contributing to the pathophysiology of several human diseases (6). Among them are Parkinson disease (7), cancer (8), multiple sclerosis (9), autoimmune diseases (10), cardiovascular diseases as atherosclerosis and myocardial infarction (4, 11, 12).

MPO represents about 5% of the total neutrophil dry weight (13), indicating its key role in the function of these cells. In fact, MPO deficiency leads to a decrease in cytokine release (3). Additionally, MPO plays an important role in NETosis progression (14). NETosis is a neutrophil death processes characterized by the ejection of neutrophil chromatin together with degranulation to trap microorganisms (15). Although these neutrophil extracellular traps (NETs) have microbicide functions, it can contribute to the pathophysiology of some diseases (16). An elevated content of NETs were found in plasma, tracheal aspirate and lungs of Covid-19 patients and an *in vitro* study has indicated that NETs released by Sars-Cov-2 activated neutrophils caused lung epithelial cell death (17).

In gout arthritis, an inflammatory disease caused by uric acid precipitation into the joints and that affects approximately 7% of the world population (18), neutrophil activation led to inflammation without affect resolution (19). Interestingly, this same study found a significant increase in MPO activity in the mice paws from a gouty arthritis model (19). In spite of this evidence, there is no studies showing MPO inhibitors as anti-inflammatory agents in gout. Uric acid is a substrate of MPO and its oxidation generates the strong pro-oxidant urate hydroperoxide, which has been associated with inflammatory processes (20, 21). Taking these findings into account, MPO itself is as a promising molecular target for the development of new anti-inflammatory agents against several diseases, including gout arthritis (22).

Although there are no MPO inhibitors approved for clinical use, several approaches have been employed in the discovering of MPO inhibitors, molecular docking and pharmacophoric models are examples of virtual screening methods, and high throughput screening (HTS) (23–26). However, all these methodologies haven't found yet the combination of a good hit rate, chemical diversity and *in vivo* efficacy. We recently reported a virtual screening methodology that integrated an inhibitor-like rule and molecular docking. This methodology is promising for the discovery of new MPO inhibitors with high hit ratios and chemical diversity (27). The inhibitor-like rule was developed with descriptors classically used to predict the permeability/bioavailability of molecules and applied to known MPO inhibitors. The rule states that MPO inhibition and the respective bioavailability of its inhibitors will be more likely for molecules presenting the following parameters:

Molecular mass between 174 and 396 Da.

ACD/logP between 0.1 and 4.37

Hydrogen bonds donors up to 7 and hydrogen bond receptors between 2 and 9

Rotatable bonds count up to 9

Topological surface area (TPSA) between 18 and 122 Å².

To confirm the potential of this rule, we selected a new set of potential MPO inhibitors that satisfied the MPO inhibitor-like rule and validated them in a complete pipeline composed of enzymatic, cellular and animal experiments. In agreement to the methodology robustness, MPO

chlorinating and peroxidatic activities were tested and inhibitors success rate was 66% and 72%, respectively to each catalytic cycle. The methodology recovered compounds with different mechanisms of action, including reversible inhibitors and HOCl scavengers. Additionally, three out of four compounds inhibited HOCl production by human neutrophils and by the neutrophil-like cultured cells dHL-60 (differentiated human leukemic cells). All tested MPO inhibitors decreased NETosis *in vitro*. The four compounds that were selected to test against a murine model of monosodium urate crystal-induced arthritis inhibited paw edema when administered intraperitoneally and three out of these four inhibited it when administered orally. Together, this study reveals the discovery of new MPO inhibitors by a computational screening with an unprecedented success rate when challenged against isolated MPO activity. The selected compounds were also effective in more complex assays, including HOCl production and NETosis by cells and *in vivo* in the inflammation caused by monosodium urate crystals.

RESULTS

Revalidation of the molecular docking protocol

To confirm that our previously described methodology generated an enriched MPO inhibitors sub-library, we reanalyzed the set of 242 computational hits that matched with MPO inhibitor-like rule and that had a good binding mode in the molecular docking (27). Before compounds selection, the molecular docking protocol was re-evaluated. Alignments of newly deposited MPO structures PDB 5QJ2, 5QJ3, 6WXZ, 6WY0, 6WY5, 6WY7, 6WYD, 7LAE, 7LAG, 7LAL and 7LAN revealed a low number of conserved water molecules (Fig. S1A). Furthermore, these clusters were located on the periphery of the catalytic cavity, except for the catalytic waters located under the hemic iron atom. This water cluster can potentially clog ligands that would coordinate with the iron atom. Thus, all water molecules were removed before the molecular docking simulations.

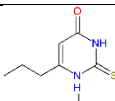
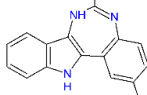
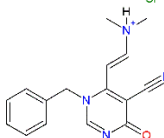
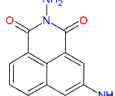
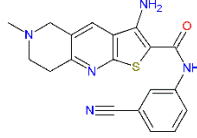
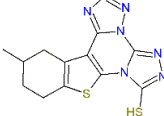
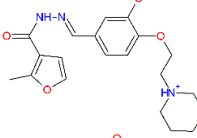
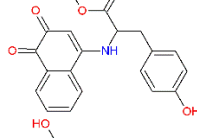
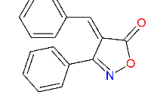
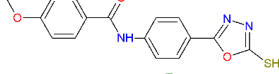
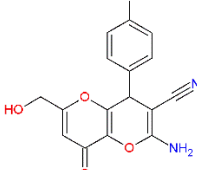
The flexibility of MPO active site also was reanalyzed by alignment. Similarly, to our previously reported data, visual inspection indicates that residues in MPO active site are mostly rigid. The most flexible ones follow the order: Asp218, Glu116 and Met411 (Fig. S1B) (27). Additionally, Glu102 also presented a certain level of flexibility. Despite the flexibility of these four residues, their external location relatively to the cavity suggests a low importance for the binding of small molecules, since the mobility may be attributed to intrinsic motion in solution but not to an induced fitting. Thus, during molecular docking simulation, MPO was configured as a rigid body. In the next validation step, the molecular docking protocol was revalidated by cross-docking because of the great number of co-crystallized MPO ligands available. For this, PDB 7LAG and 7LAN ligands were simulated into MPO active site using PDB 1CXP structure. Cross-docking simulation indicated that the molecular docking parameters were optimized to recover the experimental conformation of MPO inhibitor, as seen by the superposition of the simulated (green) and experimental (yellow) conformations of the two co-crystallized inhibitors (Fig. S1C e D). In concordance with this data, the reference Root Mean Square (refRMS) values were 1.07 and 0.81 Å² to PDB 7LAG and 7LAN ligands, respectively. Additionally, the histogram profile was clean, validating the molecular docking protocol (28). Considering the good cross-docking parameters that were obtained with the rigid receptor, the flexibility of some external residues could indeed be attributed to solvent motion and not to an induced fitting.

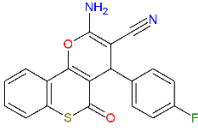
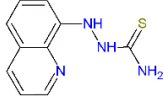
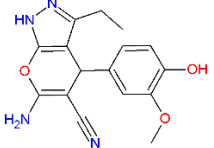
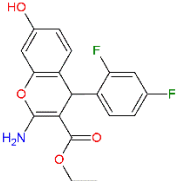
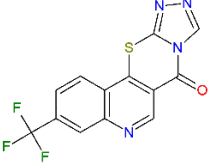
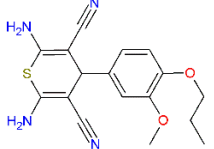

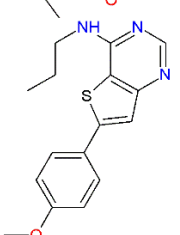
Identification of new MPO inhibitors

After molecular docking revalidation, the binding mode of the 242 potential MPO inhibitors previously selected was reanalyzed following the parameters: chemical diversity, uniqueness, binding energy, number of hydrogen bonds, π -stacking interaction and conformational histogram profile (27). Analogous molecules and compounds that had already been reported by their inhibitory activity were removed to avoid overestimation of the hit rate. By the end, 18 potential MPO inhibitors were acquired from the company Specs (Zoetermeer, Netherlands). Before experiments, compounds purity was evaluated by mass spectrometry (data not show). Twelve out of 18

compounds: RL1, RL6, RL7, RL9, RL17, RL18, RL19, RL21, RL23, RL24, RL26 and RL27 inhibited MPO chlorinating activity with an inhibition range between 18% and 92%. Six compounds: RL4, RL15, RL16, RL20, RL25 and RL28 were inactive (Table 1), indicating a 66% success rate. Although the chlorinating activity is the main MPO physiological function, *in vitro* assays for this activity are end point and susceptible to interference since some compounds can scavenger hypochlorous acid or taurine chloramine (29). Thus, all compounds were also tested against MPO peroxidatic activity.

Table 1. Inhibition of Myeloperoxidase chlorinating and peroxidatic activities by computational hits

Structure	In House	Compound codes		% Inhibition (at 20 μ M)	
		ZINC12	Specs	Chlorinating	Peroxidatic
	PTU	4640636	-	92.3 \pm 11.6	94.1 \pm 26.4
	RL1	5903548	AH-262/34227041	50.2 \pm 4.0	81.0 \pm 15.1
	RL4	235057	AH-262/34870001	INACTIVE	INACTIVE
	RL6	-	AG-690/09921025	86.5 \pm 15.3	73.0 \pm 13.4
	RL7	1427930	AM-807/42860464	84.9 \pm 17.0	INACTIVE
	RL9	6556188	AL-281/42926896	92.0 \pm 3.2	42.1 \pm 7.9
	RL15	654985	AK-968/40605613	INACTIVE	36.1 \pm 1.8
	RL16	2067366	AG-690/34551055	INACTIVE	67.1 \pm 8.1
	RL17	108018	AH-487/13582003	63.0 \pm 6.2	24.0 \pm 4.1
	RL18	6230338	AL-281/41935375	73.0 \pm 19.7	INACTIVE
	RL19	2327750	AM-807/41931995	48.6 \pm 3.5	61.8 \pm 5.9

	RL20	1429243	AM-807/42859873	INACTIVE	34.0 ± 4.3
	RL21	13545899	AH-034/11364177	89.6 ± 6.7	57.4 ± 5.3
	RL23	4453402	AM-807/15032394	57.8 ± 13.9	25.1 ± 3.2
	RL24	614461	AM-807/12739043	40.1 ± 5.5	59.1 ± 2.9
	RL25	19796894	AO-476/43407325	INACTIVE	INACTIVE
	RL26	4631443	AM-807/12426055	81.0 ± 5.8	78.7 ± 4.2
	RL27	19797067	AO-476/43415550	18.6 ± 1.6	29.5 ± 2.9
	RL28	19797146	AO-476/43415685	INACTIVE	INACTIVE

Chlorinating activity was performed in presence of MPO (10 nM), phosphate buffer (20 mM, pH 7.4), compounds (20 μM), DTPA (100 μM), CTAC (0.03%), taurine (5 mM) and NaCl (140 mM). After 15 minutes of incubation at 37°C, the reaction was started by adding 40 μM H₂O₂ and stopped with catalase (20 μg/mL) after 8 minutes of reaction. Taurine chloramine was quantified by TMB oxidation in presence of NaI at 650 nm. Peroxidase activity was measured by AmplexRed® oxidation. The product resorufin was detected by fluorescence (530, 580 nm) in a medium containing phosphate buffer (50 mM, pH 7.4), MPO (100 pM), DTPA (100 μM), CTAC (0.03%), AmplexRed® (40 μM), NaCl (140 mM) and the tested compounds (20 μM). Reactions were started with hydrogen peroxide (2 μM).

In the peroxidatic assay, MPO activity was measured by direct AmplexRed® probe oxidation, generating resorufin that is quantified by fluorescence (30). Although it uses an artificial substrate, peroxidatic test is less susceptible to scavenger interference. Thirteen out of 18 compounds (RL1, RL6, RL9, RL15, RL16, RL17, RL19, RL20, RL21, RL23, RL24, RL26 e RL27) inhibited peroxidase activity in a range from 24 to 81% and only compounds RL4, RL7, RL18, RL25 and RL28 were inactive (Table 1), generating a success rate of 72%. A similar success rate (60%) was found in our previous study (27). Ten compounds exhibited an inhibitory consensus in the two assays: RL1, RL6, RL9, RL17, RL19, RL21, RL23, RL24, RL26 and RL27. Three, RL15, RL16 and RL20, were active only in the peroxidatic assay and two, RL7 and RL18, only against the

chlorinating activity (Tab. 1 and Fig. 1A). The exclusive inhibition of RL7 and RL18 upon chlorinating assay (Fig. 1A and 1B) suggests that they are hypochlorous acid or taurine chloramine scavengers. The inactivity of RL15, RL16 and RL20 compounds in chlorinating assay can be attributed to the high chloride concentrations used in the assay (140 mM) that can compete with inhibitors for the MPO active site. Although the compounds RL9, RL17 and RL23 inhibited peroxidase activity (Tab. 1), the chlorinating/peroxidatic ratio (Fig. 1B) also suggests an important scavenger mechanism. A chlorinating/peroxidatic ratio ~ 1 is indicative of a true enzyme inhibitor (Fig. 1B). Structural analysis of the active compounds shows a high number of novel chemical and pharmacological backbones including benzodiazepine (RL1), naphthalimide (RL6), azoles (RL9, RL18, RL23 and RL25) and thiourea (RL21) (Tab. 1).

Active compounds exhibit diversified interaction mode

To better understand how active compounds bind to MPO active site, interactions with residues from the active site were analyzed (Fig. 1C). Compound LR1 is the first benzodiazepine reported as a MPO inhibitor. It performs two hydrogen bonds, one with Glu102 carboxylate and another with the heme group. Moreover, the indole substructure in LR1 is orientated under the heme plane, exhibiting a sandwich π stacking interaction with the heme π system. The benzene ring choro functionalized in LR1 also performs a π stacking interaction but with Phe99 residue and in a T-shaped angle. The indole orientation near to the iron atom suggests that it may be a good substrate to the compound I since electrons from indole ring can be removed by oxyferryl center similarly to reported in tryptamines (31). Compound RL6 exhibits structural similarity with 4-aminobenzoic acid hydrazide (ABAH), a classical irreversible MPO inhibitor (32). In spite of this, RL6 chemical class, naphthalimide, had never been reported as MPO inhibitor. It exhibits hydrogen bonds with Gln91 and heme carboxylate in addition to a sandwich π stacking interaction between the tricyclic rings and the heme group. A T-shaped π stacking interaction is also likely between the naphthalene portion and Phe99. During complex dynamics, the hydrazyl group ($\text{H}_2\text{N-N}$) putatively forms two extra hydrogen bonds with His95 (distal histidine), as proposed for hydrogen peroxide and hydroxamates inhibitors (33, 34). It also makes a hydrogen bond with Arg233, totaling 5 putative hydrogen bonds for this inhibitor. Compound RL9 can be classified as a thiol poliazole that has a stereogenic center and tautomerism, being represented by **R** and **S** enantiomers and by the thione and thiol tautomers (Tab. 1 and S1). Molecular docking of this species indicates that **R** enantiomer in the thiol form has the most favorable binding free energy (Tab. S1). It interacts by two hydrogen bonds with Gln91 and Arg233 residues. The large quadricyclic ring in this molecule forms sandwich stacking interactions with heme π system and Phe99 (T-shape angle) (Fig. 1). Interestingly, the thiol group is positioned under the hemic iron as reported for propylthiouracil (PTU) binding to lactoperoxidase (PDB 5HPW). The hydrogen is orientated to *tau* nitrogen atom in His95, suggesting a putative hydrogen bond. This is also similarly to the binding mode reported for hydrogen peroxide and hydroxamates (33, 34). Molecular docking of RL15 inhibitor, a phenyl hydrazone, indicates hydrogen bonds with Gln91, Arg233 and Glu102, the last exhibiting a high electrostatic nature. The furan and benzene rings form π stacking interactions with heme and, potentially, with Phe360, respectively. Inhibitor RL16 is an enantiomeric vicinal naphthalene dione and the **S** enantiomer presents the best binding mode (Tab S1). This species forms hydrogen bonds with Arg233, Phe141 and Arg418 residues, differently from other compounds (Fig. 1). Theoretically, the formation of a hydrogen bond with Glu102 is expected during solution dynamics. Moreover, π stacking interactions with heme (sandwich), Phe99 and Phe141 (T-shape angle) was observed. Analysis of the RL17, an oxazolone, indicates an unfavorable contact with *tau* nitrogen in His95. Despite this repulsive contact, this compound shows hydrogen bonds with Arg233 and Gln91, as well as π stacking interactions between the oxazole ring and the heme plane. Surprisingly, two benzene rings in RL17 are parallel to each other and localized between Phe99 and Phe401 residues, indicating a great sandwich π stacking contribution to complex stabilization. Molecular docking of the inhibitor RL19, a chiral chromeno, indicates that both **R** and **S** enantiomers exhibit

favorable binding parameters (Tab. S1). Binding energy values reveal a discrete favoring for the **R** enantiomer. This species forms hydrogen bonds with Glu102, Arg233 and His95. Besides, an extra bond with Gln91 could be formed with the nitrile group during protein motion. Interestingly, the orientation of the amino group related to His95 is similar to the binding mode of the hydrazyl and thiol groups in RL6 and RL9, respectively (Fig. 1). Additionally, the RL19 inhibitor is stabilized by sandwich π stacking interactions between the chromeno and the heme group. Chromeno ring also interacts with Phe99 residue but in a T-shape angle and in a dislocated π stacking interactions can be formed between fluorophenyl group and Phe401 residue. The RL19 **S** enantiomer exhibits a similar binding mode to the **R** one but the hydroxymethyl group is inside of the active site, forming a hydrogen bond with His95. The chromeno carbonyl interacts with Arg233. Finally, the amino group in the **S** enantiomer makes a hydrogen bond with Glu102. Although RL20 inhibitor is also a chiral chromeno derivative, molecular docking simulations indicates a different binding mode from the chromenos described above (Fig. 1C), being the **R** enantiomer the most likely conformation (Tab. S1). Compared to RL19, the fluorophenyl ring is in an opposite orientation and RL20 forms only one hydrogen bond with heme carboxylate and a sandwich π stacking interaction with the planar π system. The quinolinic thiourea derivative, compound RL21, has a similar binding mode to RL20 (Fig. 1) and a similar structure to the previously guanidine derivative reported by Soubhlye *et al*, which was also detected by our methodology (26, 27). RL21 forms hydrogen bonds with Thr100 and Arg233 and a sandwich π stacking interaction between the quinazoline ring and the π heme system. In addition, during protein dynamics it is possible the formation of an extra hydrogen bond with the heme carboxylate, considering the proximity and flexibility of the **HN-NH** group in RL21. RL23 exhibits similar structural and binding mode to the RL19. However, the former is a diazole and not a chromeno and the phenyl ring contains a hydroxyl group instead of a fluor. The **S** enantiomer exhibits a more concerted conformation (Tab. S1), forming hydrogen bonds with Arg233, Glu102 and with the heme carboxylate (Fig. 1C). Pi stacking interactions are observed between the diazole ring and the heme π system, as well as with the Phe401 by the methoxyphenol portion. RL24 compound is a chiral chromeno derivative that has significant analogy with RL19. The RL24 **R** enantiomer is the most favorable to interact with MPO active site (Tab. S1). As for RL19, RL24 also forms hydrogen bond with His95, but the hydroxyl group is phenolic in the latter, whereas is an alkyl hydroxyl in the former. This phenol hydroxyl forms hydrogen bond with Gln91. RL24 also interacts through hydrogen bonds with Arg233 and Glu102 by the oxygen heteroatom from the chromeno ring and by the amino group, respectively. A sandwich π stacking interaction is observed between the heme π system and the chromeno ring. RL26 inhibitor is a tadpole-shaped molecule that exhibits a symmetrical thiopyran ring functionalized with two amino and nitriles groups. This molecule forms one hydrogen bond with Glu102 and, considering the motion in solution, can potentially form other two hydrogen bonds with heme carboxylates and Arg233. One symmetric nitrile group performs an unfavorable contact with *tau* nitrogen in His95. Furthermore, the phenyl ring bonded to thiopyran exhibits a π stacking interaction with Phe401 in T-shape angle. The aromaticity of the thiopyran ring might also interact with the heme π system. The hydrophobicity of the propyl chain in RL26, which is accommodated in a pocket between the Arg233 and Phe401, can contribute to complex stabilization. The last inhibitor, compound RL27, displays a structural similarity with the known MPO inhibitors thioxanthines (35). In spite of this similarity, RL27 has the differential of a hydrazyl group and the thiofuran as the five-members ring. Furthermore, this molecule can be represented by **R** and **S** enantiomers and by a thiol/thione tautomer. Molecular docking studies indicate that the **S** enantiomer - thiol tautomer exhibits the best binding energy to MPO active site (Tab. 1).

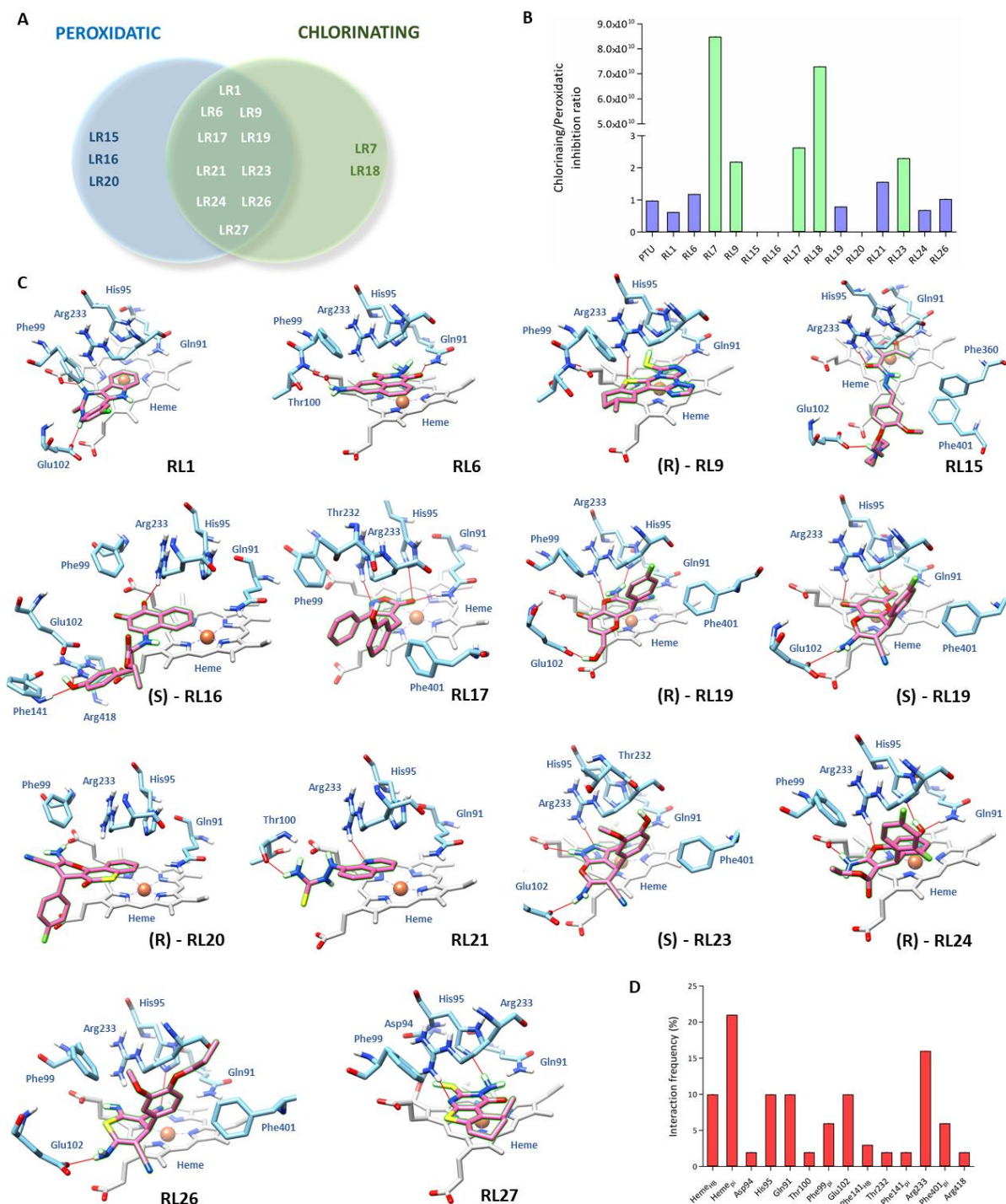


Fig. 1. Inhibitors discovered by virtual screening and their binding modes obtained from molecular docking. (A) Venn diagram showing the active compounds in the peroxidase and chlorinating tests. **(B)** Chlorinating/peroxidatic activity inhibition ratio of the compounds. **(C)** Binding mode of the compounds showing the major interactions with MPO active site. Residues are shown in blue, heme group in grey and ligands in pink. Hydrogen bonds and polar contacts are shown as red lines. For racemic compounds the enantiomer is identified. Molecular docking simulation was performed using AutoDock4 program and MPO structure PDB 1CXP. The grid box was configured to 36 x 40 x 40 Å and centralized at 24.123 × 3.191 × 43.257 coordinates. The Lamarckian Genetic algorithm was run 100 times to each ligand. **(D)** Frequency of interactions involved in the inhibitors binding mode.

Inspection of the MPO-RL27 complex reveals hydrogen bonds with Arg233 and His 95 residues. Similarly to RL6 compound, the **N-NH₂** group in RL27 is oriented as seen for hydrogen peroxide and hydroxamates (33, 34). The proximity between the thiol and the carbonyl group of Asp94 suggests a hydrogen bond during protein dynamics. Molecular docking of RL27 also indicates a sandwich π stacking interaction with heme π group.

Finally, interaction frequency analysis indicates that π stacking with heme group is the most frequent interaction (Fig. 2D), representing 21% of total interactions, followed by 16% hydrogen bonds with Arg233, heme, His95, Gln91 and Glu102. *Pi* stacking with Phe99 and Phe401 represents 6% and other interactions represent 2-3% (Asp94, Thr100, Phr141_{HB}, Thr232, Phe141_{pi}, Arg418).

RL6 is a nanomolar reversible inhibitor

The inhibitors potency was measured by plotting IC₅₀ curves for those compounds that inhibited the chlorinating activity around 70% when at 20 μ M.

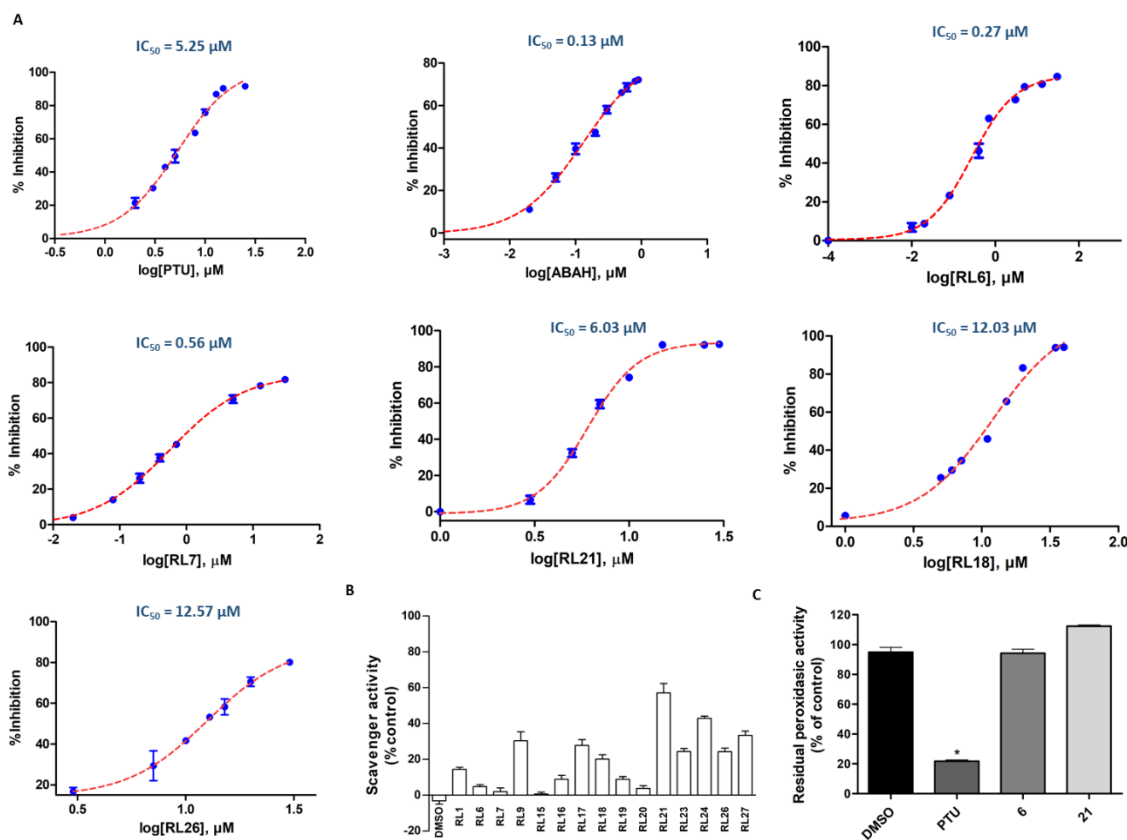


Fig. 2. Potency and action mechanism of MPO modulators. (A) Dose-response curve showing the IC₅₀ values for compounds PTU, ABAH, RL6, RL7, RL18 and RL21 in chlorinating assay. (B) Taurine chloramine scavenger activity. Taurine chloramine was produced by mixing HOCl (2.81 mM) with taurine (5 mM) in phosphate buffer (20 mM, pH 7.4) in presence of NaCl (140 mM), DTPA (100 μ M) and CTAC (0.03%). After 5 min of reaction, the compounds were added and incubated at 37° by 15 minutes. The remaining taurine chloramine was detected by TMB oxidation as previously described. (C) Residual peroxidatic activity showing the inhibition reversibility. Compounds RL6 and RL21 (20 μ M) were incubated in phosphate buffer (20 mM, pH 7.4), MPO (100 nM), CTAC 0.03% and hydrogen peroxide (40 μ M) at 37°C during for 30 minutes. After dilution (200-fold), the residual peroxidatic activity was measured by TMB at 655 in presence of new hydrogen peroxide buster (2 μ M). Bars represent the mean \pm S.E.M of three independent experiments (n = 3). Statistical analysis was performed using one-way ANOVA, followed by Bonferroni posthoc test. * Indicates statistically different (p < 0.01) compared to the control group (DMSO).

RL6 and RL7 exhibited IC_{50} in the nanomolar range (Fig. 2A). With an IC_{50} equal to 270 nM, RL6 was the most potent compound. It did not scavenge taurine chloramine (Fig. 2B), suggesting it as a true enzyme inhibitor. In agreement, RL6 presented a chlorinating/peroxidase activity ratio close to 1 (Fig. 1B). The second most potent inhibitor, RL7, had an IC_{50} equal to 560 nM, but differently from RL6, it might be a HOCl scavenger because the inhibition of the chlorinating activity was much higher than the peroxidatic one (Fig. 1B). RL21 and RL26 presented IC_{50} of 6.03 and 12.57 μ M, respectively. These values were attributed to both enzyme inhibition and scavenger activity, since they decreased taurine chloramine (Fig. 2B) but also inhibited MPO peroxidatic activity (Tab. 1 and Fig. 2B). RL18 compound had an IC_{50} equal to 12.03 μ M that was exclusive to a scavenger capacity (Fig. 2B), considering that it did not inhibit MPO peroxidatic activity (Tab. 1, Fig. 1B). After diluting samples to IC_{50} determination, compound RL9 was the only one to lose inhibitory activity (data not shown), a common behavior of aggregation, even though the samples contained 0.03% CTAC. The dose-response curve and IC_{50} calculations were validated using two known MPO irreversible inhibitors: PTU and ABAH. The calculated IC_{50} was 5.25 and 0.13 μ M, respectively (Fig. 2A), much close to those already reported, 3.38 and 0.30 μ M, respectively (36, 37).

Inhibition reversibility of the most potent compounds RL6 and RL21, among the four compounds, was evaluated by diluting samples and testing MPO residual activity. Reversible inhibitors dissociate from the enzyme and the latter recovers activity (38, 39). This is not the case for PTU, which permanently inactivated the enzyme (Fig. 2C). Both inhibitors, RL6 and RL21, lost effect after dilution, revealing a reversible inhibition mode (Fig. 2C). Reversible inhibitors are of particular interest since they usually have lower toxicity. RL6 is special because it has a potency higher than PTU and similar to ABAH, both known MPO irreversible inhibitors (Fig 2A).

Although other information can be obtained from dose-response curves, such as number of interacting site, multiple ligand binding and promiscuous inhibitor aggregators (40, 41), Hill fit parameter analysis did not distinguish between true inhibitors and scavengers agents (data not reported).

RL6 and RL7 are not consumed by the MPO

We next evaluate whether RL6 and RL7 would be oxidized by MPO or by HOCl. Fluorescence spectra indicated the excitation and emission wavelengths for monitoring the consumption of both compounds (Fig. S4). The other constituents of the system MPO, DMSO and hydrogen peroxide do not have relevant fluorescence at the wavelengths selected for excitation/emission (Fig. 3). RL6 concentration does not decay in the presence of hydrogen peroxide and MPO, suggesting that it is not oxidized by the enzyme (Fig. 3A). However, RL6 could be a substrate for MPO compound I but not for compound II, trapping the enzyme as the compound II intermediate, similarly as occurs with tryptophan (42). RL6 was not consumed by MPO in presence of chloride as well (Fig. 3B), confirming that the compound is not a HOCl scavenger (Fig. 2B). Although absence of RL6 consumption strongly suggests an inhibition mechanism independent of compound oxidation, MPO spectrum in presence of the compound should be performed to confirm it.

To best explain the high potency of RL6 reversible inhibitor compared to ABAH, an aromaticity study using DFT (density functional theory) was conducted to quantify the importance of this property to the binding. For this, the aromaticity index HOMA (harmonic oscillator model of aromaticity) was calculated (43). Interestingly, the total HOMA value for RL6 aromatic rings was 1.6364, a value higher than that observed for the ABAH, 0.9456, indicating that naphthalimide ring in RL6 exhibits more aromaticity, which can contribute to π stacking interactions with the heme π system and, consequently, to RL6 potency.

Differently from RL6, RL7 underwent a slight spontaneous fluorescence decrease but it was not influenced by hydrogen peroxide/MPO (Fig. 3C). However, RL7 was further consumed in the full reaction system in presence of chloride (Fig. 3F). This data supports a scavenger role for RL7, in accordance with the high chlorinating/peroxidatic activity ratio (Tab. 1 and Fig. 1B). Since RL7

did not scavenge taurine chloramine, it likely reacts with HOCl directly. We then incubated 20 μM RL7 with 250 μM HOCl using stopped flow to follow fluorescence decay in a millisecond scale. A spontaneous linear decrease of RL7 fluorescence was seen within 1 s and an exponential decay was observed upon incubation with HOCl (Fig. 3E and F), indicating that this compound rapidly reacts with HOCl. RL7 contains several amino groups that can react with HOCl to form chloramines derivatives. In addition, this molecule exhibits a sulfur atom into the thiophene ring, which can be oxidized generating oxo and/or dioxo derivatives. All these functional groups can explain the high scavenger capacity of RL7 against HOCl.

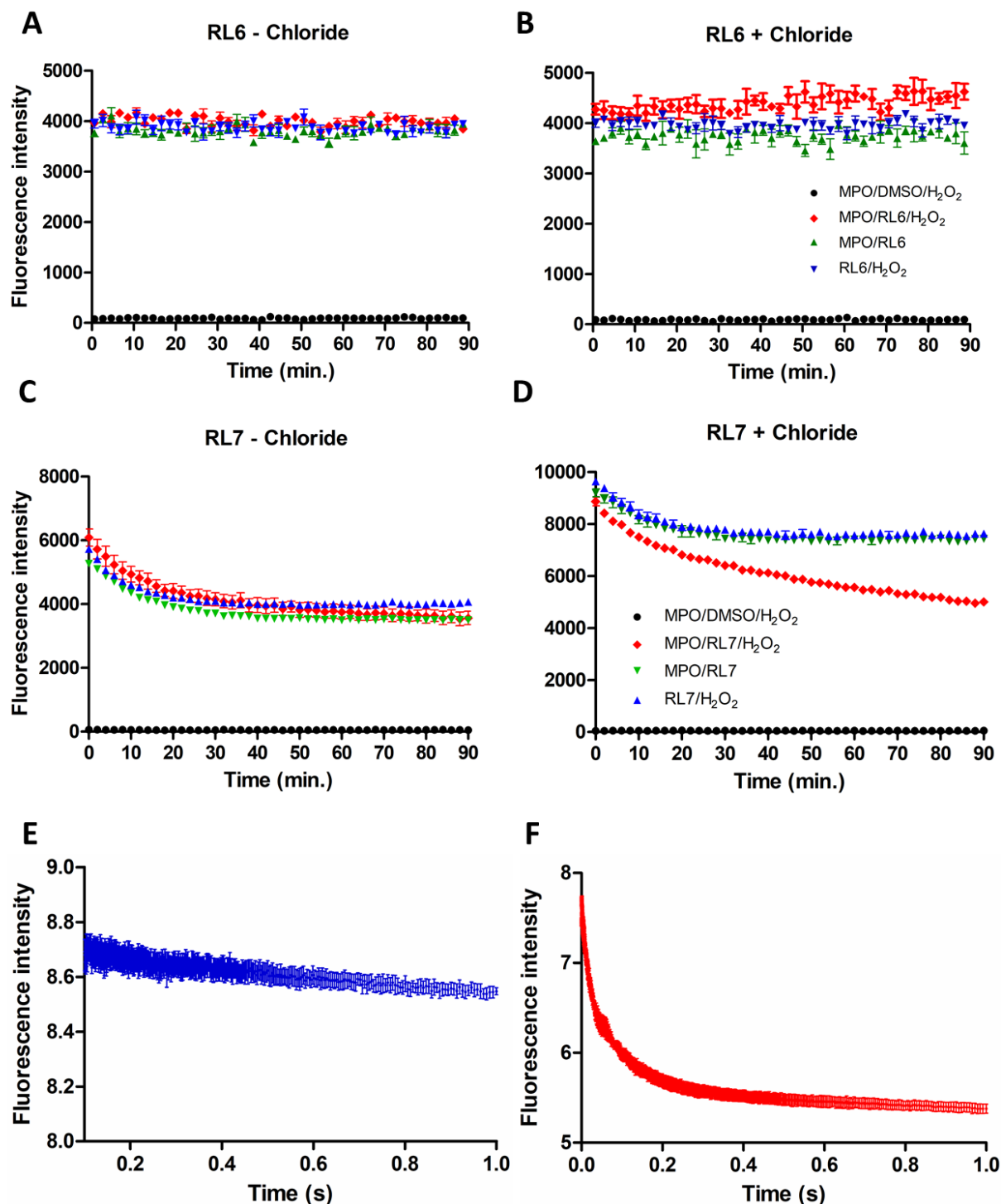


Fig. 3. Evaluation of RL6 and RL7 consumption by fluorescence decay. (A-B) RL6 and (C-D) RL7 fluorescence in absence or presence of chloride. Fluorescence decay of 1 μM RL6 (λ_{ex}

= 347, λ_{em} = 413 nm) or 1 μ M RL7 (λ_{ex} = 306, λ_{em} = 376 nm) was assessed in a medium containing phosphate buffer (20 mM, pH 7.4), MPO (10 nM), with or without NaCl (140 mM), CTAC 0.03%, DTPA (100 μ M), taurine (5 Mm) and H₂O₂ (40 μ M). For chloride free systems the CTAC was replaced by CTA bisulfate. Fluorescence of (E) RL7 alone or (F) in presence of 250 μ M HOCl was assessed by stopped flow at λ_{ex} = 306, λ_{em} = above 340 nm in phosphate buffer (20 mM, pH 7.4), NaCl (140 mM) and DTPA (100 μ M) up to 1 second. Kinetics represent the mean \pm S.E.M of three independent experiments (n = 3).

MPO inhibitors decrease NETosis and HOCl production by dHL-60 cells and neutrophils

RL6, RL7 and RL21 significantly inhibited HOCl production by cultured neutrophil-like dHL-60 cells and by peripheral blood neutrophils, whereas RL18 displayed no effect (Fig. 4B). Since in PMA-induced oxidative burst the oxidants are produced in the extracellular milieu, the inhibition or not is not related to a more or less permeability to cell membrane. The absence of RL18 effect in this assay could be explained by an exclusive scavenger activity rather than a direct enzyme inhibition. Even though scavenger of HOCl was also the main effect of RL7, this compound was about 20-fold more potent than RL18 (Fig. 2A). As expected, the irreversible inhibitor PTU was the most efficacious to counteract HOCl by both cell types (Fig. 4B).

The cell active compounds RL6, RL7, RL21 and ZINC9089086, this last a previously described MPO inhibitor in dHL-60 and neutrophils (27), were tested against the release of neutrophil extracellular traps (NETs). NETosis is a cell death process where neutrophils release their DNA material together with degranulation to trap and kill extracellular microorganisms (44). NETosis has been described as an important mechanism of tissue damage in aseptic conditions (45). In addition, MPO activity has an important role in NETosis progression (14). Therefore, MPO inhibitors are putative anti-netotic agents contributing to an anti-inflammatory effect (46). Several aseptic conditions can trigger NETosis, urate crystals are a classical one (47). In our hands, incubation of human neutrophils with monosodium urate crystals (MSU) induced nuclear decompaction and formation of large DNA nets (Fig. 4A). The netotic process was strongly inhibited by MPO inhibitors PTU, RL6 and RL21. The HOCl scavenger RL7 exhibited a notorious anti-netotic effect. Although urate crystals-induced NET has been described as a redox species-independent mechanism (47), HOCl seems to contribute to this process. These data are in agreement with the inhibition of PMA-induced NETosis by the MPO inhibitor ABAH (47).

The MPO inhibitor ZINC9089086 previously reported by our group (27) was ineffective to inhibit NETs formation. These results indicate that MPO inhibitors and HOCl scavengers can be good approaches to remedy NETosis process, being an additional mechanism to counteract inflammation.

RL6 does not inhibit PARP1

To analyze possible off-target biological effects, a literature review was carried out for the most potent compounds RL6 and RL7. This analysis revealed that the compound RL7 was initially synthesized as an antiviral agent against dengue. However, it had low potency (48). The inhibitor RL6 is a 1,8-naphthalimide derivative and this chemical class is known for diverse biological activities, including anticancer, antibacterial, antiviral and antiprotozoal (49). A 1,8-naphthalimide derivative, named 4ANI, was reported as a potent PARP1 inhibitor, with a IC₅₀ equal to 180 nM (50). PARP1 belongs to a family of proteins that are involved in DNA repair and genomic stability maintenance (51). Although PARP1 inhibition may contribute to anti-inflammatory effects (52), many toxic effects are associated with inhibition of this class of enzymes (53). Considering the high similarity between RL6 and 4ANI structures (Fig. S3A), molecular docking simulations were conducted to compare their binding mode to the PARP1 active site. After a proper redocking, 4ANI showed hydrogen bonds with Gly863 and Glu988, as well as π stacking interactions with His862, Tyr896 and Tyr907 (Fig. S3B-left), whereas RL6 presented a \sim 45° rotation in the 1,8-naphthalimide plane, a non-analogous hydrogen bond with Gly863, but maintained the same π stacking

interactions (Fig. S3B-right). Additionally, RL6 presented two conformational clusters against one in 4ANI. However, RL6 has a better binding energy. The different binding mode could be attributed to the presence of an extra amino in the hydrazyl group and in the different position of the amino group from the naphthalimide ring. These changes excluded hydrogen bonds with Glu988 and modified the optimal interactions with Gly863. They also discretely increased molecular dimensions and modified the molecular shape. Inhibition of PARP1-induced ADP-ribosylation by RL6 was assessed after incubating RPE1-hTERT cells with H₂O₂. RL6 (1 μ M, 10 μ M and 50 μ M) was not able to inhibit H₂O₂-induced ADP-ribosylation, whereas the known PARP1 inhibitor, Olaparib, significantly decreased it (Fig. S3C and D). These proved that, despite the similarity between 4ANI and RL6 molecules, PARP1 is not a RL6 off-target and that this similarity is not enough to cause side-effects. Although the RL6 compounds did not inhibit PARP1, this molecular target must be taken into account in the development of selective MPO inhibitors.

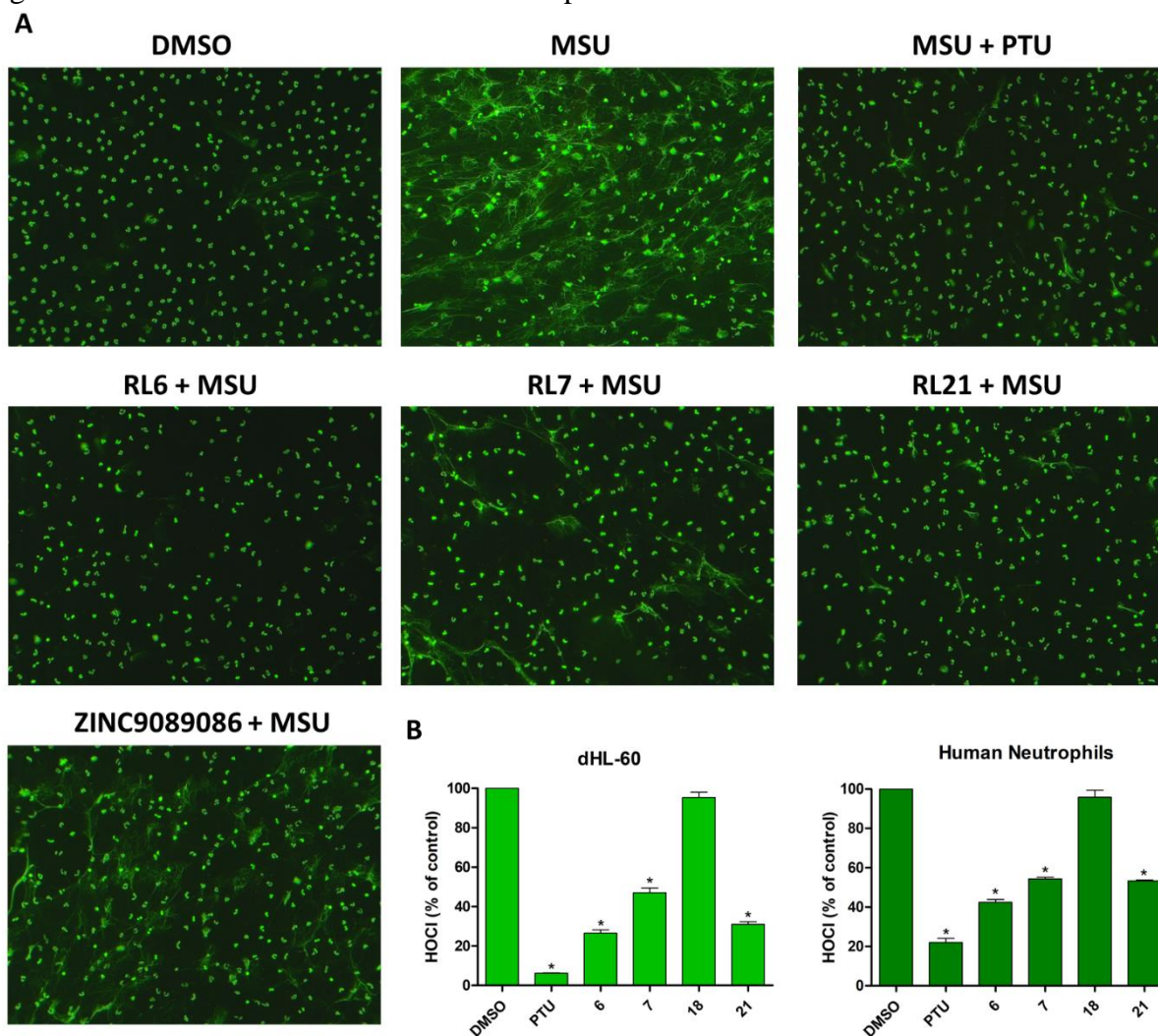


Fig. 4. MPO inhibitors decrease NETosis and HOCl production in cells. (A) Fluorescence microscopy of DNA stained with Sytox green stimulated with monosodium urate crystals (MSU). DMSO (MPO inhibitors vehicle) was used as control. Human neutrophils adhered to lysine-coated surface were incubated with the compounds (20 μ M) in RPMI medium at 37°C in a 5% CO₂ atmosphere by 15 minutes, followed by addition of MSU crystals (250 μ g/mL). After 90 minutes, the medium was removed and cells were fixed with paraformaldehyde (4%) overnight. After fixation, the paraformaldehyde was removed and washed with tris-HCl buffer (20 mM, pH 7.4). DNA was stained by Sytox green (500 nM) and lamina mounted with ProLong for images acquisition. (B) Inhibition of HOCl production from dHL-60 cell line (left) or human peripheral blood neutrophils (right). dHL-60 or human neutrophils (10^6 cells) were incubated in PBS (10

mM Na₂HPO₄, 2 mM KH₂PO₄, 0.5 mM MgCl₂, 1 mM CaCl₂, 140 mM NaCl, 5.5 mM dextrose) containing DTPA (100 μM), taurine (5 mM) and tested compounds (20 μM) and activated with PMA (100 nM) at 37° by 1 h. After incubation, taurine chloramine was measured by TMB method. Inhibition is relative to HOCl production in control (DMSO). Statistical analyses were performed by one-way ANOVA followed by Bonferroni's post-hoc, * p < 0.01 from vehicle. Bars represent the mean ± S.E.M of three independent experiments (n = 3).

***In vivo* candidates have good theoretical ADME/Tox profile**

To analyze the toxicological potential of RL6, RL7, RL21 and ZINC9089086 before animal studies, we evaluated several theoretical toxicological and pharmacokinetics parameters. Interestingly, all compounds exhibited a high gastrointestinal absorption and bioavailability scores. RL7 only is a potential substrate for P-gp, a glycoprotein that pumps out xenobiotics, decreasing absorption and bioavailability (54). Only ZINC9089086 showed potential to cross the blood-brain barrier, suggesting that this molecule could be used in neuroinflammation. Regarding toxicological indicators, ZINC9089086 presented the best security profile with absence of cardiotoxicity, cytotoxicity, carcinogenicity, immunogenicity, hepatotoxicity and a high LD₅₀. Compounds RL6 and RL21 exhibited potential to carcinogenicity and hepatotoxicity. RL7 was the second compound with the lowest toxicological potential, presenting only cardiotoxicity, as indicated by hERG inhibition and it was the only one with low LD₅₀ (10 mg/kg) (Table 4). Thus, ADME/Tox analysis indicates that, to exception of RL21, all compounds have a good profile for *in vivo* studies.

Table 4. Theoretical ADME/Tox potential for *in vivo* candidates

	RL6	RL7	RL21	ZINC9089086
GI absorption	High ^a	High ^a	High ^a	High ^a
P-gp substrate	No	Yes	No	No
Bioavailability score	0.55	0.55	0.55	0.55
BBB permeant	No	No	No	Yes
hERG inhibitor	No (0.66) ^b	Yes (0.50) ^b	No (0.60) ^b	No (0.60) ^b
Cytotoxicity	No (0.71) ^b	No (0.59) ^b	No (0.80) ^b	No (0.79) ^b
Carcinogenicity	Yes (0.77) ^b	No (0.55) ^b	Yes (0.50) ^b	No (0.51) ^b
Immunogenicity	No (0.82) ^b	No (0.99) ^b	No (0.95) ^b	No (0.99) ^b
Hepatotoxicity	Yes (0.55) ^b	No (0.57) ^b	Yes (0.72) ^b	No (0.61) ^b
LD ₅₀ (mg/kg)	1300 mg/kg	1000 mg/kg	10 mg/kg	3000 mg/kg

^a Probability of F > 10 % in rat; GI – gastrointestinal; BBB – brain-blood barrier; P-gp – Glycoprotein-P; hERG - human ether-a-go-go related gene. ^b Probability for respective biological effect.

MPO inhibitors and the HOCl scavenger decreased MSU-induced paw edema in mice

Finally, to confirm that MPO inhibition by the compounds would extend to an anti-inflammatory effect *in vivo*, RL6, RL7, RL21 and ZINC9089086 were tested in a MSU-induced gouty arthritis murine model (19). Intraplantar injection of MSU induced an increase in paw volume in vehicle pretreated animals (VEH + MSU: 0.29 ± 0.03 mL), when compared to the animals that received vehicle via intraplantar (VEH + VEH: 0.07 ± 0.02 mL) (Fig. 5). The time-dependent edema had a similar profile to that previously reported (19), with an inverted V-shape. In our hands though, the maximum edema occurred at the 4th hour instead of the 6th. The intraperitoneal treatment with 30 mg/Kg NSAID mefenamic acid (positive control) prevented paw edema up to 4h (Fig 5A). RL6, 10 and 30 mg/Kg prevented paw edema during all 5h and the compound was also effective at the 3 mg/kg dose (Fig 5B).

The HOCl scavengers, RL7 and RL21, and the previously described MPO inhibitor, ZINC908908, also inhibited paw edema at all tested dose. For RL7, the lowest dose tested (0.3 mg/Kg) had a punctual significant effect only at the peak of the paw edema (4th hour). The compound was effective from 1 to 4 hours at 3 and 30 mg/Kg (Fig 5C). For RL21 and ZINC908908 all tested doses were effective up to 4 hours and the highest dose, 30 mg/Kg, also inhibited edema in the 5th hour (Fig 5D).

Time-dependent area under the curve revealed that mefenamic acid (30 mg/Kg) reduced paw edema by 67.6% when compared to the “VEH + MSU” group. RL6 significantly decreased paw volume by 59.6% and 61.7% at 10 and 30 mg/Kg, and RL7 by 61.4% and 66.9% at 3 and 30 mg/Kg. RL21 was the most effective as it decreased paw edema by 90% at 30 mg/Kg. ZINC908908 displayed a significant effect only at the highest dose, 30 mg/Kg, reducing by 69.3% paw edema (Fig 5F).

We then selected the highest dose of the compounds to test their inhibitory effect when administered by gavage. By being effective through this route, it would be possible to confirm that by filtering compounds using Lipinski/Veber parameters is indeed a good way to recover molecules with suitable oral bioavailability (27). For a better comparison, the dose of the compounds was adjusted to an equimolar concentration. RL21 was adopted as the reference compound since it promoted the best antiedematogenic effect. As expected, the intraplantar administration of MSU increased paw volume (VEH + MSU: 0.29 ± 0.02 mL) in vehicle pretreated animals (v.o.) compared to the “VEH+VEH” group (0.07 ± 0.01 mL). Compounds RL6, RL7, RL21 and the positive control, mefenamic acid, inhibited edema by 43.4, 50.6, 52.2 and 58.9% compared to the “VEH + MSU” group (Fig. 6). However, ZINC908908 displayed no significant inhibition. It is noteworthy to mention that RL6, RL7 and RL21 were not structurally modified to optimize parameters such as solubility, lipophilicity and metabolic stability, which directly impact on bioavailability and consequently therapeutic suitability. Additionally, none of the compounds tested caused animal death or noticeable symptoms of acute toxicity, though no specific studies were used for this purpose.

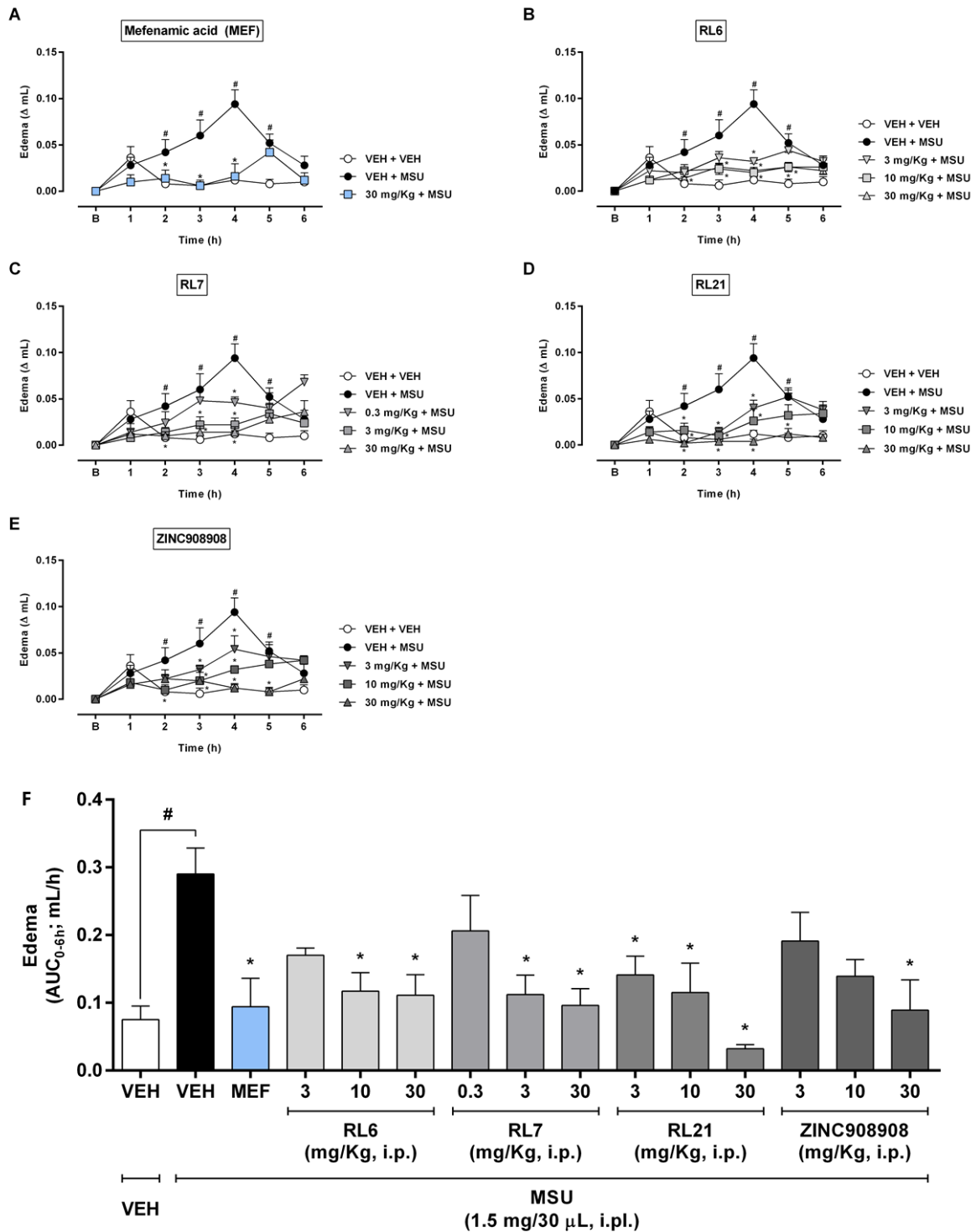


Fig. 5. Antiedematogenic effect of MPO-inhibitors and HOCl scavengers in monosodium urate (MSU)-induced paw edema. Mice were pretreated with vehicle (VEH: 5% DMSO; 0.5% tween 80 in PBS, i.p.), mefenamic acid (A, MEF: 30 mg/Kg, i.p.), RL6 (B, 3, 10 and 30 mg/Kg, i.p.), RL7 (C, 0.3, 3 and 30 mg/Kg, i.p.), RL21 (D, 3, 10 and 30 mg/Kg, i.p.) or ZINC908908 (E: 3, 10 and 30 mg/Kg, i.p.). After 30 min, mice received vehicle (VEH: PBS, 30 μL, i.pl.) or MSU (1.5 mg/30 μL, i.pl.). Paw volume (mL) was evaluated before (B, baseline), and after pretreatments for 6 h. Statistical analyses were performed by two-way ANOVA followed by Bonferroni's post-hoc * $P < 0.05$ compared to the "VEH + VEH" group; * $P < 0.05$ comparing to the "VEH + MSU" group, $n = 5$ /group.

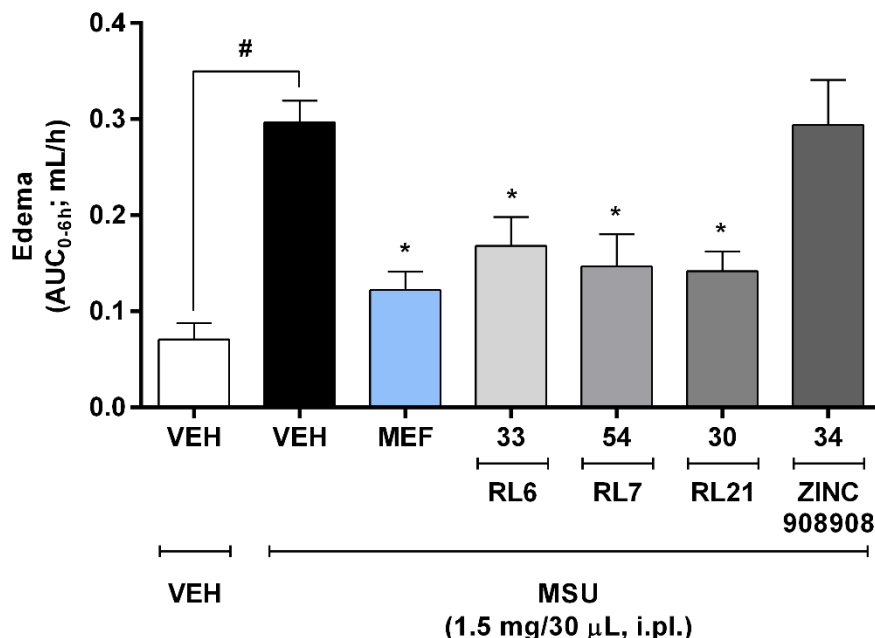


Fig. 6. Antiedematogenic effect of the gavage administration of MPO-inhibitors and HOCl scavengers in monosodium urate (MSU)-induced paw edema. RL6 (33 mg/Kg), RL7 (54 mg/Kg), RL21 (30 mg/Kg) and ZINC908908 (34 mg/Kg). After 30 min, mice received vehicle (VEH: PBS, 30 μ L, i.pl.) or MSU (1.5 mg/30 μ L, i.pl.). Paw volume (mL) was evaluated before (B, baseline), and after pretreatments for 6 h. Statistical analyses were performed by two-way ANOVA followed by Bonferroni's post-hoc [#] $P < 0.05$ compared to the "VEH + VEH" group; * $P < 0.05$ comparing to the "VEH + MSU" group, $n = 5$ /group.

DISCUSSION

In this work we demonstrated that the use of the MPO inhibitor-like rule together with structure-based virtual screening is a golden approach to the discovery of potent MPO inhibitors with *in vivo* anti-inflammatory action. Validation of the structure-based virtual screening including the alignment of new MPO crystal structures confirmed the low residues flexibility in the active site (27). In addition, the calculation of charges from heme atoms by PM7 Hamiltonian was a good approach to recover ligands experimental conformations in cross-docking validation simulations. The confirmation of the validation of this methodology allowed us to reanalyze a sub-library that satisfies the MPO inhibitor-like rule previously described by our group (27). This reanalysis allowed selecting 18 putative inhibitors with high chemical diversity not previously described.

This methodology proved to be robust considering that most of the compounds were active both in the chlorinating and peroxidatic activities assay, exhibiting one of the highest hit rates reported in the search for MPO inhibitors (66% and 72%, respectively) and validating our previous results (23–27). These high success rate can be attributed to the use of a methodology validated both at the level of ranking and molecular docking (55), as well as to experimental knowledge about the enzymology of MPO included in the inhibitor-like rule determination (27). The computational hits validation through chlorinating and peroxidatic activities proved to be valuable for the detection of HOCl scavengers, considering that a high chlorinating/peroxidatic ratio strongly suggests a predominant or exclusive HOCl scavenger activity. Although the present methodology is not free from scavengers, its high certainty rate demonstrates its predictive capacity for the discovery of new MPO inhibitors.

The inspection of new backbone hits indicates that MPO inhibitor-like rule is an efficient approach for discovering new structurally diverse inhibitors. Although this rule was developed from

known inhibitors (27), unlike pharmacophoric models (25, 26), the use of molecular descriptors in the elaboration of inhibitor-like rule allows the characterization of the MPO chemical space without compromising the chemical diversity. In addition, MPO inhibitor-like rule demonstrated to be capable of performing bioisosteric approaches. For instance, RL6, mirrors the known inhibitor ABAH and RL21 results from the acyclization of the thiouracil ring.

Molecular docking indicates that π stacking interactions with heme group from MPO active site represent the most common interaction. It is followed by hydrogen bond formation with Arg233, heme carboxylate, His95, Gln91 and Glu102. Of note, hydrogen bond with Arg233 had not been reported in previous studies as a frequent interaction between inhibitors and MPO active site (24, 26, 27, 56). This unusual type of interaction suggests that the employed methodology recovers inhibitors with different binding modes. Molecular docking simulations also showed that five inhibitors, RL9, RL20, RL21, RL26 and RL27, exhibit a sulfur atom between the heme carboxylate, near to Glu102 and Thr100 residues. This finding suggests that this region of the active site has a stereochemical complementarity for sulfur. In accordance with this data, the presence of sulfur has been implicated in the high binding potency reported in the biotin-avidin complex (57). This information could be better explored for planning more potent and selective MPO inhibitors.

The formation of π stacking interactions and several hydrogens bonds, including an orientation near to His95 that mimics the transition state observed in hydrogen peroxide-MPO (33), explains the nanomolar potency observed for RL6. Additionally, aromaticity index HOMA revealed higher aromaticity of RL6 compared to ABAH. This property corroborates the nanomolar potency of RL6 because it favors the binding and permanency of the compound within MPO active site.

The discovery of new MPO inhibitors confirm that the inhibitor-like rule is a useful approach not only for the discovery of active compounds in enzymatic systems, as well as to recover active compounds in neutrophil-like HL-60 cells and human neutrophils. A high success rate (75 %) was achieved in cell assays. Furthermore, this methodology discovered molecules that inhibit NETosis cell death. Besides *in vitro* activity, all four tested compounds have antiedematous effect in an MSU-induced gout arthritis model when administered intraperitoneally. When given orally, three of the four had anti-edematous effects in this model of inflammation, confirming that the inhibitor-like MPO rule recovers compounds with privileged pharmacodynamic and pharmacokinetic properties. Although HOCl scavengers are highlighted as interferers in screening pipeline, we have demonstrated that both a true MPO enzyme inhibitor and HOCl scavenger may be promising pharmacological approaches for inflammation, in special for reducing edema in gouty arthritis.

Finally, the integration of an inhibitor-like rule and structure-based virtual screening demonstrated a gold methodology to search for orally active MPO inhibitors and the application of this methodology to new databases, such as ZINC20, will propitiate a better exploration of chemical space and help to uncover new diversified preclinical candidates.

MATERIALS AND METHODS

Virtual screening

A virtual sub-library composed by 242 potential MPO inhibitors was used for the selection of compounds. This set was obtained from our previous studies using the Zinc12 database containing more than 35 million compounds. The library was filtered by an inhibitor-like rule and docked into MPO active site using the GOLD version 5.4 molecular docking program (27). The molecular docking methodology was re-evaluated through the alignment of new reported MPO structures (PDB 5QJ2, 5QJ3, 6WXZ, 6WY0, 6WY5, 6WY7, 6WYD, 7LAE, 7LAG, 7LAL and 7LAN) using Pymol 1.8 and Chimera 1.10.1 visualization programs. The alignment of MPO structures was used to re-evaluate the presence of conserved water molecules and the flexibility of active site residues by visual inspection. The protonation and conformation of active site residues in PDB 1CXP were adjusted as well as the atomic charges of the heme group, which were calculated by the PM7

Hamiltonian as recently published (27). Molecular docking simulations with AutoDock 4.2.3 was re-evaluated by cross-docking using PDB 7LAG and 7LAN ligands and docked into PDB 1CXP MPO active site as previously described (27). The refRMS (**reference Root Mean Square**) values between the poses and the experimental conformations was calculated by AutoDock 4.2.3. The computational hits were selected using the followed criteria: hydrogen bonds number, presence of π stacking interactions, histogram profile and binding energy (27). The lower energy conformation inside the most populous cluster was used to select the bioactive pose to be analyzed.

Chlorinating activity assay

Chlorinating activity was carried out in phosphate buffer (20 mM, pH 7.4). Compounds (20 μ M) were dissolved in 0.03% DMSO, MPO (10 nM), diethylenetriaminepentaacetic acid (100 μ M), cetyltrimethylammonium chloride (0.03%), NaCl (140 mM) and taurine (5 mM) (27). This mixture was incubated at 37°C for 15 minutes before adding 40 μ M hydrogen peroxide. The reaction run for 8 minutes and was then stopped by catalase (20 μ g/mL). Oxidation of TMB (3,3,5,5-tetramethylbenzidine) by taurine chloramine catalyzed by iodide was quantified at 650 nm (29). Results were expressed as percentage of the control (vehicle). IC₅₀ was calculated by non-linear regression using the Hill equation present in GraphPad Prism 5 software.

Peroxidatic activity assay

MPO peroxidase activity was kinetically monitored using the artificial peroxidase substrate AmplexRed®, which is oxidized to resorufin and can be detected by fluorescence (30). Reactions were carried out in phosphate buffer (50 mM, pH 7.4), MPO (100 pM), cetyltrimethylammonium chloride (0.03%), diethylenetriaminepentaacetic acid (100 μ M), AmplexRed (30 μ M) and compounds (20 μ M in 0.3% DMSO). The reaction started by adding 2 μ M hydrogen peroxide. The reaction product was assessed by fluorescence $\lambda_{ex} = 530$ nm, $\lambda_{em} = 580$ nm. The initial velocity was calculated by the slope of the linear regression at the first minutes of reaction. Inhibition is represented as percentage of the control (vehicle).

Taurine chloramine scavenger assay

Taurine chloramine was prepared by mixing hypochlorous acid (2.81 mM) with taurine (5 mM), cetyltrimethylammonium chloride (0.03%), NaCl (140 mM), diethylenetriaminepentaacetic acid (100 μ M) in phosphate buffer (20 mM, pH 7.4). The system was kept at 37°C for 5 minutes for complete chloramine taurine formation. The compounds were added to this mixture and incubated for 15 minutes at 37°C. Taurine chloramine was quantified by oxidation of TMB catalyzed by iodide (29).

Reversibility test

Reversibility of the inhibition was analyzed by peroxidase residual activity (39). MPO (100 nM) was incubated with inhibitors (20 μ M, 0.33% DMSO) in phosphate buffer (20 mM, pH 7.4) containing cetyltrimethylammonium chloride (0.03%) and hydrogen peroxide (40 μ M) at 37°C for 30 minutes. After incubation, the system was diluted 200-fold using acetate buffer (200 μ M, pH 5.4) in presence of TMB (2 mM dissolved in 10% dimethylformamide). After a new hydrogen peroxide addition (2 μ M), oxidation of TMB was quantified at 655 nm.

Kinetics for the oxidation of the compounds

Before kinetic studies, the absorption and fluorescence spectra of RL6 and RL7 were determined. RL6 and RL7 (1 μ M in 0.3% DMSO) were incubated in phosphate buffer (20 mM, pH 7.4), in presence of MPO (10 nM), diethylenetriaminepentaacetic acid (100 μ M), taurine (5 mM), cetyltrimethylammonium chloride (0.03%) and NaCl (140 mM). In the chloride free system, NaCl was omitted and cetyltrimethylammonium chloride was replaced by cetyltrimethylammonium bisulfate. The reaction was started by adding 40 μ M hydrogen peroxide. RL6 and RL7 consumption was monitored by fluorescence using specific excitation/emission wavelengths (RL6_{347/413 nm} and RL7_{306/376 nm}) in a microplate reader.

The fast oxidation of RL7 was monitored in a stopped-flow spectrophotometer (Applied Photophysics SX-18MV) using the intrinsic RL7 fluorescence ($\lambda_{ex} = 306$ nm, $\lambda_{em} =$ above 340 nm).

The reaction of RL7 (20 μM in 0.3% DMSO) with HOCl (250 μM) was performed in phosphate buffer (20 mM, pH 7.4), diethylenetriaminepentaacetic acid (100 μM) and NaCl (140 mM). Data were obtained within 1 second.

HOMA calculation

The geometry of RL6 and ABAH were optimized by the B3LYP/6-31G(d) method. The aromatic index HOMA (harmonic oscillator model of aromaticity) was calculated using Multiwfn 3.8 software (58).

Cell culture

Human promyelocytic leukemic cells (HL-60) (BCRJ, RJ, Brazil) were cultivated in RPMI with fetal bovine serum (10%), penicillin (62 $\mu\text{g}/\text{mL}$), streptomycin (100 $\mu\text{g}/\text{mL}$) at 37°C in 5% CO_2 atmosphere. HL-60 cells were differentiated to neutrophil-like (dHL-60) by DMSO (1.25%) during 4 days (59).

Peripheral blood neutrophils

Human neutrophils were obtained from healthy individual (60). The experiments were approved by the local ethic committee (CEPSH-ICB 1435/18).

Preparation of urate crystals

In sterile conditions, 1 gram of crystalline uric acid was mixed with 200 mL sterile ultrapure water. The mixture was solubilized by shaking and 20% NaOH addition until complete solubilization (61). In the next step, the solution was heated to 70°C, pH was adjusted to 7.4 by adding HCl. Finally, the solution was slowly cooled. Crystals were vacuum dehydrated overnight and kept in a desiccator containing anhydrous silica gel until use. Crystals were resuspended in sterile PBS immediately before use.

HOCl cell production

Before any assay, the oxidative burst of dHL-60 or neutrophils was evaluated by incubating it with phorbol myristate acetate (100 nM). The reduction of cytochrome *c* due to the production of superoxide was monitored over time at 550nm, $\epsilon = 21,000 \text{ M}^{-1} \text{ cm}^{-1}$. Measurement of HOCl production by 1×10^6 dHL-60 or neutrophils was carried out in PBS (10 mM Na_2HPO_4 , 2 mM KH_2PO_4 , 0.5 mM MgCl_2 , 1 mM CaCl_2 , 140 mM NaCl, 5.5 mM dextrose, 100 μM diethylenetriaminepentaacetic acid, 5 mM taurine in presence of the compounds (20 μM in 0.3% DMSO) or 0.3% DMSO (control). Cells were activated with phorbol myristate acetate (100 nM) at 37°C for 1 h. After incubation, cells were centrifuged at 1400 rpm by 10 minutes and the supernatant was diluted three-fold. Finally, 240 μL of this supernatant was added to 60 μL acetate buffer (400 mM, pH 5.4) containing NaI (100 μM) and TMB (2 mM in DMFO 10%). Taurine chloramine was quantified by TMB oxidation at 655 nm (29). Inhibition of HOCl production was calculated as the percentage of control (vehicle).

NETosis experiment

NETosis assay was conducted on human neutrophils adhered to lysine-coated glass coverslips as previously reported (62). After adhesion, the compounds were diluted in RPMI medium (free of phenol red and fetal bovine serum) at 20 μM (0.15% DMSO) final concentration and incubated by 15 minutes at 37°C in a 5% CO_2 atmosphere. Then, the netotic agent monosodium urate crystals (250 $\mu\text{g}/\text{mL}$) were added. After 90 min incubation, the medium was carefully removed, paraformaldehyde was added (500 μL at 4%) and incubated at 4°C overnight. In the day after, paraformaldehyde was removed and cells were washed three-fold with tris-HCl buffer (20 mM, pH 7.4) and reserved into same buffer at 4°C for lamina preparation. Tris-HCl buffer was carefully removed and DNA was stained by adding 500 μL sytox green (500 nM diluted in Tris-HCl buffer). The system was reserved for 30 minutes at room temperature protected from light. After staining, the coverslips were mounted on the lamina using ProLongTM Diamond Antifade Mountant fixation medium. Before reading, slides were cleaned with 70% alcohol. Fluorescence images were acquired by the fluorescence microscope Axiovert 200 (Carl Zeiss) with the Zeiss Filter Set 09, $\lambda_{\text{ex}} = 450 - 490 \text{ nm}$, $\lambda_{\text{em}} = \text{above } 515 \text{ nm}$.

PARP1 off-target assay

RPE1-hTERT cells were grown in DMEM-F12 medium supplemented with 10% fetal bovine serum and penicillin/streptomycin mix at 100 U/mL and 100 µg/mL, respectively (15140122, Thermo), and grown at 37°C in a humidified atmosphere containing 5% CO₂. 10⁵ cells were seeded per well in a 12 well plate and grown for 24h. On the following day, fresh medium containing 10µM PARGi (PDD00017273- Sigma) and either DMSO, 10 µM olaparib (Selleckchem) or 1, 10 or 50 µM RL6 was added and cells were kept at 37°C for 1h. The medium was removed and 600 µM H₂O₂ (Sigma) in PBS was added. After 10 minutes at 37°C, the solution was removed and cells were lysed in pre-heated Laemmli buffer devoid of beta-mercaptoethanol and bromophenol blue. Lysates were boiled for 15 min. Protein concentration was determined using BCA protein quantification kit (Pierce) and normalized. Beta-mercaptoethanol and bromophenol blue were then added, and the lysates were boiled again for 15 min. SDS-PAGE (10% gels) was run and gels were transferred to nitrocellulose membranes (Bio-Rad). After staining with Ponceau Red and trimming, membranes were blocked with 5% milk for 1h and incubated with pan-ADP-ribose binding reagent (1:1000, MABE1016, Millipore) at 4°C overnight, followed by incubation with secondary anti-rabbit-HRP antibody (1:5000, SAB3700934-2MG, Sigma) for 1h. Membranes were incubated with ECL Prime (Amersham) and the signals were detected using a Chemidoc MP Imaging System (Bio-Rad). Membranes were then reprobbed with anti-actin primary antibody (1:5000, MAB1501, Sigma), and secondary anti-mouse-HRP antibody (1:5000, SAB3701105-2MG, Sigma), followed by ECL incubation and imaging as above. Signals were quantified using ImageJ software.

Animals

All experiments were conducted using male C57BL/6 mice (7 – 8 weeks old, 20–25 g) provided by the local vivarium from Faculty of Medicine (University of São Paulo, Brazil). The animals were kept in polypropylene cage (5 mice/cage) and housed in controlled temperature (22 ± 2 °C) and luminosity (12 h light/dark cycle), air exhaustion, and free access to water and food (Nuvilab CR-1, Quimtia S/A, Brazil). All experimental protocols were previously approved by the local Ethics Committee of Animal Experimentation (CEUA/IQ, n° 100/2018) and conducted in agreement with the Brazilian Council for Control of Animal Experimentation (CONCEA) guidelines and according to the National Council for Animal Experimentation Control principles, consistent with the Animal Welfare Act. At final experiment, animals were euthanized by exsanguination under anesthesia with inhaled isoflurane (2% v/v in O₂).

MSU-induced paw edema

MSU-induced edema was performed as previously described (19). The compounds were diluted in tween 80 (0.5%) plus DMSO (5%) and resuspended in PBS prior to administration. The animals were intraperitoneally (i.p.) treated with: vehicle (VEH: 5% DMSO; 0.5% tween 80 in PBS), mefenamic acid (non-steroid anti-inflammatory drug: 30 mg/Kg), RL6 (3, 10 and 30 mg/Kg), RL7 (0.3, 3 and 30 mg/Kg), RL21 (3, 10 and 30 mg/Kg) or ZINC9089086 (3, 10 and 30 mg/Kg) (27). After 30 min, mice were anaesthetized with inhaled isoflurane (2% v/v in O₂). By using a hypodermic syringe (31 g needle, BD, Franklin Lakes, NJ, USA), mice received via intraplantar route (i.pl.), in the right hind paw, vehicle (VEH: PBS, 30 µL) or MSU 1.5 mg/30 µL (Fig. 7).

The paw volume (mL) was evaluated before (baseline, B) and 1, 2, 3, 4, 5 and 6 hours (h) after MSU injection by a plethysmometer (Ugo Basile, Comerio, Italy) (Fig. 7). The edema is expressed as “variation in paw volume (Δ mL)”. To evaluate the anti-edematogenic effect of MPO-inhibitors administrated orally (v.o.) by gavage. The animals were fasted for 1 h and subsequently treated with equimolar doses: vehicle (VEH: 5% DMSO; 0.5% tween 80 in PBS), mefenamic acid (30 mg/Kg), RL 6 (3.3, 33 and 103 mg/Kg), RL 7 (54 mg/Kg), RL 21 (30 mg/Kg) or ZINC9089086 (34 mg/Kg). After 1 h, anaesthetized mice (2% isoflurane, v/v in O₂) received vehicle (PBS, 30 µL, i.pl.) or 1.5 mg/30 µL MSU (i.pl.).

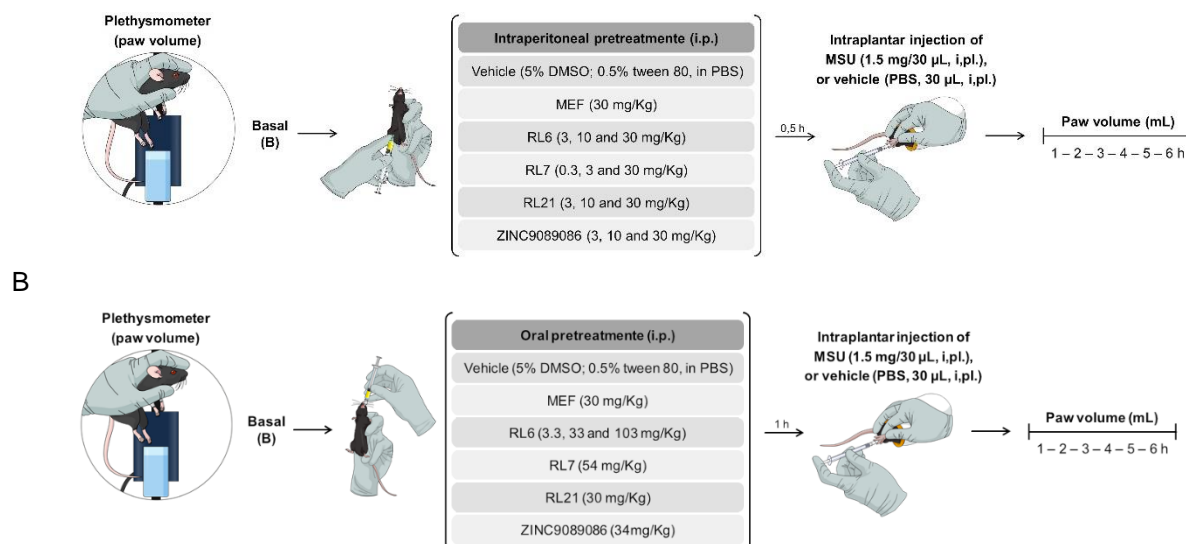


Fig. 7. Flowchart of the (MSU)-induced paw edema experiment. Design for intraperitoneal (**A**) or oral (**B**) treatment.

Statistical Analysis

The analyses were performed using the GraphPad Prism® version 6.0 (GraphPad Software, San Diego, USA). The data were analyzed by one-way analysis of variance (ANOVA) or two-way analysis of variance (ANOVA) with repeated measures, followed by Bonferroni's multiple comparisons post-hoc test. All the results are presented as mean \pm standard error of mean (SEM) and the level of significance was set as * , $\#P < 0.05$ or 0.01 .

References

1. M. Zamocky, C. Jakopitsch, P. G. Furtmüller, C. Dunand, C. Obinger, The peroxidase-cyclooxygenase superfamily: Reconstructed evolution of critical enzymes of the innate immune system. *Proteins Struct. Funct. Genet.* **72**, 589–605 (2008).
2. S. Gellhaar, D. Sunnemark, H. Eriksson, L. Olson, D. Galter, Myeloperoxidase-immunoreactive cells are significantly increased in brain areas affected by neurodegeneration in Parkinson's and Alzheimer's disease. *Cell Tissue Res.* **369**, 445–454 (2017).
3. Y. Aratani, Myeloperoxidase: Its role for host defense, inflammation, and neutrophil function. *Arch. Biochem. Biophys.* **640**, 47–52 (2018).
4. T. S. McMillen, J. W. Heinecke, R. C. LeBoeuf, Expression of human myeloperoxidase by macrophages promotes atherosclerosis in mice. *Circulation.* **111**, 2798–2804 (2005).
5. C. C. Winterbourn, A. J. Kettle, Redox Reactions and Microbial Killing in the Neutrophil Phagosome. *Antioxid. Redox Signal.* **18**, 642–660 (2013).
6. B. S. van der Veen, M. P. J. de Winther, P. Heeringa, Myeloperoxidase: Molecular Mechanisms of Action and Their Relevance to Human Health and Disease. *Antioxid. Redox Signal.* **11**, 2899–2937 (2009).
7. D.-K. Choi, S. Pennathur, C. Perier, K. Tieu, P. Teismann, D.-C. Wu, V. Jackson-Lewis, M. Vila, J.-P. Vonsattel, J. W. Heinecke, S. Przedborski, Ablation of the inflammatory enzyme myeloperoxidase mitigates features of Parkinson's disease in mice. *J. Neurosci.* **25**, 6594–6600 (2005).
8. G. M. Saed, R. Ali-Fehmi, Z. L. Jiang, N. M. Fletcher, M. P. Diamond, H. M. Abu-Soud, A. R. Munkarah, Myeloperoxidase serves as a redox switch that regulates apoptosis in epithelial ovarian cancer. *Gynecol. Oncol.* **116**, 276–281 (2010).
9. R. M. Nagra, B. Becher, W. W. Tourtellotte, J. P. Antel, D. Gold, T. Paladino, R. A. Smith, J. R. Nelson, W. F. Reynolds, Immunohistochemical and genetic evidence of myeloperoxidase involvement in multiple sclerosis. *J. Neuroimmunol.* **78**, 97–107 (1997).
10. A. Strzepa, K. A. Pritchard, B. N. Dittel, Myeloperoxidase: A new player in autoimmunity. *Cell. Immunol.* **317**, 1–8 (2017).
11. M. M. Omran, F. M. Zahran, M. Kadry, A. A. M. Belal, T. M. Emran, Role of myeloperoxidase in early diagnosis of acute myocardial infarction in patients admitted with chest pain. *J. Immunoassay Immunochem.* **39**, 337–347 (2018).
12. N. Anatoliotakis, S. Deftereos, G. Bouras, G. Giannopoulos, D. Tsounis, C. Angelidis, A. Kaoukis, C. Stefanadis, Myeloperoxidase: expressing inflammation and oxidative stress in cardiovascular disease. *Curr. Top. Med. Chem.* **13**, 115–138 (2013).
13. J. Schultz, K. Kaminker, Myeloperoxidase of the leucocyte of normal human blood. I. Content and localization. *Arch. Biochem. Biophys.* **96**, 465–467 (1962).
14. K. D. Metzler, C. Goosmann, A. Lubojemska, A. Zychlinsky, V. Papayannopoulos, A myeloperoxidase-containing complex regulates neutrophil elastase release and actin dynamics during NETosis. *Cell Rep.* **8**, 883–896 (2014).
15. V. Brinkmann, U. Reichard, C. Goosmann, B. Fauler, Y. Uhlemann, D. S. Weiss, Y. Weinrauch, A. Zychlinsky, Neutrophil Extracellular Traps Kill Bacteria. *Science (80-)*. **303**, 1532–1535 (2004).
16. V. Papayannopoulos, Neutrophil extracellular traps in immunity and disease. *Nat. Rev. Immunol.* **18**, 134–147 (2018).
17. F. P. Veras, M. C. Pontelli, C. M. Silva, J. E. Toller-Kawahisa, M. de Lima, D. C. Nascimento, A. H. Schneider, D. Caetité, L. A. Tavares, I. M. Paiva, R. Rosales, D. Colón, R. Martins, I. A. Castro, G. M. Almeida, M. I. F. Lopes, M. N. Benatti, L. P. Bonjorno, M. C. Giannini, R. Luppino-Assad, S. L. Almeida, F. Vilar, R. Santana, V. R. Bollela, M.

- Auxiliadora-Martins, M. Borges, C. H. Miranda, A. Pazin-Filho, L. L. P. da Silva, L. D. Cunha, D. S. Zamboni, F. Dal-Pizzol, L. O. Leiria, L. Siyuan, S. Batah, A. Fabro, T. Mauad, M. Dolhnikoff, A. Duarte-Neto, P. Saldiva, T. M. Cunha, J. C. Alves-Filho, E. Arruda, P. Louzada-Junior, R. D. Oliveira, F. Q. Cunha, SARS-CoV-2-triggered neutrophil extracellular traps mediate COVID-19 pathology. *J. Exp. Med.* **217** (2020), doi:10.1084/jem.20201129.
18. M. Dehlin, L. Jacobsson, E. Roddy, Global epidemiology of gout: prevalence, incidence, treatment patterns and risk factors. *Nat. Rev. Rheumatol.* **16**, 380–390 (2020).
 19. L. L. Reber, N. Gaudenzio, P. Starkl, S. J. Galli, Neutrophils are not required for resolution of acute gouty arthritis in mice. *Nat. Med.* **22** (2016), pp. 1382–1384.
 20. F. C. Meotti, G. N. L. Jameson, R. Turner, D. T. Harwood, S. Stockwell, M. D. Rees, S. R. Thomas, A. J. Kettle, Urate as a physiological substrate for myeloperoxidase: implications for hyperuricemia and inflammation. *J. Biol. Chem.* **286**, 12901–12911 (2011).
 21. E. S. Patrício, F. M. Prado, R. P. da Silva, L. A. C. Carvalho, M. V. C. Prates, T. Dadamos, M. Bertotti, P. Di Mascio, A. J. Kettle, F. C. Meotti, Chemical Characterization of Urate Hydroperoxide, A Pro-oxidant Intermediate Generated by Urate Oxidation in Inflammatory and Photoinduced Processes. *Chem. Res. Toxicol.* **28**, 1556–1566 (2015).
 22. C. J. A. Ramachandra, K. P. M. M. Ja, J. Chua, S. Cong, W. Shim, D. J. Hausenloy, Myeloperoxidase As a Multifaceted Target for Cardiovascular Protection. *Antioxid. Redox Signal.* **32**, 1135–1149 (2020).
 23. F. Duclos, L. M. Abell, D. G. Harden, K. Pike, K. Nowak, G. A. Locke, G. J. Duke, X. Liu, G. Fernando, S. A. Shaw, B. P. Vokits, N. R. Wurtz, A. Viet, M. N. Valente, S. Stachura, P. Slep, J. A. Khan, J. Gao, A. R. Dongre, L. Zhao, R. R. Wexler, D. A. Gordon, E. K. Kick, Triazolopyrimidines identified as reversible myeloperoxidase inhibitors. *Medchemcomm.* **8**, 2093–2099 (2017).
 24. I. Aldib, J. Soubhye, K. Z. Boudjeltia, M. Vanhaeverbeek, A. Rousseau, P. G. Furtmüller, C. Obinger, F. Dufrasne, J. Nève, P. Van Antwerpen, M. Prévost, Evaluation of new scaffolds of myeloperoxidase inhibitors by rational design combined with high-throughput virtual screening. *J. Med. Chem.* **55**, 7208–7218 (2012).
 25. A. Malvezzi, R. F. Queiroz, L. de Rezende, O. Augusto, A. T. Amaral, MPO Inhibitors Selected by Virtual Screening. *Mol. Inform.* **30**, 605–613 (2011).
 26. J. Soubhye, I. Chikh Alard, I. Aldib, M. Prévost, M. Gelbcke, A. De Carvalho, P. G. Furtmüller, C. Obinger, J. Flemmig, S. Tadrent, F. Meyer, A. Rousseau, J. Nève, V. Mathieu, K. Zouaoui Boudjeltia, F. Dufrasne, P. Van Antwerpen, Discovery of Novel Potent Reversible and Irreversible Myeloperoxidase Inhibitors Using Virtual Screening Procedure. *J. Med. Chem.* **60**, 6563–6586 (2017).
 27. I. de A. Matos, N. B. da Costa Júnior, F. C. Meotti, Integration of an Inhibitor-like Rule and Structure-based Virtual Screening for the Discovery of Novel Myeloperoxidase Inhibitors. *J. Chem. Inf. Model.* **60**, 6408–6418 (2020).
 28. M. Su, Q. Yang, Y. Du, G. Feng, Z. Liu, Y. Li, R. Wang, Comparative Assessment of Scoring Functions: The CASF-2016 Update. *J. Chem. Inf. Model.* **59**, 895–913 (2019).
 29. J. M. Dypbukt, C. Bishop, W. M. Brooks, B. Thong, H. Eriksson, A. J. Kettle, A sensitive and selective assay for chloramine production by myeloperoxidase. *Free Radic. Biol. Med.* **39**, 1468–1477 (2005).
 30. J. Ward, S. N. Spath, B. Pabst, P. A. Carpino, R. B. Ruggeri, G. Xing, A. E. Speers, B. F. Cravatt, K. Ahn, Mechanistic characterization of a 2-thioxanthine myeloperoxidase inhibitor and selectivity assessment utilizing click chemistry-activity-based protein profiling. *Biochemistry.* **52**, 9187–9201 (2013).
 31. J. Soubhye, M. Prévost, P. Van Antwerpen, K. Zouaoui Boudjeltia, A. Rousseau, P. G. Furtmüller, C. Obinger, M. Vanhaeverbeek, J. Ducobu, J. Nève, M. Gelbcke, F. Dufrasne,

- Structure-based design, synthesis, and pharmacological evaluation of 3-(Aminoalkyl)-5-fluoroindoles as myeloperoxidase inhibitors. *J. Med. Chem.* **53**, 8747–8759 (2010).
32. A. J. Kettle, C. A. Gedye, C. C. Winterbourn, Mechanism of inactivation of myeloperoxidase by 4-aminobenzoic acid hydrazide. *Biochem. J.* **321**, 503–508 (1997).
 33. M. C. M. Vissers, M. B. Hampton, A. J. Kettle, Eds., in *Hydrogen Peroxide Metabolism in Health and Disease* (CRC Press, 2017; <https://www.taylorfrancis.com/books/9781498776165/chapters/10.1201/9781315154831-15>), pp. 365–385.
 34. L. V. Forbes, T. Sjögren, F. Auchère, D. W. Jenkins, B. Thong, D. Laughton, P. Hemsley, G. Pairedeau, R. Turner, H. Eriksson, J. F. Unitt, A. J. Kettle, Potent reversible inhibition of myeloperoxidase by aromatic hydroxamates. *J. Biol. Chem.* **288**, 36636–36647 (2013).
 35. A.-K. Tidén, T. Sjögren, M. Svensson, A. Bernlind, R. Senthilmohan, F. Auchère, H. Norman, P.-O. Markgren, S. Gustavsson, S. Schmidt, S. Lundquist, L. V. Forbes, N. J. Magon, L. N. Paton, G. N. L. Jameson, H. Eriksson, A. J. Kettle, 2-Thioxanthines Are Mechanism-based Inactivators of Myeloperoxidase That Block Oxidative Stress during Inflammation. *J. Biol. Chem.* **286**, 37578–37589 (2011).
 36. A. J. Kettle, C. A. Gedye, M. B. Hampton, C. C. Winterbourn, Inhibition of myeloperoxidase by benzoic acid hydrazides. *Biochem. J.* **308**, 559–563 (1995).
 37. R. B. Ruggeri, L. Buckbinder, S. W. Bagley, P. A. Carpino, E. L. Conn, M. S. Dowling, D. P. Fernando, W. Jiao, D. W. Kung, S. T. M. Orr, Y. Qi, B. N. Roche, A. Smith, J. S. Warmus, Y. Zhang, D. Bowles, D. W. Widlicka, H. Eng, T. Ryder, R. Sharma, A. Wolford, C. Okerberg, K. Walters, T. S. Maurer, Y. Zhang, P. D. Bonin, S. N. Spath, G. Xing, D. Hepworth, K. Ahn, A. S. Kalgutkar, Discovery of 2-(6-(5-Chloro-2-methoxyphenyl)-4-oxo-2-thioxo-3,4-dihydropyrimidin-1(2H)-yl)acetamide (PF-06282999): A Highly Selective Mechanism-Based Myeloperoxidase Inhibitor for the Treatment of Cardiovascular Diseases. *J. Med. Chem.* **58**, 8513–8528 (2015).
 38. D. Josephy, T. Eling, R. Mason, The Horseradish Peroxidase-catalyzed Oxidation of 3,5,3',5'-Tetramethylbenzidine. *J. Biol. Chem.* **257**, 3669–3675 (1982).
 39. F. C. Meotti, R. Senthilmohan, D. T. Harwood, F. C. Missau, M. G. Pizzolatti, A. J. Kettle, Myricitrin as a substrate and inhibitor of myeloperoxidase: implications for the pharmacological effects of flavonoids. *Free Radic. Biol. Med.* **44**, 109–120 (2008).
 40. B. K. Shoichet, Interpreting Steep Dose-Response Curves in Early Inhibitor Discovery. *J. Med. Chem.* **49**, 7274–7277 (2006).
 41. H. Prinz, Hill coefficients, dose-response curves and allosteric mechanisms. *J. Chem. Biol.* **3**, 37–44 (2010).
 42. S. Galijasevic, I. Abdulhamid, H. M. Abu-Soud, Potential role of tryptophan and chloride in the inhibition of human myeloperoxidase. *Free Radic. Biol. Med.* **44**, 1570–1577 (2008).
 43. N. Trinajstić, New developments in Hückel theory. *Int. J. Quantum Chem.* **12**, 469–477 (2009).
 44. H. R. Thiam, S. L. Wong, D. D. Wagner, C. M. Waterman, Cellular Mechanisms of NETosis. *Annu. Rev. Cell Dev. Biol.* **36**, 191–218 (2020).
 45. T. Németh, M. Sperandio, A. Mócsai, Neutrophils as emerging therapeutic targets. *Nat. Rev. Drug Discov.* **19**, 253–275 (2020).
 46. O. Soehnlein, S. Steffens, A. Hidalgo, C. Weber, Neutrophils as protagonists and targets in chronic inflammation. *Nat. Rev. Immunol.* **17**, 248–261 (2017).
 47. S. M. Chatfield, K. Grebe, L. W. Whitehead, K. L. Rogers, T. Nebl, J. M. Murphy, I. P. Wicks, Monosodium Urate Crystals Generate Nuclease-Resistant Neutrophil Extracellular Traps via a Distinct Molecular Pathway. *J. Immunol.*, ji1701382 (2018).
 48. C. M. Byrd, (12) Patent Application Publication (10) Pub . No .: US 2013 / 0129677 A1. **1** (2013).

49. A. Kamal, N. R. Bolla, P. S. Srikanth, A. K. Srivastava, Naphthalimide derivatives with therapeutic characteristics: a patent review. *Expert Opin. Ther. Pat.* **23**, 299–317 (2013).
50. A. Ruf, G. de Murcia, G. E. Schulz, Inhibitor and NAD⁺ Binding to Poly(ADP-ribose) Polymerase As Derived from Crystal Structures and Homology Modeling. *Biochemistry*. **37**, 3893–3900 (1998).
51. A. Ray Chaudhuri, A. Nussenzweig, The multifaceted roles of PARP1 in DNA repair and chromatin remodelling. *Nat. Rev. Mol. Cell Biol.* **18**, 610–621 (2017).
52. A. R. Fehr, S. A. Singh, C. M. Kerr, S. Mukai, H. Higashi, M. Aikawa, The impact of PARPs and ADP-ribosylation on inflammation and host-pathogen interactions. *Genes Dev.* **34**, 341–359 (2020).
53. C. J. LaFargue, G. Z. Dal Molin, A. K. Sood, R. L. Coleman, Exploring and comparing adverse events between PARP inhibitors. *Lancet. Oncol.* **20**, e15–e28 (2019).
54. M. Elmeliegy, M. Vourvahis, C. Guo, D. D. Wang, Effect of P-glycoprotein (P-gp) Inducers on Exposure of P-gp Substrates: Review of Clinical Drug-Drug Interaction Studies. *Clin. Pharmacokinet.* **59**, 699–714 (2020).
55. B. J. Bender, S. Gahbauer, A. Lutten, J. Lyu, C. M. Webb, R. M. Stein, E. A. Fink, T. E. Balias, J. Carlsson, J. J. Irwin, B. K. Shoichet, A practical guide to large-scale docking. *Nat. Protoc.* **16**, 4799–4832 (2021).
56. J. Soubhye, F. Meyer, P. Furtmüller, C. Obinger, F. Dufrasne, P. Van Antwerpen, Characterization of chemical features of potent myeloperoxidase inhibitors. *Future Med. Chem.* **8**, 1163–1177 (2016).
57. D. B. McConnell, Biotin's Lessons in Drug Design. *J. Med. Chem.* **64**, 16319–16327 (2021).
58. T. Lu, F. Chen, Multiwfn: A multifunctional wavefunction analyzer. *J. Comput. Chem.* **33**, 580–592 (2012).
59. L. A. C. Carvalho, J. P. P. B. Lopes, G. H. Kaihami, R. P. Silva, A. Bruni-Cardoso, R. L. Baldini, F. C. Meotti, Uric acid disrupts hypochlorous acid production and the bactericidal activity of HL-60 cells. *Redox Biol.* **16**, 179–188 (2018).
60. R. P. Silva, L. A. C. Carvalho, E. S. Patricio, J. P. P. Bonifacio, A. B. Chaves-Filho, S. Miyamoto, F. C. Meotti, Identification of urate hydroperoxide in neutrophils: A novel pro-oxidant generated in inflammatory conditions. *Free Radic. Biol. Med.* **126**, 177–186 (2018).
61. L. J. Moilanen, M. Hämäläinen, L. Lehtimäki, R. M. Nieminen, E. Moilanen, Urate crystal induced inflammation and joint pain are reduced in transient receptor potential ankyrin 1 deficient mice - Potential role for transient receptor potential ankyrin1 in gout. *PLoS One*. **10**, 1–13 (2015).
62. V. Brinkmann, B. Laube, U. Abu Abed, C. Goosmann, A. Zychlinsky, Neutrophil Extracellular Traps: How to Generate and Visualize Them. *J. Vis. Exp.* (2010), doi:10.3791/1724.

Supplementary Materials

Targeting Myeloperoxidase Ameliorates Gouty Arthritis in Mice: A Virtual Screening Success Story

Isaac de Araujo Matos, Jorge Luiz Dallazen, Nivan Bezerra da Costa Júnio, Lorena Rocha Reis, Graziella Eliza Ronsein, Luiz Felipe de Souza, Nicolas Hoch, Soraia Kátia Pereira Costa, Flávia Carla Meotti.

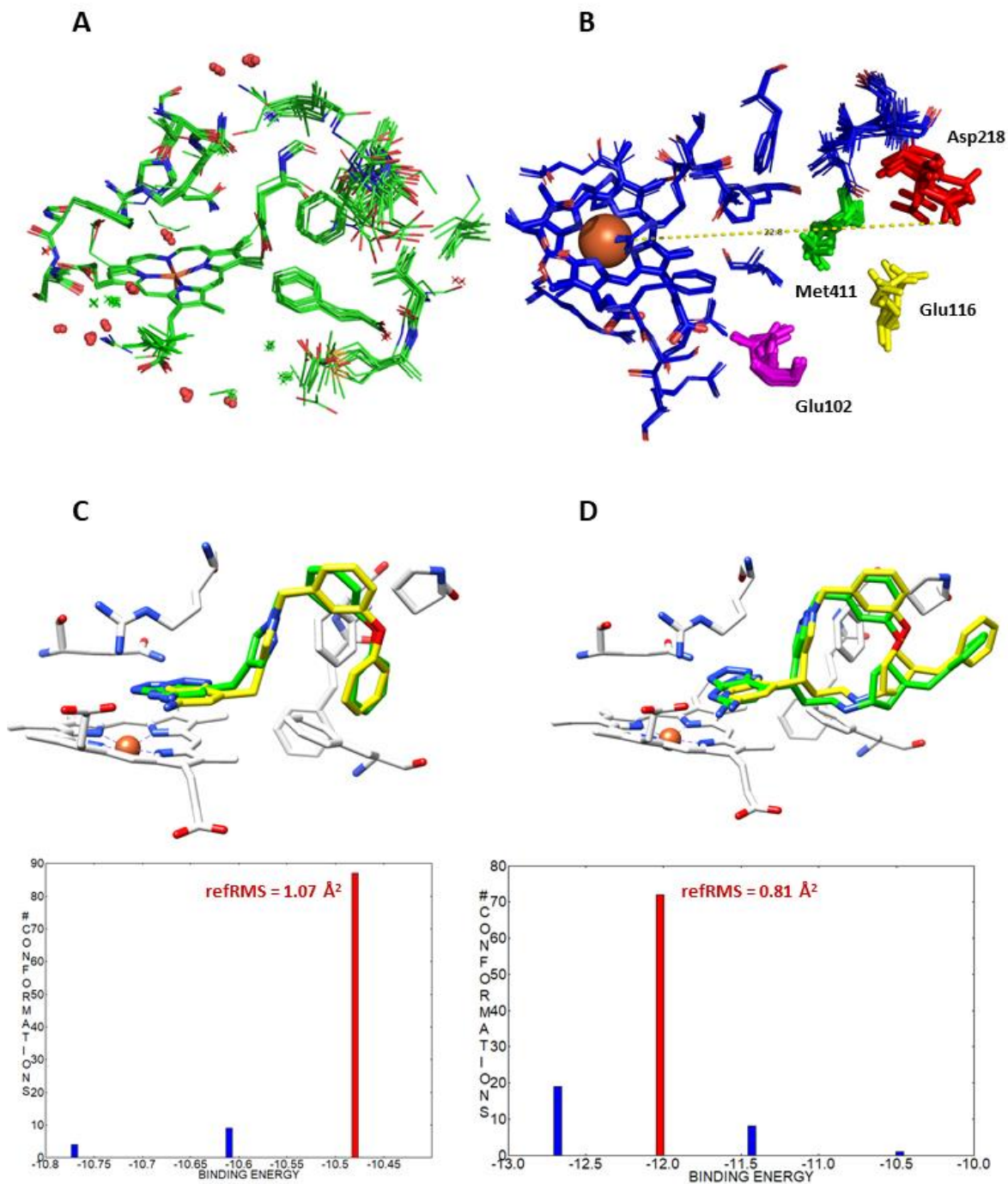
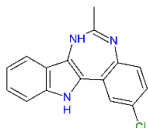
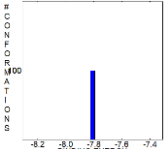
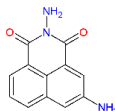
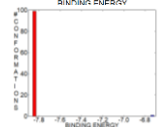
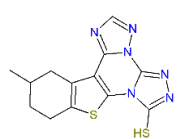
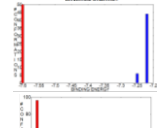

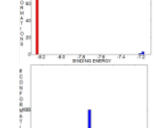
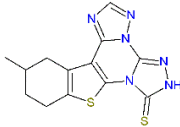
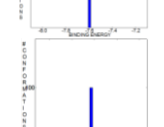

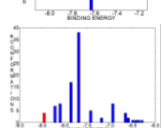
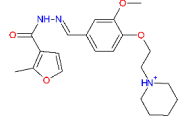
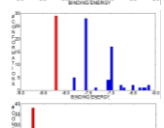
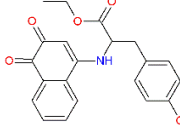
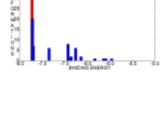


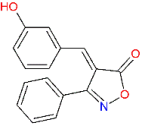
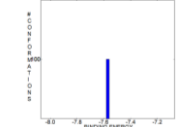
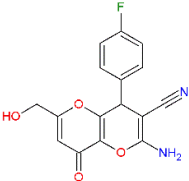
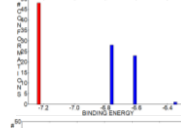
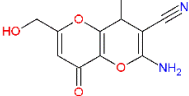
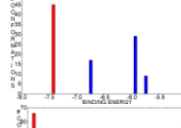
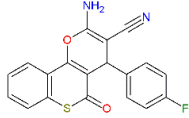
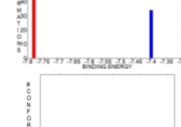

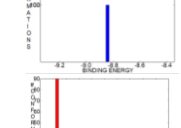
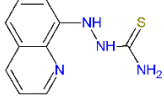
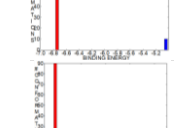
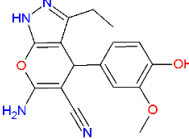
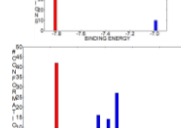
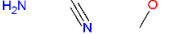
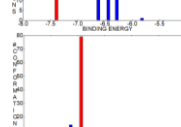
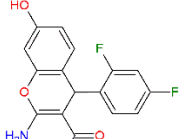
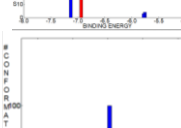

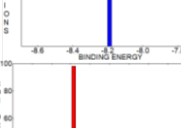
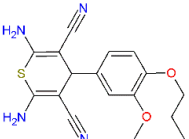




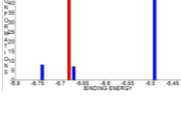


Fig. S1. Alignments of MPO crystal structures PDB 5QJ2, 5QJ3, 6WXZ, 6WY0, 6WY5, 6WY7, 6WYD, 7LAE, 7LAG, 7LAL and 7LAN. A - groups of conserved water molecules are shown as red spheres. B - Rigid residues are shown in blue lines and the flexible ones in green (Met411), red (Asp218), yellow (Glu116) and magenta (Glu102). Distance between iron atom and Asp218 is shown in yellow dot line. Cross-docking of MPO inhibitor into the active site of PDB 7LAG (C) and 7LAN (D) ligands. Pose are shown in green and crystallographic conformation in yellow. The respective conformational histograms are shown on the right with the most populous cluster in red and the refRMS value.

Table S1. Molecular docking Parameters to MPO inhibitors from AutoDock								
Structure	In house	$\Delta G_{\text{binding}}$	K_i (nM)	Ligand Efficiency	Desolvation energy	Electrostatic energy	Hydrogen bonds	Histogram
	RL1	-7.81	1,900	-0.39	-7.62	-0.19	2	
	RL6	-7.84	1,810	-0.46	-8.38	-0.05	1	
	(S) RL9	-7.6	2700	-0.36	-8.12	-0.67	2	
	(R) RL9	-8.24	0.906	-0.39	-8.68	-0.75	2	
	(S) RL9	-7.60	2690	-0.36	-7.55	-0.95	0	
	(R) RL9	-7.63	2570	-0.36	-7.57	-0.95	0	
	RL15	-8.45	0.638	-0.3	-9.3	-1.54	3	
	(S) RL16	-8.21	0.963	-0.3	-10.48	-0.11	3	
	(R) RL16	-7.73	2160	-0.29	-10.04	-0.08	2	

	RL17	-7.57	2,832	-0.38	-8.43	-0.03	2	
	(S) RL19	-7.23	5,000	-0.31	-8.4	-0.02	3	
	(R) RL19	-7.43	3590	-0.32	-8.47	-0.15	3	
	(S) RL20	-7.78	1980	-0.31	-8.27	-0.11	2	
	(R) RL20	-8.84	0.333	-0.35	-9.23	-0.2	1	
	RL21	-6.64	11,550	-0.45	-7.68	0.05	1	
	(S) RL23	-7.81	1,890	-0.34	-8.95	-0.35	4	
	(R) RL23	-7.39	3840	-0.32	-8.68	-0.21	3	
	(S) RL24	-6.94	8160	-0.28	-8.58	-0.15	2	
	(R) RL24	-8.19	0.999	-0.33	-9.84	-0.14	4	
	RL26	-7.37	3,930	-0.31	-9.1	-0.36	2	
	(S) RL27	-7.09	6350	-0.42	-7.42	0.03	1	
	(R) RL27	-6.68	12670	-0.39	-6.86	-0.12	0	

	(S) RL27	-7.62	2590	-0.45	-8.08	-0.13	1	
	(R) RL27	-6.94	8170	-0.41	-7.48	-0.06	0	

<

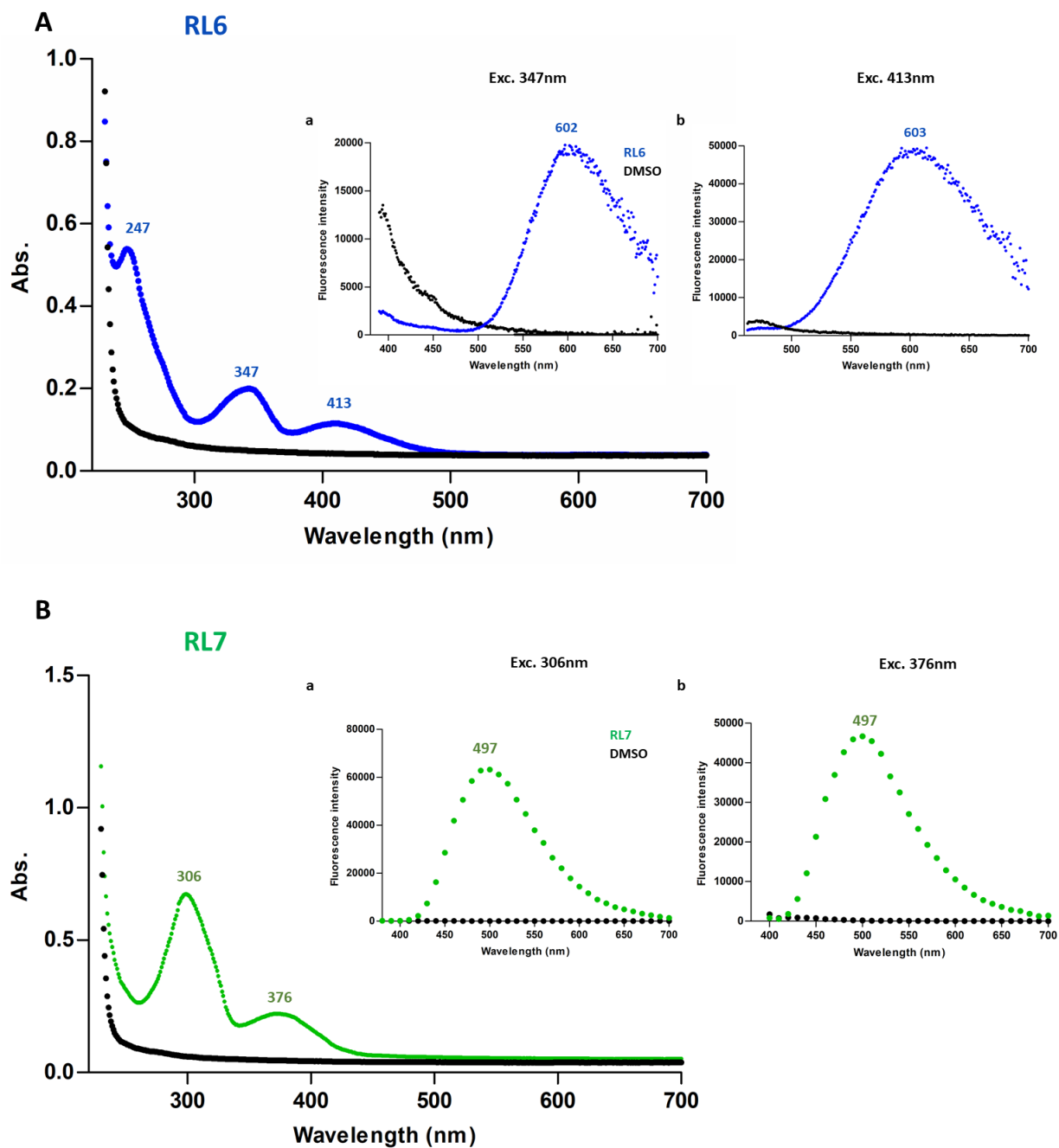


Fig. S2. UV/Vis and fluorescence scans for RL6 and RL7 compounds. (A) RL6 absorbance spectrum (left) and its respective fluorescence emission when excited at 347 and 413 nm (right). (B) RL7 absorbance spectrum and its respective fluorescence emission spectrum excited at 306 and 376 nm. Spectra were obtained at 20 μ M in DMSO with a gain 100 to RL7 and 150 to RL6 using a microplate reader.

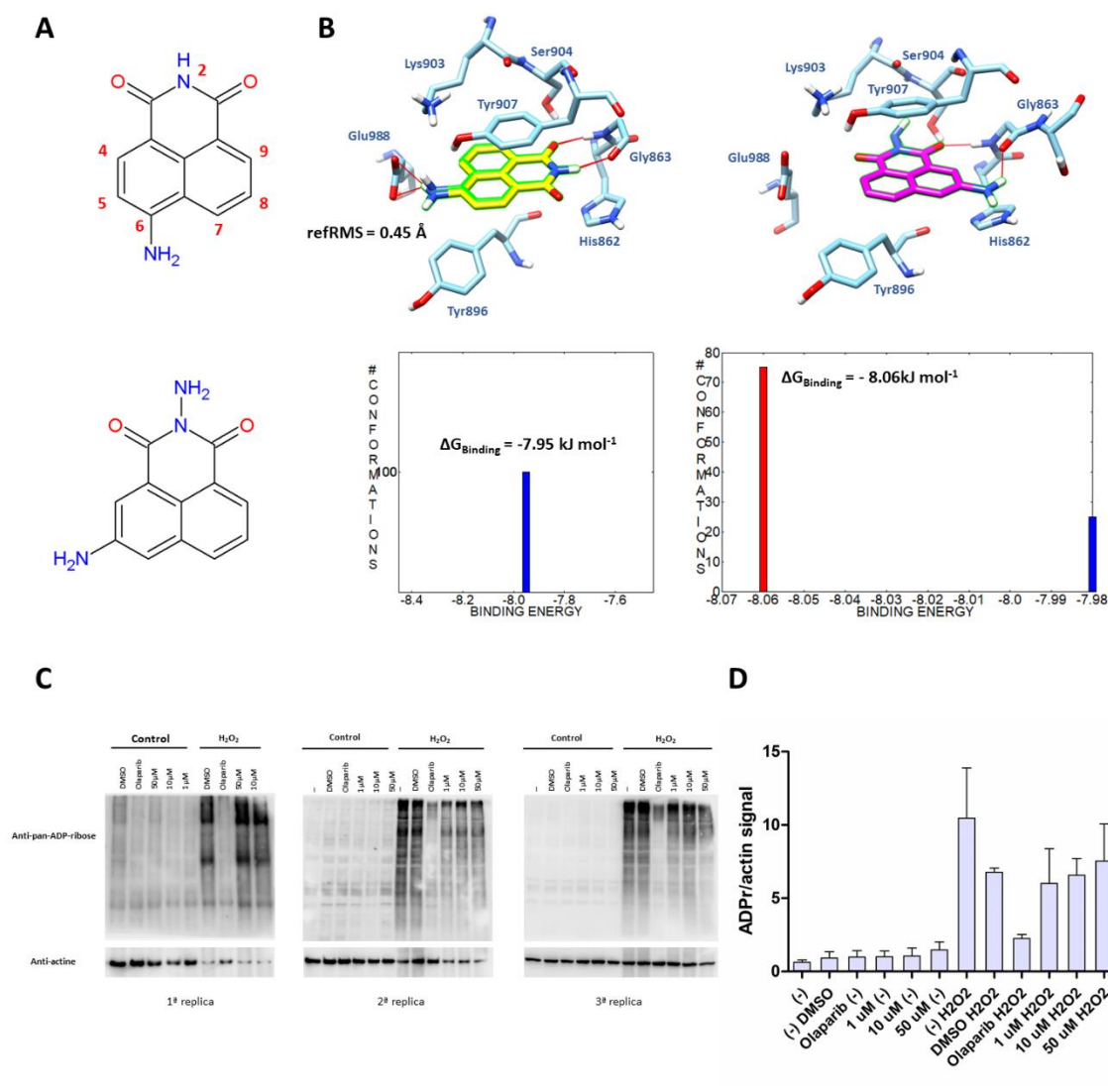


Fig. S3 Evaluation of the RL6 off-target assay. (A) Molecular structure of the PARP1 inhibitor 4ANI (top) and RL6 (bottom) showing their structural similarity (B) Left, 4ANI redocking to into the PARP1 active site showing the crystallography experimental conformation (green) and redocked (yellow). Molecular docking of RL6 (magenta) at the right. The respective histograms and binding energies are shown below. For RL6, the conformation with the best binding energy of the most populous cluster was selected. For molecular docking studies with PARP1, the PDB 2PAX structure was selected, the hydrogens were added and water molecules were maintained during simulation. All simulations were performed using AutoDock 4.2.3 in a box of 40x, 40y,40z dimensions and centered in the coordinates 40.852x, 22.791y, 21.55z. The Lamarckian genetic algorithm was selected and it was run 100 times. Other parameters were kept as default. (C) ADP-ribosylation stimulated by H₂O₂ (600 μM) and incubated for 10 min in RPE1-hTERT cells. (D) Gel densitometry quantified by ImageJ software.

REFERENCES

1. Rosales C. Neutrophil: A cell with many roles in inflammation or several cell types? *Front Physiol.* 2018;9(FEB):1–17.
2. Görgens A, Radtke S, Möllmann M, Cross M, Dürig J, Horn PA, et al. Revision of the Human Hematopoietic Tree: Granulocyte Subtypes Derive from Distinct Hematopoietic Lineages. *Cell Rep* [Internet]. 2013 May;3(5):1539–52. Available from: <https://linkinghub.elsevier.com/retrieve/pii/S2211124713002076>
3. Yvan-Charvet L, Ng LG. Granulopoiesis and Neutrophil Homeostasis: A Metabolic, Daily Balancing Act. *Trends Immunol.* 2019;40(7):598–612.
4. von Vietinghoff S, Ley K. Homeostatic Regulation of Blood Neutrophil Counts. *J Immunol* [Internet]. 2008 Oct 15;181(8):5183–8. Available from: <http://www.jimmunol.org/lookup/doi/10.4049/jimmunol.181.8.5183>
5. Lawrence SM, Corriden R, Nizet V. The Ontogeny of a Neutrophil: Mechanisms of Granulopoiesis and Homeostasis. *Microbiol Mol Biol Rev.* 2018;82(1).
6. Rørvig S, Østergaard O, Heegaard NHH, Borregaard N. Proteome profiling of human neutrophil granule subsets, secretory vesicles, and cell membrane: correlation with transcriptome profiling of neutrophil precursors. *J Leukoc Biol* [Internet]. 2013 Oct;94(4):711–21. Available from: <http://doi.wiley.com/10.1189/jlb.1212619>
7. Kjeldsen L, Sengeløv H, Lollike K, Nielsen MH, Borregaard N. Isolation and characterization of gelatinase granules from human neutrophils. *Blood.* 1994 Mar;83(6):1640–9.
8. Jacobsen LC, Theilgaard-Mönch K, Christensen EI, Borregaard N. Arginase 1 is expressed in myelocytes/metamyelocytes and localized in gelatinase granules of human neutrophils. *Blood.* 2007 Apr;109(7):3084–7.
9. Valenti P, Antonini G. Lactoferrin: an important host defence against microbial and viral attack. *Cell Mol Life Sci.* 2005 Nov;62(22):2576–87.
10. Siqueiros-Cendón T, Arévalo-Gallegos S, Iglesias-Figueroa BF, García-Montoya IA, Salazar-Martínez J, Rascón-Cruz Q. Immunomodulatory effects of lactoferrin. *Acta Pharmacol Sin* [Internet]. 2014;35(5):557–66. Available from: <https://doi.org/10.1038/aps.2013.200>
11. SCHULTZ J, KAMINKER K. Myeloperoxidase of the leucocyte of normal human blood. I. Content and localization. *Arch Biochem Biophys.* 1962 Mar;96:465–7.
12. Odobasic D, Kitching AR, Holdsworth SR. Neutrophil-Mediated Regulation of Innate and Adaptive Immunity: The Role of Myeloperoxidase. *J Immunol Res.* 2016;2016:2349817.
13. Klebanoff SJ, Rosen H. The role of myeloperoxidase in the microbicidal activity of polymorphonuclear leukocytes. *Ciba Found Symp.* 1978 Jun;(65):263–84.
14. Binder V, Ljubojevic S, Haybaeck J, Holzer M, El-Gamal D, Schicho R, et al. The Myeloperoxidase Product Hypochlorous Acid Generates Irreversible High-Density Lipoprotein Receptor Inhibitors. *Arterioscler Thromb Vasc Biol* [Internet]. 2013 May;33(5):1020–7. Available from: <https://www.ahajournals.org/doi/10.1161/ATVBAHA.113.301235>
15. Korkmaz B, Moreau T, Gauthier F. Neutrophil elastase, proteinase 3 and cathepsin G: physicochemical properties, activity and physiopathological functions. *Biochimie.* 2008 Feb;90(2):227–42.
16. Döhrmann S, Cole JN, Nizet V. Conquering Neutrophils. *PLoS Pathog.* 2016;12(7):1–8.
17. Ley K, Laudanna C, Cybulsky MI, Nourshargh S. Getting to the site of inflammation: The

- leukocyte adhesion cascade updated. *Nat Rev Immunol.* 2007;7(9):678–89.
18. Mayadas TN, Cullere X, Lowell CA. The multifaceted functions of neutrophils. *Annu Rev Pathol.* 2014;9:181–218.
 19. Gullberg U, Andersson E, Garwicz D, Lindmark A, Olsson I. Biosynthesis, processing and sorting of neutrophil proteins: insight into neutrophil granule development. *Eur J Haematol.* 1997 Mar;58(3):137–53.
 20. Fittschen C, Henson PM. Linkage of azurophil granule secretion in neutrophils to chloride ion transport and endosomal transcytosis. *J Clin Invest [Internet].* 1994 Jan 1;93(1):247–55. Available from: <http://www.jci.org/articles/view/116952>
 21. Uribe-Quero E, Rosales C. Control of phagocytosis by microbial pathogens. *Front Immunol.* 2017;8(OCT):1–23.
 22. Winterbourn CC, Kettle AJ. Redox reactions and microbial killing in the neutrophil phagosome. *Antioxidants Redox Signal.* 2013;18(6):642–60.
 23. Németh T, Sperandio M, Mócsai A. Neutrophils as emerging therapeutic targets. *Nat Rev Drug Discov [Internet].* 2020;19(4):253–75. Available from: <https://doi.org/10.1038/s41573-019-0054-z>
 24. Soehnlein O, Steffens S, Hidalgo A, Weber C. Neutrophils as protagonists and targets in chronic inflammation. *Nat Rev Immunol.* 2017 Apr;17(4):248–61.
 25. Brinkmann V, Reichard U, Goosmann C, Fauler B, Uhlemann Y, Weiss DS, et al. Neutrophil extracellular traps kill bacteria. *Science.* 2004 Mar;303(5663):1532–5.
 26. Papayannopoulos V. Neutrophil extracellular traps in immunity and disease. *Nat Rev Immunol.* 2018;18(2):134–47.
 27. Röhm M, Grimm MJ, D'Auria AC, Almyroudis NG, Segal BH, Urban CF. NADPH oxidase promotes neutrophil extracellular trap formation in pulmonary aspergillosis. *Infect Immun.* 2014 May;82(5):1766–77.
 28. Hiroki CH, Toller-Kawahisa JE, Fumagalli MJ, Colon DF, Figueiredo LTM, Fonseca BALD, et al. Neutrophil Extracellular Traps Effectively Control Acute Chikungunya Virus Infection. *Front Immunol.* 2019;10:3108.
 29. Azevedo EPC, Guimarães-Costa AB, Torezani GS, Braga CA, Palhano FL, Kelly JW, et al. Amyloid fibrils trigger the release of neutrophil extracellular traps (NETs), causing fibril fragmentation by NET-associated elastase. *J Biol Chem.* 2012 Oct;287(44):37206–18.
 30. Castanheira FVS, Kubes P. Neutrophils and NETs in modulating acute and chronic inflammation. *Blood.* 2019;133(20):2178–85.
 31. Franck G, Mawson TL, Folco EJ, Molinaro R, Ruvkun V, Engelbertsen D, et al. Roles of PAD4 and NETosis in Experimental Atherosclerosis and Arterial Injury. *Circ Res [Internet].* 2018 Jun 22;123(1):33–42. Available from: <https://www.ahajournals.org/doi/10.1161/CIRCRESAHA.117.312494>
 32. Martínez-Alemán SR, Campos-García L, Palma-Nicolas JP, Hernández-Bello R, González GM, Sánchez-González A. Understanding the Entanglement: Neutrophil Extracellular Traps (NETs) in Cystic Fibrosis. *Front Cell Infect Microbiol [Internet].* 2017 Apr 6;7. Available from: <http://journal.frontiersin.org/article/10.3389/fcimb.2017.00104/full>
 33. Veras FP, Pontelli M, Silva C, Toller-Kawahisa J, de Lima M, Nascimento D, et al. SARS-CoV-2 triggered neutrophil extracellular traps (NETs) mediate COVID-19 pathology. *J Exp Med.* 2020;217(12).
 34. Khan MA, Farahvash A, Douda DN, Licht J-C, Grasemann H, Swezey N, et al. JNK Activation Turns on LPS- and Gram-Negative Bacteria-Induced NADPH Oxidase-Dependent Suicidal NETosis. *Sci Rep [Internet].* 2017;7(1):3409. Available from:

- <https://doi.org/10.1038/s41598-017-03257-z>
35. Guiducci E, Lemberg C, Küng N, Schraner E, Theocharides APA, LeibundGut-Landmann S. Candida albicans-induced NETosis is independent of peptidylarginine deiminase 4. *Front Immunol.* 2018;9(JUL):1–15.
 36. Arcanjo A, Logullo J, Menezes CCB, de Souza Carvalho Giangiarulo TC, dos Reis MC, de Castro GMM, et al. The emerging role of neutrophil extracellular traps in severe acute respiratory syndrome coronavirus 2 (COVID-19). *Sci Rep.* 2020;10(1):1–11.
 37. Zucoloto AZ, Jenne CN. Platelet-Neutrophil Interplay: Insights Into Neutrophil Extracellular Trap (NET)-Driven Coagulation in Infection. *Front Cardiovasc Med.* 2019;6(June):1–8.
 38. Chatfield SM, Grebe K, Whitehead LW, Rogers KL, Nebl T, Murphy JM, et al. Monosodium Urate Crystals Generate Nuclease-Resistant Neutrophil Extracellular Traps via a Distinct Molecular Pathway. *J Immunol.* 2018;ji1701382.
 39. Papayannopoulos V, Metzler KD, Hakkim A, Zychlinsky A. Neutrophil elastase and myeloperoxidase regulate the formation of neutrophil extracellular traps. *J Cell Biol.* 2010;191(3):677–91.
 40. Metzler KD, Fuchs TA, Nauseef WM, Reumaux D, Roesler J, Schulze I, et al. Myeloperoxidase is required for neutrophil extracellular trap formation: Implications for innate immunity. *Blood.* 2011;117(3):953–9.
 41. Warnatsch A, Ioannou M, Wang Q, Papayannopoulos V. Inflammation. Neutrophil extracellular traps license macrophages for cytokine production in atherosclerosis. *Science.* 2015 Jul;349(6245):316–20.
 42. Wang Y, Wysocka J, Sayegh J, Lee Y-H, Perlin JR, Leonelli L, et al. Human PAD4 regulates histone arginine methylation levels via demethylimination. *Science.* 2004 Oct;306(5694):279–83.
 43. Li P, Li M, Lindberg MR, Kennett MJ, Xiong N, Wang Y. PAD4 is essential for antibacterial innate immunity mediated by neutrophil extracellular traps. *J Exp Med.* 2010 Aug;207(9):1853–62.
 44. Leonard TA, Róycki B, Saidi LF, Hummer G, Hurley JH. Crystal structure and allosteric activation of protein kinase C β II. *Cell.* 2011;144(1):55–66.
 45. Karlsson A, Nixon JB, McPhail LC. Phorbol myristate acetate induces neutrophil NADPH-oxidase activity by two separate signal transduction pathways: Dependent or independent of phosphatidylinositol 3-kinase. *J Leukoc Biol.* 2000;67(3):396–404.
 46. Choi HK, Atkinson K, Karlson EW, Willett W, Curhan G. Purine-Rich Foods, Dairy and Protein Intake, and the Risk of Gout in Men. *N Engl J Med [Internet].* 2004 Mar 11;350(11):1093–103. Available from: <http://www.nejm.org/doi/abs/10.1056/NEJMoa035700>
 47. Choi HK, Atkinson K, Karlson EW, Willett W, Curhan G. Alcohol intake and risk of incident gout in men: a prospective study. *Lancet [Internet].* 2004 Apr;363(9417):1277–81. Available from: <https://linkinghub.elsevier.com/retrieve/pii/S0140673604160005>
 48. Dehlin M, Jacobsson L, Roddy E. Global epidemiology of gout: prevalence, incidence, treatment patterns and risk factors. *Nat Rev Rheumatol [Internet].* 2020 Jul 15;16(7):380–90. Available from: <http://www.nature.com/articles/s41584-020-0441-1>
 49. So AK, Martinon F. Inflammation in gout: Mechanisms and therapeutic targets. *Nat Rev Rheumatol.* 2017;13(11):639–47.
 50. Maiuolo J, Oppedisano F, Gratteri S, Muscoli C, Mollace V. Regulation of uric acid metabolism and excretion. *Int J Cardiol.* 2016;213:8–14.

51. Kratzer JT, Lanaspá MA, Murphy MN, Cicerchi C, Graves CL, Tipton PA, et al. Evolutionary history and metabolic insights of ancient mammalian uricases. *Proc Natl Acad Sci U S A*. 2014;111(10):3763–8.
52. Ames BN, Cathcart R, Schwiers E, Hochstein P. Uric acid provides an antioxidant defense in humans against oxidant- and radical-caused aging and cancer: a hypothesis. *Proc Natl Acad Sci U S A*. 1981 Nov;78(11):6858–62.
53. Rodrigues TC, Maahs DM, Johnson RJ, Jalal DI, Kinney GL, Rivard C, et al. Serum uric acid predicts progression of subclinical coronary atherosclerosis in individuals without renal disease. *Diabetes Care*. 2010 Nov;33(11):2471–3.
54. Santana MS, Nascimento KP, Lotufo PA, Benseñor IM, Meotti FC. Allantoin as an independent marker associated with carotid intima-media thickness in subclinical atherosclerosis. *Brazilian J Med Biol Res [Internet]*. 2018;51(8). Available from: http://www.scielo.br/scielo.php?script=sci_arttext&pid=S0100-879X2018000800613&tlng=en
55. Chaudhary K, Malhotra K, Sowers J, Aroor A. Uric Acid - key ingredient in the recipe for cardiorenal metabolic syndrome. *Cardiorenal Med*. 2013 Oct;3(3):208–20.
56. AL DOSSARI D, KAMAL D. Clinical Practice: Clinical Practice. *J Gastroenterol Hepatol*. 2015;30(S3):13–26.
57. Murea M, Tucker BM. The physiology of uric acid and the impact of end-stage kidney disease and dialysis. *Semin Dial*. 2019;32(1):47–57.
58. Lukkunaprasit T, Rattanasiri S, Turongkaravee S, Suvannang N, Ingsathit A, Attia J, et al. The association between genetic polymorphisms in ABCG2 and SLC2A9 and urate: an updated systematic review and meta-analysis. *BMC Med Genet*. 2020;21(1):1–13.
59. Stark K, Reinhard W, Grassl M, Erdmann J, Schunkert H, Illig T, et al. Common polymorphisms influencing serum uric acid levels contribute to susceptibility to gout, but not to coronary artery disease. *PLoS One*. 2009;4(11).
60. Champion EW, Glynn RJ, DeLabry LO. Asymptomatic hyperuricemia. Risks and consequences in the Normative Aging Study. *Am J Med*. 1987 Mar;82(3):421–6.
61. Howard RG, Pillinger MH, Gyftopoulos S, Thiele RG, Swearingen CJ, Samuels J. Reproducibility of musculoskeletal ultrasound for determining monosodium urate deposition: concordance between readers. *Arthritis Care Res (Hoboken)*. 2011 Oct;63(10):1456–62.
62. Dalbeth N, House ME, Aati O, Tan P, Franklin C, Horne A, et al. Urate crystal deposition in asymptomatic hyperuricaemia and symptomatic gout: a dual energy CT study. *Ann Rheum Dis*. 2015 May;74(5):908–11.
63. Martinon F, Pétrilli V, Mayor A, Tardivel A, Tschopp J. Gout-associated uric acid crystals activate the NALP3 inflammasome. *Nature*. 2006;440(7081):237–41.
64. Guo H, Callaway JB, Ting JP-Y. Inflammasomes: mechanism of action, role in disease, and therapeutics. *Nat Med [Internet]*. 2015;21(7):677–87. Available from: <https://doi.org/10.1038/nm.3893>
65. Dalbeth N, Gosling AL, Gaffo A, Abhishek A. Gout. *Lancet [Internet]*. 2021 May;397(10287):1843–55. Available from: <https://linkinghub.elsevier.com/retrieve/pii/S0140673621005699>
66. Bauernfeind FG, Horvath G, Stutz A, Alnemri ES, MacDonald K, Speert D, et al. Cutting Edge: NF-κB Activating Pattern Recognition and Cytokine Receptors License NLRP3 Inflammasome Activation by Regulating NLRP3 Expression. *J Immunol [Internet]*. 2009 Jul 15;183(2):787–91. Available from:

- <http://www.jimmunol.org/lookup/doi/10.4049/jimmunol.0901363>
67. Martinon F, Burns K, Tschopp J. The inflammasome: a molecular platform triggering activation of inflammatory caspases and processing of proIL-beta. *Mol Cell*. 2002 Aug;10(2):417–26.
 68. Reber LL, Gaudenzio N, Starkl P, Galli SJ. Neutrophils are not required for resolution of acute gouty arthritis in mice. *Nat Med*. 2016;22(12):1382–4.
 69. Neogi T. Gout. *N Engl J Med* [Internet]. 2011 Feb 3;364(5):443–52. Available from: <http://www.nejm.org/doi/abs/10.1056/NEJMcp1001124>
 70. Cicero AFG, Fogacci F, Cincione RI, Tocci G, Borghi C. Clinical Effects of Xanthine Oxidase Inhibitors in Hyperuricemic Patients. *Med Princ Pract* [Internet]. 2021;30(2):122–30. Available from: <https://www.karger.com/DOI/10.1159/000512178>
 71. Tátrai P, Erdő F, Dörnyei G, Krajcsi P. Modulation of urate transport by drugs. *Pharmaceutics*. 2021;13(6):1–22.
 72. Marquez LA, Huang JT, Dunford HB. Spectral and kinetic studies on the formation of myeloperoxidase compounds I and II: roles of hydrogen peroxide and superoxide. *Biochemistry*. 1994 Feb;33(6):1447–54.
 73. Kettle AJ. Myeloperoxidase: Unleashing the Power of Hydrogen Peroxide. In: *Hydrogen Peroxide Metabolism in Health and Disease*. 2017. p. 365–85.
 74. Nauseef WM. Biosynthesis of human myeloperoxidase. *Arch Biochem Biophys*. 2018;642(January):1–9.
 75. Van Antwerpen P, Slomianny MC, Boudjeltia KZ, Delporte C, Faid V, Calay D, et al. Glycosylation pattern of mature dimeric leukocyte and recombinant monomeric myeloperoxidase: Glycosylation is required for optimal enzymatic activity. *J Biol Chem*. 2010;285(21):16351–9.
 76. Booth KS, Kimura S, Lee HC, Ikeda-Saito M, Caughey WS. Bovine myeloperoxidase and lactoperoxidase each contain a high affinity site for calcium. *Biochem Biophys Res Commun*. 1989 Apr;160(2):897–902.
 77. Shin K, Hayasawa H, Lönnnerdal B. Mutations affecting the calcium-binding site of myeloperoxidase and lactoperoxidase. *Biochem Biophys Res Commun*. 2001;281(4):1024–9.
 78. Zederbauer M, Furtmüller PG, Ganster B, Moguilevsky N, Obinger C. The vinyl-sulfonium bond in human myeloperoxidase: impact on compound I formation and reduction by halides and thiocyanate. *Biochem Biophys Res Commun*. 2007 May;356(2):450–6.
 79. Zederbauer M, Furtmüller PG, Brogioni S, Jakopitsch C, Smulevich G, Obinger C. Heme to protein linkages in mammalian peroxidases: impact on spectroscopic, redox and catalytic properties. *Nat Prod Rep* [Internet]. 2007;24(3):571–84. Available from: <http://xlink.rsc.org/?DOI=B604178G>
 80. Carpena X, Vidossich P, Schroettner K, Calisto BM, Banerjee S, Stampfer J, et al. Essential Role of Proximal Histidine-Asparagine Interaction in Mammalian Peroxidases. *J Biol Chem* [Internet]. 2009 Sep;284(38):25929–37. Available from: <https://linkinghub.elsevier.com/retrieve/pii/S0021925818810663>
 81. Arnhold J, Furtmüller PG, Regelsberger G, Obinger C. Redox properties of the couple compound I/native enzyme of myeloperoxidase and eosinophil peroxidase. *Eur J Biochem*. 2001 Oct;268(19):5142–8.
 82. Furtmüller PG, Burner U, Obinger C. Reaction of myeloperoxidase compound I with chloride, bromide, iodide, and thiocyanate. *Biochemistry*. 1998 Dec;37(51):17923–30.
 83. Furtmüller PG, Burner U, Jantschko W, Regelsberger G, Obinger C. The reactivity of

- myeloperoxidase compound I formed with hypochlorous acid. *Redox Rep* [Internet]. 2000 Aug 1;5(4):173–8. Available from: <https://doi.org/10.1179/135100000101535717>
84. Kettle AJ, Winterbourn CC. A kinetic analysis of the catalase activity of myeloperoxidase. *Biochemistry*. 2001 Aug;40(34):10204–12.
 85. Kettle AJ, Sangster DF, Gebicki JM, Winterbourn CC. A pulse radiolysis investigation of the reactions of myeloperoxidase with superoxide and hydrogen peroxide. *Biochim Biophys Acta*. 1988 Aug;956(1):58–62.
 86. Heinecke JW, Li W, Daehnke HL 3rd, Goldstein JA. Dityrosine, a specific marker of oxidation, is synthesized by the myeloperoxidase-hydrogen peroxide system of human neutrophils and macrophages. *J Biol Chem*. 1993 Feb;268(6):4069–77.
 87. Meotti FC, Jameson GNL, Turner R, Harwood DT, Stockwell S, Rees MD, et al. Urate as a physiological substrate for myeloperoxidase: implications for hyperuricemia and inflammation. *J Biol Chem*. 2011 Apr;286(15):12901–11.
 88. Galijasevic S, Abdulhamid I, Abu-Soud HM. Melatonin is a potent inhibitor for myeloperoxidase. *Biochemistry*. 2008 Feb;47(8):2668–77.
 89. Ximenes VF, Maghzal GJ, Turner R, Kato Y, Winterbourn CC, Kettle AJ. Serotonin as a physiological substrate for myeloperoxidase and its superoxide-dependent oxidation to cytotoxic tryptamine-4,5-dione. *Biochem J*. 2009 Dec;425(1):285–93.
 90. Pálinkás Z, Furtmüller PG, Nagy A, Jakopitsch C, Pirker KF, Magierowski M, et al. Interactions of hydrogen sulfide with myeloperoxidase. *Br J Pharmacol*. 2015 Mar;172(6):1516–32.
 91. Bolscher BG, Zoutberg GR, Cuperus RA, Wever R. Vitamin C stimulates the chlorinating activity of human myeloperoxidase. *Biochim Biophys Acta*. 1984 Jan;784(2–3):189–91.
 92. Kettle AJ, Anderson RF, Hampton MB, Winterbourn CC. Reactions of superoxide with myeloperoxidase. *Biochemistry*. 2007;46(16):4888–97.
 93. Abu-Soud HM, Raushel FM, Hazen SL. A novel multistep mechanism for oxygen binding to ferrous hemoproteins: rapid kinetic analysis of ferrous-dioxy myeloperoxidase (compound III) formation. *Biochemistry*. 2004 Sep;43(36):11589–95.
 94. Jantschko W, Georg Furtmüller P, Zederbauer M, Lanz M, Jakopitsch C, Obinger C. Direct conversion of ferrous myeloperoxidase to compound II by hydrogen peroxide: an anaerobic stopped-flow study. *Biochem Biophys Res Commun*. 2003 Dec;312(2):292–8.
 95. Sicking W, Somnitz H, Schmuck C. DFT calculations suggest a new type of self-protection and self-inhibition mechanism in the mammalian heme enzyme myeloperoxidase: nucleophilic addition of a functional water rather than one-electron reduction. *Chemistry*. 2012 Aug;18(35):10937–48.
 96. Paumann-Page M, Furtmüller PG, Hofbauer S, Paton LN, Obinger C, Kettle AJ. Inactivation of human myeloperoxidase by hydrogen peroxide. *Arch Biochem Biophys*. 2013 Nov;539(1):51–62.
 97. Hoogland H, van Kuilenburg A, van Riel C, Muijsers AO, Wever R. Spectral properties of myeloperoxidase compounds II and III. *Biochim Biophys Acta*. 1987 Nov;916(1):76–82.
 98. Forbes L V., Sjögren T, Auchère F, Jenkins DW, Thong B, Laughton D, et al. Potent reversible inhibition of myeloperoxidase by aromatic hydroxamates. *J Biol Chem*. 2013;288(51):36636–47.
 99. Queiroz RF, Vaz SM, Augusto O. Inhibition of the chlorinating activity of myeloperoxidase by tempol: revisiting the kinetics and mechanisms. *Biochem J*. 2011 Nov;439(3):423–31.
 100. Galijasevic S, Abdulhamid I, Abu-Soud HM. Potential role of tryptophan and chloride in the inhibition of human myeloperoxidase. *Free Radic Biol Med* [Internet]. 2008

- Apr;44(8):1570–7. Available from:
<https://linkinghub.elsevier.com/retrieve/pii/S0891584908000269>
101. Meotti FC, Senthilmohan R, Harwood DT, Missau FC, Pizzolatti MG, Kettle AJ. Myricitrin as a substrate and inhibitor of myeloperoxidase: implications for the pharmacological effects of flavonoids. *Free Radic Biol Med*. 2008 Jan;44(1):109–20.
 102. Shiba Y, Kinoshita T, Chuman H, Taketani Y, Takeda E, Kato Y, et al. Flavonoids as Substrates and Inhibitors of Myeloperoxidase: Molecular Actions of Aglycone and Metabolites. *Chem Res Toxicol* [Internet]. 2008 Aug 1;21(8):1600–9. Available from: <https://doi.org/10.1021/tx8000835>
 103. Tien M. Myeloperoxidase-catalyzed oxidation of tyrosine. *Arch Biochem Biophys*. 1999 Jul;367(1):61–6.
 104. Marquez LA, Dunford HB. Kinetics of oxidation of tyrosine and dityrosine by myeloperoxidase compounds I and II. Implications for lipoprotein peroxidation studies. *J Biol Chem*. 1995 Dec;270(51):30434–40.
 105. Marquez LA, Dunford HB, Van Wart H. Kinetic studies on the reaction of compound II of myeloperoxidase with ascorbic acid. Role of ascorbic acid in myeloperoxidase function. *J Biol Chem*. 1990 Apr;265(10):5666–70.
 106. Vlasova II, Sokolov A V, Arnhold J. The free amino acid tyrosine enhances the chlorinating activity of human myeloperoxidase. *J Inorg Biochem*. 2012 Jan;106(1):76–83.
 107. Kettle AJ, Gedye CA, Winterbourn CC. Mechanism of inactivation of myeloperoxidase by 4-aminobenzoic acid hydrazide. *Biochem J*. 1997;321(2):503–8.
 108. Ward J, Spath SN, Pabst B, Carpino PA, Ruggeri RB, Xing G, et al. Mechanistic characterization of a 2-thioxanthine myeloperoxidase inhibitor and selectivity assessment utilizing click chemistry--activity-based protein profiling. *Biochemistry*. 2013 Dec;52(51):9187–201.
 109. Ruggeri RB, Buckbinder L, Bagley SW, Carpino PA, Conn EL, Dowling MS, et al. Discovery of 2-(6-(5-Chloro-2-methoxyphenyl)-4-oxo-2-thioxo-3,4-dihydropyrimidin-1(2H)-yl)acetamide (PF-06282999): A Highly Selective Mechanism-Based Myeloperoxidase Inhibitor for the Treatment of Cardiovascular Diseases. *J Med Chem*. 2015 Nov;58(21):8513–28.
 110. Duclos F, Abell LM, Harden DG, Pike K, Nowak K, Locke GA, et al. Triazolopyrimidines identified as reversible myeloperoxidase inhibitors. *Medchemcomm* [Internet]. 2017;8(11):2093–9. Available from: <http://dx.doi.org/10.1039/C7MD00268H>
 111. Taylor AM. The Resurrection of Myeloperoxidase as a Therapeutic Target: Is it Lazarus or Just an Apparition? *JACC Basic to Transl Sci* [Internet]. 2016;1(7):644–6. Available from: <http://dx.doi.org/10.1016/j.jacbts.2016.10.003>
 112. Malle E, Furtmüller PG, Sattler W, Obinger C. Myeloperoxidase: a target for new drug development? *Br J Pharmacol*. 2007 Nov;152(6):838–54.
 113. Aratani Y. Myeloperoxidase: Its role for host defense, inflammation, and neutrophil function. *Arch Biochem Biophys*. 2018 Feb;640:47–52.
 114. Nagra RM, Becher B, Tourtellotte WW, Antel JP, Gold D, Paladino T, et al. Immunohistochemical and genetic evidence of myeloperoxidase involvement in multiple sclerosis. *J Neuroimmunol*. 1997 Sep;78(1–2):97–107.
 115. Churg A, Marshall C V., Sin DD, Bolton S, Zhou S, Thain K, et al. Late intervention with a myeloperoxidase inhibitor stops progression of experimental chronic obstructive pulmonary disease. *Am J Respir Crit Care Med*. 2012;185(1):34–43.
 116. Stefanova N, Georgievska B, Eriksson H, Poewe W, Wenning GK. Myeloperoxidase

- Inhibition Ameliorates Multiple System Atrophy-Like Degeneration in a Transgenic Mouse Model. *Neurotox Res.* 2012;21(4):393–404.
117. Choi DK, Pennathur S, Perier C, Tieu K, Teismann P, Wu DC, et al. Ablation of the inflammatory enzyme myeloperoxidase mitigates features of Parkinson's disease in mice. *J Neurosci.* 2005;25(28):6594–600.
 118. Ramachandra CJA, Ja KPMM, Chua J, Cong S, Shim W, Hausenloy DJ. Myeloperoxidase As a Multifaceted Target for Cardiovascular Protection. *Antioxid Redox Signal.* 2020 May;32(15):1135–49.
 119. Stamp LK, Turner R, Khalilova IS, Zhang M, Drake J, Forbes L V, et al. Myeloperoxidase and oxidation of uric acid in gout: implications for the clinical consequences of hyperuricaemia. *Rheumatology (Oxford).* 2014 Nov;53(11):1958–65.
 120. Liu C, Desikan R, Ying Z, Gushchina L, Kampfrath T, DeJulius J, et al. Effects of a novel pharmacologic inhibitor of myeloperoxidase in a mouse atherosclerosis model. *PLoS One.* 2012;7(12):e50767.
 121. Ali M, Pulli B, Courties G, Tricot B, Sebas M, Iwamoto Y, et al. Myeloperoxidase Inhibition Improves Ventricular Function and Remodeling After Experimental Myocardial Infarction. *JACC Basic to Transl Sci.* 2016 Dec;1(7):633–43.
 122. Tshako MH, Augusto O, Linares E, Chadi G, Giorgio S, Pereira CA. Tempol ameliorates murine viral encephalomyelitis by preserving the blood-brain barrier, reducing viral load, and lessening inflammation. *Free Radic Biol Med.* 2010;48(5):704–12.
 123. Hirche TO, Gaut JP, Heinecke JW, Belaaouaj A. Myeloperoxidase plays critical roles in killing *Klebsiella pneumoniae* and inactivating neutrophil elastase: effects on host defense. *J Immunol.* 2005 Feb;174(3):1557–65.
 124. Schürmann N, Forrer P, Casse O, Li J, Felmy B, Burgener AV, et al. Myeloperoxidase targets oxidative host attacks to *Salmonella* and prevents collateral tissue damage. *Nat Microbiol* [Internet]. 2017;2(January):1–9. Available from: <http://dx.doi.org/10.1038/nmicrobiol.2016.268>
 125. Lehrer RI, Cline MJ. Leukocyte myeloperoxidase deficiency and disseminated candidiasis: the role of myeloperoxidase in resistance to *Candida* infection. *J Clin Invest.* 1969 Aug;48(8):1478–88.
 126. Cech P, Papathanassiou A, Boreux G, Roth P, Miescher PA. Hereditary myeloperoxidase deficiency. *Blood.* 1979 Mar;53(3):403–11.
 127. Moosmann K, Bojanovsky A. [Recurrent candidiasis in bone-marrow peroxidase deficiency]. *Monatsschr Kinderheilkd.* 1975 May;123(5):408–9.
 128. Nelander K, Lagerstrom-Fermer M, Amilon C, Michaëlsson E, Heijer M, Kjaer M, et al. Early Clinical Experience With AZD4831, A Novel Myeloperoxidase Inhibitor, Developed for Patients With Heart Failure With Preserved Ejection Fraction. *Clin Transl Sci* [Internet]. 2021 May 1;14(3):812–9. Available from: <https://doi.org/10.1111/cts.12859>
 129. Thomas D, Moisidis A, Tsiakalos A, Alexandraki K, Syriou V, Kaltsas G. Antithyroid drug-induced aplastic anemia. *Thyroid.* 2008 Oct;18(10):1043–8.
 130. Watanabe N, Narimatsu H, Noh JY, Yamaguchi T, Kobayashi K, Kami M, et al. Antithyroid drug-induced hematopoietic damage: a retrospective cohort study of agranulocytosis and pancytopenia involving 50,385 patients with Graves' disease. *J Clin Endocrinol Metab.* 2012 Jan;97(1):E49–53.
 131. Akmal A, Kung J. Propylthiouracil, and methimazole, and carbimazole-related hepatotoxicity. *Expert Opin Drug Saf.* 2014 Oct;13(10):1397–406.
 132. Soubhye J, Van Antwerpen P, Dufrasne F. A patent review of myeloperoxidase inhibitors

- for treating chronic inflammatory syndromes (focus on cardiovascular diseases, 2013-2019). *Expert Opin Ther Pat* [Internet]. 2020 Aug 2;30(8):595–608. Available from: <https://www.tandfonline.com/doi/full/10.1080/13543776.2020.1780210>
133. Forbes L V, Furtmüller PG, Khalilova I, Turner R, Obinger C, Kettle AJ. Isoniazid as a substrate and inhibitor of myeloperoxidase: identification of amine adducts and the influence of superoxide dismutase on their formation. *Biochem Pharmacol*. 2012 Oct;84(7):949–60.
 134. Kuppusamy P, Wang P, Shankar RA, Ma L, Trimble CE, Hsia CJ, et al. In vivo topical EPR spectroscopy and imaging of nitroxide free radicals and polynitroxyl-albumin. *Magn Reson Med*. 1998 Dec;40(6):806–11.
 135. Reves R, Heilig CM, Tapy JM, Bozeman L, Kyle RP, Hamilton CD, et al. Intermittent tuberculosis treatment for patients with isoniazid intolerance or drug resistance. *Int J Tuberc Lung Dis Off J Int Union against Tuberc Lung Dis*. 2014 May;18(5):571–80.
 136. Willems H, De Cesco S, Svensson F. Computational Chemistry on a Budget: Supporting Drug Discovery with Limited Resources. *J Med Chem* [Internet]. 2020 Sep 24;63(18):10158–69. Available from: <https://doi.org/10.1021/acs.jmedchem.9b02126>
 137. DiMasi JA, Grabowski HG, Hansen RW. Innovation in the pharmaceutical industry: New estimates of R&D costs. *J Health Econ*. 2016;47:20–33.
 138. Smietana K, Siatkowski M, Møller M. Trends in clinical success rates. *Nat Rev Drug Discov* [Internet]. 2016;15(6):379–80. Available from: <https://doi.org/10.1038/nrd.2016.85>
 139. Roses AD. Pharmacogenetics in drug discovery and development: a translational perspective. *Nat Rev Drug Discov*. 2008 Oct;7(10):807–17.
 140. Hefti FF. Requirements for a lead compound to become a clinical candidate. *BMC Neurosci* [Internet]. 2008 Dec 10;9(S3):S7. Available from: <https://bmcneurosci.biomedcentral.com/articles/10.1186/1471-2202-9-S3-S7>
 141. Evans SR. Fundamentals of clinical trial design. *J Exp Stroke Transl Med* [Internet]. 2010 Jan 1;3(1):19–27. Available from: <https://pubmed.ncbi.nlm.nih.gov/21533012>
 142. Suvarna V. Phase IV of Drug Development. *Perspect Clin Res* [Internet]. 2010 Apr;1(2):57–60. Available from: <https://pubmed.ncbi.nlm.nih.gov/21829783>
 143. Martin L, Hutchens M, Hawkins C, Radnov A. How much do clinical trials cost? *Nat Rev Drug Discov* [Internet]. 2017;16(6):381–2. Available from: <https://doi.org/10.1038/nrd.2017.70>
 144. Yan XC, Sanders JM, Gao Y-D, Tudor M, Haidle AM, Klein DJ, et al. Augmenting Hit Identification by Virtual Screening Techniques in Small Molecule Drug Discovery. *J Chem Inf Model* [Internet]. 2020 Sep 28;60(9):4144–52. Available from: <https://doi.org/10.1021/acs.jcim.0c00113>
 145. Yu W, MacKerell ADJ. Computer-Aided Drug Design Methods. *Methods Mol Biol*. 2017;1520:85–106.
 146. Ou-Yang S, Lu J, Kong X, Liang Z, Luo C, Jiang H. Computational drug discovery. *Acta Pharmacol Sin* [Internet]. 2012;33(9):1131–40. Available from: <https://doi.org/10.1038/aps.2012.109>
 147. Hauri S, Khakzad H, Happonen L, Telemann J, Malmström J, Malmström L. Rapid determination of quaternary protein structures in complex biological samples. *Nat Commun* [Internet]. 2019;10(1):192. Available from: <https://doi.org/10.1038/s41467-018-07986-1>
 148. Waterhouse A, Bertoni M, Bienert S, Studer G, Tauriello G, Gumienny R, et al. SWISS-MODEL: homology modelling of protein structures and complexes. *Nucleic Acids Res* [Internet]. 2018 Jul 2;46(W1):W296–303. Available from:

- <https://academic.oup.com/nar/article/46/W1/W296/5000024>
149. Batool M, Ahmad B, Choi S. A Structure-Based Drug Discovery Paradigm. *Int J Mol Sci* [Internet]. 2019 Jun 6;20(11):2783. Available from: <https://www.mdpi.com/1422-0067/20/11/2783>
 150. Jumper J, Evans R, Pritzel A, Green T, Figurnov M, Ronneberger O, et al. Highly accurate protein structure prediction with AlphaFold. *Nature* [Internet]. 2021;596(7873):583–9. Available from: <https://doi.org/10.1038/s41586-021-03819-2>
 151. Vamathevan J, Clark D, Czodrowski P, Dunham I, Ferran E, Lee G, et al. Applications of machine learning in drug discovery and development. *Nat Rev Drug Discov* [Internet]. 2019;18(6):463–77. Available from: <https://doi.org/10.1038/s41573-019-0024-5>
 152. Carpenter KA, Huang X. Machine Learning-based Virtual Screening and Its Applications to Alzheimer’s Drug Discovery: A Review. *Curr Pharm Des*. 2018;24(28):3347–58.
 153. Oprea T. Virtual Screening in Lead Discovery: A Viewpoint. *Molecules* [Internet]. 2002 Jan 31;7(1):51–62. Available from: <http://www.mdpi.com/1420-3049/7/1/51>
 154. Lipinski CA, Lombardo F, Dominy BW, Feeney PJ. Experimental and computational approaches to estimate solubility and permeability in drug discovery and development settings. *Adv Drug Deliv Rev*. 2001 Mar;46(1–3):3–26.
 155. Veber DF, Johnson SR, Cheng H-Y, Smith BR, Ward KW, Kopple KD. Molecular Properties That Influence the Oral Bioavailability of Drug Candidates. *J Med Chem* [Internet]. 2002 Jun 1;45(12):2615–23. Available from: <https://doi.org/10.1021/jm020017n>
 156. Shultz MD. Two Decades under the Influence of the Rule of Five and the Changing Properties of Approved Oral Drugs. *J Med Chem* [Internet]. 2019 Feb 28;62(4):1701–14. Available from: <https://doi.org/10.1021/acs.jmedchem.8b00686>
 157. Malvezzi A, Queiroz RF, De Rezende L, Augusto O, Amaral ATD. MPO inhibitors selected by virtual screening. *Mol Inform*. 2011;30(6–7):605–13.
 158. Aldib I, Soubhye J, Boudjeltia KZ, Vanhaeverbeek M, Rousseau A, Furtmüller PG, et al. Evaluation of new scaffolds of myeloperoxidase inhibitors by rational design combined with high-throughput virtual screening. *J Med Chem*. 2012;55(16):7208–18.
 159. Soubhye J, Chikh Alard I, Aldib I, Prévost M, Gelbcke M, De Carvalho A, et al. Discovery of Novel Potent Reversible and Irreversible Myeloperoxidase Inhibitors Using Virtual Screening Procedure. *J Med Chem*. 2017;60(15):6563–86.
 160. Ferreira RS, Oliva G, Andricopulo AD. Integrating virtual and high-throughput screening: Opportunities and challenges in drug research and development. *Quim Nova*. 2011;34(10):1770–8.
 161. Duclos F, Abell LM, Harden DG, Pike K, Nowak K, Locke GA, et al. Triazolopyrimidines identified as reversible myeloperoxidase inhibitors. *Medchemcomm* [Internet]. 2017;8(11):2093–9. Available from: <http://xlink.rsc.org/?DOI=C7MD00268H>

APPENDIX

**COMPOSTOS DERIVADOS HIDRAZIL OU HIDROXÂMICO DO ANIDRIDO
1,8-NAFTÁLICO, COMPOSIÇÃO FARMACÊUTICA E SEU USO**

Campo da invenção:

[001] A presente invenção se insere no campo das preparações farmacêuticas contendo ingredientes ativos orgânicos, especificamente contendo compostos derivados naftálicos, mais especificamente contendo compostos que promovem a inibição da enzima mieloperoxidase.

Fundamentos da invenção:

[002] A mieloperoxidase (MPO) é uma enzima pertencente à superfamília de peroxidase presente em fungos, plantas e animais. Em animais pode-se citar a lactoperoxidase, tireoide peroxidase, eosinofil peroxidase, prostaglandina II sintase e a própria mieloperoxidase.

[003] A MPO é encontrada em células mieloides como eosinófilos, macrófagos, micróglia e principalmente em leucócitos polimorfonucleares (neutrófilos). Após maturação, apresenta-se como um homodímero onde cada monômero é formado por uma cadeia leve e outra pesada, sendo que seu grupo heme encontra-se ligado à estrutura proteica por três ligações covalentes.

[004] A MPO reduz o peróxido de hidrogênio e posteriormente oxida íons haleto, principalmente cloreto, para gerar o ácido hipocloroso, que é um forte oxidante. Sua principal função fisiológica é a eliminação de agentes microbianos durante a fagocitose. Outros haletos como iodeto e brometo também são substratos da MPO como também o pseudo-haleto tiocianato.

[005] Neutrófilos são os leucócitos mais abundantes na circulação sanguínea e possuem um importante papel na

resposta inflamatória aguda e recentemente tem sido demonstrado também sua contribuição em processos inflamatórios crônicos. O mecanismo de defesa do sistema imunológico contra microrganismos invasores mediado por neutrófilos envolve inicialmente o englobamento do patógeno para dentro do vacúolo, em que o fagossomo gerado funde-se a grânulos contendo mieloperoxidase gerando o fagolisossomo.

[006] No referido fagolisossomo, a mieloperoxidase desempenha um complexo papel catalítico por meio do uso de vários substratos como ânion radical superóxido, peróxido de hidrogênio e finalmente cloreto, culminando na produção de ácido hipocloroso, um importante agente microbicida. Este poderoso oxidante reage com diversos grupos químicos como aminas para formar cloraminas, além de aminoácidos aromáticos clorados.

[007] Macrófagos também possuem capacidade fagocítica e expressam a mieloperoxidase podendo contribuir para a lesão oxidativa desencadeada pela MPO, embora a atividade desta seja muito inferior à encontrada em neutrófilos.

[008] As ações catalíticas da MPO não estão confinadas ao meio intracelular, sendo que seu extravasamento para os tecidos adjacentes, bem como para a circulação geral, é uma característica importante dessa enzima em muitos processos inflamatórios agudos e crônicos.

[009] As ações catalíticas da mieloperoxidase, principalmente sua ação clorinante, têm sido correlacionadas à fisiopatologia de várias doenças inflamatórias, como fibrose cística, asma, doença obstrutiva pulmonar crônica, artrite reumatoide e aterosclerose. Sua participação no processo aterosclerótico tem sido bem documentada, com

efeitos como desestabilização do ateroma e oxidação das lipoproteínas apoB100 da LDLs (do inglês, *low density lipoproteins*) e apoAI da HDL (do inglês, *high density lipoprotein*), ambos atribuídos às ações deletérias da MPO na aterosclerose. Além disso, seu potencial pró-inflamatório tem sido associado também às desordens neuro-inflamatórias como a doença de Alzheimer, Parkinson e esclerose dos múltiplos sistemas. Ainda, a doença emergente COVID-19, por exemplo, produz uma resposta inflamatória durante a fase de síndrome respiratória aguda grave, que está associada a um infiltrado neutrofílico pulmonar significativo e níveis elevados de MPO circulante.

[010] Devido ao papel proeminente da MPO em uma variedade de doenças e condições, estudos anteriores investigaram os efeitos de nocaute ou inibição de MPO e mostraram que atenuar a atividade dessa enzima fornece efeitos protetores em modelos inflamatórios. Nesse sentido, a MPO parece ser um alvo promissor para novos agentes terapêuticos que podem ser usados no tratamento de doenças inflamatórias e crônicas. Atualmente, existem diversas classes de inibidores da MPO. Inicialmente, hidroxamatos e hidrazidas foram os primeiros inibidores de MPO relatados. Posteriormente, outras classes químicas foram identificadas, incluindo polifenóis, indóis, antimaláricos, benzodioxóis, triptaminas, nitróxidos, naftalenos, tiouracilos e tioxantinas.

[011] No entanto, todos esses inibidores prospectivos falharam em ensaios clínicos e as agências reguladoras não os aprovaram. Portanto, a busca por novos inibidores com maior potência, biodisponibilidade e especificidade é particularmente relevante. Diversas estratégias

computacionais têm sido empregadas para identificar novos inibidores de MPO. A primeira metodologia de triagem virtual foi desenvolvida por Malvezzi *et al.* e usou uma abordagem baseada em ligante e estrutura com o programa de acoplamento GOLD e um modelo de farmacóforo.

[012] Esta metodologia exibiu uma alta taxa de sucesso, mas baixa diversidade química porque todos os inibidores descobertos eram hidrazidas. Pouco tempo depois, usando o software de docagem molecular Glide, Aldib *et al.* recuperaram um conjunto de inibidores de MPO com um número diversificado de novos esqueletos moleculares, mas com uma baixa taxa de sucesso. Mais recentemente, Soubhye *et al* obtiveram a melhor taxa de sucesso, usando vários modelos de farmacóforo e o programa de acoplamento FlexX. No entanto, uma análise mais detalhada dos compostos ativos revelou muitos análogos e inibidores relatados anteriormente.

[013] Neste contexto, a presente invenção analisou as propriedades moleculares de 143 inibidores de MPO publicados anteriormente e gerou um perfil semelhante a um inibidor para a criação de um banco de dados enriquecido. Em seguida, a metodologia de triagem virtual validada foi aplicada ao banco de dados, seguida de docagem molecular com os programas GOLD e AutoDock. Acertos computacionais foram selecionados com base em sua estéreo-especificidade para o sítio ativo, que incluiu a análise do número de ligações de hidrogênio, energia de ligação e perfil do histograma.

[014] Em seguida, os resultados foram validados avaliando a inibição da atividade de cloração da MPO *in vitro*. Com base nesses resultados, o IC₅₀ de cada composto foi calculado.

[015] A reversibilidade da inibição foi avaliada pelo método de diluição e a inibição da atividade de cloração também foi testada em células dHL-60 e neutrófilos de sangue periférico. A presente invenção demonstra que integrar uma regra semelhante a um inibidor e uma metodologia baseada em estrutura validada é uma abordagem excelente para descobrir novos inibidores enzimáticos estruturalmente distintos dos conhecidos. Assim, ao melhorar a taxa de sucesso e a diversidade molecular dos compostos, diversos inibidores da MPO novos e potentes foram identificados, como, por exemplo, os derivados naftálicos, que possuem diversas atividades farmacológicas já reportadas, como atividade oncolítica, antimicrobiana, ansiolítica, antitrombótica, anti-hipertensiva, antidepressiva, analgésica e antiepilética.

[016] Desse modo, fica evidente a necessidade de identificação de um fármaco que possa inibir ou pelo menos reduzir a atividade indesejável da mieloperoxidase, atuando na prevenção e/ou tratamento de condições inflamatórias.

Estado da técnica:

[017] Alguns documentos do estado da técnica descrevem compostos com certa similaridade química, que proporcionam atividade anti-inflamatória, analgésica e imunomoduladora, tendo como mecanismos de ação a inibição de enzimas, no entanto, não conseguem resolver de maneira eficiente o problema técnico em questão.

[018] Godina M. A. (2017) revela a obtenção de derivados de ftalamida, com foco na análise atividade anti-inflamatória, analgésica e imunomoduladora dos referidos derivados, em diferentes ensaios pré-clínicos, sugerindo uma redução enzimática da mieloperoxidase.

[019] No entanto, ressalta-se que os compostos citados no referido artigo se referem a derivados N-alkil alcoólicos e N-alkil nitrados da ftalamida e não da naftalamida, que não satisfazem a fórmula Markush da presente invenção. Em suma, os referidos derivados N-alkil alcoólicos e N-alkil nitrados reportados, possuem modificações em porções do anel ftalâmico que impedem a inibição direta da atividade enzimática da MPO, sendo que a diminuição da atividade da MPO e da inflamação reportada se deve a mecanismos secundários. Nota-se que qualquer anti-inflamatório diminui a atividade da MPO, porém em níveis menores, e não por inibição direta, mas sim por modular vias que irão diminuir o influxo de neutrófilos e conseqüentemente a atividade da MPO.

[020] Mora (2003) revela sobre compostos de ftalimidas alkil/aryl substituídas e sua capacidade inibitória sob a enzima mieloperoxidase. Ainda, refere-se à influência dos compostos na produção e regulação do fator de necrose tumoral- α , adicionalmente, revela sobre a atividade antipsicótica desses derivados.

[021] Em suma, apesar de o referido artigo revelar uma inibição de MPO se verifica que não há alta similaridade ou identidade com os compostos da presente invenção.

[022] Cunha (2010) estuda a síntese e a atividade imunomoduladora de ftalimidas n-substituídas, considerando a obtenção de novas matrizes moleculares multi-alvos, porém para inibição de TNF- α , sendo este o fator de necrose tumoral alfa, também relacionado a processos inflamatórios.

[023] Entretanto, comparando-se com a presente invenção, não há ensaios ou testes que comprovem uma inibição frente

à MPO como mecanismo de ação para a atividade terapêutica.

[024] Vasconcelos (2016) revela sobre a terapia fotodinâmica com um derivado ftálico que atua sobre os níveis de enzimas envolvidas no estresse oxidativo e defesas antioxidantes. Ainda, o protocolo utilizado neste experimento demonstra maior influência da terapia sobre os mecanismos antioxidantes inespecíficos.

[025] O referido artigo apesar de apresentar mecanismo de ação similar, utiliza composto com estrutura química distinta, ftalocianinas, para modular o processo inflamatório.

[026] WO2017160632/A1 descreve um conjunto de derivados triazolpiridínicos como inibidores da mieloperoxidase. Estes compostos são úteis no tratamento e/ou profilaxia da falência cardíaca, doença pulmonar obstrutiva crônica (DPOC), aterosclerose e desordens relacionadas. No entanto, não descreve os compostos tais como identificados na presente invenção.

[027] Em suma, a presente invenção resolve o problema técnico relacionado às condições inflamatórias provenientes das ações catalíticas da MPO estabelecendo um composto estável e uma composição farmacêutica capaz de inibir ou pelo menos reduzir a atividade indesejável da mieloperoxidase na prevenção e/ou tratamento de condições inflamatórias.

Breve descrição da invenção:

[028] A presente invenção tem por objetivo propor um composto, ou um sal farmacêuticamente aceitável, de derivados hidrazil (N-NH₂) ou hidroxâmico (N-OH) do anidrido 1,8-naftálico com mecanismo de ação competitivo frente ao

sítio ativo da enzima mieloperoxidase.

[029] Em uma segunda modalidade, a invenção propõe uma composição farmacêutica contendo ingredientes ativos orgânicos, especificamente contendo os compostos derivados naftálicos supracitados, que são capazes de inibir ou pelo menos reduzir a atividade indesejável da mieloperoxidase na prevenção e/ou tratamento de condições inflamatórias.

[030] Em uma terceira modalidade a presente invenção refere-se ao uso da referida composição farmacêutica visando a profilaxia ou o tratamento de qualquer doença ou condição nas quais a enzima mieloperoxidase (MPO) e outras peroxidases como eosinófilo peroxidase, tireoide peroxidase e peroxidase possuam relevância fisiopatológica.

Breve descrição das figuras:

[031] Para obter uma visualização completa dos resultados adquiridos a partir dos testes de concretização desta invenção, são apresentadas as figuras as quais se faz referências, conforme se segue.

[032] Na Figura 1 apresenta-se um fluxo da triagem virtual para seleção de possíveis compostos inibidores da mieloperoxidase.

[033] Na Figura 2 representa-se a distribuição de frequência de propriedade molecular para 143 inibidores da MPO conhecidos. As barras azuis representam a distribuição de frequência considerando todos os inibidores e as barras amarelas representam os inibidores com valores de IC_{50} inferiores a 500 nM. Siglas: MW - Peso molecular; ACD/log P - coeficiente de partição de octanol/água; n_{OHNH} - número de doadores de hidrogênio; n_{ON} - número de aceptores de hidrogênio; RBC - contagem de ligação rotativa; TPSA - área

de superfície polar 2D.

[034] Na Figura 3 apresenta-se um gráfico referente a uma representação 2D dos espaços químicos referentes a Lipinski/Veber (amarelo) e de inibidores da MPO (verde). Siglas: MW - Peso molecular; ACD/log P - coeficiente de partição de octanol/água; nOHNH - Número de doadores de hidrogênio; nON - número de aceptores de hidrogênio; RBC - contagem de ligações rotativas; TPSA - área superficial polar 2D.

[035] Na Figura 4 representa-se as métricas estatísticas usadas para validar os protocolos de triagem virtual, em que (A) apresenta a AUC - área sob a curva ROC, (B) apresenta o RIE - enriquecimento inicial robusto, (C) apresenta a BEDROC - distribuição aprimorada de Boltzmann do operador receptor e (D) apresenta o EF - fator de enriquecimento. Os dados são apresentados como a média \pm desvio padrão médio de três simulações independentes. Os resultados foram analisados estatisticamente usando ANOVA de uma via, seguido pelo teste *posthoc* de Bonferroni. O asterisco (*) representa uma diferença estatística ($p < 0,05$) quando comparado aos grupos ChemScore, GoldScore ou AutoDockVina.

[036] Na Figura 5 apresenta-se a validação da docagem molecular. Ligantes cristalográficos HX1 (PDB ID 4C1M, painel superior) e o análogo de triazol (PDB ID 5WDJ, painel inferior) foram docados de forma cruzada na estrutura PDB 1CXP. Os valores RMSD foram calculados entre a conformação simulada (azul) e cristalográfica (amarelo). Os respectivos histogramas e energias de ligação são exibidos nos painéis à direita das imagens do sítio ativo.

[037] Na Figura 6 representa-se a docagem molecular de

compostos ativos no sítio ativo da MPO, em que os inibidores são mostrados em verde, o grupo heme em cinza e os aminoácidos e ligações de hidrogênio em amarelo.

[038] Na Figura 7 apresenta-se o IC₅₀ (concentração capaz de inibir 50% da atividade enzimática) do composto I no ensaio de atividade clorinante da MPO e a dose dependência deste composto.

[039] Na Figura 8 apresenta-se o percentual de inibição da atividade clorinante em células dHL-60 (modelo celular neutrofílico).

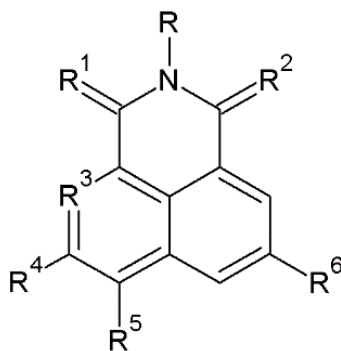
[040] Na Figura 9 apresenta-se o percentual de inibição da atividade clorinante em neutrófilos humanos extraídos de indivíduos saudáveis.

[041] Na Figura 10 apresenta-se um gráfico relativo à reversibilidade do composto intitulado ZINC9089086. Em que a MPO (100 nM) foi incubada com PTU (propiltiouracil) ou ZINC9089086 (20 µM) por 30 min a 37 °C e diluída 200 vezes em tampão acetato (0,2 M pH 5,4) com TMB (2 mM em DMF 10%). Em seguida, peróxido de hidrogênio (40 µM) foi adicionado para iniciar a reação. A atividade residual da peroxidase é expressa como a porcentagem do controle (0,33% DMSO - dimetilsulfóxido). A análise estatística foi realizada por ANOVA de uma via, seguida do teste *posthoc* de Bonferroni. O asterisco (*) indica resultados estatisticamente diferentes ($p < 0,01$) quando comparados ao grupo DMSO.

[042] Na Figura 11 apresentam-se os resultados da atividade anti-inflamatória em camundongos do composto em doses equivalentes ao fármaco anti-inflamatório padrão ácido mefenâmico no modelo de artrite gotosa induzida por cristais de urato de sódio.

Descrição detalhada da invenção:

[043] A presente invenção compreende um composto, ou um sal farmacologicamente aceitável de derivados hidrazil (N-NH₂) ou hidroxâmico (N-OH) do anidrido 1,8-naftálico (I) com mecanismo de ação competitivo frente ao sítio ativo da enzima mieloperoxidase. Os átomos polares dos grupos R, R¹, R² presentes na fórmula abaixo (I), bem como a planaridade do anel naftalênico são essenciais para a interação com resíduos específicos e com o grupo heme do sítio ativo, sendo conseqüentemente essenciais à atividade inibitória frente a MPO. O referido composto consiste em:



(I)

em que R é um átomo de hidrogênio, oxigênio ou nitrogênio;

em que R¹ é um átomo de oxigênio, enxofre ou nitrogênio;

em que R² é um átomo de oxigênio, enxofre ou nitrogênio;

em que R³ é um átomo de carbono ou nitrogênio;

em que R⁴ representa os átomos de hidrogênio, halogênios e os grupos -CX₃, -CHX₂, -CH₂X, -OCX₃, -OCR₂X, -OCHX, -N₃, -CN, -SOR, -SONRR, -NHC(O)NRR, -N(O), -NRR, -C(O)R, -C(O)-OR, -C(O)NRR, -OR, -NRSO₂R, -NRC(O)R, -NRAC(O)OR, -NROR, substituídos ou não por grupos alquil como heteroalquil, ciclo-alquil, heterociclo-alquil, aril ou hetero-aril;

em que R⁵ representa os átomos de hidrogênio, halogênios

e os grupos $-CX_3$, $-CHX_2$, $-CH_2X$, $-OCX_3$, $-OCR_2X$, $-OCHX$, $-N_3$, $-CN$, $-SOR$, $-SONRR$, $-NHC(O)NRR$, $-N(O)$, $-NRR$, $-C(O)R$, $-C(O)-OR$, $-C(O)NRR$, $-OR$, $-NRSO_2R$, $-NRC(O)R$, $-NRAC(O)OR$, $-NROR$, substituídos ou não por grupos alquil como heteroalquil, ciclo-alquil, heterociclo-alquil, aril ou hetero-aril;

em que R^6 representa os átomos de hidrogênio, halogênios e os grupos $-CX_3$, $-CHX_2$, $-CH_2X$, $-OCX_3$, $-OCR_2X$, $-OCHX$, $-N_3$, $-CN$, $-SOR$, $-SONRR$, $-NHC(O)NRR$, $-N(O)$, $-NRR$, $-C(O)R$, $-C(O)-OR$, $-C(O)NRR$, $-OR$, $-NRSO_2R$, $-NRC(O)R$, $-NRAC(O)OR$, $-NROR$, substituídos ou não por grupos alquil como heteroalquil, ciclo-alquil, heterociclo-alquil, aril ou hetero-aril.

[044] O termo halogênios aqui empregado refere-se aos átomos de flúor, cloro, bromo e iodo.

[045] O termo amínicos aqui empregado refere-se à função química amina seja ela primária, secundária ou terciária funcionalizada ou não com grupos alquil.

[046] O termo alquil refere-se a grupos alquílicos de cadeia simples, ramificada ou cíclica composta de um a doze átomos de carbono incluindo metil, etil, propil, butil, pentil, hexil, heptil, octil, decil, dodecil e seus isômeros.

[047] O termo amino-alquilas aqui empregado refere-se a grupamentos $-NR_3$ onde R representa 1, 2 ou 3 átomos de hidrogênio bem como grupamentos alquílicos de um a doze átomos de carbono incluindo metil, etil, propil, butil, pentil, hexil, heptil, octil, decil, dodecil e seus isômeros.

[048] O termo hidroxialquilas aqui empregado refere-se a grupamentos C_n-OH onde n representa de um a doze átomos de carbono incluindo metil, etil, propil, butil, pentil, hexil, heptil, octil, decil, dodecil e seus isômeros.

[049] O termo aril-alquilas aqui empregado refere-se a

grupamentos alquílicos de um a doze átomos de carbono incluindo metil, etil, propil, butil, pentil, hexil, heptil, octil, decil, dodecil simples, ramificados ou cíclicos ligados a anéis de 5 e 6 membros contendo opcionalmente 1, 2, 3 ou 4 hetero-átomos como N, O ou S, incluindo fenil, piridinil, pirrol, tienil, furanil, imidazol, triazol, tetrazol ou semelhantes funcionalizados ou não por halogênio, grupos alquil, fenil, hidroxil, amino, ciano ou nitro por exemplo.

[050] O termo guanido-alquilas aqui empregado refere-se a grupamentos alquílicos de um a doze átomos de carbono incluindo metil, etil, propil, butil, pentil, hexil, heptil, octil, decil, dodecil simples, ramificados ou cíclicos ligados a anéis de 5 e 6 membros contendo opcionalmente 1, 2, 3 ou 4 hetero-átomos como N, O ou S, incluindo fenil, piridinil, pirrol, tienil, furanil, imidazol, triazol, tetrazol e semelhantes.

[051] O referido composto foi identificado por meio de similaridade de propriedades moleculares com base na análise de inibidores conhecidos da MPO. Os quais apresentavam as seguintes faixas de propriedades moleculares: valores da massa molecular (174 a 396 u.m.a), do coeficiente de partição octanol/água (0,1 a 4,37), do número de doadores (0 a 7) e aceptadores de ligação de hidrogênio (2 a 9), do número de ligações rotacionáveis (0 a 8) e da área superficial polar (18 a 122) usadas na descoberta do referido composto.

[052] A partir de tais parâmetros, a referida regra de triagem foi aplicada em um banco de dados abrangente de compostos, p. ex. ZINC 12 (recentemente atualizado para ZINC 15), recuperando um total de 6546 moléculas que se

enquadrassem nos critérios estabelecidos dentre as mais de 35 milhões de moléculas.

[053] Na tentativa de selecionar quais dessas moléculas poderiam possuir maior potencial de inibição da MPO *in vitro*, realizou-se um estudo computacional empregando docagem molecular com auxílio de um programa específico (p. ex. *Gold*).

[054] A docagem molecular consiste em simular o encaixe dos possíveis inibidores dentro do sítio ativo da enzima. Essa etapa é a mais reprodutível, embora a natureza não determinística dos métodos de docagem dificultem a obtenção de um resultado idêntico estatisticamente, no que tange aos compostos elencados.

[055] Após essa etapa foi realizada a análise visual do resultado, sendo aplicados os critérios de análise como: número de ligações de hidrogênio, contatos desfavoráveis e estéreo-especificidade geométrica geral para eleger quais compostos seriam selecionados para a próxima etapa. Essa etapa recuperou um total de 242 moléculas que apresentaram um maior potencial teórico em inibir a MPO. Em seguida, os compostos foram submetidos a um novo experimento de docagem, porém em outro programa, sendo preferencialmente o AutoDock.

[056] Após essa etapa foi realizada uma nova análise com base no número de ligações de hidrogênio, perfil do histograma, energia livre de ligação, eficiência de ligação, constante de inibição e diversidade química, sendo selecionados 10 compostos que foram adquiridos pela empresa Specs (Zoetermeer, Netherlands) e desafiados frente a testes *in vitro* com a enzima MPO.

[057] Destes, 6 apresentaram atividade inibitória na

concentração de 20 uM, sendo a naftalamida o composto de maior atividade.

[058] A presente invenção engloba ainda uma composição farmacêutica que compreende:

0,001 a 20 % do composto ou sal farmaceuticamente aceitável de derivado hidrazil (N-NH₂) ou hidroxâmico (N-OH) do anidrido 1,8-naftálico, da Fórmula (I), na presença ou ausência de qualquer percentual de coadjuvante e/ou excipiente farmacotécnico líquido, sólido ou semissólido;

em que os referidos coadjuvantes e/ou excipientes farmacotécnicos são escolhidos dentre espessante e/ou aglutinante e/ou desagregante e/ou lubrificante e/ou agente molhante.

[059] Em uma modalidade preferencial utiliza-se de 2 a 20% de um espessante escolhido dentre: lactose, manitol, amido, celulose microcristalina, fosfato de cálcio dibásico diidratado, ou outro agente usado como espessante.

[060] Em uma modalidade preferencial utiliza-se de 2 a 20% de um aglutinante escolhido dentre: amido, PVP, derivados de celulose, gelatina, amido pré-gelatinizado ou outra substância com a mesma finalidade.

[061] Em uma modalidade preferencial utiliza-se de 2 a 20% de um desagregante, escolhido dentre: amido, celulose microcristalina, PVP modificado, amido pré-gelatinizado ou qualquer outro agente com a mesma função.

[062] Em uma modalidade preferencial utiliza-se de 1 a 3% de um lubrificante escolhido dentre: ácido esteárico, talco, estearato de magnésio ou qualquer outro agente com a mesma função.

[063] Em uma modalidade preferencial utiliza-se 0 a 1%

de um agente molhante escolhido dentre: lauril sulfato de sódio, polissorbatos: Tween® 20 (C₅₈H₁₁₄O₂₆), Tween® 60 (C₃₂H₆₂O₁₀), Tween® 80 (C₆₄H₁₂₄O₂₆), ou qualquer outro agente com a mesma função.

[064] O referido composto promoveu atividade inibitória *in vitro* e *in vivo* frente à enzima mieloperoxidase (MPO), caracterizando seu uso em formulações farmacêuticas veterinárias ou humanas compreendendo tal composto ou seus respectivos sais, visando a preparação de um medicamento para tratar condições inflamatórias agudas ou crônicas que envolvam a atividade inflamatória mediada pela enzima mieloperoxidase.

[065] As referidas doenças tratadas são principalmente fibrose cística, asma, aterosclerose, doença obstrutiva pulmonar crônica, artrite reumatoide, aterosclerose, doença de Alzheimer, doença de Parkinson, esclerose dos múltiplos sistemas, psoríase e insuficiência respiratória aguda grave (IRAG) gerada por infiltração neutrofílica.

Testes de concretização

[066] Uma revisão inicial da literatura científica e patentária revela que a naftalamida possui alguma similaridade com o clássico inibidor da MPO 4-hidrazida do ácido benzoico (ABAH), embora possua marcantes diferenças estruturais e de mecanismo de ação, como a inibição reversível, além de ser uma classe química e farmacológica distinta (naftalamida), desse modo, testes foram realizados para evidenciar seu efeito técnico.

[067] Para demonstrar todo o seu potencial, a presente invenção será mais detalhadamente descrita sob aspecto dos testes realizados assim como dos resultados obtidos.

Design de regras do tipo de inibidor MPO.

[068] Um conjunto de 143 inibidores de MPO, relatados anteriormente, foi usado para caracterizar o espaço químico desses inibidores e gerar a regra do tipo inibidor. As propriedades moleculares, incluindo massa molecular (MM), contagem de ligações rotativas (RBC), área de superfície polar topológica (TPSA), doadores de ligações de hidrogênio (OH, NH) e números de aceitadores (O, N) foram calculados por Molinspiration (www.molinspiration.com). O coeficiente de partição octanol-água (log P) foi estimado por ChemSketch (<https://www.acdlabs.com/>).

Preparação da estrutura do receptor.

[069] Três estruturas cristalográficas da MPO (PDB IDs 1CXP, 4C1M e 5WDJ) foram usadas para todos os estudos de docagem molecular. As estruturas da proteína foram editadas usando o software CAChe WorkSpace, onde todos os ligantes e moléculas de água foram removidos e átomos de hidrogênio adicionados. Os aminoácidos flexíveis foram identificados por sobreposição dos seguintes IDs de MPO PDB: 1DNU, 1DNW, 1MHL, 3F9P, 3ZS0, 3ZS1, 4C1M, 4DL1, 5FIW, 1CXP, 1D2V, 1D5L e 1D7W. Como as conformações e formas tautoméricas de alguns resíduos nos cristais de MPO são incompatíveis com o mecanismo catalítico da enzima, alguns ajustes foram realizados. Por exemplo, a histidina distal (His95) na enzima nativa exibe uma forma tautomérica *N π* sem carga que é essencial para a coordenação com peróxido de hidrogênio. Além disso, a espectroscopia de ressonância Raman e as simulações de dinâmica molecular demonstraram que a ionização do imidazol em imidazolato na histidina proximal (His336) maximiza as ligações de hidrogênio pela alteração

da orientação da Asn421.

Cálculo das cargas do grupo Heme.

[070] Nos estudos de docagem com AutoDock 4.2.3, as cargas de ferro e átomos próximos foram calculadas com o software MOPAC2016, usando as palavras-chave PRECISE, UHF, MS = 2,5, CHARGE = 1, METAL = (FE (+3)), PDBOUT, PL, GRADIENTES, NOOPT OPT-H e XYZ. Os Hamiltonianos PM6, PM6-D3, PM6-D3H4, PM6-D3H4X, PM6-DH +, PM6-DH2, PM6-DH2X e PM7 também foram avaliados. Para este cálculo, o sítio ativo foi representado pelo grupo heme e os seguintes aminoácidos: Asn421, Arg424, Arg333, His336, Glu242, Met243, Asp94, Asp98, Phe99 e Thr100.

Simulação de docagem molecular.

[071] As simulações de docagem molecular foram realizadas com os programas AutoDock 4.2.3, AutoDock Vina 1.1.2 e GOLD 5.4. Durante as simulações, a proteína foi mantida rígida e os ligantes flexíveis. Nas simulações com AutoDock e Vina, hidrogênios não polares foram mesclados e cargas de Gasteiger foram adicionadas. A caixa de grade tinha tamanho de $36 \times 40 \times 40 \text{ \AA}$, com uma distância do ponto de rede de $0,375 \text{ \AA}$, e estava centralizada nas coordenadas $24,123 \times 3,191 \times 43,257$. Cada simulação de docagem consistiu em 100 execuções e o algoritmo Genético Lamarckiano foi selecionado como o método de otimização. Para os estudos de docagem usando GOLD 5.4, o raio da simulação foi definido como 10 \AA , as funções de pontuação ASP, ChemPLP, GoldScore e ChemScore foram testadas e o parâmetro de eficiência foi definido em 30%. Todos os outros parâmetros foram definidos com os valores padrão. Após as simulações de docagem molecular, os resultados foram validados por docagem cruzada. Para isso,

a conformação experimental do inibidor hidroxamato (HX1) em PDB ID 4C1M e o análogo de triazol em PDB ID 5WDJ foram alinhadas à posição simulada na estrutura PDB ID 1CXP e o programa VMD foi usado para calcular as distâncias RMSD entre os átomos de ligante.

Validação de triagem virtual.

[072] Para validar as diferentes metodologias de triagem virtual baseadas em estrutura, o servidor *DUD-E* foi utilizado para gerar um conjunto de 456 iscas de 24 inibidores de MPO conhecidos. As métricas estatísticas, área sob a curva de característica de operação do receptor (AUC), fator de enriquecimento (EF), aprimoramento inicial robusto (RIE) e discriminação aprimorada de Boltzmann da característica de operação do receptor (BEDROC) foram calculadas usando Rv3.3.2 (www.r-project.org) e software RStudio v1.0.1.3.6 (www.rstudio.com).

Ensaio de inibição de MPO

[073] A naftalamida foi validada experimentalmente pela medição da atividade de clorinante mediada pela MPO. A mistura de reação incluiu MPO (10 nM), NaCl 140 mM, taurina 5 mM, cloreto de cetiltrimetilamônio 0,03% (CTAC), ácido dietilenotriaminopentaacético 0,1 mM (DTPA), tampão fosfato 20 mM pH 7,4 e o composto a ser testado (20 µM). Todos esses componentes foram incubados por 15 min a 37 °C e, em seguida, a reação foi iniciada pela adição de 40 µM (H₂O₂). Após 8 minutos, a reação foi interrompida com 20 µg/mL de catalase. A taurina cloramina foi quantificada monitorando a oxidação do TMB (3,3,5,5-tetrametilbenzidina) pelo iodeto. Para este ensaio, 240 µL da mistura de reação acima foram misturados com 60 µL de 2 mM TMB contendo 10% de dimetilformamida e 100

μM de iodeto de potássio (KI) em 400 mM de tampão de acetato (pH 5,4). Após 8 min, a absorvância a 650 nm foi medida em um leitor de microplacas. O grau de inibição foi baseado na atividade da amostra de controle, que continha 0,3% de DMSO (veículo). A concentração que inibiu 50% da atividade enzimática (IC_{50}) foi determinada usando oito concentrações diferentes de cada composto, e as curvas foram ajustadas usando regressão não-linear com o software *GraphPad Prism 5*.

[074] Inicialmente, um conjunto de 143 inibidores da MPO conhecidos foi analisado para verificar a distribuição de frequência de propriedades moleculares críticas relacionadas à biodisponibilidade oral e toxicidade.

[075] Como ilustrado na Figura 2, os compostos mais potentes (isto é, $\text{IC}_{50} \leq 500$ nM, barras amarelas) têm um perfil de distribuição semelhante quando comparado a todos os inibidores (barras azuis). É importante notar que a maioria dos inibidores de MPO selecionados para construir a regra do tipo inibidor de MPO não foram descobertos por metodologias que incluíram filtros de biodisponibilidade. Além disso, ao analisar todos os compostos em conjunto, a distribuição de frequência indicou biodisponibilidade oral limitada, de acordo com as regras de Lipinski e Veber (Tabela 1). Por outro lado, quando os inibidores mais potentes ($\text{IC}_{50} \leq 500$ nM) foram agrupados separadamente, eles obedeceram às regras de Lipinski e Veber, exceto quando a propriedade nOHNH foi analisada (Tabela 1):

Tabela 1: Propriedades moleculares de Inibidores de MPO

Regras	Propriedades	Alcance	
		Todos (não)	Mais potente
Lipinski	Peso molecular (≤ 500)	136-610	174-396 (sim)

Lipinski	ACD/log P (≤ 5)	-1,59-6,26	0,1-4,37 (sim)
Lipinski	nOHNH (≤ 5)	0-10	0-7 (não)
Lipinski	nON (≤ 10)	2-16	2-9 (sim)
Veber	RBC (≤ 10)	0-11	0-8 (sim)
Veber	TPSA ($\leq 140 \text{ \AA}^2$)	18-269	18-122 (sim)

[076] Esses resultados demonstram uma boa sobreposição entre os espaços químicos de alta potência e biodisponibilidade oral, um requisito na busca de novos inibidores orais ativos. Além disso, os compostos mais potentes exibem valores mais baixos de log P e TPSA mais altos, indicando menor toxicidade e uma janela terapêutica mais alta para este subconjunto. A análise dos valores do descritor indicou que as regras de Lipinski e Veber possuem apenas o limite superior. Comparando esses valores com os limites superior e inferior da regra semelhante ao inibidor de MPO (Tabela 1), é possível notar que o espaço químico semelhante a inibidor é um subespaço dentro dos espaços químicos de Lipinski e Veber, mas com uma pequena zona externa (OH/NH). Usando o banco de dados Zinc 12 (<http://zinc.docking.org>), que contém mais de 35 milhões de compostos, aplicou-se a regra semelhante a inibidor da MPO para procurar compostos exibindo propriedades inibitórias e biodisponibilidade oral. Esta abordagem de filtragem rendeu 6546 ligantes potenciais.

Primeira etapa baseada na estrutura

[077] Antes das simulações de docagem molecular, foi realizada a sobreposição das estruturas de cristal de MPO para detectar aminoácidos flexíveis. A superposição resultante das estruturas mostrou que as cadeias laterais Glu116, Asp218 e Met411 são flexíveis, mas distantes do sítio

ativo. Com base nessas observações, optou-se por configurar o MPO como um corpo rígido durante as simulações. Em seguida, os protocolos de docagem molecular foram testados e validados para a triagem virtual baseada em estrutura, usando iscas, redocagem e abordagens de docagem cruzada com três estruturas cristalográficas da MPO (PDB IDs 1CXP, 4C1M e 5WDJ). Para validar os programas GOLD 5.4 e *AutoDockVina*, foram geradas 456 iscas de 24 inibidores de MPO.

[078] Segundo Mysinger (2012), devido ao grande número de algoritmos de busca e funções de pontuação disponíveis, é importante avaliar o desempenho desses programas estatisticamente. Para tanto, foram avaliadas as seguintes quatro métricas estatísticas: área sob a curva ROC (AUC-ROC), BEDROC (discriminação aprimorada de Boltzmann do operador receptor), RIE (enriquecimento inicial robusto) e EF (fator de enriquecimento). Os valores de AUC-ROC, um indicador da capacidade de distinguir entre inibidores e não inibidores, foram altamente semelhantes entre as cinco metodologias, mas ASP e CHEMPLP tiveram valores significativamente maiores (Figura 4A). Da mesma forma, os valores RIE (Figura 4B) e BEDROC (Figura 4C) para ASP e CHEMPLP também eram superiores significativamente quando comparados com *ChemScore*, *GoldScore* e *AutoDockVina*, que foram determinados como tendo um baixo desempenho. Além disso, esses dois métodos exibiram valores elevados de FE (Figura 4D).

[079] Esses resultados demonstram que ASP e CHEMPLP tiveram o melhor desempenho em termos de reconhecimento precoce de inibidores da MPO. Assim, as funções de pontuação ASP e CHEMPLP foram selecionadas para a triagem virtual

baseada em estrutura. Curiosamente, um estudo anterior pesquisando inibidores da β -glucuronidase relatou que a ASP teve o pior desempenho na recuperação de inibidores, enquanto o *ChemScore* apresentou melhor desempenho. Esses dados sugerem que o desempenho do programa de docagem molecular e suas funções de pontuação são dependentes da enzima alvo, reforçando a importância de validar cada programa antes de iniciar uma metodologia virtual.

[080] A implementação desta etapa de validação sem dúvida aumenta a probabilidade de descoberta de novos inibidores. Aqui, as simulações de docagem molecular GOLD 5.4, em um modo de triagem rápida, reduziram efetivamente os candidatos a inibidor de 6546 para 242 (Figura 1). Nesta seleção, o modo de ligação molecular dos compostos 50% superiores (3273) foi analisado por inspeção visual, levando em consideração sua complementaridade estereoquímica. Este último foi analisado por meio da energia de ligação, o número de ligações de hidrogênio, o número de interações π e o perfil do histograma de docagem.

Segunda etapa baseada na estrutura

[081] Para melhorar a precisão da abordagem e confirmar as conformações dos ligantes acoplados, uma nova etapa de acoplamento molecular foi adicionada, usando o programa *AutoDock 4*. Neste caso, as cargas dos átomos hêmicos foram calculadas usando diferentes hamiltonianos semi-empíricos no programa MOPAC. Conforme resumido na Tabela 2, algumas das cargas adicionadas melhoraram a simulação de redocagem do ligante HX1 na estrutura PDB ID 4C1M. Por exemplo, a carga de ferro PM7 semi-empírica produziu a estrutura com o melhor RMSD (1,04Å) tanto para o cluster mais populoso quanto para

o de menor energia.

Tabela 2: Dados do agrupamento para o hidroxamato (HX1) em simulação de redocagem usando diferentes cargas semi-empíricas na estrutura da MPO PDB ID 4C1M.

Método	RMSD (Å) da população/cluster mais populoso	RMSD (Å) da população/cluster de menor energia	Número total do Cluster
Gasteiger	1,19 (57)	1,19 (57)	12
PM6	1,07 (60)	1,07 (60)	13
PM6-D3	1,07 (65)	1,07 (65)	9
PM6-D3H4	1,13 (69)	1,13 (69)	9
PM6-D3H4X	1,20 (64)	1,20 (64)	9
PM6-DH+	1,19 (61)	1,19 (61)	13
PM6-DH2	1,32 (62)	3,23 (20)	8
PM6-DH2X	1,22 (57)	3,41 (17)	15
PM7	1,04 (69)	1,04 (69)	11

[082] Além disso, a carga de ferro PM7 apresentou uma população elevada em ambos os agrupamentos. É plausível que o método PM7 aprimore a descrição das interações não-covalentes presentes neste Hamiltoniano, que são importantes para as interações intermoleculares. Para a validação de cross-docagem, HX1 e um análogo de triazol, ligantes da MPO presentes nas estruturas cristalinas PBD IDs 4C1M e 5WDJ, respectivamente, foram acoplados à estrutura de cristal MPO PBD ID 1CXP usando o programa *AutoDock* 4 (Figura 5). Os valores RMSD da docagem cruzada para os ligantes HX1 e o análogo de triazol foram 1,09 e 0,75 Å, respectivamente. Como esses valores eram menores que 2 Å, o protocolo de docagem molecular foi validado. Com o protocolo validado, agora usando o *AutoDock*, os 242 compostos identificados

anteriormente foram acoplados à MPO (PDB ID 1CXP). Usando os mesmos critérios descritos anteriormente para a seleção (6546 a 242 candidatos) e também, selecionando um grupo químico diverso (removendo réplicas). Todos os 242 complexos de docagem molecular foram analisados e os 10 principais inibidores de MPO potenciais foram adquiridos para testar a atividade da enzima. Digno de nota, algumas classes químicas anteriormente relatadas como inibidores de MPO também foram recuperadas na metodologia de triagem virtual. Estes incluíam flavonoides, hidrazinas e hidroxamatos. Além disso, a metodologia selecionou uma guanidina quinazolina idêntica e derivados previamente relatados como inibidores irreversíveis de MPO.

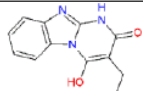
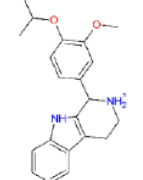
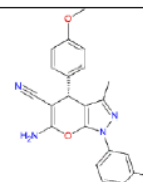
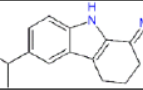
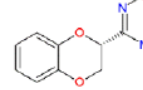
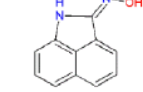
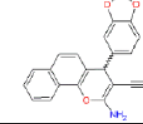
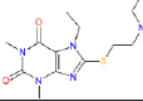
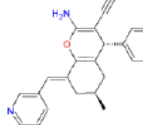
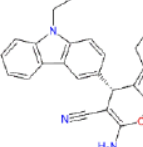
[083] Como o efeito inibitório desses compostos sobre a MPO já foi estabelecido, eles não foram incluídos para teste contra a enzima, pois superestimaria a taxa de sucesso da metodologia de triagem virtual. Os inibidores de MPO descritos recentemente aminopiridinas e um novo arcabouço de indol combinaram com o perfil semelhante ao inibidor de MPO em todos os parâmetros, apesar do fato de que eles não foram incluídos na elaboração da regra do tipo inibidor de MPO. Juntos, esses dados corroboram a precisão da regra do tipo inibidor de MPO para descobrir novos inibidores de MPO.

Validação e caracterização dos "hits"

[084] Os 10 compostos identificados foram subsequentemente adquiridos da Specs (Zoetermeer, Holanda), e a estrutura e pureza de cada um foram confirmadas por espectrometria de massa. Em seguida, um ensaio de cloração de MPO foi empregado para avaliar a ação inibitória desses compostos. Quando aplicados a 20 μM , seis dos 10 compostos

inibiram a cloração relacionada ao MPO em mais de 20% (faixa de 20 a 74%) quando comparados às amostras de controle (veículo) (Tabela 3):

Tabela 3: Lista dos 10 compostos selecionados para o ensaio de cloração e os respectivos códigos *Zinc*, *Specs*, estruturas, energias de ligação e atividades inibitórias.

Zinc code	Specs Code	Estrutura	Energia de ligação (kcal/mol)	Inibição at 20 μ M (%)
9089086	AI-204/31685032		-8.31	74 \pm 15
99474	AK-968/41705263		-9.35	60 \pm 10
660255	AM-807/13614268		-8.57	51 \pm 5.0
478529	AH-262/34342005		-7.31	48 \pm 1.0
13466360	AH-262/32490010		-6.29	40 \pm 1.0
4471880	AH-034/04864059		-7.18	20 \pm 1.0
208265	AH-034/11650405		-9.07	8.0 \pm 8.0
4134843	AG-690/40721604		-8.47	0.0 \pm 8.0
19796886	AO-476/43407309		-8.77	1.0 \pm 2.0
4450397	AM-807/41928974		-8.78	3.0 \pm 1.0

[085] As inibições exibidas pelos outros quatro compostos variaram entre 0-8% (Tabela 3). Esses resultados foram interpretados como uma taxa de sucesso de 60%. Os compostos apresentaram alta diversidade química, e nenhum foi relatado anteriormente como inibidor de MPO. Quatro dos inibidores têm um anel benzimidazol semelhante ao indol presente em muitos inibidores de MPO conhecidos.

[086] Notavelmente, o composto ZINC9089086 inibiu a atividade de cloração de MPO em mais de 70% a 20 μM , e a curva de resposta à dose indicou um IC_{50} de $2,2 \pm 0,1 \mu\text{M}$ (Figura 7). Os compostos que falharam em inibir a cloração mediada por MPO foram ZINC208265, ZINC4134843, ZINC19796886 e ZINC4450397 (Tabela 3). Deve ser salientado que a ausência de inibição por ZINC208265 e ZINC4134843 foi inesperada porque estes compostos contêm um benzodioxol e um fragmento de purina, respectivamente, que estão presentes em inibidores de MPO bem conhecidos e previamente descritos. A ausência de inibição por estes dois compostos revelou que outras propriedades, que não foram incluídas nas simulações de docagem molecular (por exemplo, o potencial redox) e potencialmente modificações que impactam a estrutura global do composto, também são importantes para conferir a inibição frente à MPO.

Estudo teórico ADME/Tox

[087] Os seguintes parâmetros farmacocinéticos teóricos, a saber, absorção gastrointestinal, biodisponibilidade oral, permeação da barreira hematoencefálica (BBB) e o substrato da glicoproteína P dos compostos ativos foram calculados pelo *SwissADME* (<http://www.swissadme.ch/>).

[088] A cardiotoxicidade foi medida pelo risco de

bloqueio do canal h-ERG por meio do servidor Pred-hERG 4.3 (<http://predherg.labmol.com.br/>). O potencial toxicológico, incluindo o risco de carcinogenicidade, citotoxicidade, hepatotoxicidade, imunotoxicidade e toxicidade aguda, foi calculado usando ProTox-II (http://tox.charite.de/protox_II/).

[089] A análise dos parâmetros farmacocinéticos de absorção gastrointestinal, índice de biodisponibilidade e substrato P-gp (Glicoproteína-P) revelou que todos os compostos ativos têm uma alta probabilidade de absorção gastrointestinal e biodisponibilidade oral (Tabela 4). Além disso, esses resultados fornecem evidências adicionais de que a aplicação de um filtro semelhante a um inibidor no fluxo de trabalho de triagem virtual facilita a recuperação de compostos com características moleculares privilegiadas para administração oral.

Tabela 4: Perfis teóricos ADME / Tox de compostos ativos

Farmacocinética						
Zinc Code	Absorção de GI	Pontuação de biodisponibilidade	BBB permeante			P-gp substrato
9089086	alta	0,56	Sim			Não
99474	alta	0,55	Sim			Sim
660255	alta	0,55	Não			Não
478529	alta	0,55	Sim			Sim
134466360	alta	0,55	Não			Não
4471880	alta	0,55	Sim			Não
Toxicidade						
Zinc Code	Inibidor hERG	Carcinogenicidade	Citotoxicidade	Hepatotoxicidade	Imunotoxicidade	LD₅₀ mg/kg
9089086	Não	Não	Não	Não	Não	300
99474	Sim	Não	Não	Não	Sim	595
660255	Sim	Não	Não	Sim	Não	900
478529	Sim	Sim	Não	Não	Não	374
134466360	Não	Sim	Não	Não	Não	348

30/39

4471880	Não	Não	Não	Sim	Não	4617
---------	-----	-----	-----	-----	-----	------

*Probabilidade de F> 10% no camundongo; GI - Gastrointestinal; BBB - Barreira hematoencefálica; P-gp - glicoproteína P; hERG - gene relacionado ao éter a-go-go.

[090] Surpreendentemente, foram identificados três inibidores (ZINC 9089086, ZINC99474 e ZINC478529) que eram permeáveis a BBB, embora nenhum filtro para penetração de BBB tenha sido aplicado na triagem. Esta observação é particularmente relevante porque foi relatado anteriormente que os inibidores de MPO permeáveis a BBB poderiam tratar doenças neuroinflamatórias. Além disso, o perfil ADME/Tox mostrou que cerca de 20% dos compostos apresentam riscos toxicológicos, exceto para cardiotoxicidade, onde 50% dos compostos provavelmente inibem o hERG. No entanto, os compostos selecionados apresentam baixa toxicidade aguda, evidenciada pelos valores de DL₅₀ acima de 300 mg/kg. Notavelmente, a análise integrativa desses parâmetros farmacocinéticos mostrou que ZINC9089086, o inibidor de MPO mais potente, apresenta riscos de toxicidade calculados reduzidos. Portanto, esse composto foi considerado o melhor candidato para otimizar e testar o modelo inflamatório.

[091] É importante ressaltar que os histogramas de docagem molecular mostram uma predominância clara de um único cluster para cinco dos seis compostos ativos. O composto ZINC660255 exibiu dois modos de ligação distintos. A conformação de menor energia (menos populosa) foi selecionada por apresentar mais ligações de hidrogênio. Os compostos ZINC9089086, ZINC99474 e ZINC660255 exibiram energias de ligação mais baixas (Tabela 3) do que o ligante HX1 cocrystalizado (Figura 5) e o composto ZINC99474 tinha uma energia de ligação mais baixa do que o triazol cocrystalizado (Figura 5). As simulações de docagem molecular mostraram que o inibidor mais potente, ZINC9089086, forma ligações de hidrogênio com Arg233 e o

carboxilato hêmico.

[092] Além disso, esse composto faz uma interação de empilhamento π entre seu anel benzimidazol e o pirrol hêmico (Figura 6). O composto ZINC99474 apresenta uma orientação do indol semelhante e forma uma ponte salina com o carboxilato hêmico. O composto ZINC660255 faz uma ligação de hidrogênio com Glu102 e outra com Gln91 e interações de empilhamento π com o heme, Phe360 e Phe401. O composto ZINC478529 contém uma orientação de sistema de três anéis, semelhante a ZINC9089086 e ZINC99474, formando uma ligação de hidrogênio com o carboxilato hêmico, um grupo hidrazina que participa de uma ligação de hidrogênio com His95 e um anel fenil que faz uma interação em forma de T com a Phe99.

[093] O composto ZINC13466360 forma ligações de hidrogênio com Arg233, Glu102 e o carboxilato hêmico e uma interação de empilhamento π deslocada com o pirrol hêmico. Por último, o composto ZINC4471880 faz uma interação de empilhamento π entre o anel tricíclico e o heme e forma ligações de hidrogênio com Gln91 e His95. Esses resultados são consistentes com estudos anteriores, demonstrando que essas interações são essenciais para o reconhecimento molecular entre o sítio ativo da MPO e os inibidores.

[094] De fato, a orientação dos grupos hidrazina e oxima entre o átomo de ferro e His95, como em ZINC478529 e ZINC4471880, é análoga à conformação catalítica proposta de peróxido de hidrogênio no sítio ativo do MPO nativo. Com base no fato de que a interação mais observada foi entre o pirrol hêmico e o sistema aromático dos ligantes, parece que a aromaticidade é uma propriedade essencial para a ação inibitória. Além disso, interações com o carboxilato hêmico

e Glu102 também foram comumente identificadas, indicando a importância desses elementos estruturais. Curiosamente, a última interação com Glu102 também está presente em vários inibidores potentes da MPO.

Cultura de células

[095] Células leucêmicas promielocíticas humanas (HL-60) foram cultivadas em meio RPMI 1640 com soro fetal bovino (20%) e penicilina (100 U/mL) em atmosfera umidificada de 5% CO₂ a 37°C. Para diferenciar as células HL-60 em células dHL-60, dimetilsulfóxido (1,25%) foi adicionado ao meio de crescimento acima e as células foram incubadas por 4 dias.

Isolamento de neutrófilos humanos.

[096] Neutrófilos de sangue periférico foram isolados do sangue de voluntários saudáveis (tendo em vista a aprovação do Comitê de ética CEPESH-ICB 1435/18) por centrifugação em um gradiente histopaque e dextrano, sedimentação e lise hipotônica dos glóbulos vermelhos.

Produção de ácido hipocloroso em células.

[097] Antes de medir a produção de ácido hipocloroso, as células dHL-60 e os neutrófilos humanos foram centrifugados a 1400 rpm por 10 min, lavados com solução salina estéril e suspensos em glicose PBS (Na₂HPO₄ 10 mM, KH₂PO₄ 2 mM, NaCl 140 mM, CaCl₂ 1 mM, 0,5 MgCl₂ mM e 1 g/L de glicose). Em seguida, as células (1×10⁶) foram ativadas com 100 nM de acetato de forbol miristato (PMA) e a taxa de produção de superóxido, com base na redução do citocromo c ($\lambda_{550\text{nm}} = 21.000 \text{ M}^{-1}\text{cm}^{-1}$), foi calculada para verificar a explosão oxidativa. O ácido hipocloroso foi quantificado usando o método TMB. Em resumo, o dHL-60 ou neutrófilos humanos (1×10⁶) foram incubados em PBS glicose contendo DTPA 0,1 mM, taurina 5 mM,

compostos de teste 20 μM e PMA 100 nM por 1 h a 37°C. As células de controle foram incubadas com DMSO a 0,3%. As amostras foram centrifugadas a 1400 rpm por 10 min, uma alíquota do sobrenadante foi diluída (três vezes) no mesmo tampão e 240 μL desta mistura foram incubados com 60 μL de tampão de acetato 0,4 M pH 5,4 contendo NaI 0,1 mM e TMB 2 mM dissolvido em 10% de dimetilformamida (DMF). A absorbância a 655 nm foi usada para monitorar a oxidação do TMB.

[098] O ensaio em células dHL-60 revelou que a naftalamida inibiu a atividade clorinante da mieloperoxidase em mais de 50% (Figura 8), apresentando uma alta potência em célula mesmo sendo um inibidor reversível.

[099] A potência *in vitro* da naftalamida foi determinada por meio de uma curva dose resposta.

[100] A atividade inibitória da naftalamida foi determinada por meio de diferentes concentrações desta no ensaio de atividade clorinante da MPO (Figura 7). A naftalamida apresentou um valor de IC_{50} na região nanomolar (275 nM), indicando alta potência inibitória.

Teste de reversibilidade

[101] Os compostos (20 μM) foram incubados com 100 nM de MPO em tampão de fosfato 20 mM pH 7,4 contendo 0,03% de CTAC a 37 ° C por 30 min. A reação foi iniciada pela adição de peróxido de hidrogênio 40 μM . Em seguida, uma alíquota foi diluída 200 vezes em tampão de acetato 0,2 M pH 5,4 contendo TMB 2 mM (10% DMF), e a atividade da peroxidase residual foi medida monitorando a oxidação de TMB a 655 nm após uma nova adição de peróxido de hidrogênio 40 μM .

[102] Após diluição, a quantificação da atividade residual de peroxidase indicou recuperação total da

atividade enzimática (Figura 10), indicando que após diluição, a naftalamida dissocia-se da MPO, o que sugere um mecanismo de inibição reversível, distinto do observado para o inibidor conhecido ABAH, que apresenta inibição irreversível.

Inibição da produção de ácido hipocloroso in vitro

[103] A inibição da atividade de cloração da MPO foi avaliada usando células dHL-60. Foi demonstrado anteriormente que diferenciar células HL-60 adicionando 1,25% de DMSO ao meio de cultura por 4-5 dias aumenta a expressão das subunidades NADPH oxidase, o que aumenta substancialmente a produção de superóxido, peróxido de hidrogênio e, conseqüentemente, ácido hipocloroso (HOCl) por essas células.

[104] Conforme mostrado na Tabela 5, ZINC9089086, o inibidor mais potente da atividade de cloração da MPO purificada, diminuiu a produção de ácido hipocloroso em células dHL-60.

Tabela 5: Produção de ácido hipocloroso em células

	Produção de HOCl (% de controle)	
	dHL-60	Neutrófilos humanos
PTU	6,2 ± 0,4	22 ± 4,2
ZINC9089086	31 ± 2,7	53 ± 4,2

[105] dHL-60 ou neutrófilos humanos (1×10^6) foram incubados em glicose PBS contendo 0,1 mM de DTPA, 5 mM de taurina, 20 μ M de composto de teste e 100 nM de PMA por 1 h a 37 °C. As amostras foram então centrifugadas a 1400 rpm por 10 min. Uma alíquota do sobrenadante foi diluída (três vezes) no mesmo tampão. A mistura de reação continha 240 μ L

do sobrenadante diluído, 60 μ L de tampão de acetato 0,4 M pH 5,4 contendo NaI 0,1 mM e TMB 2 mM dissolvido em DMF a 10%. A oxidação do TMB foi medida a 655 nm. Os valores são expressos como médias \pm DP, n = 4. As análises estatísticas envolveram ANOVA de uma via, seguida do teste *posthoc* de Bonferroni. O asterisco (*) representa resultados estatisticamente diferentes (p <0,05) quando comparados ao controle (DMSO).

[106] Para confirmar a inibição da cloração mediada por MPO, um conjunto semelhante de experimentos foi realizado usando neutrófilos humanos e foi observado um perfil de inibição semelhante (Tabela 5). Embora o composto ZINC9089086 tenha sido menos eficiente na inibição de MPO do que o inibidor irreversível propiltiouracil (PTU), ele exibiu maior inibição em neutrófilos do que outros inibidores de MPO descobertos recentemente.

[107] Embora a naftalimida se diferencie estruturalmente e no mecanismo de inibição do clássico inibidor de peroxidases, ABAH, por apresentar uma inibição reversível, estudos em neutrófilos humanos também indicaram que a naftalamida apresenta atividade inibitória frente a MPO comparável a inibidores irreversíveis, inibindo a produção de ácido hipocloroso em mais de 50%, indicando a alta potência desse composto.

Mecanismo de Inibição

[108] Estudos anteriores determinaram que existem três grupos de inibidores de MPO:

(i) inibidores de ligação (por exemplo, hidroxamatos);

(ii) inibidores baseados em mecanismo (por exemplo, 2-

tiouracil); e

(iii) acumuladores do composto II (por exemplo, indóis).

[109] Para elucidar o mecanismo de inibição de MPO mediada por ZINC9089086, o composto foi incubado com MPO por 30 min, a mistura de reação foi diluída 200 vezes e a atividade residual da peroxidase foi medida. Conforme mostrado na Figura 10, a atividade residual de MPO foi completamente restaurada após a diluição da amostra. Este resultado demonstra que ZINC9089086 é um inibidor reversível e significa que é um inibidor de ligação forte ou um acumulador do composto II. Com relação aos acumuladores do composto II, este grupo de inibidores de MPO não é considerado o melhor porque substratos fisiológicos do composto II de MPO (por exemplo, tirosina, ácido úrico e ascorbato) podem restaurar a enzima à sua forma férrica nativa. Assim, mais estudos com foco na discriminação entre esses dois mecanismos inibitórios são necessários.

Atividade anti-inflamatória - Modelo em camundongo

[110] Finalmente, para confirmar se a naftalamida apresentava atividade anti-inflamatória, foi realizado um estudo em camundongos usando um modelo de artrite gotosa (gota). Nesse modelo, os animais foram pré-tratados com a naftalamida e um fármaco de referência (ácido mefenâmico), nas doses de 3, 10 e 30 mg/kg pela via intraperitoneal dissolvidos em DMSO 5%. Após 15 minutos o edema de pata foi induzido pela administração na região plantar de cristais de urato de sódio na dose de 1,5 mg. O edema foi monitorado até a 6^a hora após a indução.

[111] A administração da naftalimida em doses

equivalentes ao fármaco anti-inflamatório padrão ácido mefenâmico no modelo de artrite gotosa induzida por cristais de urato de sódio revelou que a mesma apresenta atividade anti-edematosa comparável ao anti-inflamatório não-esteroidal, reduzindo o edema em aproximadamente 50% (Figura 11) e caracterizando, portanto, um composto de alta potência *in vivo*.

[112] Em conclusão, a presente invenção revela que a integração de uma regra semelhante a um inibidor com uma metodologia baseada em estrutura validada pode efetivamente gerar um banco de dados alvo enriquecido e identificar compostos com uma alta taxa de sucesso e diversidade química.

Referências Bibliográficas

[113] Aldib, I.; Soubhye, J.; Zouaoui Boudjeltia, K.; Vanhaeverbeek, M.; Rousseau, A.; Furtmüller, P. G.; Obinger, C.; Dufrasne, F.; Neve, J.; Van Antwerpen, P.; Prevost, M. Evaluation of New Scaffolds of Myeloperoxidase Inhibitors by Rational Design Combined with HighThroughput Virtual Screening. *J. Med. Chem.* 2012, 55, 7208-7218.

[114] Lipinski, C. A.; Lombardo, F.; Dominy, B. W.; Feeney, P. J. Experimental and Computational Approaches to Estimate Solubility and Permeability in Drug Discovery and Development Settings. *Adv. Drug Delivery Rev.* 2012, 64, 4-17.

[115] Malvezzi, A.; Queiroz, R. F.; de Rezende, L.; Augusto, O.; Amaral, A. T.-d. MPO Inhibitors Selected by Virtual Screening. *Mol. Inf.* 2011, 30, 605-613.

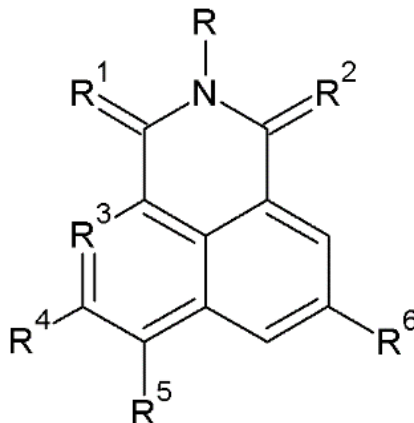
[116] Mysinger, M. M.; Carchia, M.; Irwin, J. J.; Shoichet, B. K. Directory of Useful Decoys, Enhanced (DUD-E): Better Ligands and Decoys for Better Benchmarking. *J. Med. Chem.* 2012, 55, 6582- 6594

[117] Soubhye, J.; Chikh Alard, I.; Aldib, I.; Prévost, M.; Gelbcke, M.; De Carvalho, A.; Furtmüller, P. G.; Obinger, C.; Flemmig, J.; Tadrent, S.; Meyer, F.; Rousseau, A.; Nève, J.; Mathieu, V.; Zouaoui Boudjeltia, K.; Dufrasne, F.; Van Antwerpen, P. Discovery of Novel Potent Reversible and Irreversible Myeloperoxidase Inhibitors Using Virtual Screening Procedure. *J. Med. Chem.* 2017, 60, 6563–6586.

[118] Veber, D. F.; Johnson, S. R.; Cheng, H.-Y.; Smith, B. R.; Ward, K. W.; Kopple, K. D. Molecular Properties That Influence the Oral Bioavailability of Drug Candidates. *J. Med. Chem.* 2002, 45, 2615– 2623.

REIVINDICAÇÕES

1. COMPOSTO, **caracterizado** pelo fato de ser de fórmula (I):



ou seu sal farmaceuticamente aceitável, em que:

R é um átomo de hidrogênio, oxigênio ou nitrogênio;

R¹ é um átomo de oxigênio, enxofre ou nitrogênio em que

R² é um átomo de oxigênio, enxofre ou nitrogênio;

R³ é um átomo de carbono ou nitrogênio;

R⁴, R⁵ e R⁶ são escolhidos dentre: hidrogênio, halogênios, -CX₃, -CHX₂, -CH₂X, -OCX₃, -OCR₂X, -OCHX, -N₃, -CN, -SOR, -SONRR, -NHC(O)NRR, -N(O), -NRR, -C(O)R, -C(O)-OR, -C(O)NRR, -OR, -NRSO₂R, -NRC(O)R, -NRAC(O)OR, -NROR, substituídos ou não por grupos alquil, heteroalquil, cicloalquil, heterociclo-alquil, aril ou hetero-aril.

2. COMPOSTO, de acordo com a reivindicação 1, **caracterizado** pelo fato de os halogênios serem flúor, cloro, bromo ou iodo.

3. COMPOSTO, de acordo com a reivindicação 1, **caracterizado** pelo fato de os grupos alquil serem de cadeia simples, ramificada ou cíclica composta de um a doze átomos de carbono incluindo metil, etil, propil, butil, pentil, hexil, heptil, octil, decil, dodecil e seus isômeros.

4. COMPOSTO, de acordo com a reivindicação 1, **caracterizado** pelo fato de ser preferencialmente o 2,5 diaminobenzo[de]isoquinolina-1,3-diona.

5. COMPOSIÇÃO FARMACÊUTICA, caracterizada pelo fato de compreender: 0,001 a 20 % do composto definido na reivindicação 1, na presença ou ausência de qualquer percentual de coadjuvante e/ou excipiente farmacotécnico líquido, sólido ou semissólido, em que os referidos coadjuvantes e/ou excipientes farmacotécnicos são escolhidos dentre espessante e/ou aglutinante e/ou desagregante e/ou lubrificante e/ou agente molhante.

6. COMPOSIÇÃO FARMACÊUTICA, de acordo com a reivindicação 5, caracterizado pelo fato de compreender preferencialmente 2 a 20% de um espessante escolhido dentre: lactose manitol, amido, celulose microcristalina, fosfato de cálcio dibásico diidratado.

7. COMPOSIÇÃO FARMACÊUTICA, de acordo com a reivindicação 5, caracterizado pelo fato de compreender preferencialmente 2 a 20% de um aglutinante escolhido dentre: amido, PVP, derivados de celulose, gelatina, amido pré-gelatinizado.

8. COMPOSIÇÃO FARMACÊUTICA, de acordo com a reivindicação 5, caracterizada pelo fato de compreender preferencialmente 2 a 20% de um desagregante, escolhido dentre: amido, celulose microcristalina, PVP modificado, amido pré-gelatinizado.

9. COMPOSIÇÃO FARMACÊUTICA, de acordo com a reivindicação 5, caracterizada pelo fato de compreender preferencialmente 1 a 3% de um lubrificante escolhido dentre: ácido esteárico, talco, estearato de magnésio.

10. COMPOSIÇÃO FARMACÊUTICA, de acordo com a reivindicação 5, caracterizada pelo fato de compreender

preferencialmente 0 a 1% de um agente molhante escolhido dentre: laurel sulfato de sódio, tween 20, tween 60, tween 80.

11. USO do composto conforme definido na reivindicação 1, caracterizado pelo fato de ser na preparação de um medicamento para tratar doenças inflamatórias relacionadas às ações catalíticas da enzima mieloperoxidase (MPO).

12. USO, de acordo com a reivindicação 11, caracterizado pelo fato de as referidas doenças inflamatórias serem fibrose cística, psoríase, asma, doença obstrutiva pulmonar crônica, artrite reumatoide, aterosclerose, doença de Alzheimer, doença de Parkinson, insuficiência respiratória aguda grave e esclerose dos múltiplos sistemas.

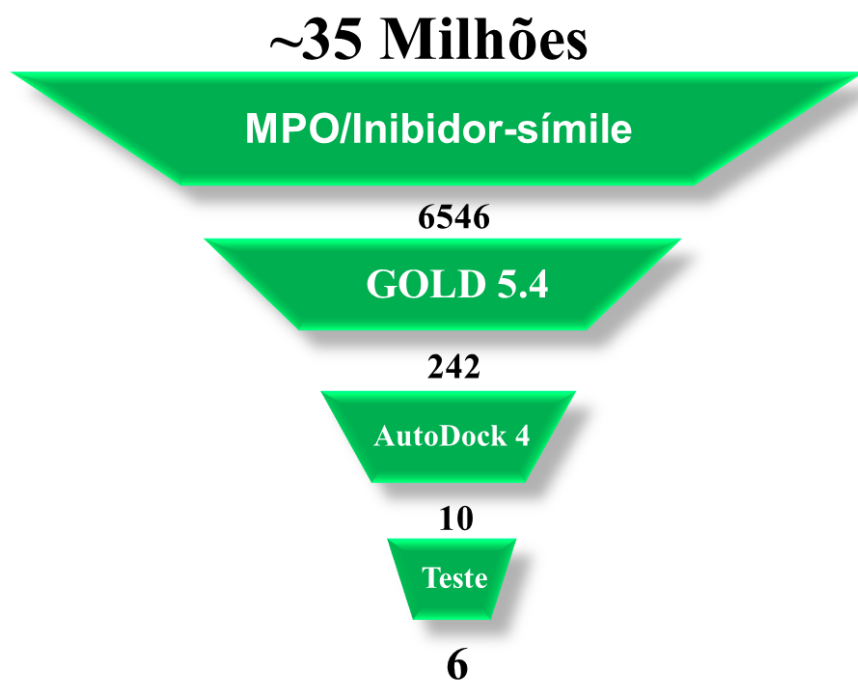


Figura 1

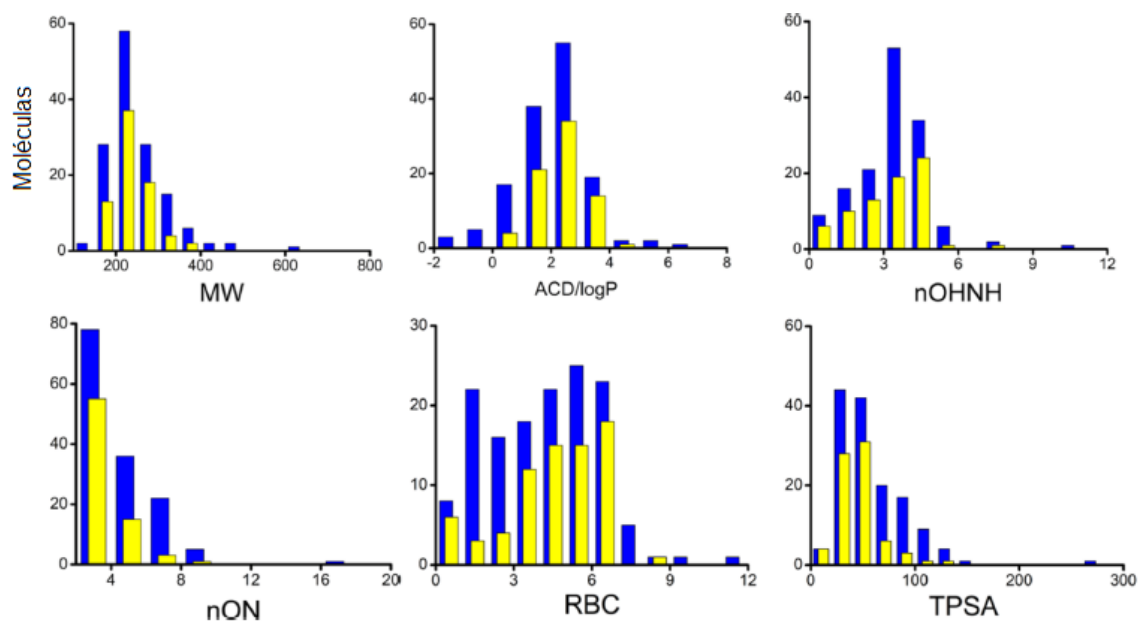


Figura 2

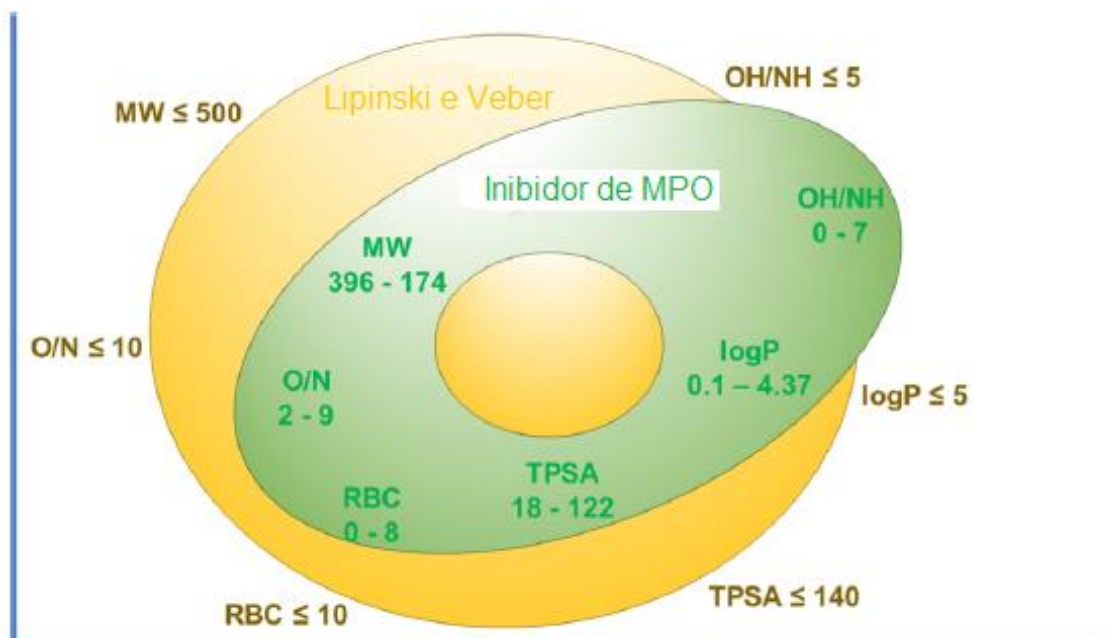


Figura 3

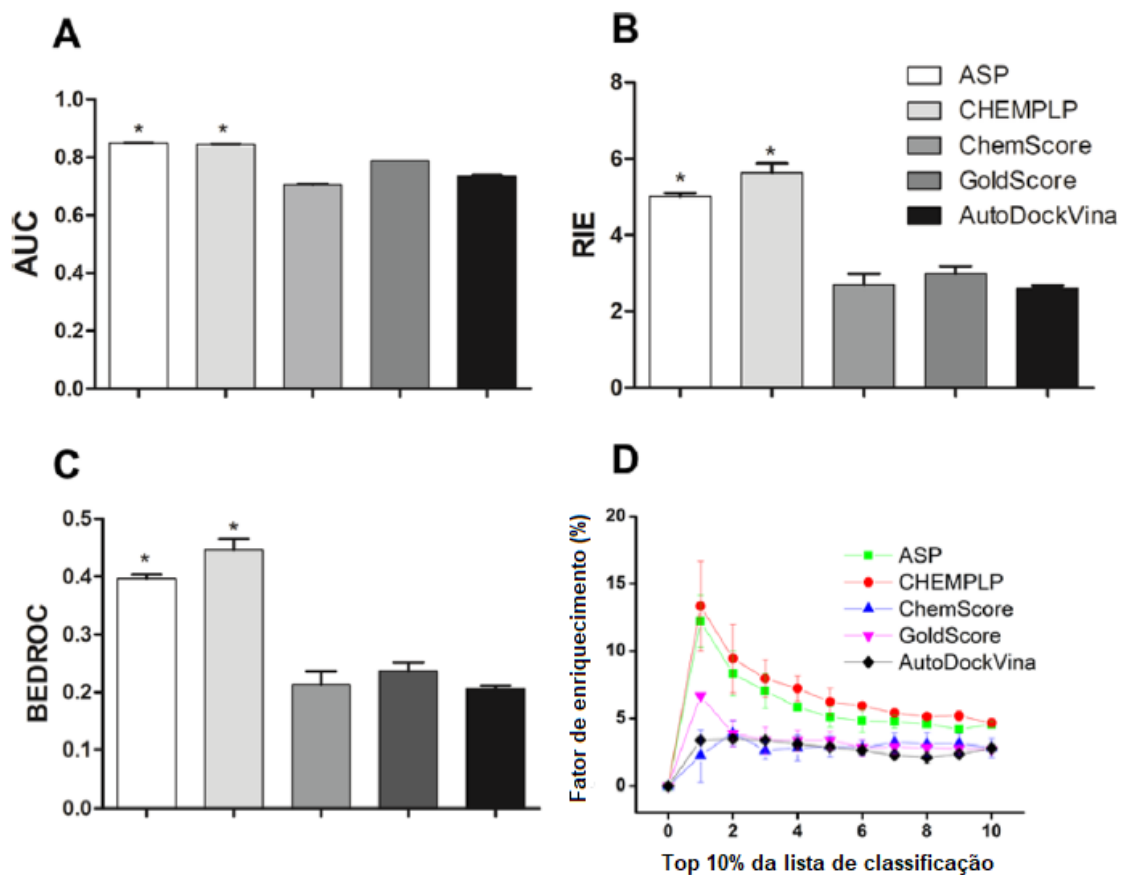


Figura 4

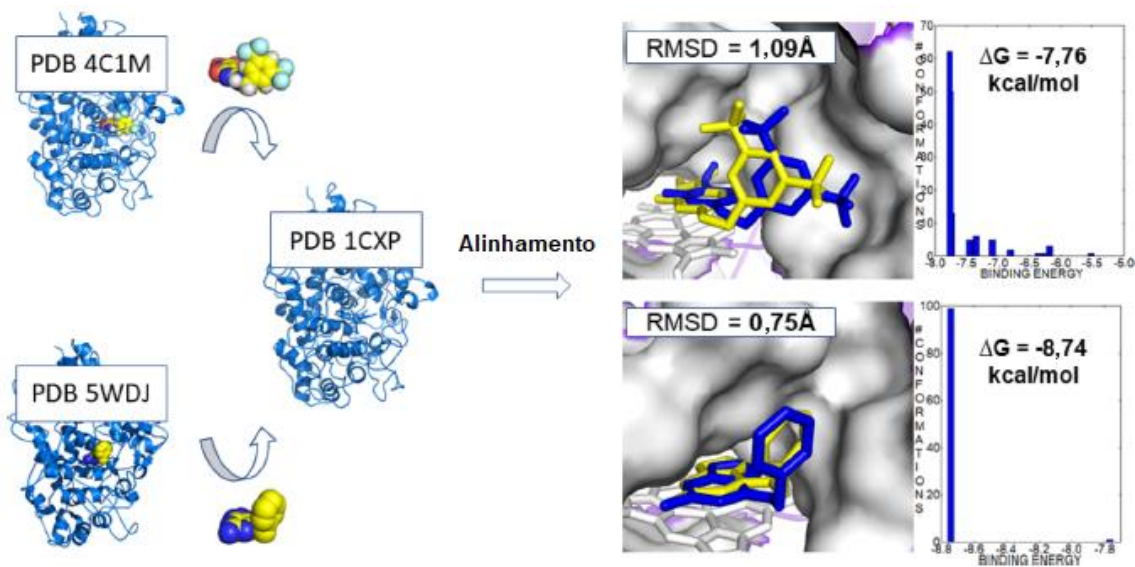


Figura 5

4 / 7

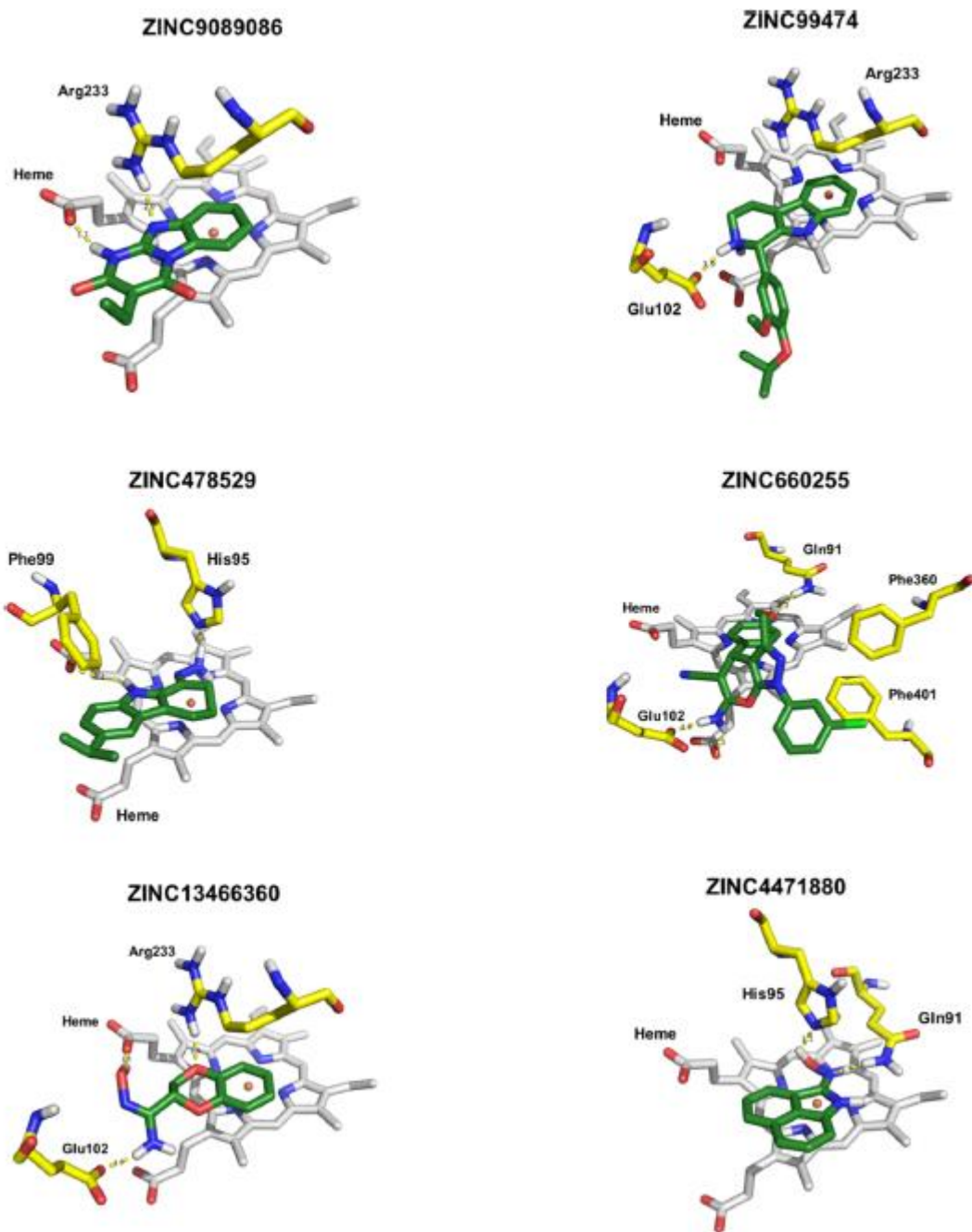


Figura 6

5/7

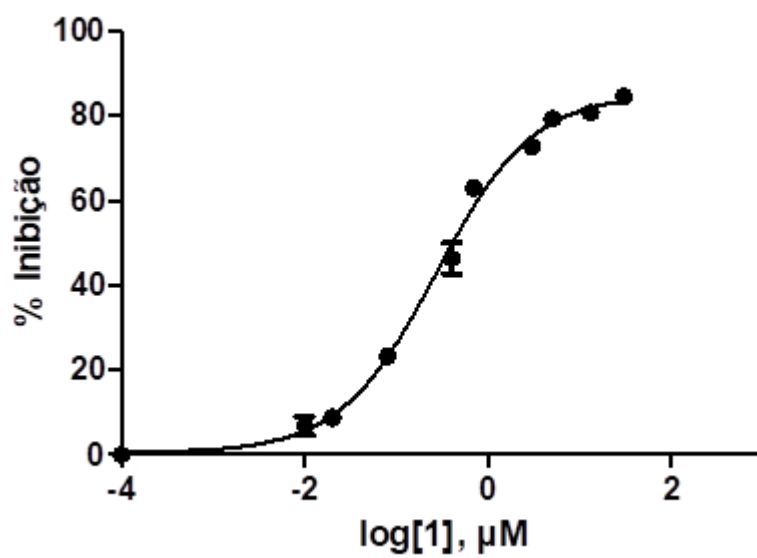


Figura 7

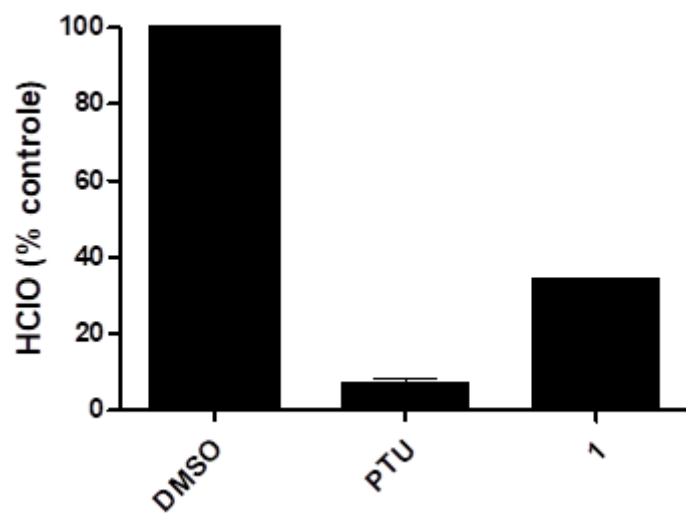


Figura 8

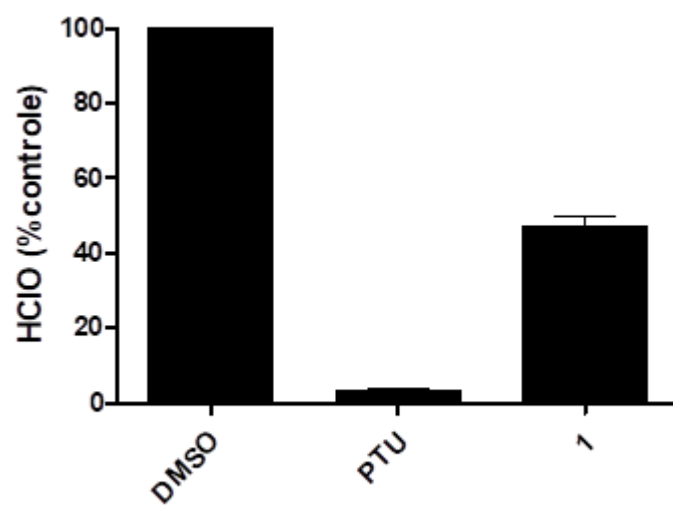


Figura 9

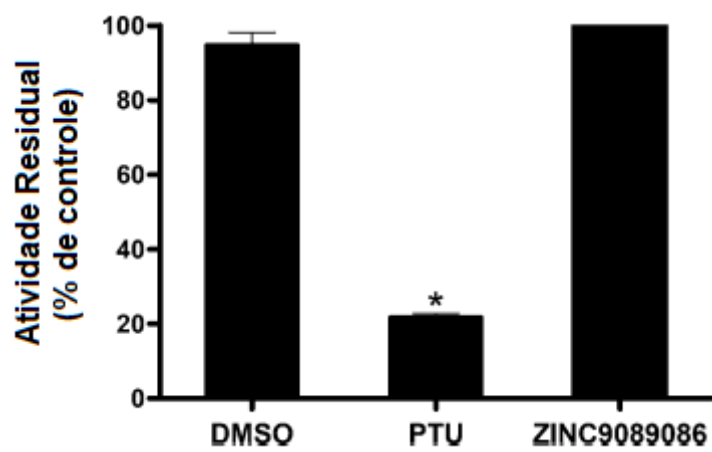


Figura 10

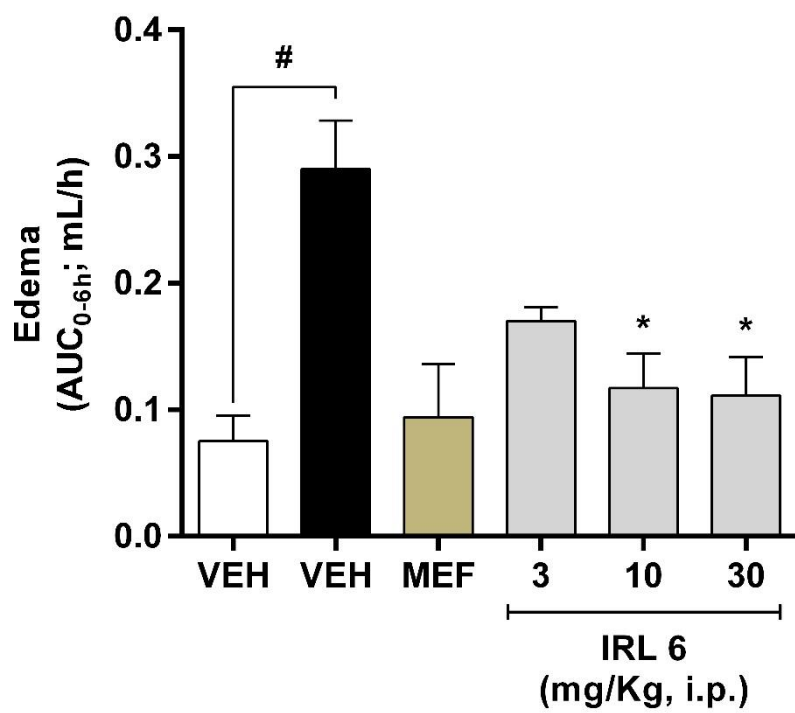


Figura 11

RESUMO**COMPOSTO DERIVADO HIDRAZIL OU HIDROXÂMICO DO ANIDRIDO 1,8-NAFTÁLICO, COMPOSIÇÃO FARMACÊUTICA E SEU USO**

A presente invenção propõe um composto, ou um sal farmacêuticamente aceitável, de derivados hidrazil (N-NH₂) ou hidroxâmico (N-OH) do anidrido 1,8-naftálico com mecanismo de ação competitivo frente ao sítio ativo da enzima mieloperoxidase. Inicialmente, a presente invenção revela os compostos derivados naftálicos, ou seus respectivos sais, como inibidores da enzima mieloperoxidase; em seguida, de posse do composto obtido, é formulada uma composição farmacêutica contendo ingredientes ativos orgânicos, especificamente contendo os compostos derivados naftálicos supracitados que são capazes de inibir ou pelo menos reduzir a atividade indesejável da mieloperoxidase na prevenção e/ou tratamento de condições inflamatórias. Adicionalmente, a presente invenção também diz respeito ao uso da referida composição farmacêutica para a profilaxia ou o tratamento de qualquer doença ou condição nas quais a enzima mieloperoxidase (MPO) e outras peroxidases como eosinófilico peroxidase, tireoide peroxidase e peroxidase de glóbulos vermelhos possuam relevância fisiopatológica.



Isaac de Araujo Matos

Endereço para acessar este CV: <http://lattes.cnpq.br/8188695724384449>

Última atualização do currículo em 25/04/2022

Resumo informado pelo autor

Isaac de Araujo Matos possui doutorado em Bioquímica no Instituto de Química da Universidade de São Paulo (USP-SP). Participa atualmente como pesquisador no Consórcio Internacional para a busca de agentes antivirais contra SARS-Cov-2 com foco na inibição do macrodomínio da proteína nsp3. Tem publicado 4 artigos em periódicos especializados, 1 depósito de patente e 19 apresentações de trabalho em anais de eventos e congressos. Possui 2 prêmios. De 2016 a 2017 lecionou como professor substituto no Departamento de Química da Universidade Federal de Sergipe. Ministrou também aula de Inibidores Enzimáticos na disciplina de Bioquímica Experimental Avançada no Instituto de Química da USP-SP. Sua área de interesse concentra-se no processo de desenvolvimento de fármacos assistido por computador e validados por métodos experimentais (in vitro, ex-vivo e in vivo). Computacionalmente domina métodos de física clássica como docagem molecular e dinâmica molecular, como também o uso de propriedades eletrônicas calculadas a níveis quânticos semi-empíricos para a compreensão de mecanismo catalítico e inibição enzimática. Possui experiências em ensaios enzimáticos, celulares em cultura e ex-vivo e no uso de modelos animais para validação do efeito terapêutico de inibidores enzimáticos (Farmacologia Experimental).

(Texto informado pelo autor)

Nome civil

Nome Isaac de Araujo Matos

Dados pessoais



Filiação Dagnoberto Ferreira de Matos e Maria Gorete de Araújo Matos

Nascimento 09/03/1987 - Aracaju/SE - Brasil

Carteira de Identidade 32942311 SSP - SE - 01/03/2004

CPF 012.684.555-71

Formação acadêmica/titulação

- 2017 - 2022** Doutorado em Ciências Biológicas (Bioquímica).
Universidade de São Paulo, USP, Sao Paulo, Brasil
Título: Planejamento de Inibidores da Enzima Mieloperoxidase como novos Agentes Anti-inflamatórios:
Um estudo in silico, in vitro e in vivo, Ano de obtenção: 2022
Orientador: Flávia Carla Meotti 
Bolsista do(a): Coordenação de Aperfeiçoamento de Pessoal de Nível Superior
- 2014 - 2016** Mestrado em Química.
Universidade Federal de Sergipe, UFS, Sao Cristovao, Brasil
Título: Planejamento in silico de Inibidores da Enzima Diidrofolato Redutase, Ano de obtenção: 2016
Orientador: Nivan Bezerra da Costa Junior 
Co-orientador: Ricardo Oliveira Freire
Bolsista do(a): Coordenação de Aperfeiçoamento de Pessoal de Nível Superior
- 2009 - 2014** Graduação em Química Tecnológica.
Universidade Federal de Sergipe, UFS, Sao Cristovao, Brasil
Título: Estudo Comparativo entre os efeitos Antidiabéticos e Moduladores do Estresse Oxidativo do Ácido Cinâmico e seu Respeetivo Complexo de Oxovanádio (IV) no Diabetes Mellitus Tipo 1
Orientador: Humberto Reis Matos
Bolsista do(a): Conselho Nacional de Desenvolvimento Científico e Tecnológico
- 2004 - 2006** Ensino Profissional de nível técnico em Técnico em Química.
Instituto Federal de Sergipe, IFS, Aracaju, Brasil

Formação complementar

- 2019 - 2019** Curso de curta duração em Redação de Patentes, Além dos Guias + Oficinas Práticas. (Carga horária: 12h).
Universidade de São Paulo, USP, Sao Paulo, Brasil
- 2015 - 2015** Extensão universitária em "I ESCOLA DE QUÍMICA UFSCAR - UFS". (Carga horária: 40h).
Universidade Federal de Sergipe, UFS, Sao Cristovao, Brasil
- 2009 - 2009** Curso de curta duração em Bioquímica. (Carga horária: 176h).
Universidade de São Paulo, USP, Sao Paulo, Brasil
- 2009 - 2009** Curso de curta duração em Utilização de Softwares em Aval. de Sim. Genética. (Carga horária: 8h).
Embrapa Tabuleiros Costeiros, EMBRAPA, Brasil
- 2009 - 2009** Curso de curta duração em Extração de DNA em Tecidos Vegetais. (Carga horária: 16h).
Embrapa Tabuleiros Costeiros, EMBRAPA, Brasil
- 2008 - 2008** Curso de curta duração em Decomposição de Amostras por Microondas. (Carga horária: 4h).
Embrapa Tabuleiros Costeiros, EMBRAPA, Brasil
- 2008 - 2008** Curso de curta duração em Métodos em Biofísica Molecular. (Carga horária: 6h).
Universidade Federal de Sergipe, UFS, Sao Cristovao, Brasil
- 2008 - 2008** Curso de curta duração em Biossegurança, Manejo e Criação de Anim. de Lab.. (Carga horária: 14h).
Universidade Federal de Sergipe, UFS, Sao Cristovao, Brasil
- 2008 - 2008** Curso de curta duração em Cromatografia Líquida de Alta Eficiência. (Carga horária: 4h).

Embrapa Tabuleiros Costeiros, EMBRAPA, Brasil

- 2008 - 2008** Curso de curta duração em Análise Cromat. de Lipídeos p/ Estudo de Ecologia. (Carga horária: 4h). Embrapa Tabuleiros Costeiros, EMBRAPA, Brasil
- 2008 - 2008** Curso de curta duração em Análise por Difração de Raios X. (Carga horária: 4h). Embrapa Tabuleiros Costeiros, EMBRAPA, Brasil
- 2005 - 2005** Curso de curta duração em Química Aplic. às Atividades de Prod. de Petróleo. (Carga horária: 6h). Universidade Federal de Sergipe, UFS, Sao Cristovao, Brasil
- 2005 - 2005** Curso de curta duração em Aproveitamento de Resíduos Sólidos. (Carga horária: 16h). Universidade Federal de Sergipe, UFS, Sao Cristovao, Brasil
- 2005 - 2005** Curso de curta duração em Segurança em Laboratório. (Carga horária: 4h). Universidade Federal de Sergipe, UFS, Sao Cristovao, Brasil
- 2005 - 2005** Curso de curta duração em Contextualizando o Ensino de Química. (Carga horária: 6h). Universidade Federal de Sergipe, UFS, Sao Cristovao, Brasil
- 2002 - 2002** Curso de curta duração em Programa de Educação Ambiental. (Carga horária: 40h). Superintendência de Recursos Hídricos, SRH SE, Brasil

Atuação profissional

1. Universidade Federal de Sergipe - UFS

Vínculo institucional

- 2016 - 2017** Vínculo: Servidor público , Enquadramento funcional: Professor Substituto , Carga horária: 20, Regime: Parcial
- 2007 - 2013** Vínculo: Iniciação Científica , Enquadramento funcional: Iniciação Científica , Carga horária: 20, Regime: Parcial
Outras informações:
Desenvolveu atividades de pesquisa relacionadas com a fisiopatologia molecular do diabetes mellitus, da inflamação e do etilismo empregando para isso análises bioquímicas , fitoquímicas e analíticas, em ensaios in vitro e modelos animais.

2. Conselho Nacional de Desenvolvimento Científico e Tecnológico - CNPq

Vínculo institucional

- 2012 - 2013** Vínculo: Bolsista , Enquadramento funcional: Iniciação Científica , Carga horária: 20, Regime: Parcial
Outras informações:
Estágio remunerado com bolsa CNPq de Apoio Técnico à Pesquisa - Nível Médio - 2A do INCT de Processos Redox em Biomedicina - Redoxoma.
- 2009 - 2011** Vínculo: Bolsista , Enquadramento funcional: Iniciação Científica , Carga horária: 20, Regime: Parcial
Outras informações:
Estágio remunerado com bolsa CNPq de Apoio Técnico à Pesquisa - Nível Médio - 2A do INCT de Processos Redox em Biomedicina - Redoxoma.

3. Empresa de Desenvolvimento Agropecuário de Sergipe - EMDAGRO

Vínculo institucional

- 2007 - 2009** Vínculo: Bolsista , Enquadramento funcional: Estagiário , Carga horária: 20, Regime: Parcial
Outras informações:
Estágio extracurricular ligado ao Projeto de Pesquisa do PRODETAB - "Métodos Alternativos para o Controle Fitossanitário em Sistema Orgânico de Produção de Hortaliças nos Tabuleiros Costeiros do Estado de Sergipe" e de Ações de Pesquisas em Diagnóstico e Caracterização Molecular de Isolados da Xylella fastidiosa dos Citros em Sergipe.

4. Universidade de São Paulo - USP

Vínculo institucional

- 2017 - 2022** Vínculo: Bolsista , Enquadramento funcional: Aluno , Carga horária: 40, Regime: Integral

Projetos

Projetos de pesquisa

- 2020 - Atual** Inibição do macromódulo viral como estratégia de tratamento para coronavírus
- Descrição: O projeto visa desenvolver inibidores para o macromódulo nsp3 do SARS-Cov-2 com atividade antiviral empregando métodos computacionais e experimentais.
Situação: Em andamento Natureza: Projetos de pesquisa
Integrantes: Isaac de Araujo Matos; Flávia Carla Meotti; Nicolas Hoch (Responsável); Déborah Schechtman; Alexandre Bruni Cardoso
- 2017 - 2022** Planejamento de Inibidores da Enzima Mieloperoxidase Candidatos a Fármacos Anti-inflamatórios: Um estudo Computacional e Experimental
- Situação: Concluído Natureza: Projetos de pesquisa
Integrantes: Isaac de Araujo Matos (Responsável); ; Flávia Carla Meotti
- 2002 - 2007** Métodos alternativos para o controle fitossanitário em sistema orgânico de produção de hortaliças nos tabuleiros costeiros do Estado de Sergipe
- Descrição: Gerar novos conhecimentos técnico-científicos sobre o uso de produtos naturais no controle de doenças e pragas para viabilizar, técnicas e economicamente, a produção de hortaliças orgânicas pelo pequeno produtor em Sergipe.
Situação: Concluído Natureza: Projetos de pesquisa
Integrantes: Isaac de Araujo Matos (Responsável); ; Luzia Nilda Tabosa Andrade; Maria Urbana Corrêa Nunes; Ivênio Rubens de Oliveira
- 2001 - 2005** Epidemiologia, danos e caracterização da Xylella fastidiosa dos citros no estado de Sergipe
- Descrição: A Clorose Variegada dos Citros, causada pela bactéria Xylella fastidiosa é atualmente considerada o mais sério problema da citricultura nacional. Sua importância decorre do fato de afetar

todas as variedades comerciais de de laranja doce, principal exploração brasileira. Os estudos epidemiológicos da CVC em Sergipe, permitirão através do mapeamento de pomares em áreas comerciais uma visão da disseminação da doença no tempo e no espaço, o dano causado e a utilização de teste molecular através de PCR para diagnóstico e caracterização de isolados da bactéria, contribuindo para adequar metodologias de controle e/ou convivência com a doença.
Situação: Concluído Natureza: Projetos de pesquisa
Integrantes: Isaac de Araujo Matos (Responsável); ; Luzia Nilda Tabosa Andrade; Paula Cristina da Silva Angelo; Luiz Mário Santos da Silva

Projeto de extensão

- 2011 - 2012** Educar, Prevenir e Reduzir as Complicações Diabéticas em Pacientes Tratados com Hipoglicemiantes e Suplementados com Vitamina C no Município de ItabaianaSE

Situação: Concluído Natureza: Projeto de extensão
Integrantes: Isaac de Araujo Matos; Humberto Reis Matos (Responsável)

Prêmios e títulos

- 2021** IX PRÊMIO QUALIDADE CIENTÍFICA PROF. DR. "JOÃO GARCIA LEME", Departamento de Farmacologia ICB USP
- 2015** Melhor Apresentação oral na II ESCOLA DE QUÍMICA UFS-UFSCAR, PROGRAMA DE PÓS-GRADUAÇÃO EM QUÍMICA - Universidade Federal de Sergipe

Produção

Produção bibliográfica

Artigos completos publicados em periódicos

- 1.** [doi](#) RUSSO, LILIAN CRISTINA; TOMASIN, REBEKA; **MATOS, ISAAC ARAÚJO**; MANUCCI, ANTONIO CARLOS; SOWA, SVEN T.; DALE, KATIE; CALDECOTT, KEITH W.; LEHTIÖ, LARI; SCHECHTMAN, DEBORAH; MEOTTI, FLAVIA C.; BRUNI-CARDOSO, ALEXANDRE; HOCH, NICOLAS CARLOS
The SARS-CoV-2 Nsp3 macrodomain reverses PARP9/DTX3L-dependent ADP-ribosylation induced by interferon signaling. *JOURNAL OF BIOLOGICAL CHEMISTRY*. [JCB](#), v.297, p.101041 - , 2021.
- 2.** [doi](#) **MATOS, ISAAC DE ARAÚJO**; DA COSTA JÚNIOR, NIVAN BEZERRA; MEOTTI, FLAVIA CARLA
Integration of an Inhibitor-like Rule and Structure-based Virtual Screening for the Discovery of Novel Myeloperoxidase Inhibitors. *Journal of Chemical Information and Modeling*. [JCB](#), v.60, p.6408 - 6418, 2020.
- 3.** [doi](#) PINTO, ISABELLA F.D.; SILVA, RAILMARA P.; FILHO, ADRIANO DE B. CHAVES; DANTAS, LUCAS S.; BISPO, VANDERSON S.; **MATOS, ISAAC A.**; OTSUKA, FELIPE A.M.; SANTOS, ALINE C.; MATOS, HUMBERTO REIS
Study of Antiglycation, Hypoglycemic, and Nephroprotective Activities of the Green Dwarf Variety Coconut Water (*Cocos nucifera* L.) in Alloxan-Induced Diabetic Rats. *Journal of Medicinal Food*. [JCB](#), v.18, p.802 - 809, 2015.
- 4.** [doi](#) SANTOS, J. L. A.; BISPO, V. S.; FILHO, A. B. C.; PINTO, I. F. D.; DANTAS, L. S.; VASCONCELOS, D. F.; ABREU, F. F.; MELO, D. A.; MATOS, I. A.; FREITAS, F. P.; GOMES, O. F.; MEDEIROS, M. H. G.; MATOS, H. R.
Evaluation of Chemical Constituents and Antioxidant Activity of Coconut Water (*Cocos nucifera* L.) and Caffeic Acid in Cell Culture. *ANAIAS DA ACADEMIA BRASILEIRA DE CIENCIAS*. [JCB](#), v.85, p.1235 - 1247, 2013.

Apresentação de trabalho e palestra

- 1.** **MATOS, I. A.**; DALLAZEN, J. L.; COSTA JUNIOR, N. B.; COSTA, S. K. P.; MEOTTI, F. C.
Descoberta de um Inibidor Nanomolar da Mieloperoxidase Oralmente Ativo em um Modelo de Artrite Gotosa usando uma Regra Inibidor-símile e Triagem Virtual Baseada no Receptor, 2021. (Simpósio, Apresentação de Trabalho)
- 2.** **MATOS, I. A.**; DALLAZEN, J. L.; COSTA, S. K. P.; COSTA JUNIOR, N. B.; MEOTTI, F. C.
Discovery of Nanomolar Myeloperoxidase Inhibitors with Anti-Arthritis Properties: A Computational, in vitro and in vivo study., 2021. (Congresso, Apresentação de Trabalho)
- 3.** COSTA, A. L. S. V.; **MATOS, I. A.**; COSTA JUNIOR, N. B.; DOMINGOS, I. G. R.; MEOTTI, FLAVIA C.
Modo de Ligação entre a Proteína Dissulfeto Isomerase A1 e seu Oxidante Hidróperóxido de Urato – Um Estudo Computacional, 2021. (Seminário, Apresentação de Trabalho)
- 4.** **MATOS, I. A.**; COSTA JUNIOR, N. B.; MEOTTI, F. C.
Identification of New Myeloperoxidase Inhibitors with Nanomolar Potency using Validated Virtual Screening Methodology, 2019. (Congresso, Apresentação de Trabalho)
- 5.** **MATOS, I. A.**; MEOTTI, F. C.
Virtual Screening for Discovery of New Myeloperoxidase Inhibitors: Integration of an Inhibitor-like Rule and Consensus Docking Approach., 2019. (Congresso, Apresentação de Trabalho)
- 6.** **MATOS, ISAAC A.**
Planejamento in silico de Inibidores da Enzima Dihidrofolato Redutase, 2015. (Outra, Apresentação de Trabalho)
- 7.** MATOS, I. A.; SILVA, R. P.; FILHO, A. B. C.; DANTAS, L. S.; SANTOS, D. M.; OTSUKA, F. A. M.; PINTO, I. F. D.; BISPO, V. S.; MATOS, H. R.; SANTOS, A. C.
Antioxidant Activity of Cinnamic Acid Derivatives in Oxidative Damage Induced by Hydrogen Peroxide in Cell Culture: A Comparative Study, 2013. (Congresso, Apresentação de Trabalho)
- 8.** SANTOS, A. C.; SILVA, R. P.; VASCONCELOS, D. F.; FILHO, A. B. C.; DANTAS, L. S.; MATOS, I. A.; PINTO, I. F. D.; OTSUKA, F. A. M.; SANTOS, D. M.; BISPO, V. S.; MATOS, H. R.
Chemical characterization, antioxidant potential and hypoglycemic activity of the bark stem hydroalcoholic extract of *Bauhinia cheilantha*, 2013. (Congresso, Apresentação de Trabalho)
- 9.** SILVA, R. P.; MATOS, I. A.; FILHO, A. B. C.; DANTAS, L. S.; OTSUKA, F. A. M.; PINTO, I. F. D.; VASCONCELOS, D. F.; SANTOS, D. M.; MATOS, H. R.
Nephroprotective and Hepatoprotective Effects of the Coconut Water and Caffeic Acid in Oxidative Stress Mediated by Acetaminophen, 2013. (Congresso, Apresentação de Trabalho)
- 10.** OTSUKA, F. A. M.; SILVA, R. P.; DANTAS, L. S.; PINTO, I. F. D.; FILHO, A. B. C.; MATOS, I. A.; VASCONCELOS, D. F.; SANTOS, D. M.; MATOS, H. R.
Study of hypoglycemic and nephroprotective activities of the green dwarf variety coconut water (*Cocos nucifera* L.) in alloxan-induced diabetic rats, 2013. (Congresso, Apresentação de Trabalho)
- 11.** SILVA, R. P.; PINTO, I. F. D.; ABREU, F. F.; VASCONCELOS, D. F.; DANTAS, L. S.; FILHO, A. B. C.; MATOS, I. A.; OTSUKA, F. A. M.; MATOS, H. R.
Study of the Antioxidant and Antidiabetic Activity of Coconut Water From Green Dwarf Variety (*Cocos nucifera* L.), 2012. (Congresso, Apresentação de Trabalho)
- 12.** FILHO, A. B. C.; VASCONCELOS, D. F.; PINTO, I. F. D.; DANTAS, L. S.; SANTOS, F. L.; SILVA, R. P.; MELO, A. J. O.; BISPO, V. S.; MATOS, I. A.; ABREU, F. F.; LIMA, E. S.; LIMA, A. S.; MATOS, H. R.
Evaluation of Antioxidant Activity and Inhibition of Digestive Enzymes of *Angico de Carço* (*Anadenanthera macrocarpa*) Stem Bark Extract, 2011. (Congresso, Apresentação de Trabalho)

13. VASCONCELOS, D. F.; ABREU, F. F.; MATOS, H. R.; FILHO, A. B. C.; PINTO, I. F. D.; DANTAS, L. S.; SANTOS, F. L.; SILVA, R. P.; MELO, A. J. O.; BISPO, V. S.; **MATOS, I. A.**
Evaluation of Hypoglycemic Activity and Antioxidant Potential of Bauhinia variegata Stem Bark Extract in Oxidative Stress Induced on alloxan diabetic rats, 2011. (Congresso, Apresentação de Trabalho)
14. PINTO, I. F. D.; MELO, A. J. O.; SANTOS, F. L.; ABREU, F. F.; MATOS, H. R.; FILHO, A. B. C.; VASCONCELOS, D. F.; DANTAS, L. S.; BISPO, V. S.; SANTOS, J. L. A.; MATOS, I. A.; SILVA, R. P.
Evaluation of Oxidative Stress in Diabetic Patients Treated with Oral Hypoglycemic Agents in Salgado-SE, 2011. (Congresso, Apresentação de Trabalho)
15. MATOS, I. A.; SANTOS, J. L. A.; BISPO, V. S.; FREITAS, F. P.; FILHO, A. B. C.; MATOS, H. R.; GOMES, O. F.; PINTO, I. F. D.; MEDEIROS, M. H. G.; ABREU, F. F.; VASCONCELOS, D. F.; DANTAS, L. S.
Antioxidant Avaluation of Four Varieties Antioxidant of Cocos nucifera L., 2010. (Congresso, Apresentação de Trabalho)
16. BISPO, V. S.; SANTOS, J. L. A.; MATOS, I. A.; FILHO, A. B. C.; PINTO, I. F. D.; VASCONCELOS, D. F.; FREITAS, F. P.; GOMES, O. F.; MEDEIROS, M. H. G.; ABREU, F. F.; DANTAS, L. S.; MATOS, H. R.
Hepatoprotecting Effect and Antioxidant Potential of the Coconut Water in Oxidative Stress Mediated by Ethanol, 2010. (Congresso, Apresentação de Trabalho)
17. ABREU, F. F.; BISPO, V. S.; SANTOS, J. L. A.; MATOS, I. A.; PINTO, I. F. D.; FILHO, A. B. C.; DANTAS, L. S.; VASCONCELOS, D. F.; FREITAS, F. P.; MATOS, H. R.
Study of the Antioxidant Activity and Antidiabetes of the Fruit of Catingueira (Caesalpinia pyramidalis), 2010. (Congresso, Apresentação de Trabalho)
18. **MATOS, I. A.**
Variabilidade Genética entre Vinte Clones de Cajueiro, 2008. (Congresso, Apresentação de Trabalho)
19. **MATOS, I. A.**
Utilização da Técnica de Perfusão para Diagnóstico por PCR da Bactéria Xylella fastidiosa dos Citros, 2007. (Congresso, Apresentação de Trabalho)

Patentes e registros

Patente

A Confirmação do status de um pedido de patentes poderá ser solicitada à Diretoria de Patentes (DIRPA) por meio de uma Certidão de atos relativos aos processos

1. MEOTTI, F. C.; **MATOS, I. A.**
Composição Farmacêutica contendo Inibidores da Mieloperoxidase para Uso Terapêutico, 2021.
Categoria: Produto. Instituição onde foi depositada: INPI - Instituto Nacional da Propriedade Industrial.
País: Brasil. Natureza: Patente de Invenção. Número do registro: BR10202102167. Número do depósito PCT: 10202102167. Data de depósito: 28/10/2021. Depositante/Titular: Universidade de São Paulo.

Página gerada pelo sistema Currículo Lattes em 12/05/2022 às 14:24:02.